General Disclaimer

One or more of the Following Statements may affect this Document

- This document has been reproduced from the best copy furnished by the organizational source. It is being released in the interest of making available as much information as possible.

- This document may contain data, which exceeds the sheet parameters. It was furnished in this condition by the organizational source and is the best copy available.

- This document may contain tone-on-tone or color graphs, charts and/or pictures, which have been reproduced in black and white.

- This document is paginated as submitted by the original source.

- Portions of this document are not fully legible due to the historical nature of some of the material. However, it is the best reproduction available from the original submission.

Produced by the NASA Center for Aerospace Information (CASI)

(NASA-CR-161945) STRUCTURAL DYNAMIC ANALYSIS OF THE SPACE SHUTTLE MAIN ENGINE Final Report (Lockheed Missiles and Space Co.) 166 p HC A08/MF A01 CSCL 21H

N82-19302

Unclas
G3/16 12339

Lockheed
Missiles & Space Company, Inc
Huntsville Research & Engineering Center

Cummings Research Park
4800 Bradford Drive,
Huntsville, Alabama

STRUCTURAL DYNAMIC ANALYSIS OF THE SPACE SHUTTLE MAIN ENGINE

FINAL REPORT

December 1981

Contract NAS8-33808

Prepared for National Aeronautics and Space Administration
Marshall Space Flight Center, Alabama 35812

by

L.P. Scott
G.T. Jamison
W.A. McCutcheon
J. M. Price

APPROVED: Leland P. Scott

for W. H. Armstrong, Manager
Structures & Mechanics Section

George D. Reny

George D. Reny
Director

FOREWORD

This final report presents a summary of the analytic model developments and results of analyses performed in the Structural Dynamic Analysis of the Space Shuttle Main Engine. This work was performed by the Structures & Mechanics Section of the Lockheed Missiles & Space Company, Huntsville Research & Engineering Center, Huntsville, Alabama, for the National Aeronautics and Space Administration, George C. Marshall Space Flight Center, Marshall Space Flight Center, Alabama. The Contracting Officer's Technical Representative for this study is Mr. Larry A. Kiefling, ED22.

Thermal and structural models of critical SSME powerhead components developed and applied in this study are documented and analyses described in this final report. These documented models, installed on MSFC computers, provide a data base for future SSME engine uprating studies and modifications.

TABLE OF CONTENTS

Section		Page
	FOREWORD	ii
1	INTRODUCTION	1-1
2	ANALYTIC MODEL DEVELOPMENTS	2-1
	2.1 SPAR LOX Post Assembly Model	2-2
	2.2 SPAR Post/Retainer Detailed Model	2-4
	2.3 APSA Post/Retainer Detail Model	2-4
	2.4 BOPACE 3-D Post/Retainer Detailed Model	2-8
	2.5 BOPACE 2-D Inertia Weld Region Model	2-8
	2.6 BOPACE 3-D Inertia Weld Region Model	2-11
	2.7 SPAR Inertia Weld Region Model	2-13
3	LOX POST ANALYSIS DISCUSSION	3-1
	3.1 LOX Post Assembly Analysis	3-1
	3.2 LOX Post Inertia Weld Region Analysis	3-24
	3.3 Inertia Weld Region Stress Concentration	3-30
	APPENDIX A - SPAR LOX Post Assembly Model	A-1a
	APPENDIX B - SPAR LOX Post Assembly Model Components	B-1
	APPENDIX C - SPAR Post/Retainer Detailed Model	C-1

1. INTRODUCTION

The objective of this structural dynamic analysis is to support development of the SSME by evaluating components subjected to critical dynamic loads, identify significant parameters and evaluate solution methods. Engine operating parameters at both rated and full power levels (RPL and FPL) were considered. Detailed structural dynamic analyses of operationally critical and life-limited components have supported the assessment of engine design modifications and environmental changes. Engine system test results which became available during the work period have been utilized to verify analytic model simulations.

The SSME Main Chamber Injector Assembly shown in Fig. 1 is an assembly of 600 injector elements which are called LOX posts. It is this critical component which is the focus of the analysis effort described herein.

The overall LOX post analysis procedure is shown in Fig. 2 where the analysis flow proceeds from thermal, structural static and dynamic loadings to the nonlinear APSA stress analysis. Later, in order to develop a more detailed view of the nonlinear cyclic loads, a BOPACE 3-D model was developed. The analysis is concluded with the fatigue life assessments. These procedures were, of course, often repeated for the evaluation of design and material changes.

A sectional view of the assembled LOX post is shown in Fig. 3 where each component is identified and a set of static applied lateral deflections are summarized.

ORIGINAL PAGE IS
OF POOR QUALITY

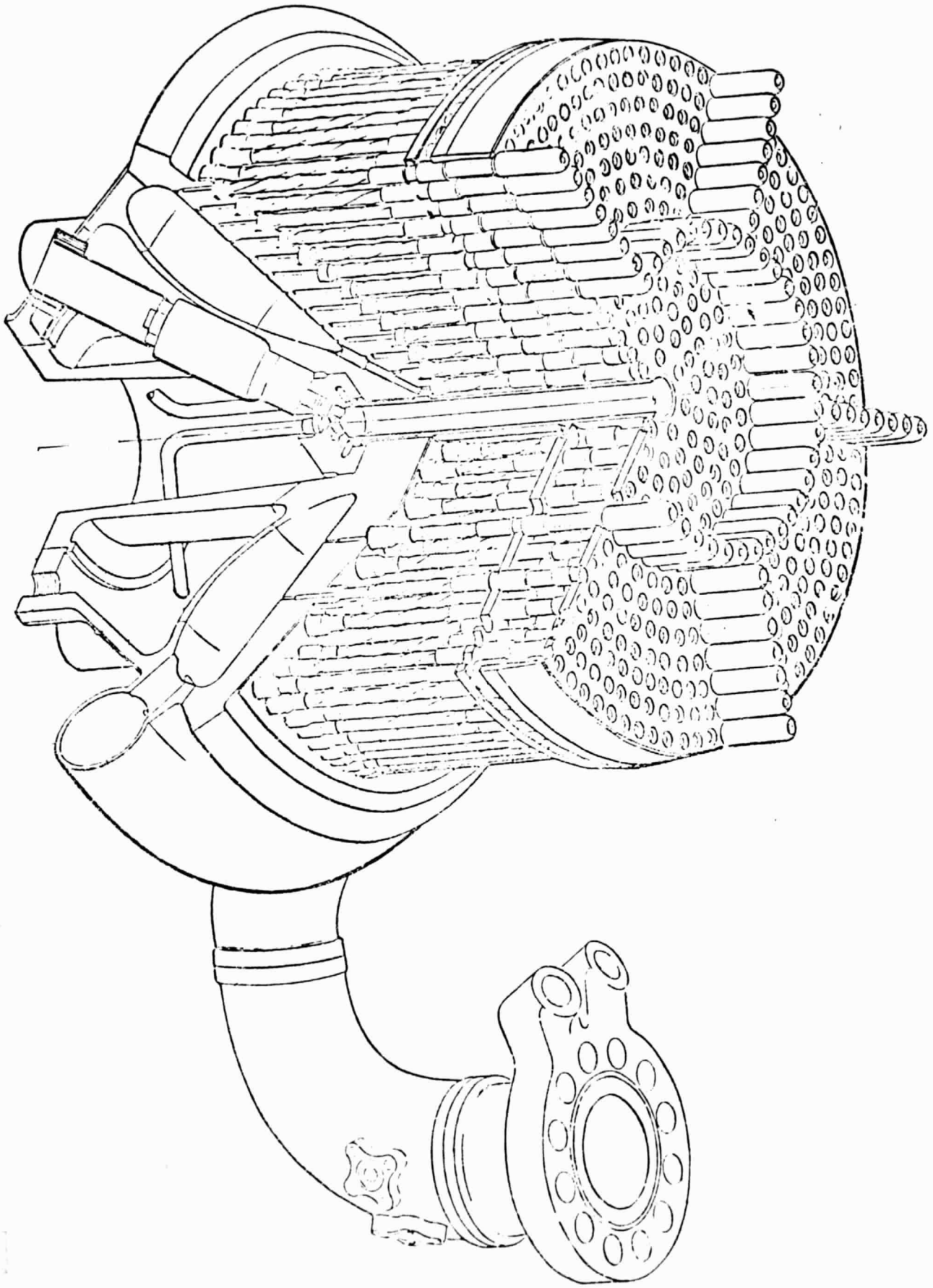

Fig. 1 - SSME Main Chamber Injector Assembly

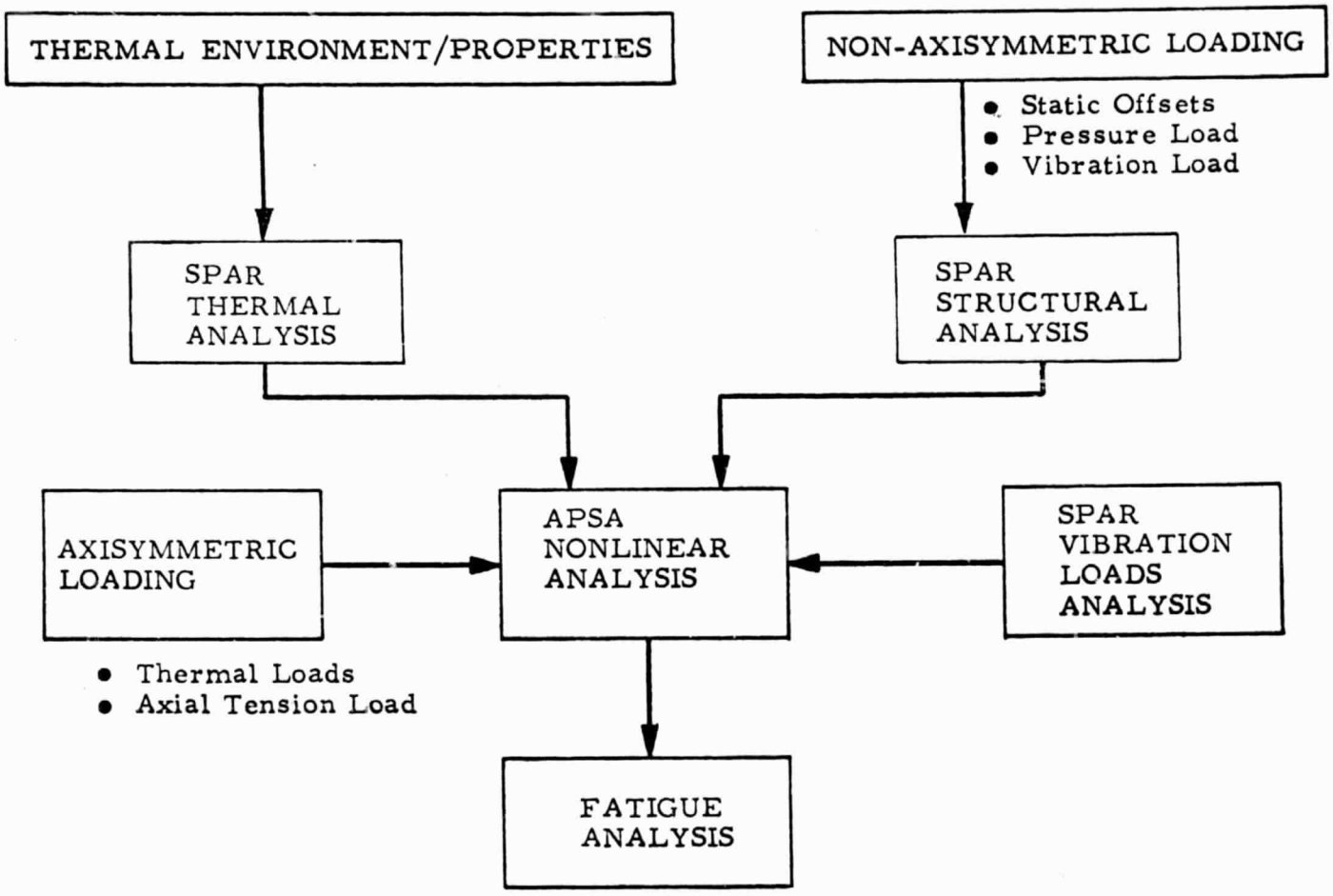

Fig. 2 - SSME LOX Post Analysis Procedure

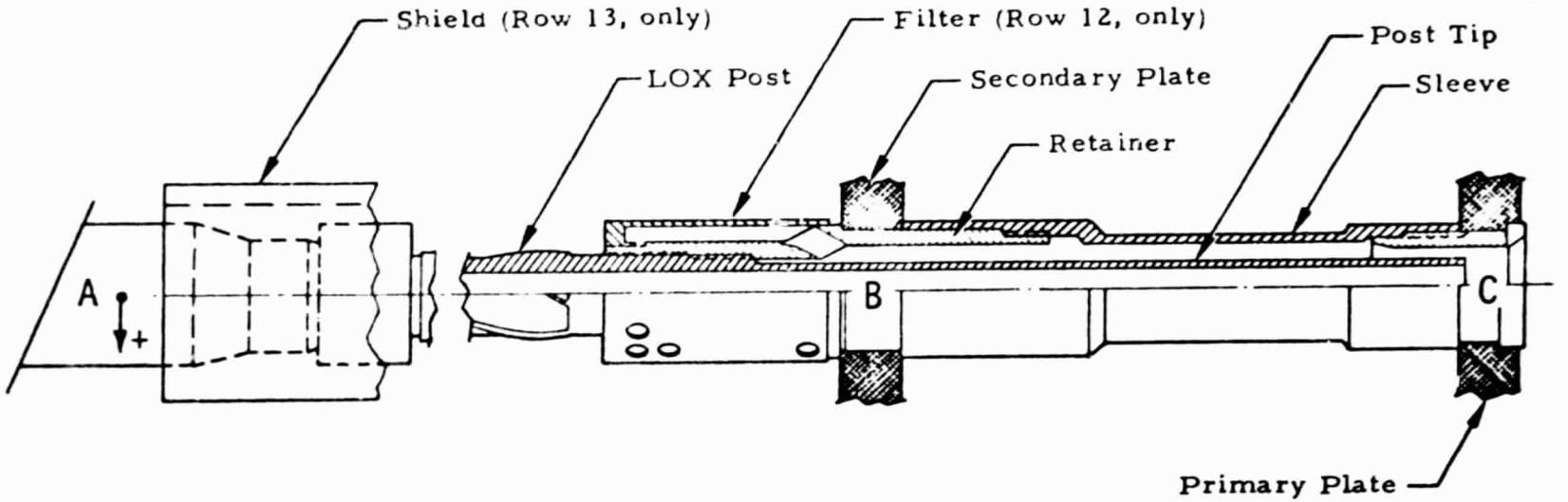

Static Applied Lateral Deflections		
	Displacement	Rotation
A	0.0176"	0.7 deg
B	-0.002"	0.0
C	0.0017"	0.0

*Tension axial load at "C" = 242 lb

Fig. 3 - SSME LOX Post Assembly Details

2. ANALYTIC MODEL DEVELOPMENTS

The finite element math models developed for the LOX post analysis are summarized as follows:

1. SPAR LOX Post Assembly Model
   - Thermal Version
   - Stress Version
   - Dynamic Version

2. SPAR Post/Retainer Detail Model
   - Thermal Version
   - Stress Version

3. APSA Post/Retainer Detail Model
   - Stress Version (Nonlinear)

4. BOPACE 3-D Post/Retainer Detail Model
   - 60 Deg Symmetric Segment

5. BOPACE 2-D Inertia Weld Region Model
   - Stress Version

6. BOPACE 3-D Inertia Weld Region Model
   - Thermal Version
   - Stress Version

7. SPAR Inertia Weld Region Model
   - Thermal Version
   - Stress Version

Two different post configurations were analyzed: (1) a one-piece 316L stainless steel post, and (2) an improved two-piece post with a Haynes 188 tip. Modified versions of the LOX post models were used to simulate posts from Rows 13, 12, 11 and 10; however, most analyses were concentrated on the Row 13 "Baseline" configuration which was investigated both with and without the outer flow shield.

2.1 SPAR LOX POST ASSEMBLY MODEL

The SPAR LOX Post Assembly Model Components are shown in Fig. 4. A layout drawing of the complete SPAR LOX Post Assembly Model and its 46 cross sections with numbered node locations are presented in Appendix A. Also shown is the one-half symmetric 13th row flow shield model details.

Assembled and exploded views of the LOX Post Assembly Model Components are presented in Appendix B.

This SPAR assembly model of the 13th row LOX Post contains 3388 nodes (2964 in the post assembly and 424 within the flow shield). The structural model possesses 10164 degrees of freedom and contains 2400 three-dimensional solid elements. The same element mesh is used for the thermal and structural models. The Row 12 model is developed from the baseline by deleting the shield and adjusting the distance between the upper post inertia weld joint and the secondary plate.

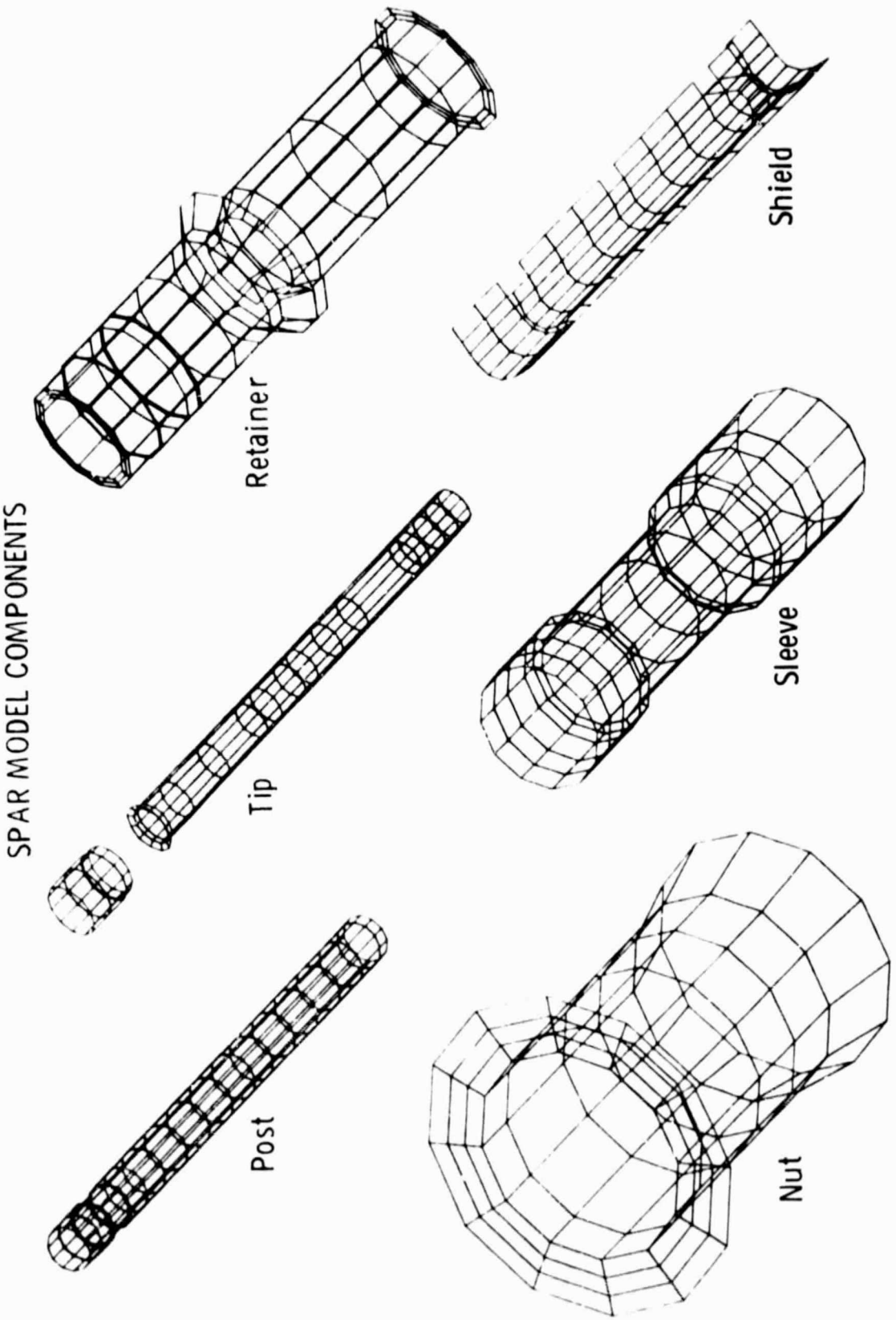

Fig. 4 - SPAR LOX Post Assembly Model Details

2.2 SPAR POST/RETAINER DETAILED MODEL

The SPAR Post/Retainer Detail Model was developed to investigate both thermal and stress levels in the post-to-retainer thread area where fatigue cracks had been observed after test firings at both RPL and FPL levels. The Post/Retainer Thermal/Structural Model is shown in Fig. 5. Additional views of the model and its components are presented in Appendix C. The detailed model consists of 2040 nodes.

2.3 APSA POST/RETAINER DETAIL MODEL

The APSA Post/Retainer Detailed Model was developed to investigate the nonlinear effects encountered in the post-to-retainer threads which resulted in cracks forming in the threads and fillet region of the post. The APSA model shares exactly identical boundary nodes with the SPAR assembly model so that computed temperature profiles from the SPAR thermal analysis could be mapped directly onto the APSA detailed model for stress analyses. The APSA axisymmetric model is shown in Fig. 6. Because of the detail involved, only the first three threads are modeled. The APSA model has 1500 nodes, 2958 degrees of freedom and is constructed using 1359 axisymmetric elements. An evaluation of the stress variations due to load sharing between the threads indicated that three threads represented an adequate modeling approach. An enlarged view of the threaded area is shown in Fig. 7 where thread contact stresses are simulated through the use of "slip" elements at the interface.

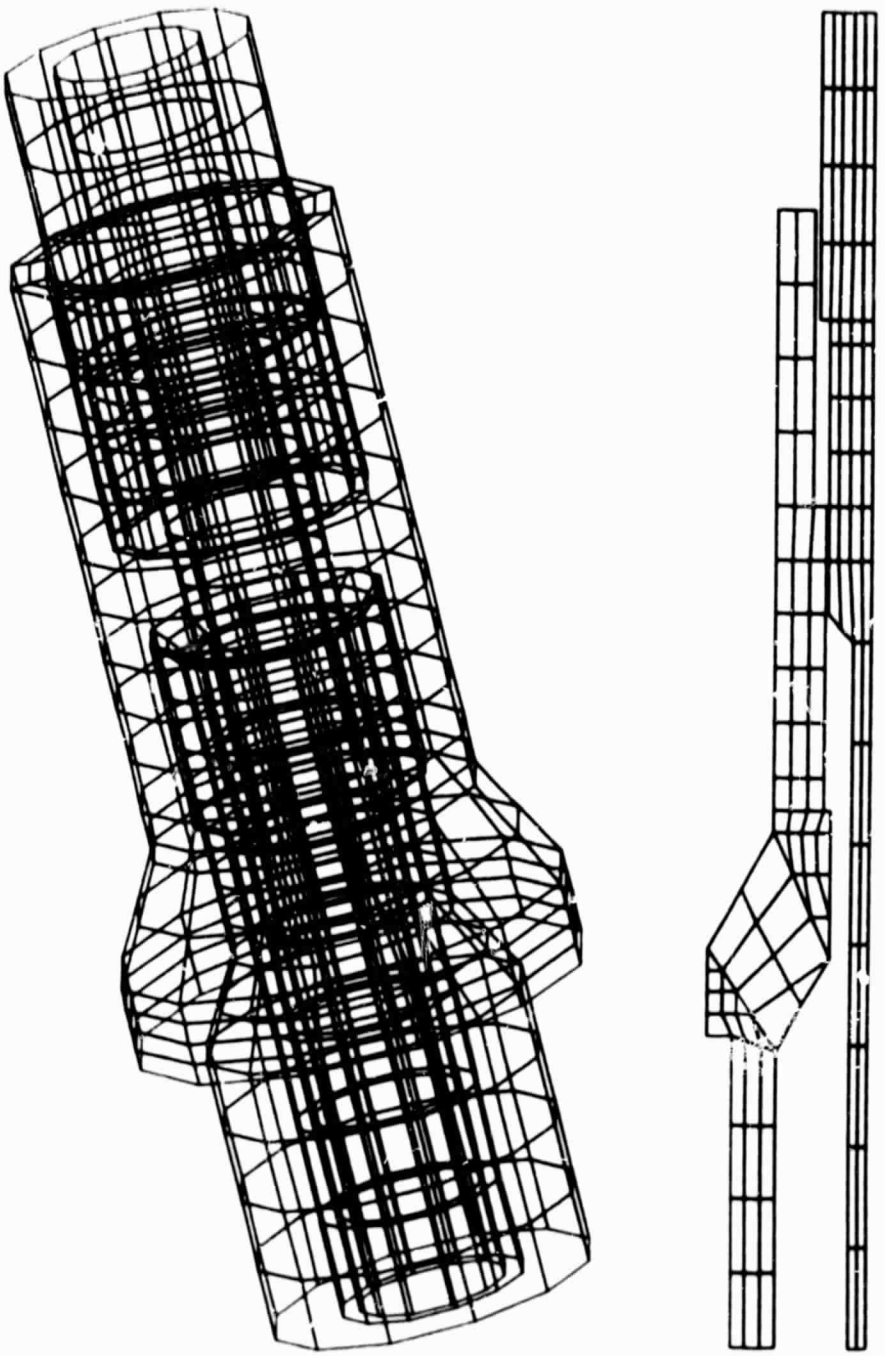

Fig. 5 - SPAR Post/Retainer Detailed Model

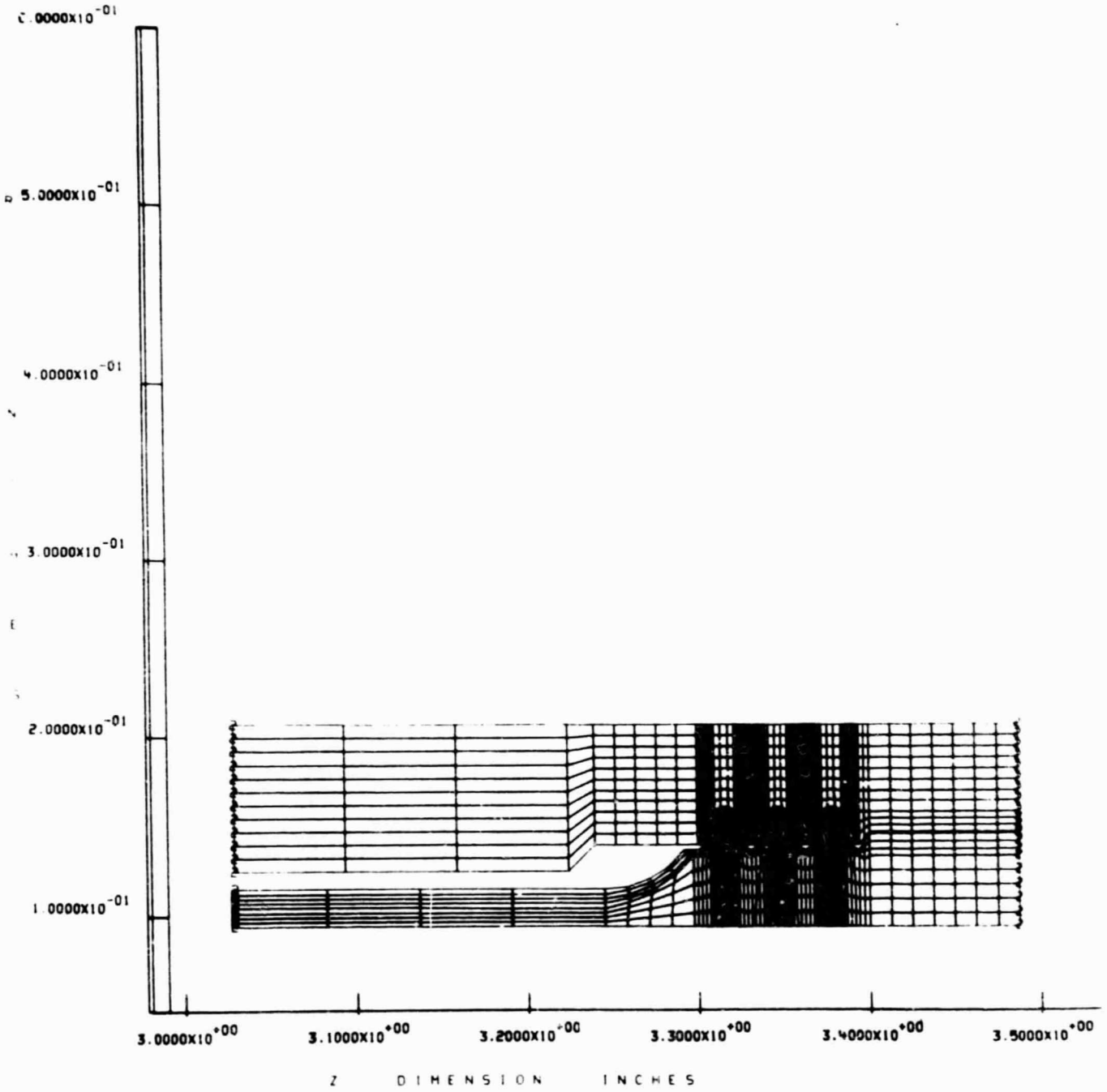

Fig. 6 - APSA LOX POST/Retainer Detailed Thread Model

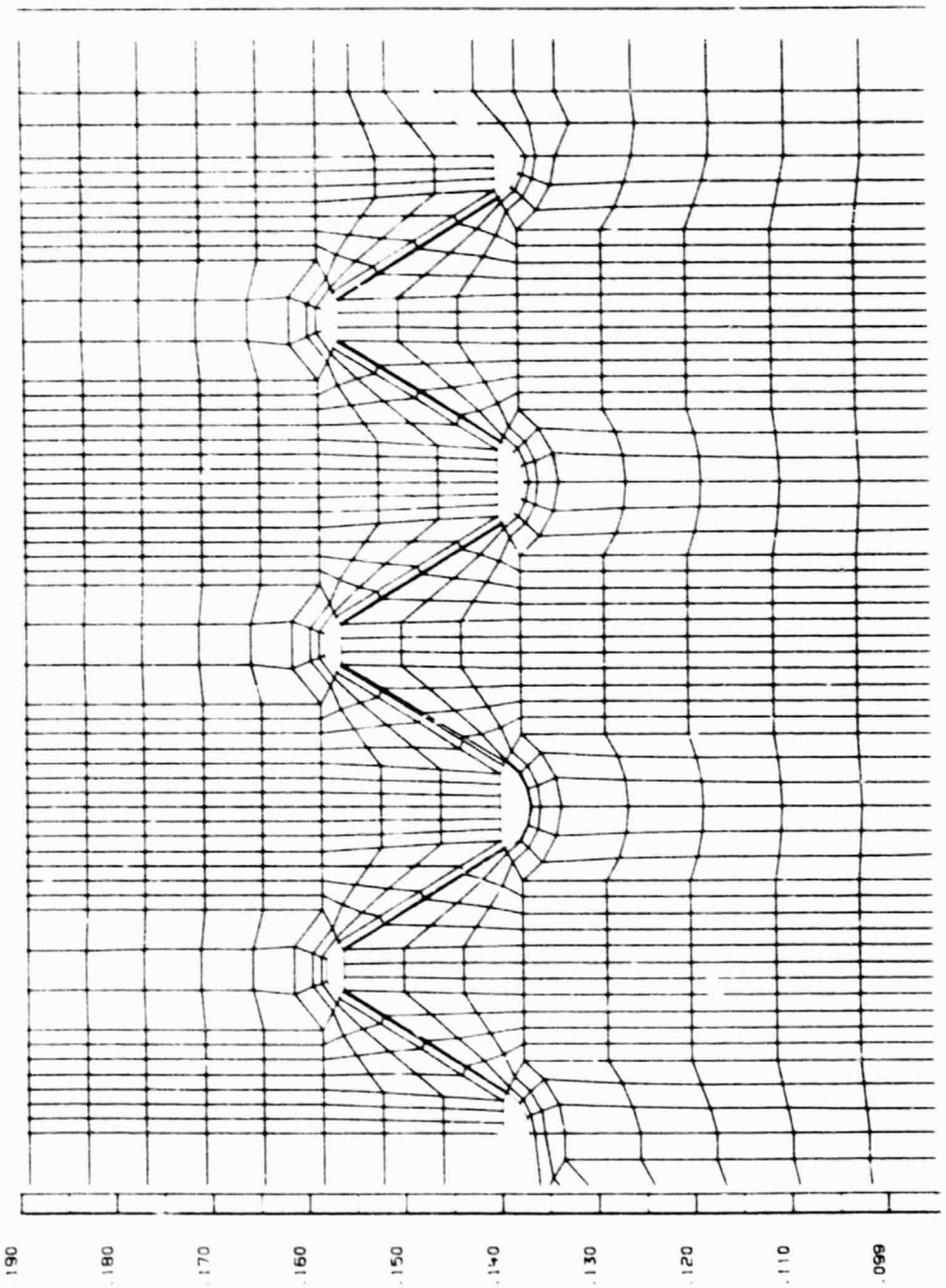

Fig. 7 - APSA Post/Retainer Detailed Model - Thread Region

2.4 BOPACE 3-D POST/RETAINER DETAILED MODEL

The BOPACE 3-D Post/Retainer Detailed Model is made up of a 60-deg symmetric segment of the thread region with 810 nodes and 405 eight-node brick elements. Elastic-plastic properties are included for 316L stainless steel and Haynes 188. At the 0-deg axial plane nodes are numbered 1 through 270, at the 30-deg plane, nodes are numbered 1001 through 1270 and at the 60-deg plane, 2001 through 2270. The current run stream is configured for processing on the IBM 360 computer system at MSFC. The model comprises the same post/retainer thread region used in the SPAR and APSA detailed models. This BOPACE simulation, however, permits multiple elastic-plastic load cycling not available in the other models. Detailed model plots have been generated and are available.

2.5 BOPACE 2-D INERTIA WELD REGION MODEL

To evaluate the stress concentration effects which exist at the LOX post inertia weld joint, a refined local two-dimensional model was constructed. This 2-D Inertia Weld Region Model is presented in Fig. 8. The refined region at the outer weld plane between the 316L and Haynes 188 materials permits accurate evaluation of the stress concentration due to the chemical etching performed after welding. An example of the method of simulating a variable depth of etching is shown in Fig. 9 where the appropriate elements are removed to simulate a 0.006-in. etch depth. The refined area around the weld is made up of ten layers each 0.001 in. thick. Both uniaxial and bending loadings were applied for the evaluation of the stress concentration as a function of etch depth.

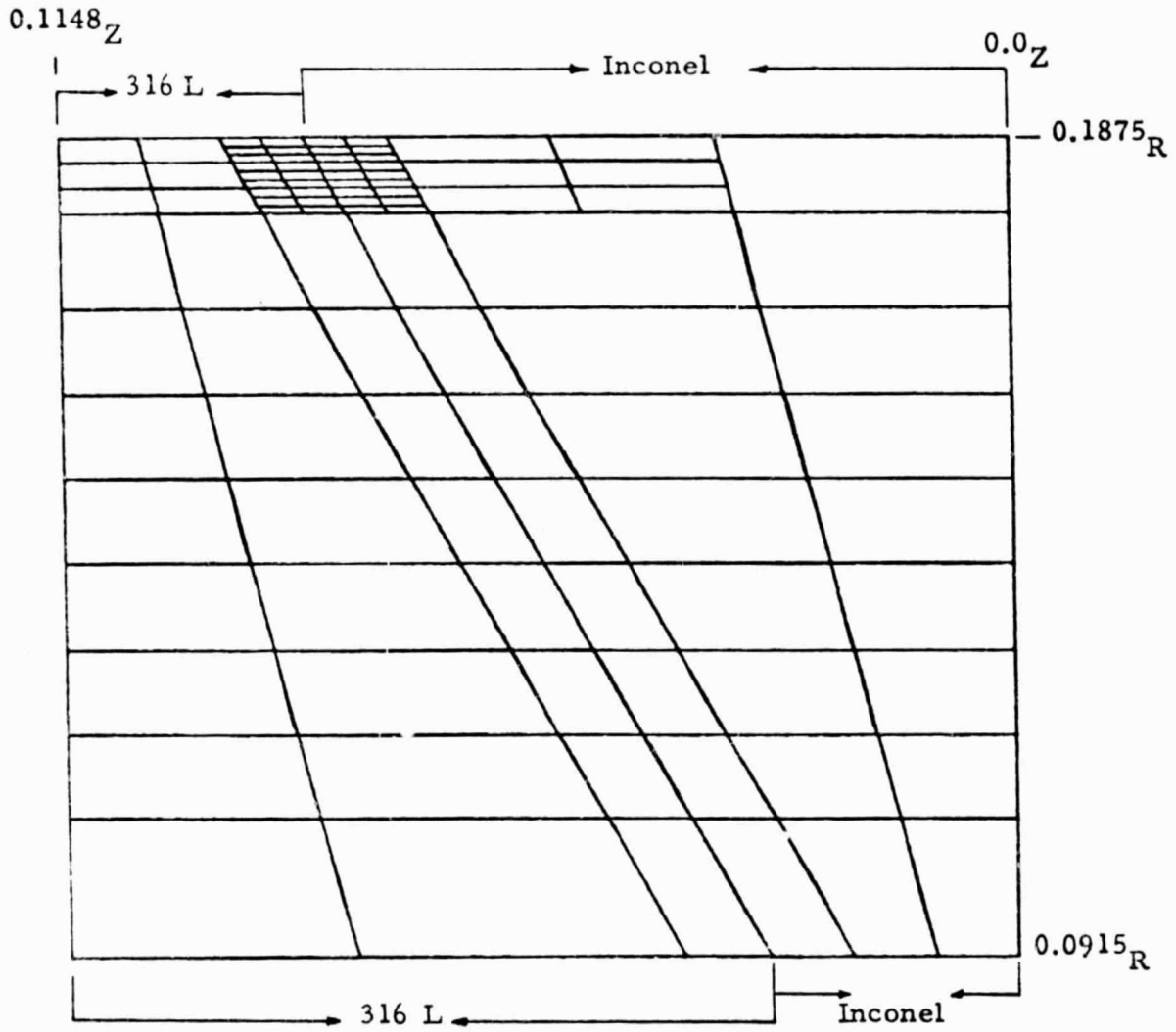

Fig. 8 - BOPACE 2-D Weld Model (Unetched)

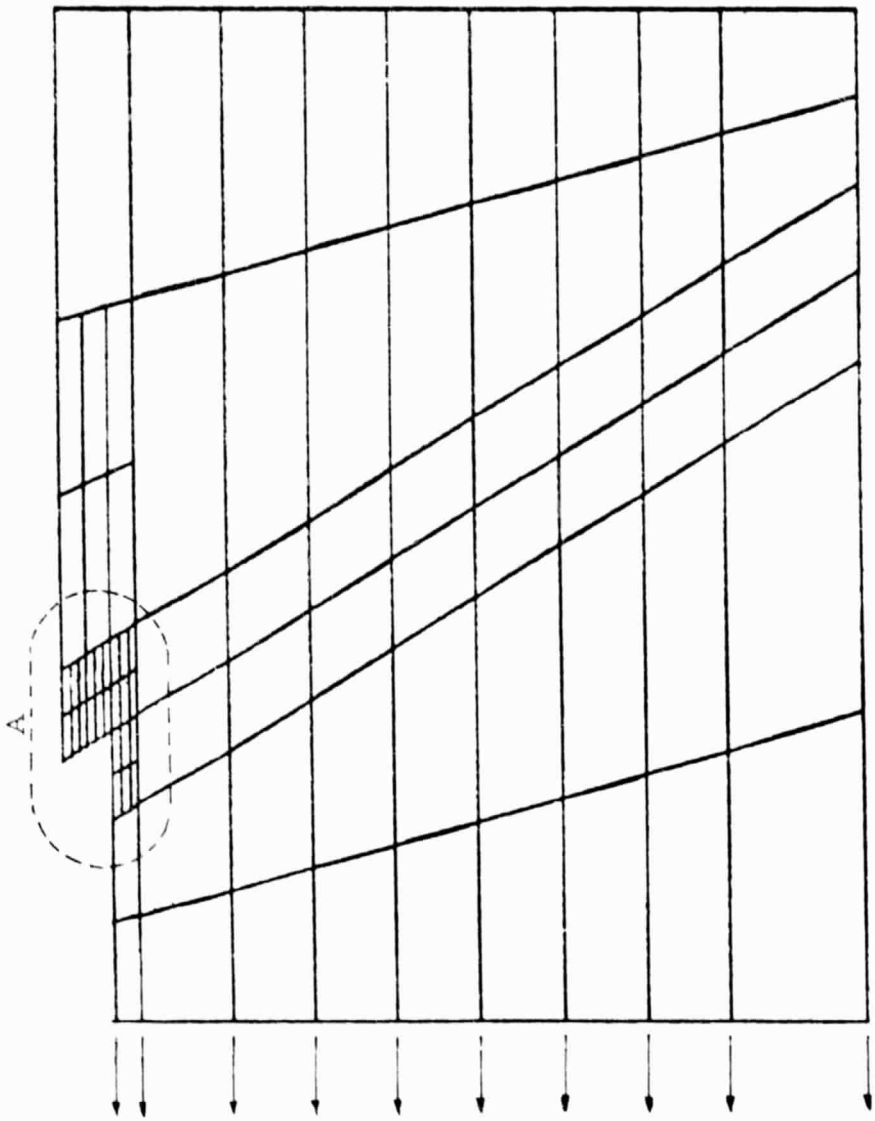

Fig. 9 - Model Loading and Element Layout for 0.006 in. Etch Depth

2.6 BOPACE 3-D INERTIA WELD REGION MODEL

Figure 10 presents the detailed BOPACE 3-D model of the inertia weld region built to investigate the post-yield performance of the weld joint. This 0.115-in. long, 5-deg segment model is built of eight-node brick elements. Test data reveal significant deformation and cracking near the weld. Thermal and structural load conditions were generated for this model.

LOX POST INERTIA WELD

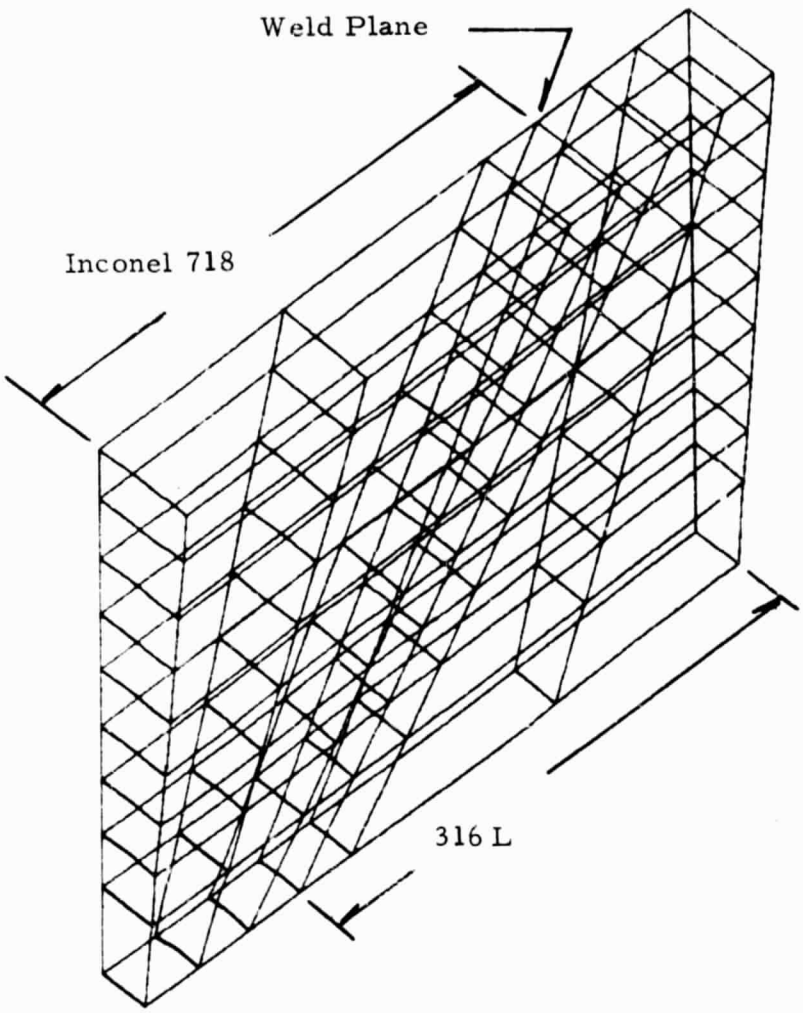

UNDEFORMED CONFIGURATION

Fig. 10 - BOPACE Model of the LOX Post Inertia Weld

2.7 SPAR INERTIA WELD REGION MODEL

In order to perform the required thermal analysis to define accurate weld region environments a detailed SPAR model of the upper post and inertia weld region was developed. The upper LOX post assembly and its components are shown in Fig. 11. The detailed SPAR model of this region is shown in Fig. 12. This 360-deg three-dimensional model contains 1932 nodes. All SPAR models are configured for processing on the MSFC Univac 1100 computer system.

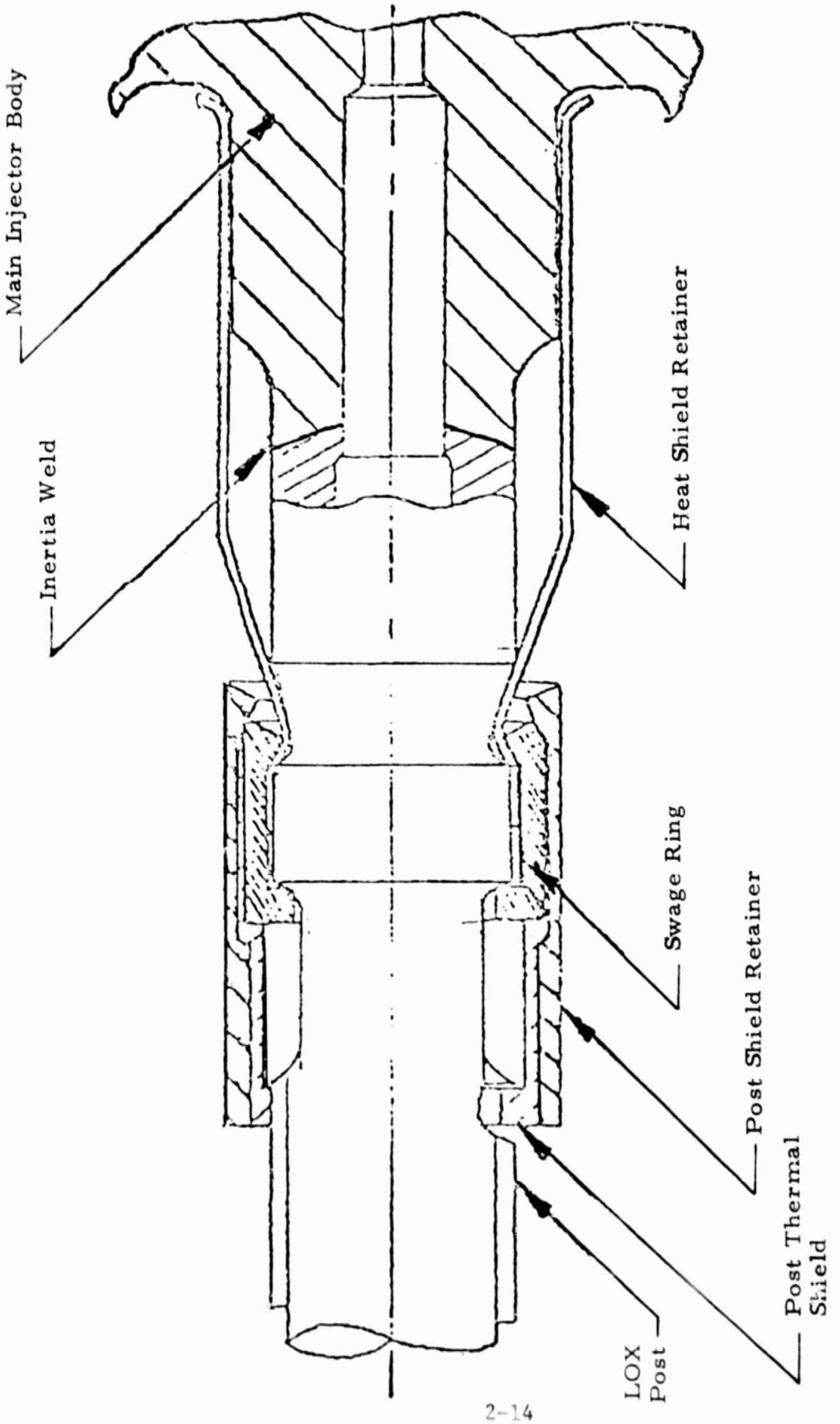

Fig. 11 - Upper LOX Post Assembly

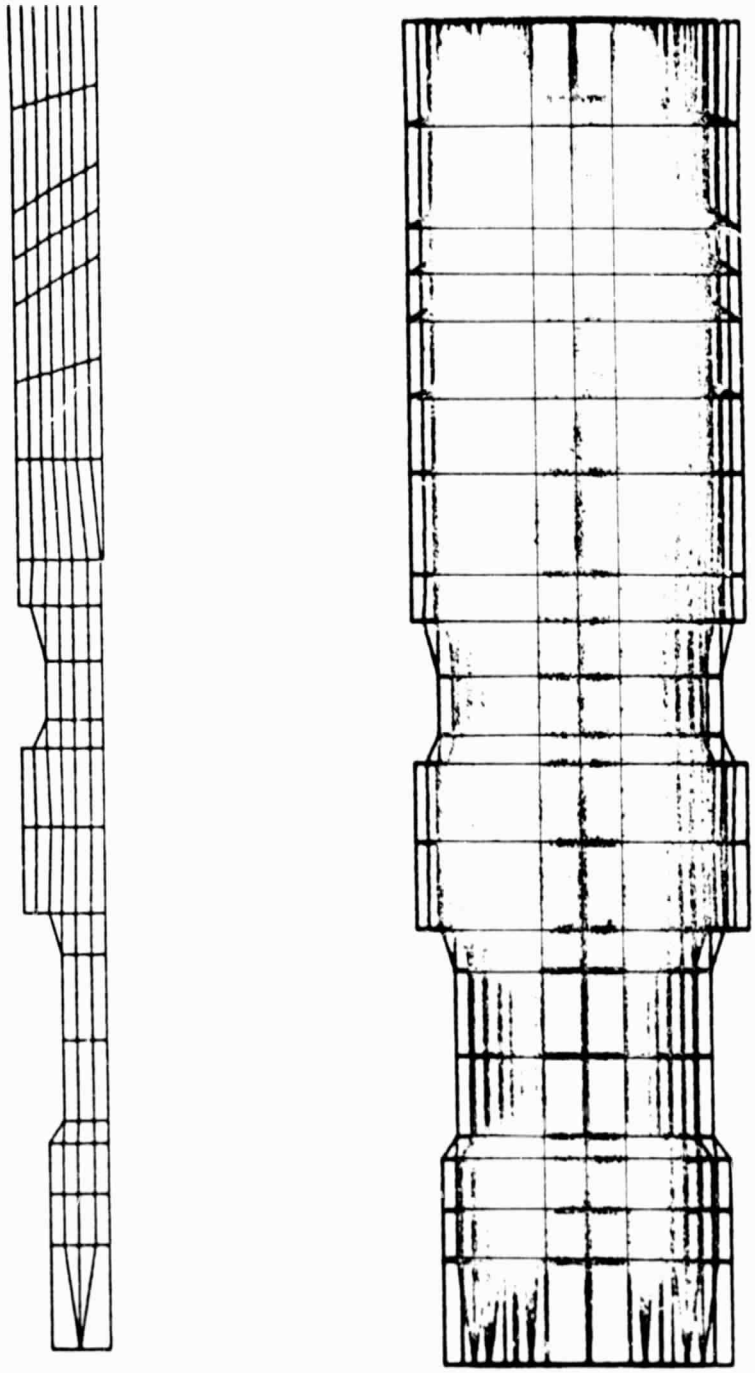

Fig.12 - Main Injector LOX Post SPAR Models

3. LOX POST ANALYSIS DISCUSSION

This discussion is subdivided into three areas which are arranged as follows:

1. LOX Post Assembly Analysis
   - Thermal
   - Structural
   - Dynamic
   - Fatigue
2. LOX Post Inertia Weld Region Analysis
   - Thermal (at FPL)
3. Inertia Weld Region Stress Concentration
   - Uniaxial Loading
   - Bending Loading

3.1 LOX POST ASSEMBLY ANALYSIS

The RPL thermal analysis was performed on the SPAR main chamber LOX post assembly model using the environmental temperatures and film coefficients identified in Fig. 13. The analysis results from the assembly model thermal run were applied to the Post/Retainer Detailed Model which was used to develop the temperature distributions summarized in Fig. 14 for the one-piece 316L stainless steel configuration and in Fig. 15 for the Haynes 188 two-piece LOX post. The radial temperature results are presented at five cross-sections through the post/retainer thread region.

RPL THERMAL BOUNDARY CONDITIONS FOR MAIN ELEMENT IN ROW 13 AND ROW 12

ZONE		PRESSURE (psia)	TEMPERATURE (F)	FILM COEFFICIENT ($B^{t}u/ft^2$-F-sec)
1	SHIELD	3216	1240	5.76
2	POST, OUTSIDE	3216	1240	3.00
3	POST, INSIDE	3722	-268	2.88
4	RETAINER, OUTSIDE	3216	1240	3.00
5	RETAINER, INSIDE	3216	1240	3.00
6	SLEEVE, OUTSIDE	3357	9	2.16
7	SLEEVE, INSIDE	3216	1240	3.60
8	POST, OUTSIDE	3216	1240	3.60
9	POST, INSIDE	3300	-268	2.88
10	NUT, INSIDE	3000	1140	3.40
11	POST/RETAINER LOWER REENTRANT REGION	3216	1100	0.30
12	POST/RETAINER UPPER REENTRANT REGION	3216	1150	0.30

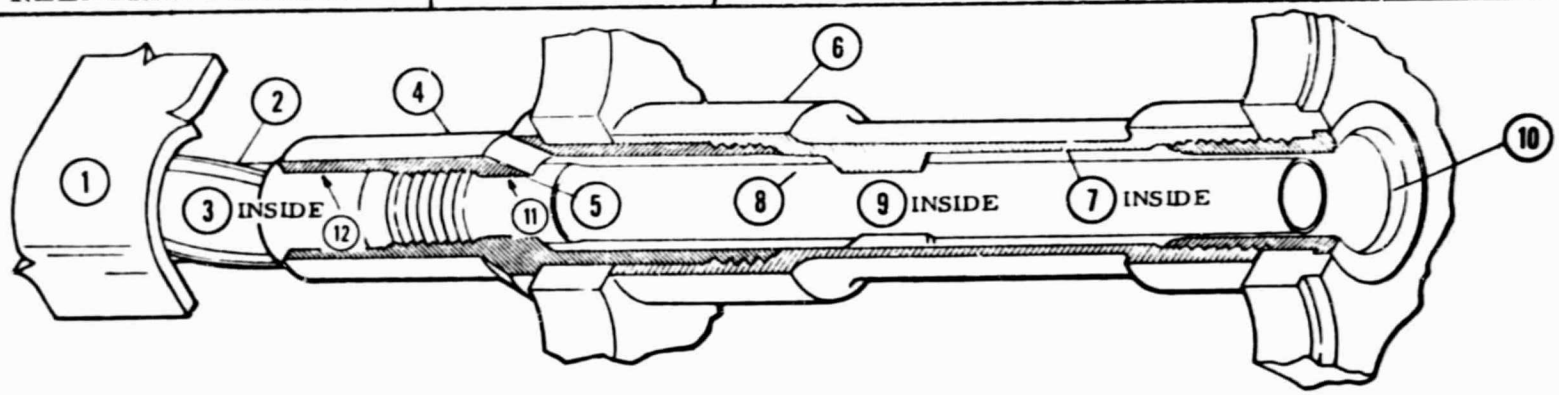

Fig. 13 - LOX Post Thermal Load Inputs for All Models

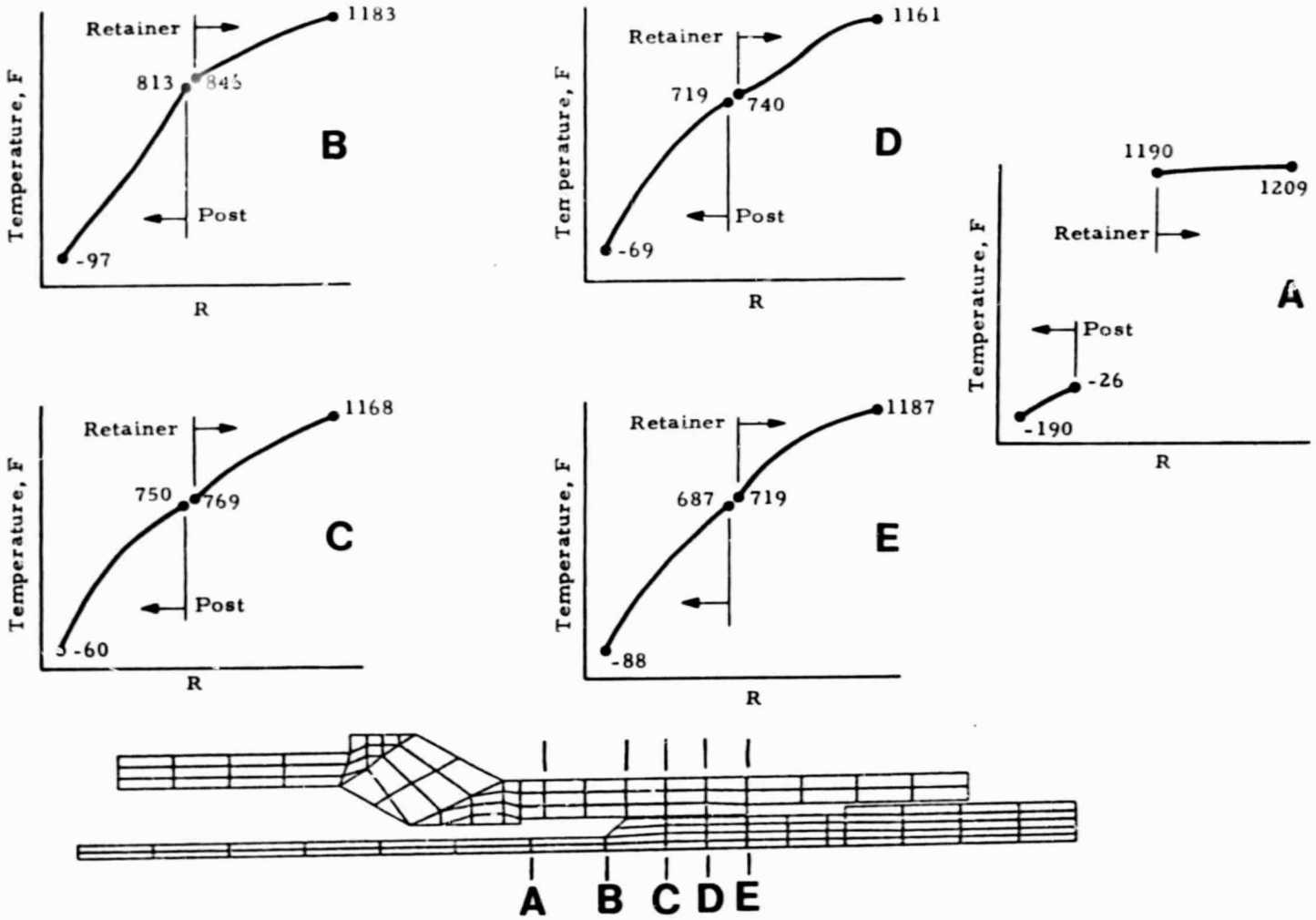

Fig. 14 - Radial Temperature Variation in Post/Retainer Thread Area for 316L One-Piece LOX Post

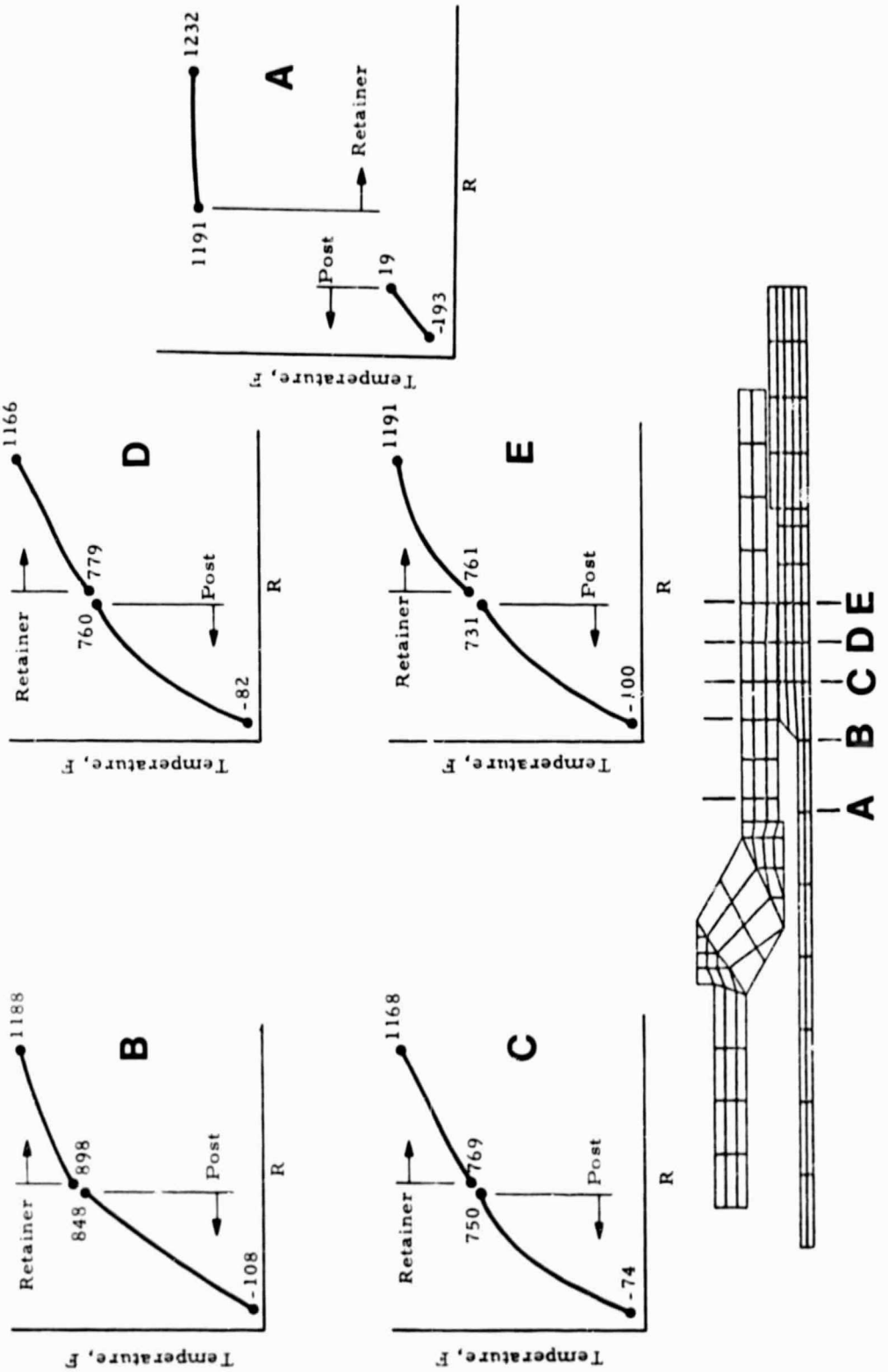

Fig. 15 - Radial Temperature Variation in Post-Retainer Thread Area for Haynes 188 Tip LOX Post

The exact RPL temperature profiles from the SPAR Post/Retainer Detailed Model were mapped onto the APSA Thread Model as shown in Figs. 16, 17 and 18. In addition, the SPAR model was used to develop the displacements due to non-axisymmetric loads (i.e., pressure and transverse motion) that exist at the detailed model boundary nodes. These loads are summarized for two cases in Fig. 19 for the one-piece 316 L configuration and in Fig. 20 for the two-piece Haynes 188 LOX Post.

Vibration induced loads were calculated using the SPAR LOX Post Assembly Model. The general procedures used are outlined in Fig. 21, where the SPAR model response is forced to reach measured levels of strain in order to access the magnitude of the vibration-induced loads.

Figure 22 summarizes the first three normal modes of each configuration both with and without the flow shield. The resultant dynamic displacements were determined and applied to the APSA model as shown in Fig. 23 for the one-piece 316 L LOX Post and in Fig. 24 for the two-piece Hynes 188 version.

All these combined loadings were evaluated in the stress analysis of the APSA model. Peak resultant stresses were identified at points D and C in Fig. 25. These maximum stresses and strains are summarized in the table in Fig. 26, where the peak effective strain of 3.2% was experienced in the 316 L stainless steel post thread area.

Stress-strain diagrams of the first one-half cycle of combined static, thermal and dynamic loading effects for each of the three peak value cases are presented in Figs. 27, 28 and 29. Here, it can be seen that for all cases the state of stress is well within the plastic or post-yield range for each case. Inspection of the S/N curves for the two materials reveals the following endurance limits:

316 L (Fig. 30) σ = 16 ksi

Haynes 188 (Fig. 31) σ = 36 ksi

Using Goodman's correction for an equivalent stress, neither of the two configurations reaches its endurance limit:

316 L: 41% of endurance limit (See Fig. 32)
Haynes 188: 20% of endurance limit (See Fig. 32)

It should be noted however that the one-piece (316 L) peak stresses are experienced in a tension field while those of the two-piece (H-188) post are in a compression stress region. The Haynes 188 material in the two-piece design can be concluded to be a superior configuration from this fatigue analysis.

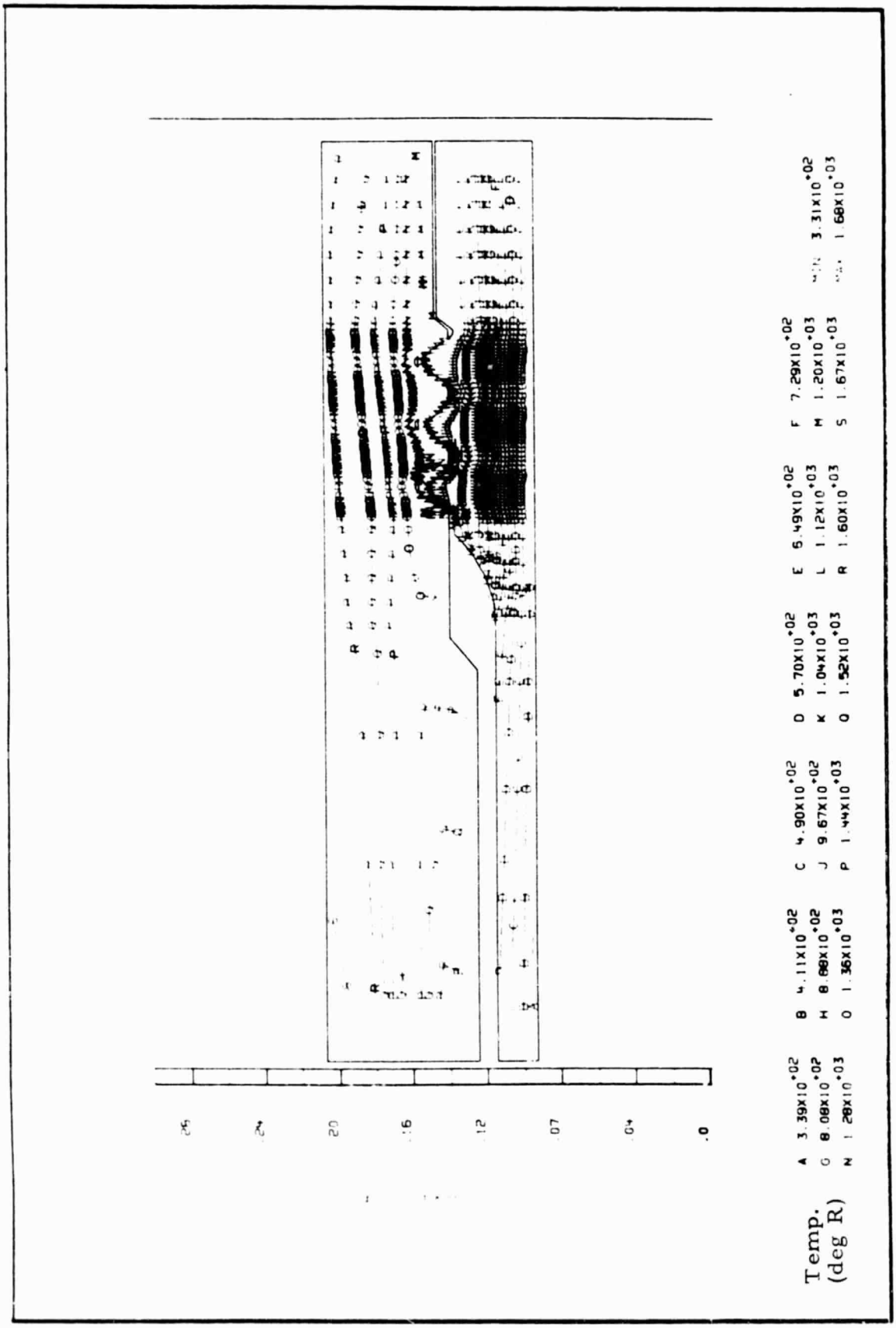

Fig. 16 - APSA Thread Fillet Model Temperature Distribution

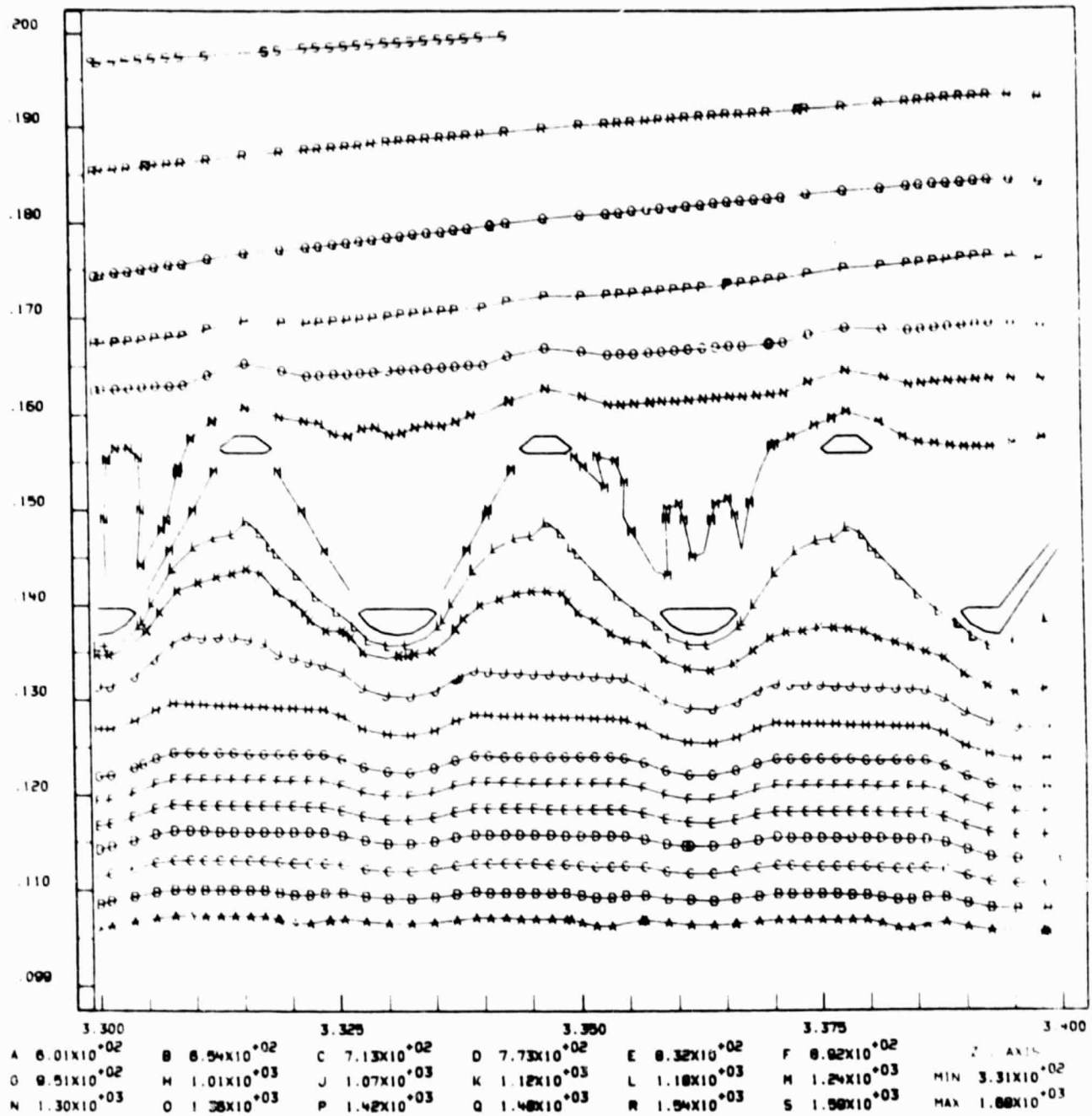

Fig. 17 - APSA Model Temperature Contours

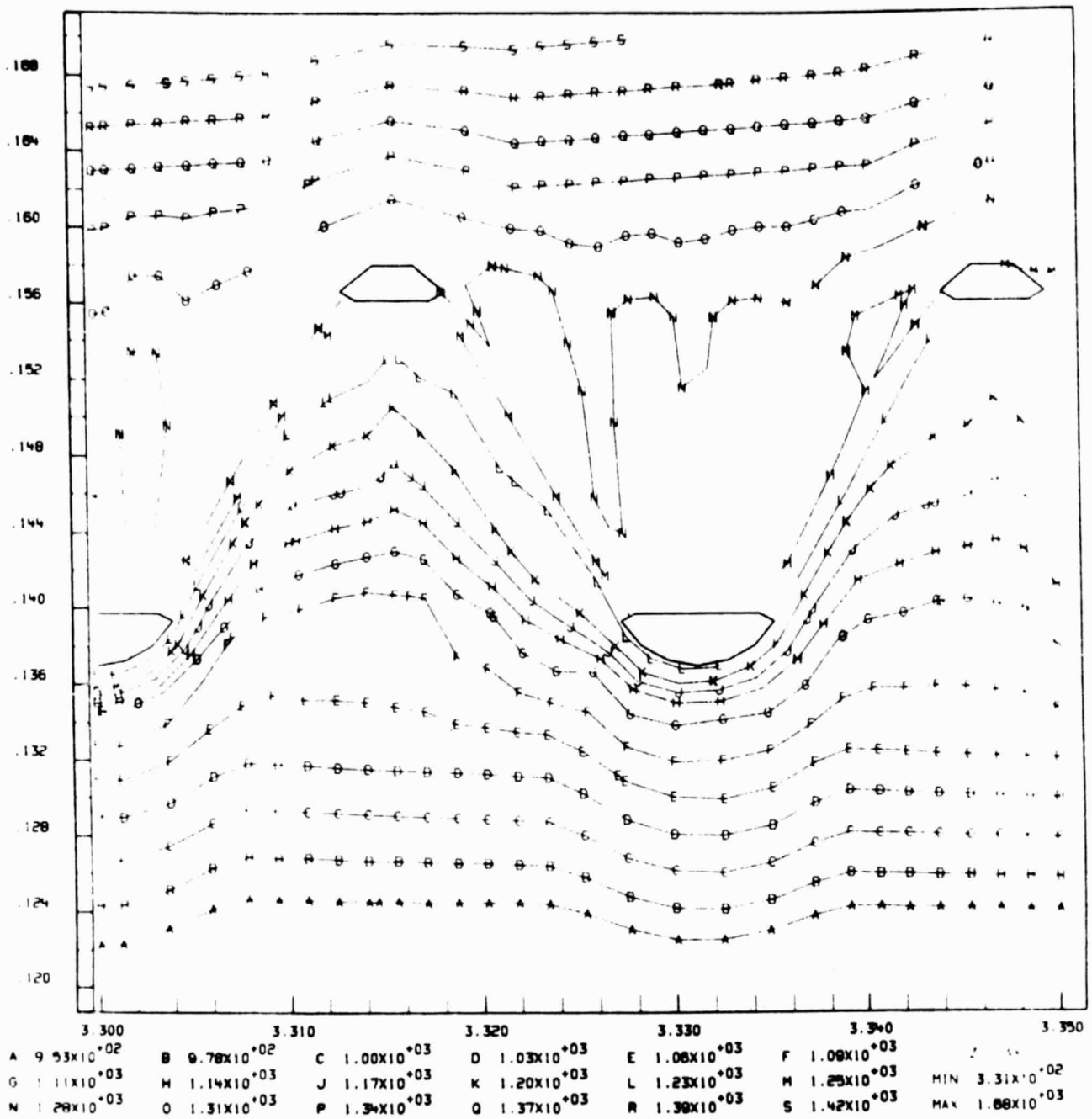

Fig. 18 - APSA Model Temperature Contours

ORIGINAL PAGE IS
OF POOR QUALITY

(Pressure, Non-Axisymmetric Force and Motion)

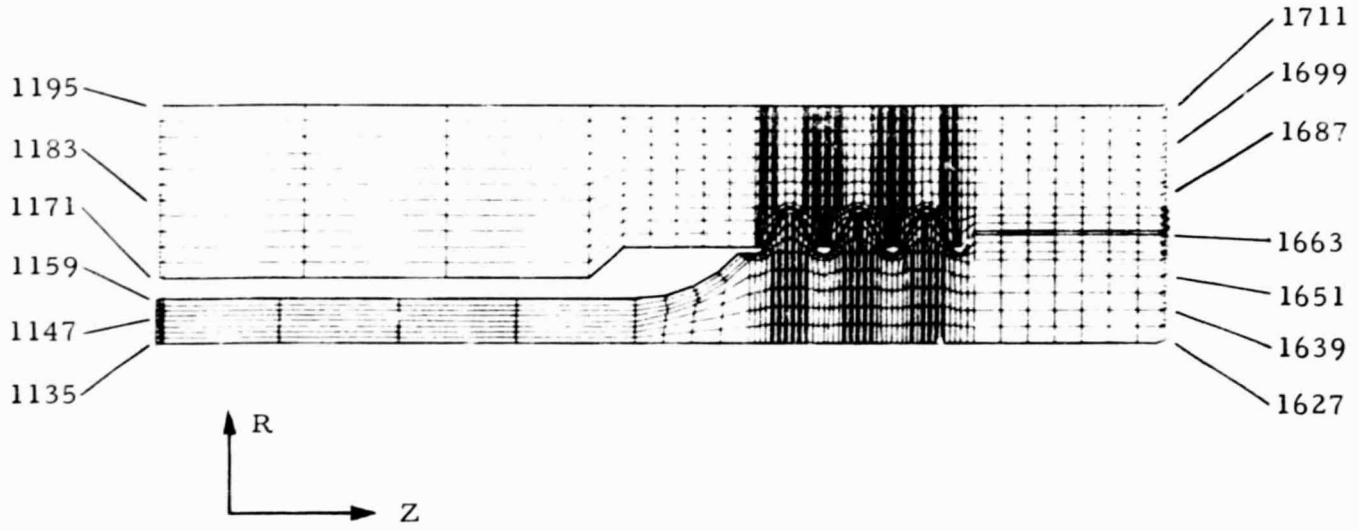

SPAR Nodes		Set 1 δZ	Set 2 δZ
Retainer	1195	.171-3	-.174-3
	1183	.180-3	-.184-3
	1171	.177-3	-.181-3
Post	1159	.108-3	-.112-3
	1147	.987-4	-.102-3
	1135	.886-4	-.923-4

SPAR Nodes		Set 1 δZ	Set 2 δZ
Retainer	1711	.185-3	-.188-3
	1699	.169-3	-.173-3
	1687	.138-3	-.142-3
Post	1663	.166-3	-.170-3
	1651	.144-3	-.148-3
	1639	.123-3	-.126-3
	1627	.102-3	-.106-3

Fig. 19 - One-Piece 316 L LOX Post Displacements Due to Non-Axisymmetric Loads

(Pressure, Non-Axisymmetric Force and Motion)

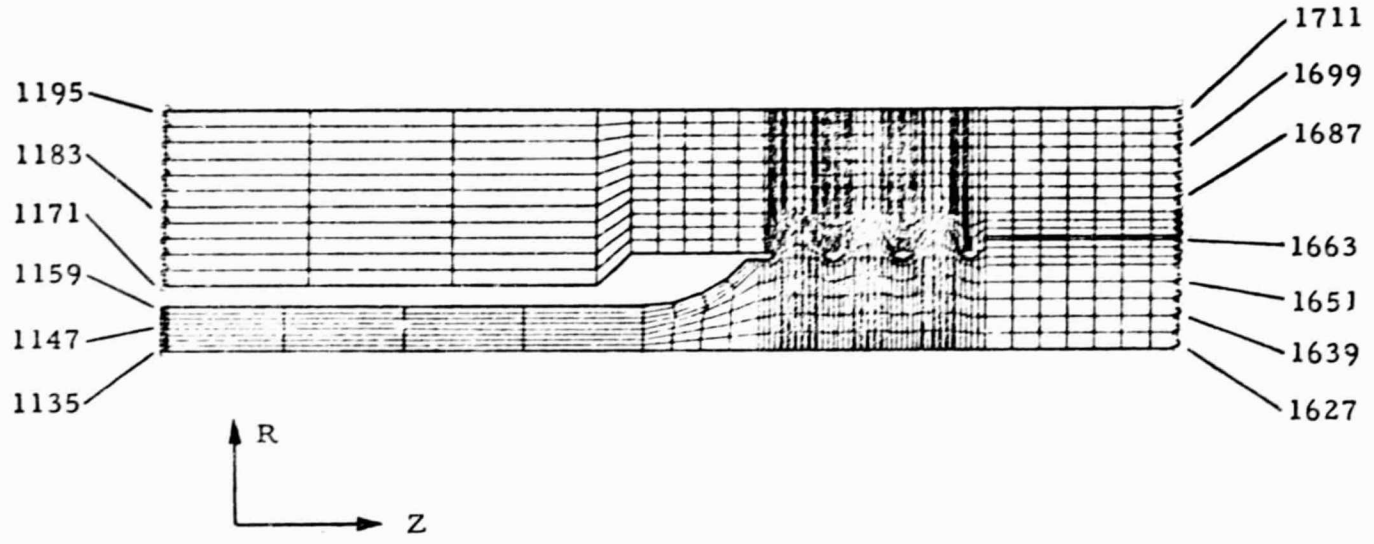

SPAR Nodes		Set 1 δZ	Set 2 δZ
Retainer	1195	.167-3	-.169-3
	1183	.176-3	-.179-3
	1171	.173-3	-.177-3
Post	1159	.111-3	-.114-3
	1147	.986-4	-.101-3
	1135	.861-4	-.889-4

SPAR Nodes		Set 1 δZ	Set 2 δZ
Retainer	1711	.178-3	-.180-3
	1699	.163-3	-.166-3
	1687	.134-3	-.137-3
Post	1663	.149-3	-.152-3
	1651	.131-3	-.134-3
	1639	.112-3	-.115-3
	1627	.929-4	-.958-4

Fig. 20 - Two-Piece (Haynes Tip) LOX Post Displacements due to Non-Axisymmetric Loads

- SPAR VIBRATION ANALYSIS EXECUTED FOR NATURAL FREQUENCIES/MODES
- SPAR NORMAL MODES MODEL
  - MODAL DAMPING FACTOR, 2%
  - TEST DATA INDICATES THAT THE SIGNIFICANT MODE IS AT 1200 HZ
- SPAR FORCED RESPONSE ANALYSIS (BASE MOTION) APPLIED VIBRATION LOADS AT LOX POST ATTACHMENTS:
  - INJECTOR BODY
  - SECONDARY PLATE
  - PRIMARY PLATE
- FORCING FUNCTION AMPLITUDES ARE DETERMINED THAT GIVE THE REQUIRED RESPONSE LEVELS AT 4.75 IN. FROM THE LOX POST TIP

BASE MOTION EXCITATION PATTERN

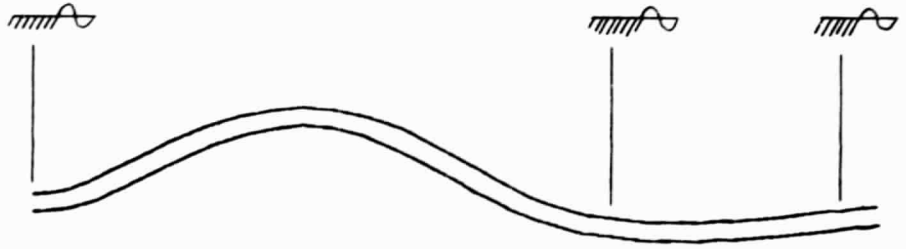

Fig. 21 - Forced Vibration Response Analysis

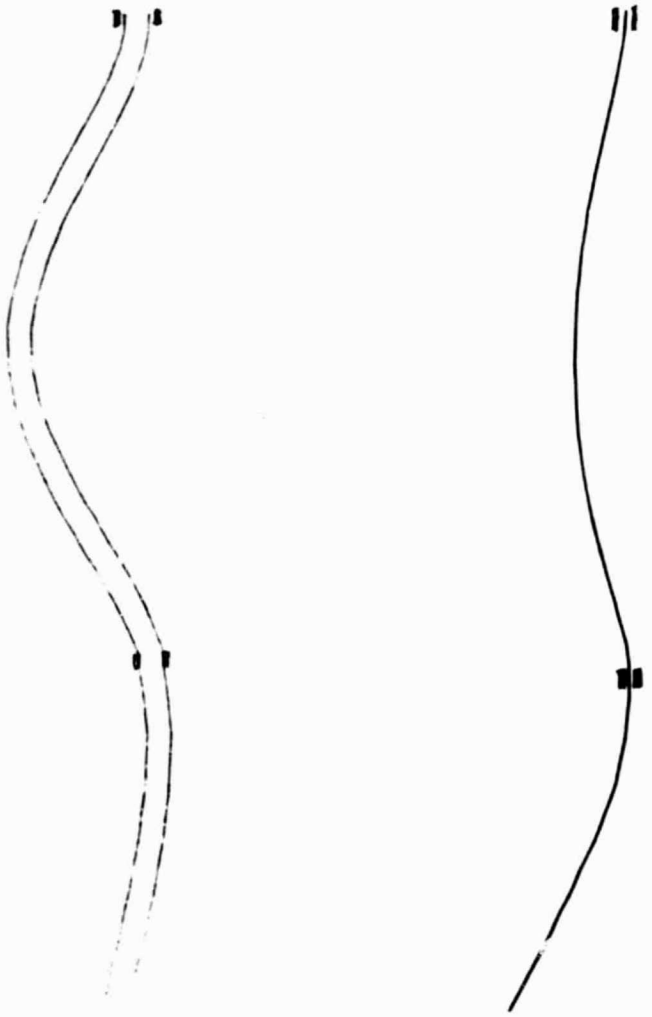

No Shield With Shield

Typical Mode Shapes (2nd Mode)

One-Piece Post (316 L)	
No Shield	
Mode	Frequency (Hz)
1	1183
2	1717
3	3982
With Shield	
Mode	Frequency (Hz)
1	1177
2	1432
3	3435

Two-Piece Post (H-188)	
No Shield	
Mode	Frequency (Hz)
1	1434
2	1890
3	4414
With Shield	
Mode	Frequency (Hz)
1	1412
2	1535
3	3759

Fig. 22 - LOX Post Dynamic Modes and Frequencies

ORIGINAL PAGE IS
OF POOR QUALITY

(Uniaxial Strain of 120 μ in./in. ~ 3000 psi,
at 1200 Hz, 4.75 in. from LOX Post Tip)

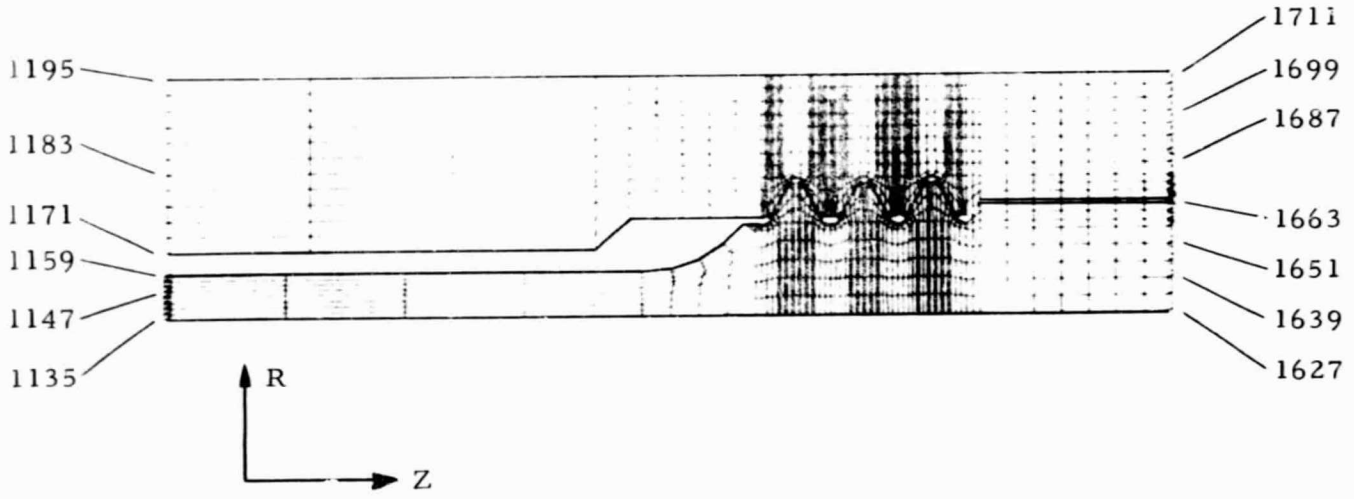

SPAR Nodes		±δZ
Retainer	1195	.367-4
	1183	.359-4
	1171	.342-4
Post	1159	.187-4
	1147	.175-4
	1135	.159-4

SPAR Nodes		±δZ
Retainer	1711	.588-4
	1699	.539-4
	1687	.441-4
Post	1663	.850-4
	1651	.712-4
	1639	.599-4
	1627	.488-4

Fig. 23 - One-Piece 316 L LOX Post Displacements due to Measured Vibration Loading

ORIGINAL PAGE IS
OF POOR QUALITY

(Uniaxial Strain of 120 μ in./in. ~ 3000 psi,
at 1200 Hz, 4.75 in. from LOX Post Tip)

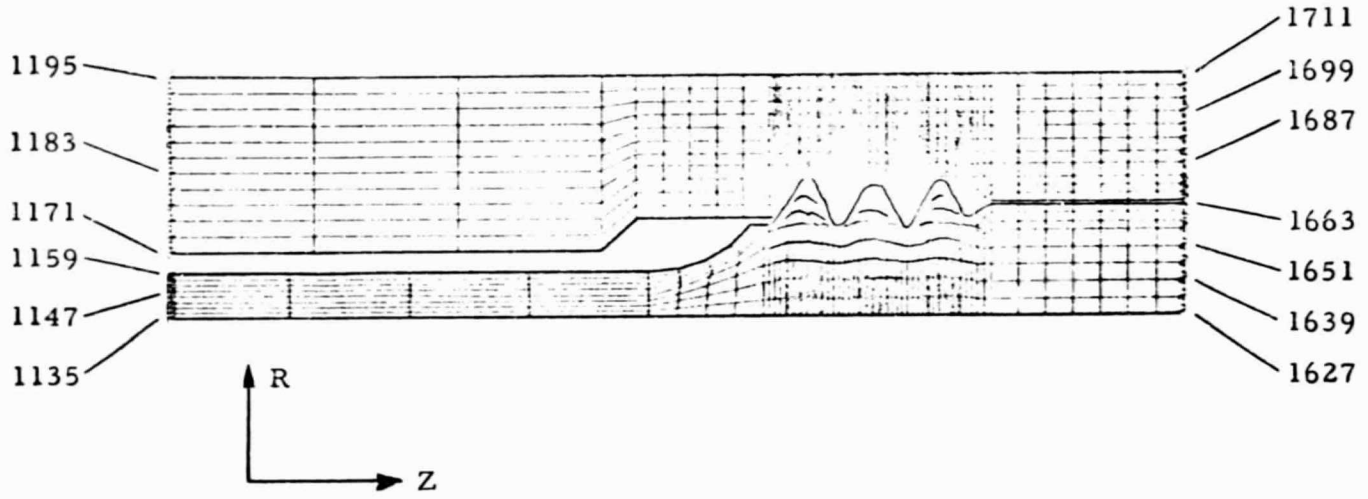

SPAR Nodes		±δZ
Retainer	1195	.425-4
	1183	.416-4
	1171	.396-4
Post	1159	.227-4
	1147	.206-4
	1135	.185-4

SPAR Nodes		±δZ
Retainer	1711	.683-4
	1699	.631-4
	1687	.520-4
Post	1663	.926-4
	1651	.798-4
	1639	.678-4
	1639	.539-4

Fig. 24 - Two-Piece (Haynes Tip) LOX Post Displacemnts Due to Measured Vibration Loading

APSA THREAD MODEL – DETAILED STRESS POINTS

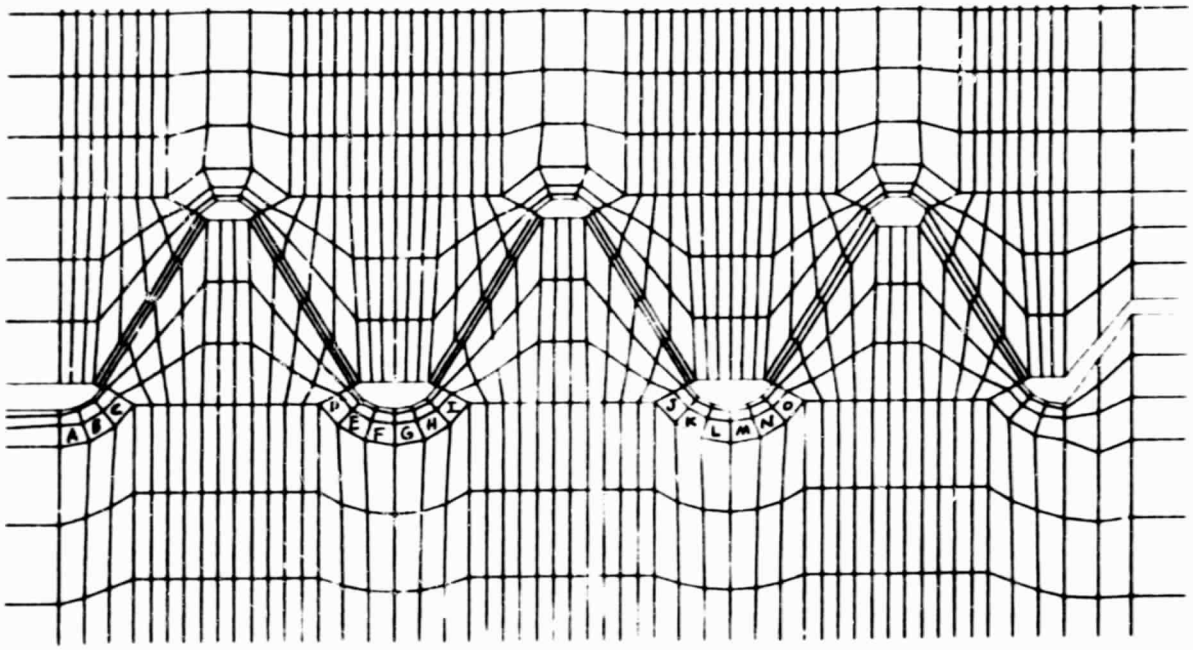

POINT D = EVALUATION ELEMENT 461

POINT C = EVALUATION ELEMENT 499

Fig. 25 - APSA Thread Model - Detailed Stress Points

MAXIMUM STRESS AND STRAIN IN ROOT AREA OF THREAD ON LOX POST
(Combined Thermal, Static and Dynamic Displacement Loads)

Post Mat'l.	Elem. No.	Local Temp. (F)	σ_R (ksi)	σ_t (ksi)	σ_Z (ksi)	τ_{RZ} (ksi)	σ_{eff} (ksi)	τ_{max} (ksi)	ϵ_{eff} (in./in.)
316 L	461	774	1.63	2.52	10.63	-13.59	25.06	14.32	.03200
H-188*	461	824	-11.27	-42.67	-7.63	-6.83	35.41	20.15	.00422
H-188*	499	823	-1.88	-41.17	-32.38	3.14	36.12	19.80	.00591

Young's Modulus

E (316 L) = 23.4×10^6 psi

E (H-188) = 28.8×10^6 psi

Coefficient of Thermal Expansion

α (316 L) = 9.45×10^{-6} in/in/F

α (H-188) = 6.85×10^{-6} in/in/F

*Peak stresses for H-188 are compressive.

Fig. 26 - APSA Thread Model Results

Post Material = 316 L

Evaluation Element 461

ϵ_T = (static/mean) $\pm$ (alternating)

ϵ_T = .0320 $\pm$ .00015

$\Delta\sigma_{alt}$ = 3.49 ksi

Stress Ratio = R = $\frac{18.13}{25.11}$ = +0.72

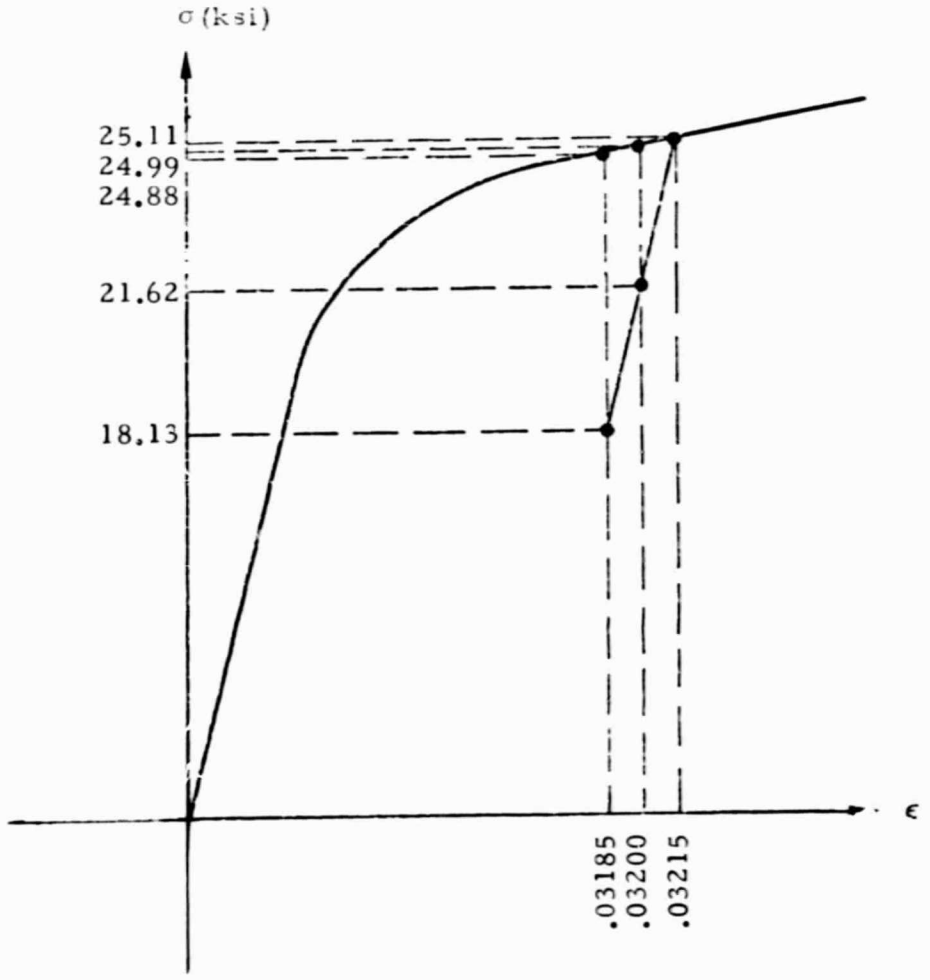

Fig. 27 - Stress-Strain Diagram for Combined Static, Thermal and Dynamic Loads at RPL Conditions

Post Material = Haynes 188

Evaluation Element 461

ϵ_T = (static mean) $\pm$ (alternating)

ϵ_T = .00422 $\pm$ .000144

$\Delta\sigma_{alt}$ = 4.15 ksi

Stress Ratio = $R = \frac{27.2}{35.5} = +0.77$

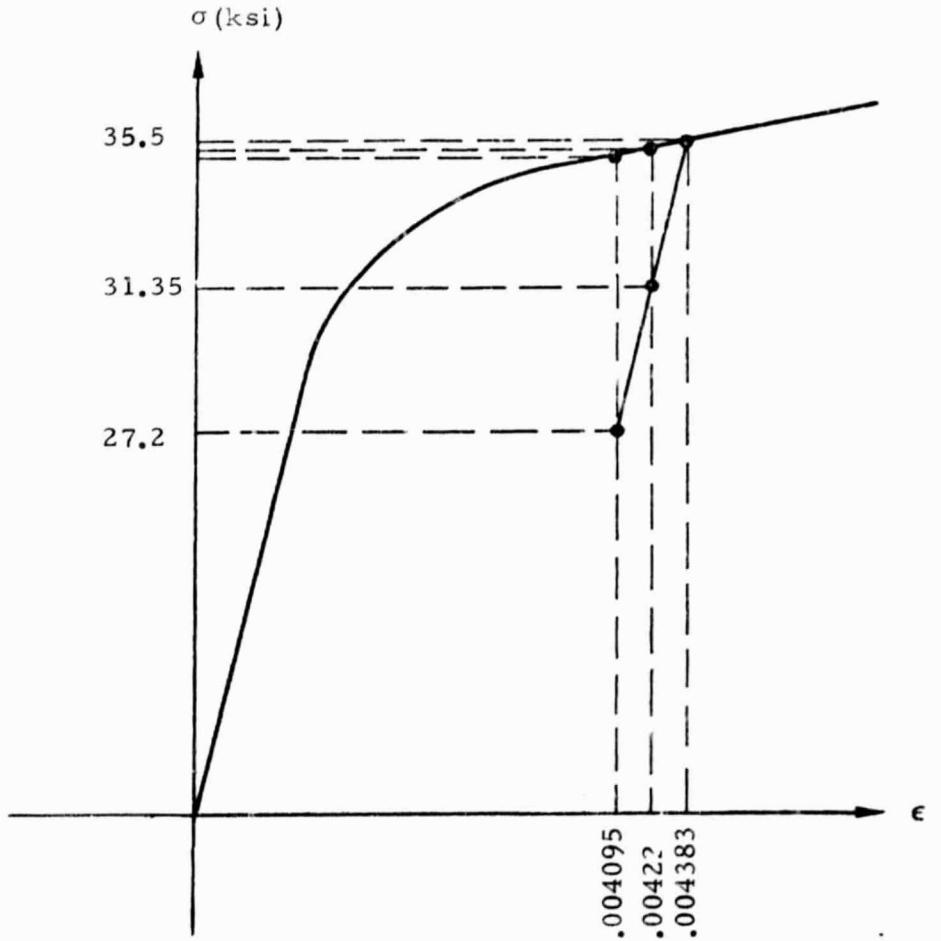

Fig. 28 - Stress-Strain Diagram for Combined Static, Thermal and Dynamic Loads at RPL Conditions

Post Material = Haynes 188

Evaluation Element 499

ϵ_T = (static/mean) $\pm$ (alternating)

ϵ_T = .00591 $\pm$ .000164

$\Delta\sigma_{alt}$ = 4.71 ksi

Stress Ratio = $R = \frac{26.78}{36.2} = +0.74$

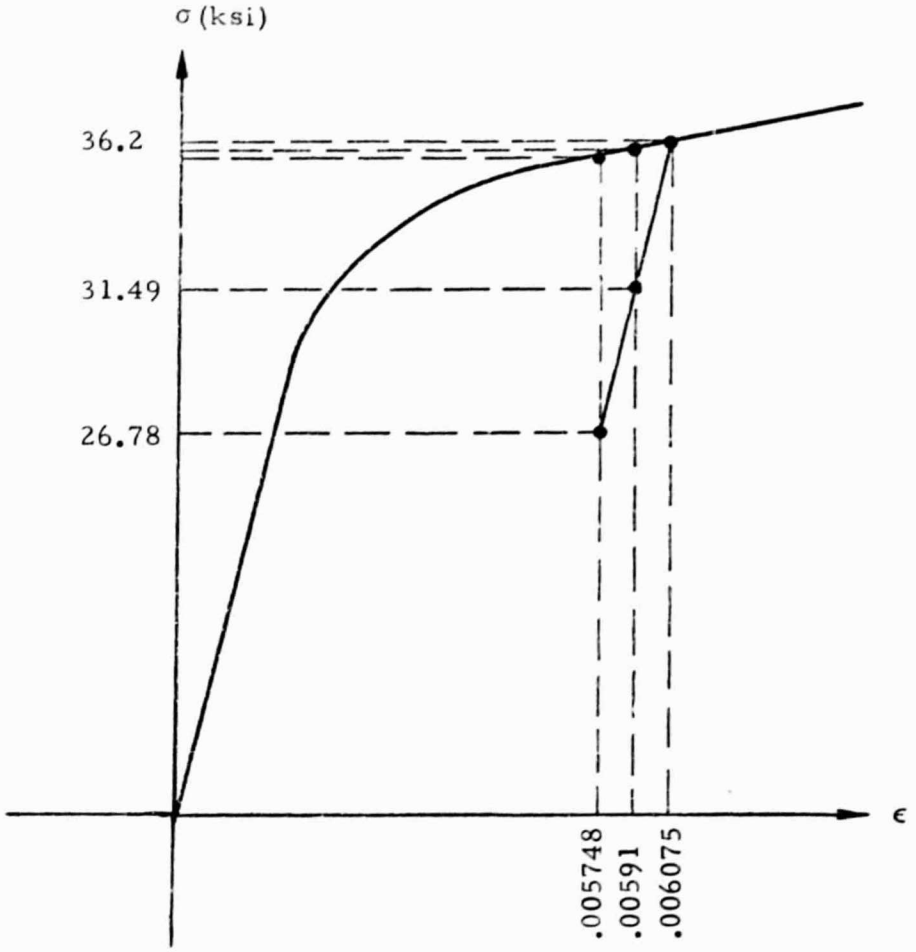

Fig. 29 - Stress-Strain Diagram for Combined Static, Thermal and Dynamic Loads at RPL Conditions

ORIGINAL PAGE IS
OF POOR QUALITY

ROCKWELL INTERNATIONAL
ROCKETDYNE DIVISION

MATERIALS PROPERTIES MANUAL

EXPECTED MINIMUM, 70F AND 600F
PREDICTED MINIMUM, 1100F-1600F
AXIAL, R = -1.0
MACHINED SURFACE
DATE- 9-1-77
REFERENCE- 2212-5
2ND EDITION PAGE- 2.8.9.1.2.11C

2212.33.10.50-2

316L STAINLESS STEEL	2212
HIGH CYCLE FATIGUE	.33
WROUGHT	.10
ANNEALED	.50
PAGE NUMBER	-2

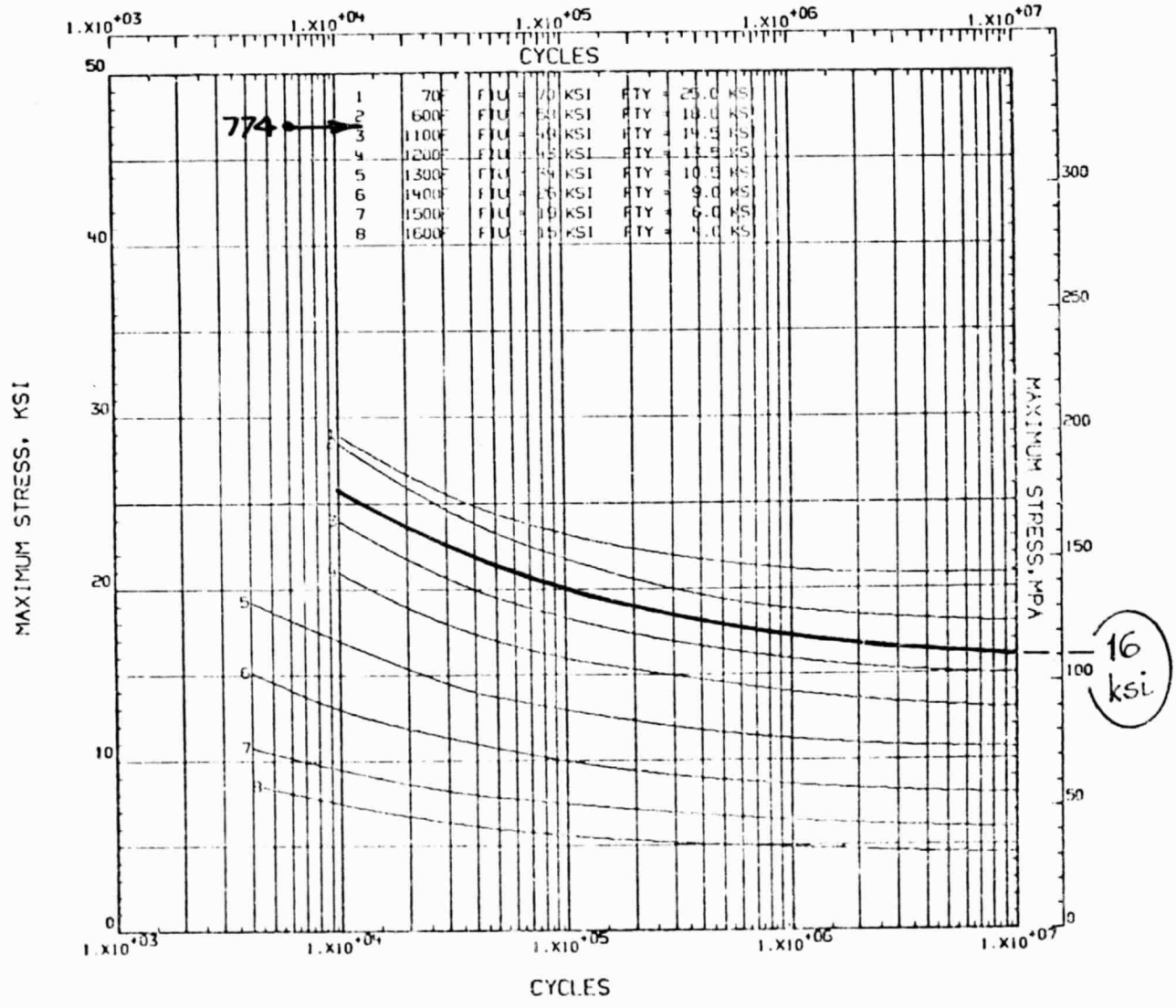

Fig. 30 - Fatigue Life Curve for 316 L

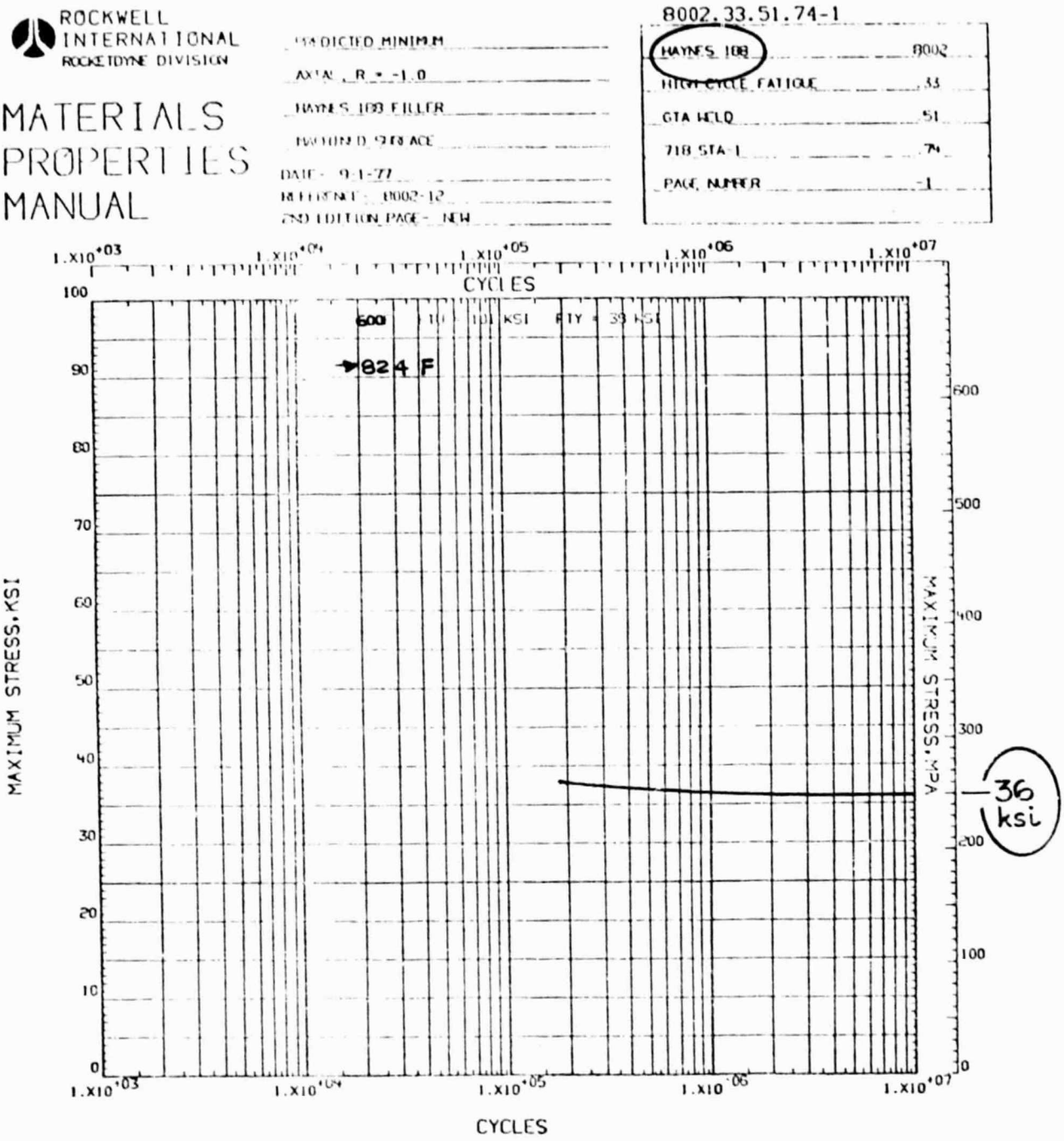

Fig. 31 - Fatigue Life Curve for Haynes 188

316-L

σ_{mean} = 25.06 ksi

σ_{alt} = 3.49 ksi

σ_{ult} = 54 ksi @ 775 F

$$\sigma_{eq} = \frac{\sigma_{alt}}{1 - \frac{\sigma_{m}}{\sigma_{u}}}$$

σ_{eq} = 6.51 ksi at Element 461

$\sigma_{(Endurance\ Limit)}$ = 16.0 ksi

Percent = 41%

Haynes 188

σ_{mean} = 35.41/36.12 ksi

σ_{alt} = 4.15/4.71 ksi

σ_{ult} = 86 ksi @ 800 F

σ_{eq} = 7.05 ksi at Element 461/8.12 ksi at Element 499

σ (Endurance Limit) = 36 ksi

Percent = 19.6%/22.6%

Fig. 32 - Calculation of Effective Dynamic Stresses

3.2 LOX POST INERTIA WELD REGION ANALYSIS

Using the existing SPAR detailed upper post model, a complete FPL thermal analysis was performed using environments and film coefficients specified by MSFC. A view of the SPAR model in the weld region is shown in Fig. 33 for both the undeformed and deformed conditions. The complete distribution of resulting FPL temperatures at the weld region are shown in Fig. 34. Significant temperature gradients can be seen between the post ID and OD surfaces. The two different materials in the area are identified. Appropriate temperature dependent conduction properties were used for each in the analysis.

Using the thermal environments determined in the above analysis, a detailed BOPACE elastic-plastic stress analysis was performed with the 5-deg BOPACE Weld Region Model. The resultant strain levels in each material are shown in Table 1 at the weld line. The effective strain ranges due to heating from room temperature to FPL and then back again are shown in the table. These values were used to assess the low cycle fatigue life of both the 316 L and Haynes 188 LOX posts.

The 316 L low cycle fatigue life at 0.32% strain range is seen in Fig. 35 to be approximately 10,000 cycles. Similarly, the Haynes 188 at 0.53% strain range has a low cycle life of approximately 2000 cycles as shown in Fig. 36.

Thus, in summary, the predicted FPL cycle does produce thermally induced plastic strain in the inertia weld region of the LOX post for both materials. The thermal strain cycle is more severe in the Haynes 188 post than in 316 L due to the lower resistance to low cycle fatigue of the Haynes material (2000 cycles in Haynes versis 10,000 for 316 L). However, in either case, adequate low-cycle fatigue life levels are predicted.

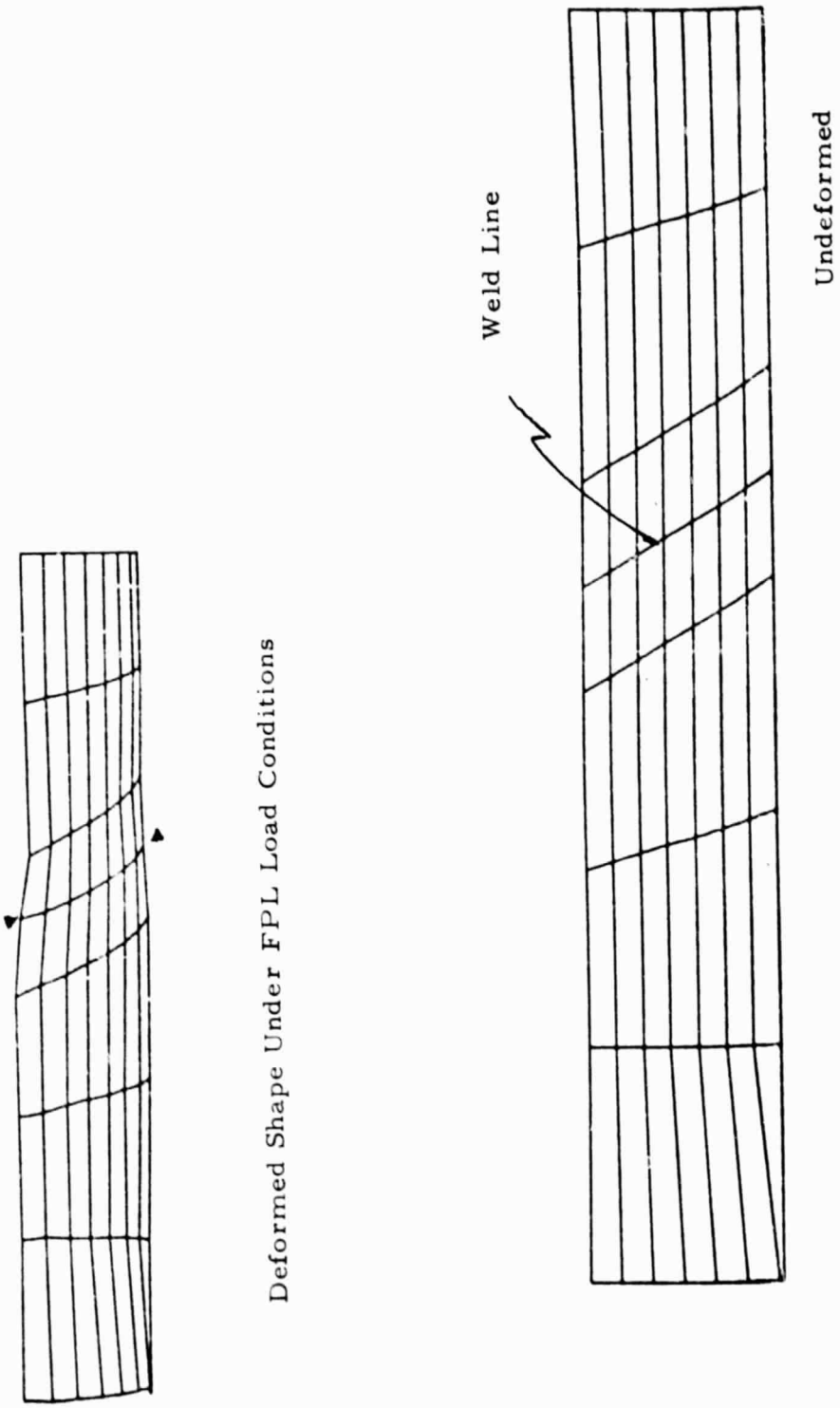

Fig. 33 - SPAR Model Response Under FPL Thermal Loads in Inertial Weld Region

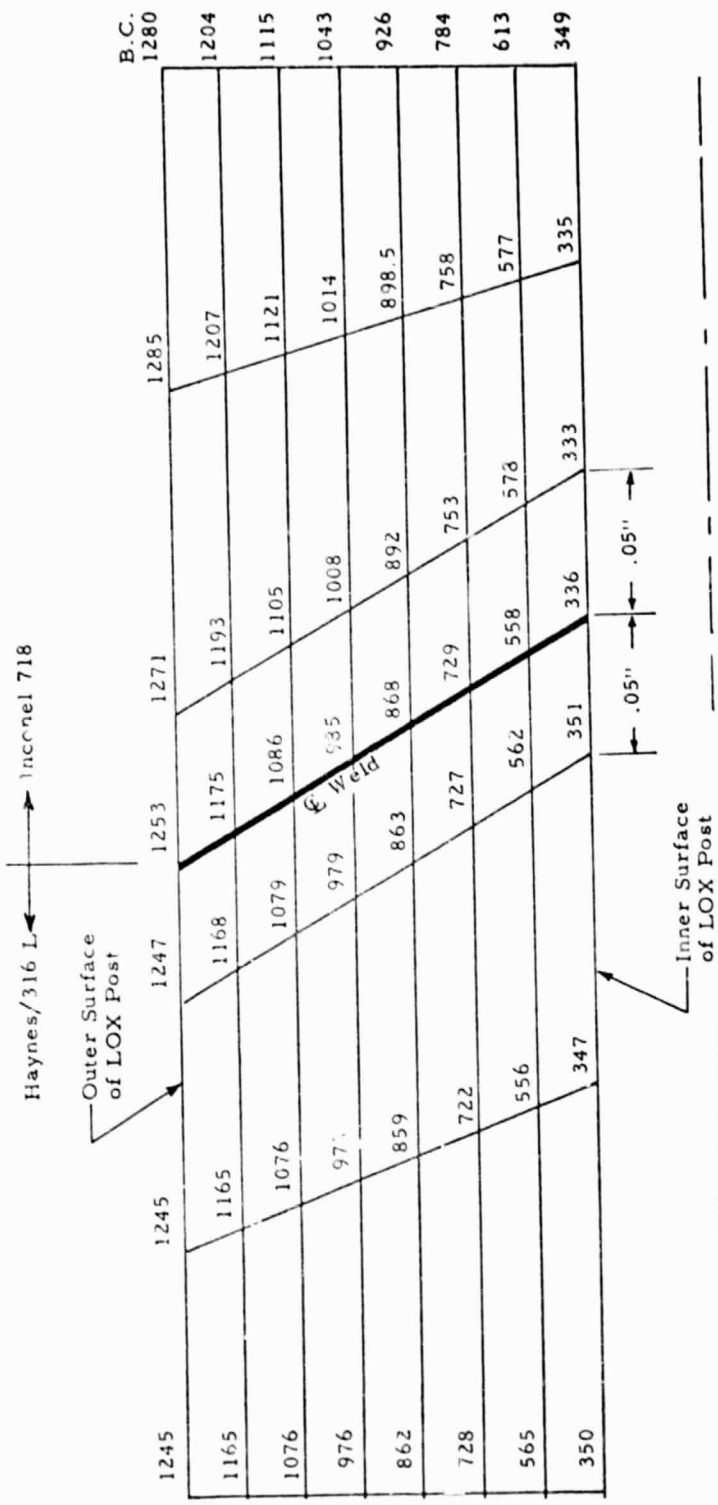

Note: Temperatures are given in degrees Rankine.

Fig. 34 - FPL Temperatures in Inertia Weld Region of SPAR Model

Table 1

BOPACE INERTIA WELD MODEL
(COMPUTED THERMAL STRAINS – FPL CYCLE)

LOX Post Material	Effective Strain, Outer Surface (%)		Effective Strain Range (%)
	at FPL	Residual at R.T.	
316 L (As Welded)	+0.48	+0.16	+0.32
Haynes 188 (As Welded)	+0.69	+0.16	+0.53

ROCKWELL INTERNATIONAL
ROCKETDYNE DIVISION

MATERIALS PROPERTIES MANUAL

PREDICTED MINIMUM
APPLIES TO 316L SIDE OF -
316L/B91718 OR 316L/B83903 JOINT
MIS DIVIDED 3
DATE- 9-1-77
REFERENCE- 2212-5
2ND EDITION PAGE- 2.8.8.3.2.4A

2212.34.51.30-1

316L STAINLESS STEEL	2212
LOW CYCLE FATIGUE	34
GTA WELDED	51
AS-WELDED	30
PAGE NUMBER	-1

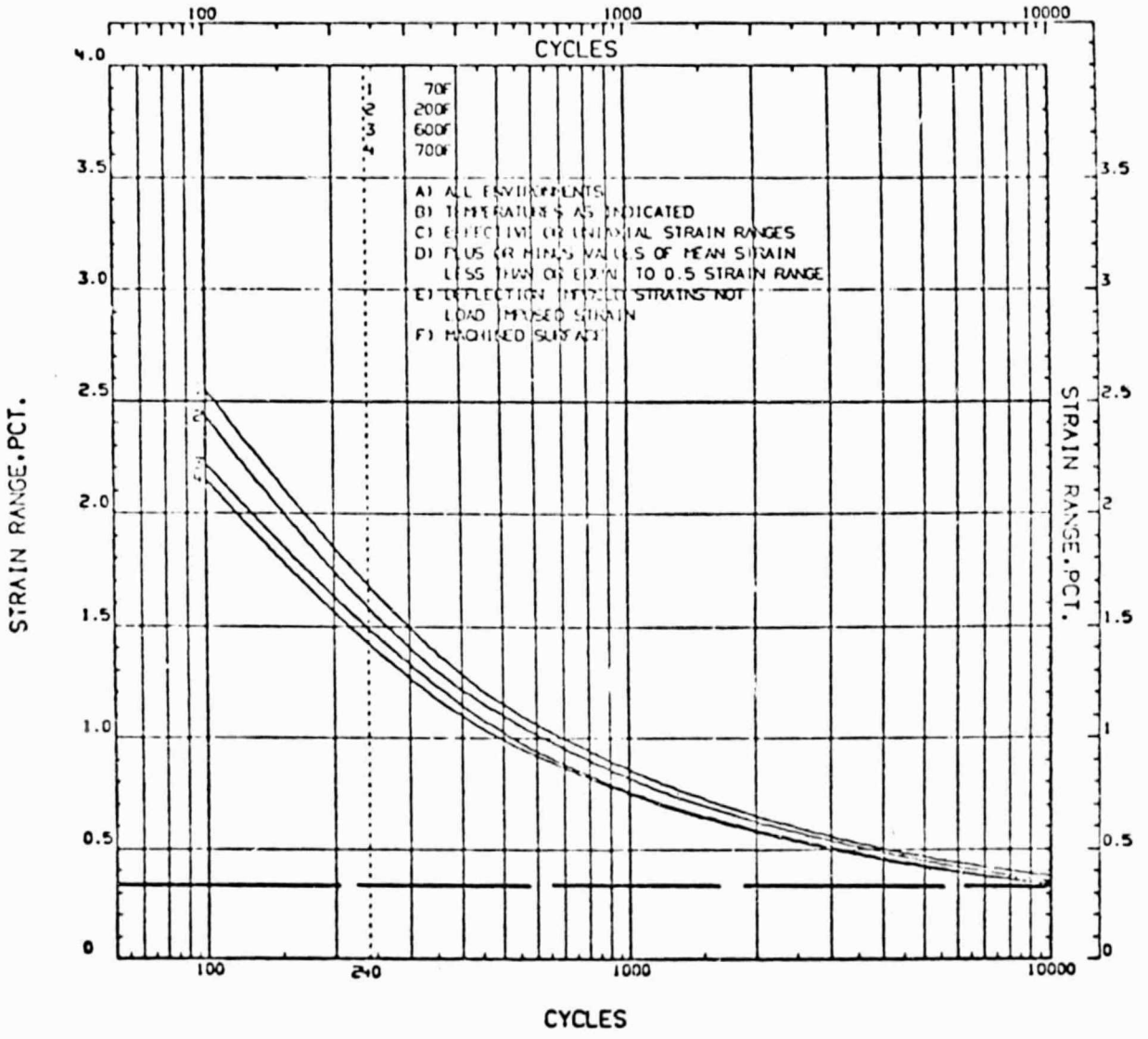

Fig. 35 - Low Cycle Fatigue Curves for 316 L

ORIGINAL PAGE IS
OF POOR QUALITY

ROCKWELL INTERNATIONAL
ROCKETDYNE DIVISION

MATERIALS PROPERTIES MANUAL

PREDICTED MINIMUM
MUSE DIVIDED BY 3
APPLIES TO HAYNES 188/INCO 718
HELD WITH INCOLOY 88 FILLER
DATE- 9-1-77
REFERENCE- 8002-14
2ND EDITION PAGE- G.4.2.3.2.4A

8002.34.51.30-2

HAYNES 188	8002
LOW CYCLE FATIGUE	34
GTA HELD	51
AS-HELDED	30
PAGE NUMBER	-2

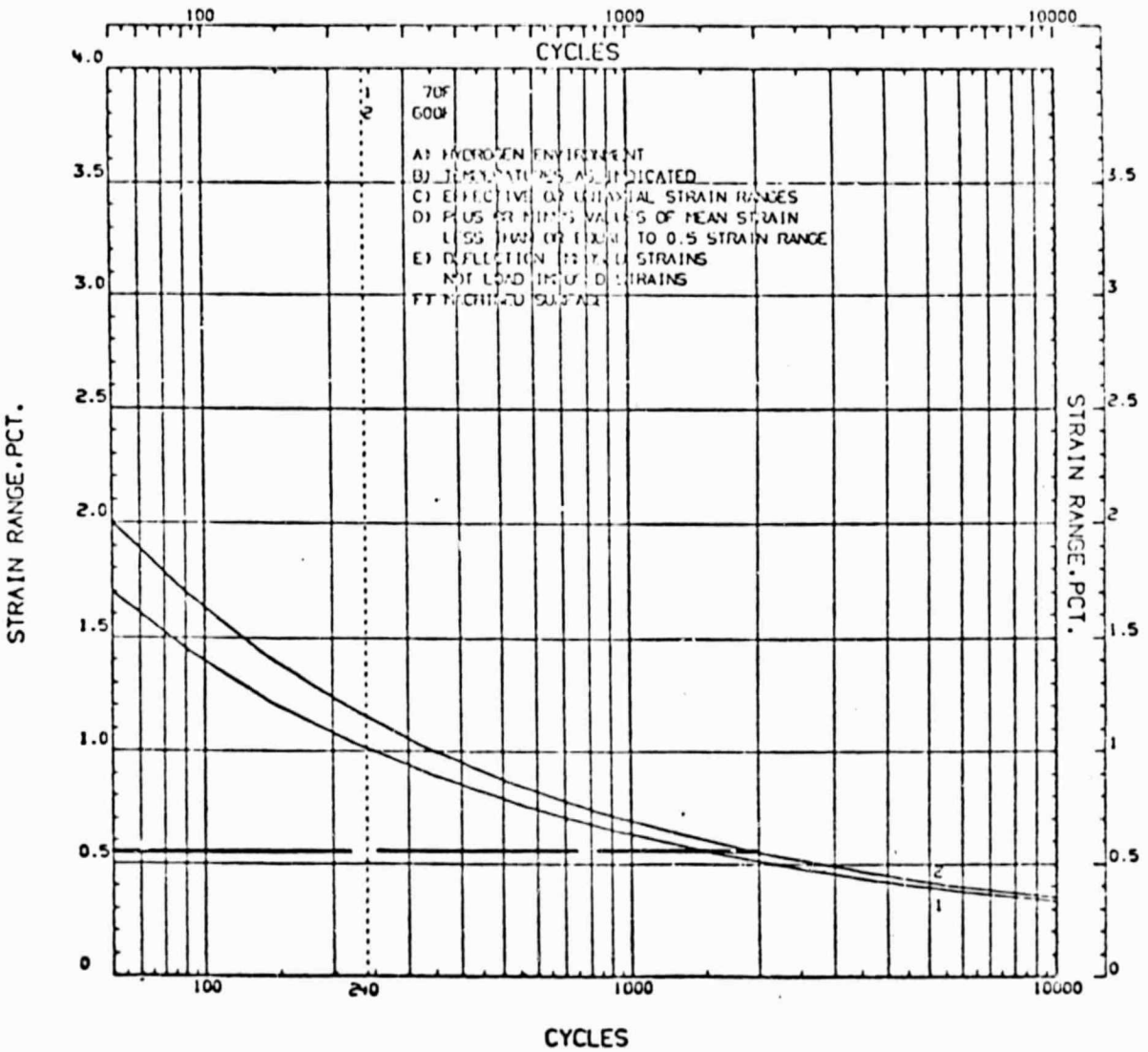

Fig. 36 - Low Cycle Fatigue Curves for Haynes 188

3.3 INERTIA WELD REGION STRESS CONCENTRATION

An analysis investigation was performed of the stress concentration factors which exist in the upper post inertia weld region of the main stage LOX post after etching is performed. A two-dimensional BOPACE analytic model of the weld region was developed as described in Section 2.5. Here the two material regions are divided by the diagonal weld line representing one side of the tubular post. The most likely crack forming location is the outside region of the weld which has been refined to simulate ten layers (each 0.001 in. thick).

A series of load cases was analyzed using uniform stress loads. Tension loads were applied to the left boundary of the model while the right side was held stationary. Etch depth variations from zero to 0.009 in. were evaluated by the sequential removal of element levels as shown in Fig. 37 where the 0.006 in. depth is depicted.

Stress resultants were determined at Points 1 and 2 as shown in the enlarged model view in Fig. 37. Stresses for each etch depth were compared with the uniform stress field of the unetched model. Stress concentration factors, K_T, were determined at each location for each etch depth. Results for the elastic range of factors are presented in Fig. 38 as a function of etch depth where a factor of 1.0 represents the zero or unetched model.

Similarly resultant elastic-plastic stress concentration factors are presented versus percent load for various etch depth in Fig. 39 where 100% corresponds to a uniform stress equal to the 316 L material yield strength for the unetched model. It can be seen that as etch depth increases the weld region stress concentration causes plastic material performance at earlier load levels. Unfortunately, this lowering of the local stresses is accompanied by work hardening of the material which in turn raises the yield stress and causes the general maintaining of elastic K_T values. For this reason, it is recommended that application of K_T values be made at the higher, i.e. elastic, values and not the lower plastic levels. Advantages of lower etch depths are clearly demonstrated in these results.

An additional evaluation was performed loading the BOPACE model as shown in Fig. 40. This load distribution was derived from a pure bending moment load on the LOX post tubular crossection. The 100% load level was adjusted to produce 316 L yield stresses at the etch gap location in the unetched model. Resultant K_T values versus depth of etch at Points 1 and 2 are shown in Fig. 41. The elastic-plastic performance is presented in Fig. 42 versus percent load. Peak K_T values for this bending moment case approach a value of 2.5; whereas for the earlier pure tension case values approach a peak of 2.0.

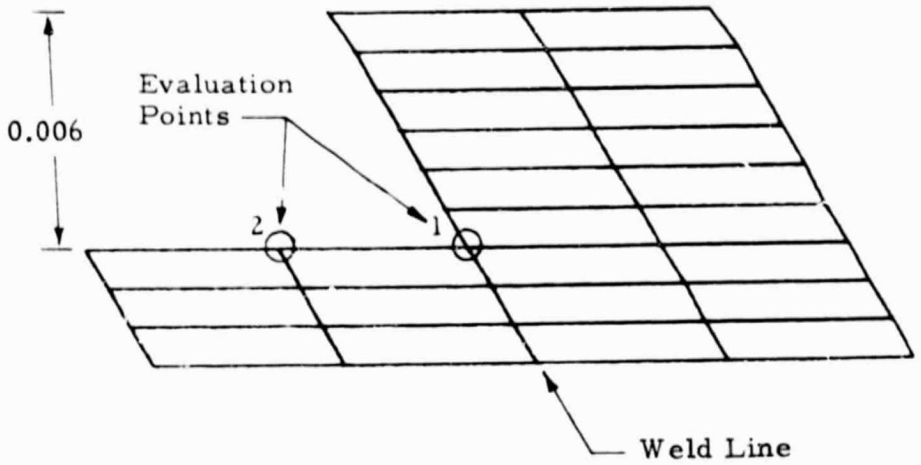

Fig. 37 - Inertia Weld Region Enlargement
Showing Stress Evaluation Points

Data Reduced from Elastic Strain Region

$$K_T = \frac{\sigma_E}{\sigma_\alpha}$$

σ_E = Etched

σ_α = Unetched

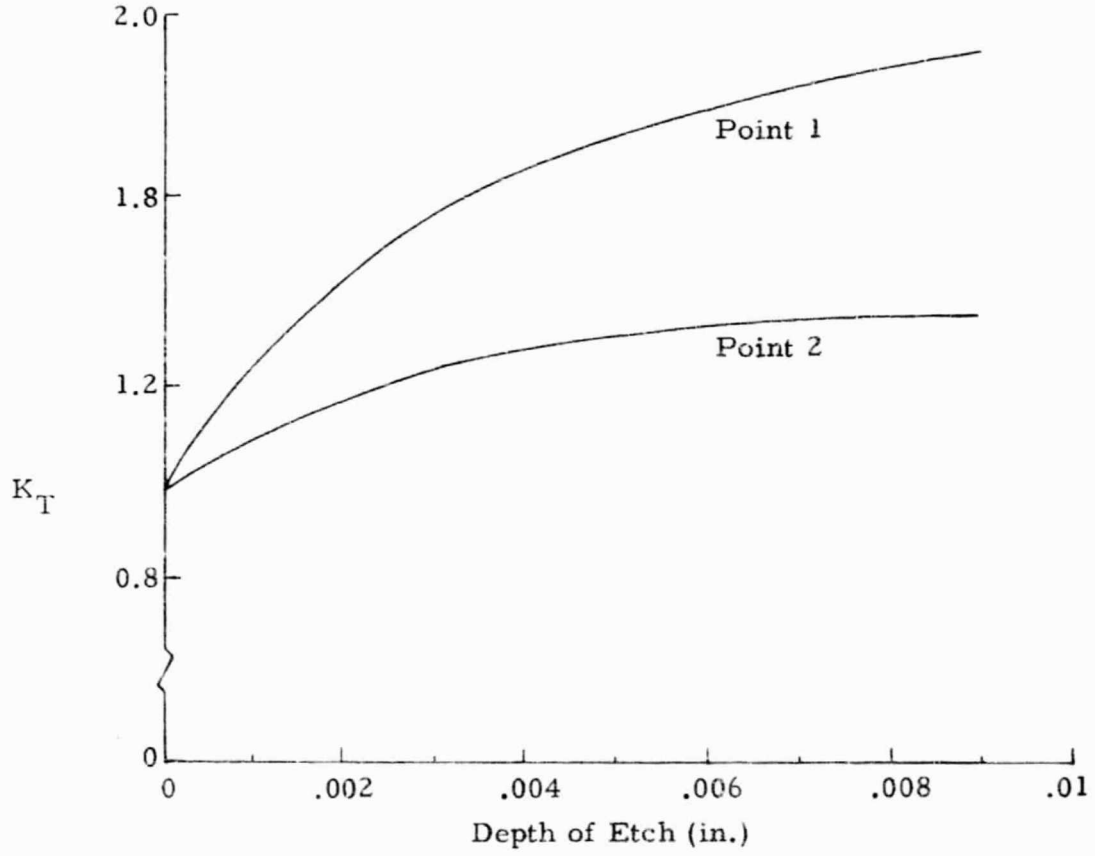

Fig. 38 - LOX Weld Stress Concentration Factor Versus Depth of Etch

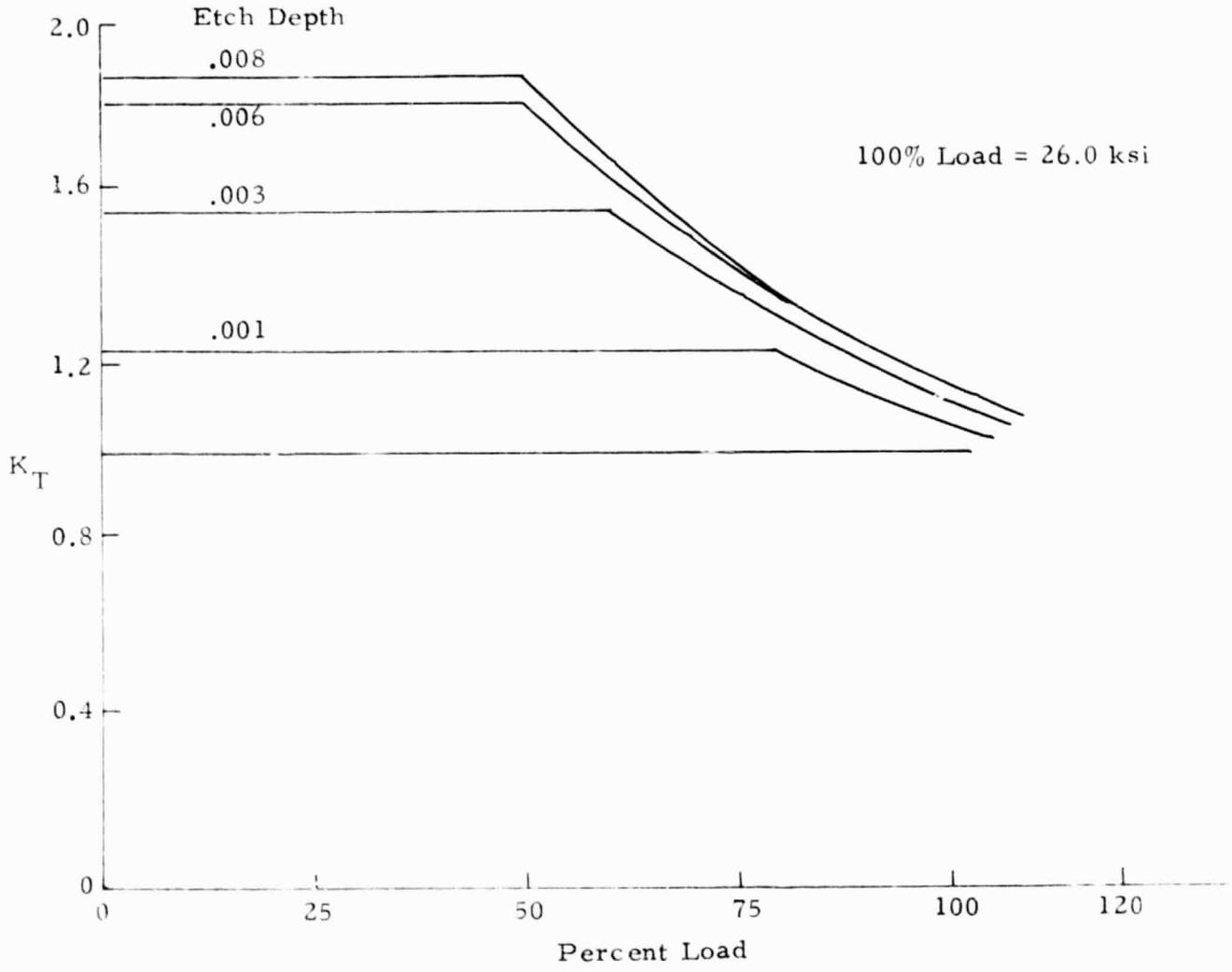

Fig. 39 - LOX Post Weld Area Stress Concentration Factor Versus Percent Load for Various Etch Depths

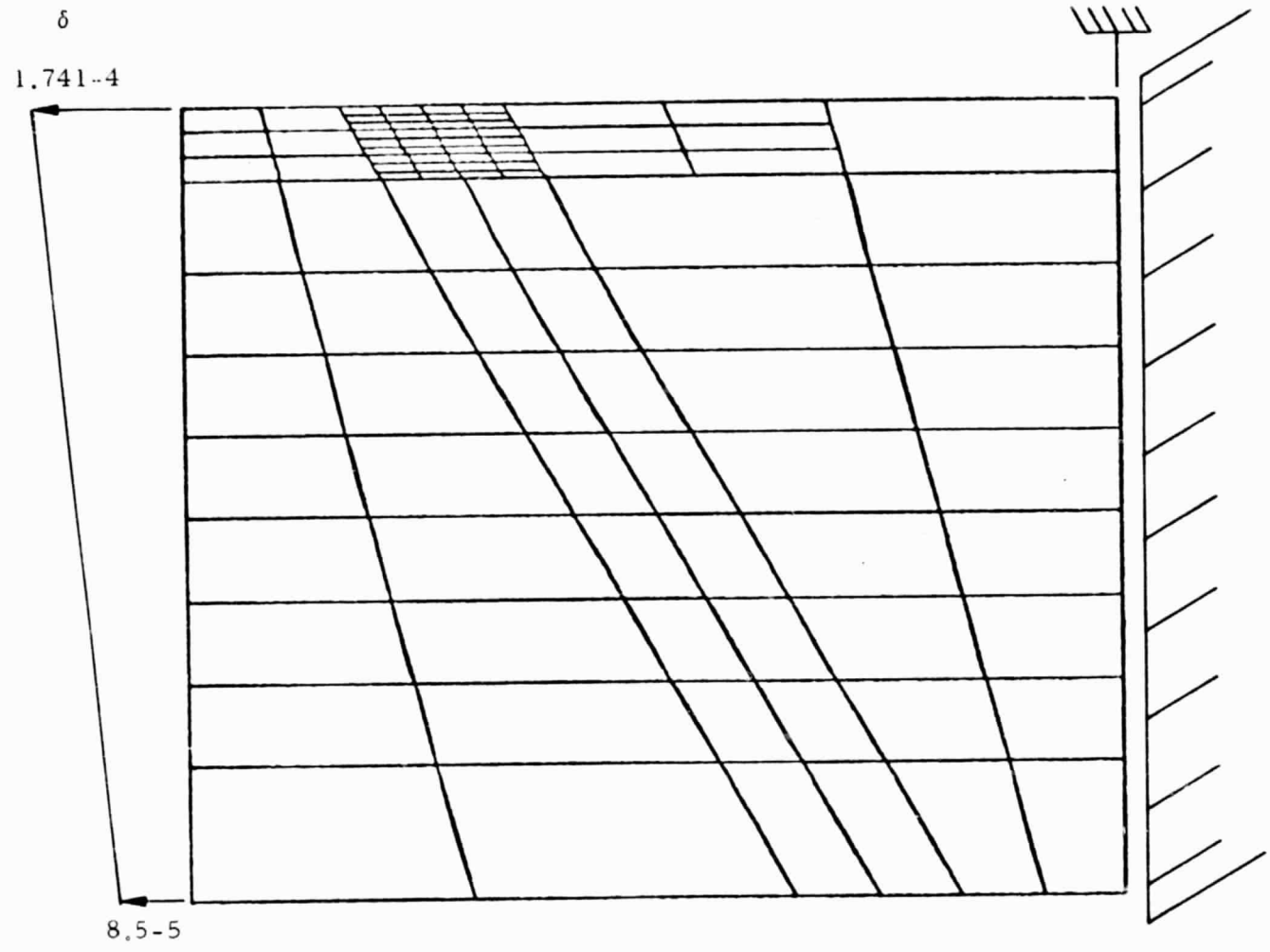

Fig. 40 - Bending Model for LOX Post Weld Area Stress Concentration Factors

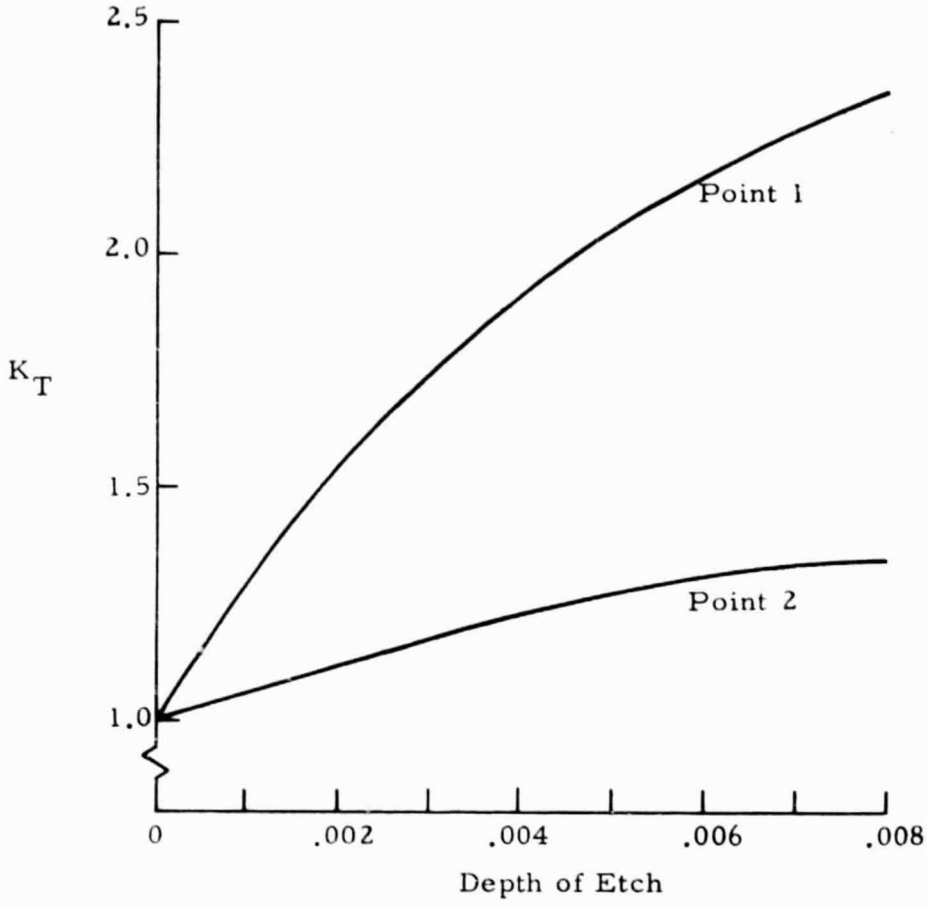

Data Reduced from Elastic Strain Region

$K_T = \frac{\sigma_E}{\sigma_\alpha}$

σ_E = etched

σ_α = unetched

Fig. 41 - LOX Post Weld Concentration Factor vs Depth of Etch for Bending Moment

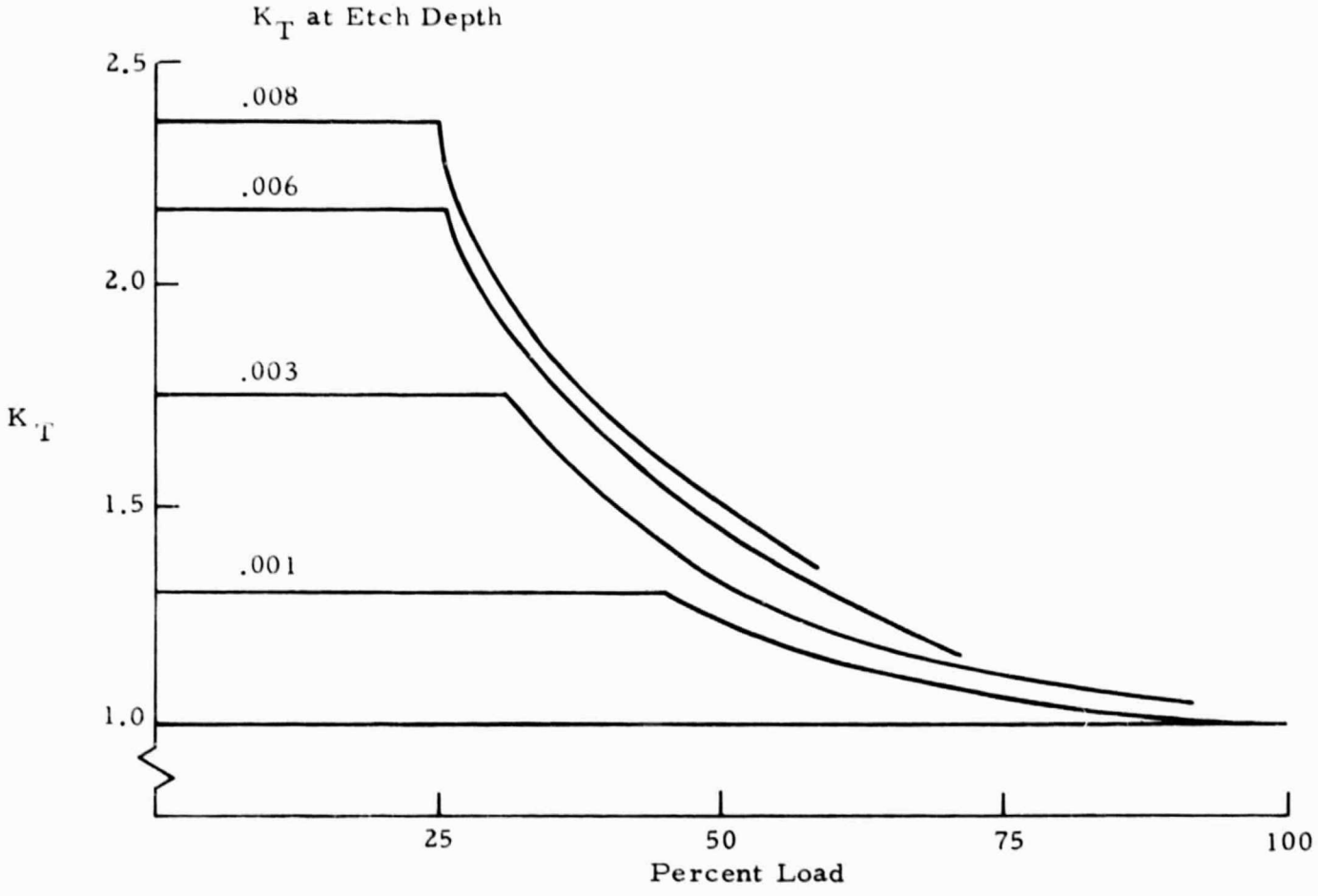

Fig. 42 - LOX Post Weld Area Stress Concentration Factor vs Percent Load for Bending Moment

Appendix A

SPAR LOX POST ASSEMBLY MODEL

Contents:

	Page
LOX Post Layout Model Drawing	A-1a
Cross-Sectional Details with Node Numbers	A-1b through A-54
Flow Shield Model Details	A-55 through A-68

ORIGINAL PAGE IS
OF POOR QUALITY

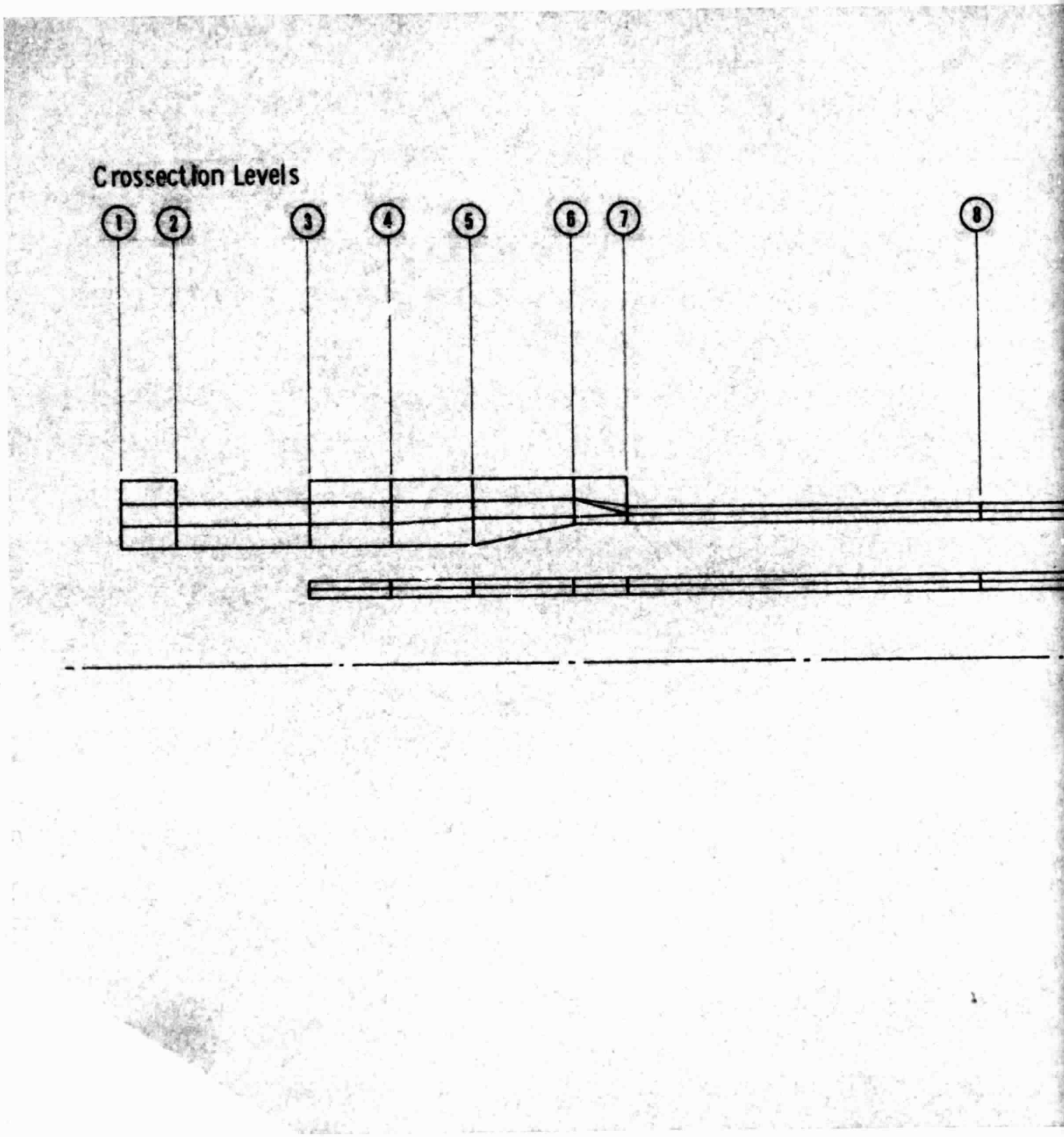

FOLDOUT FRAME

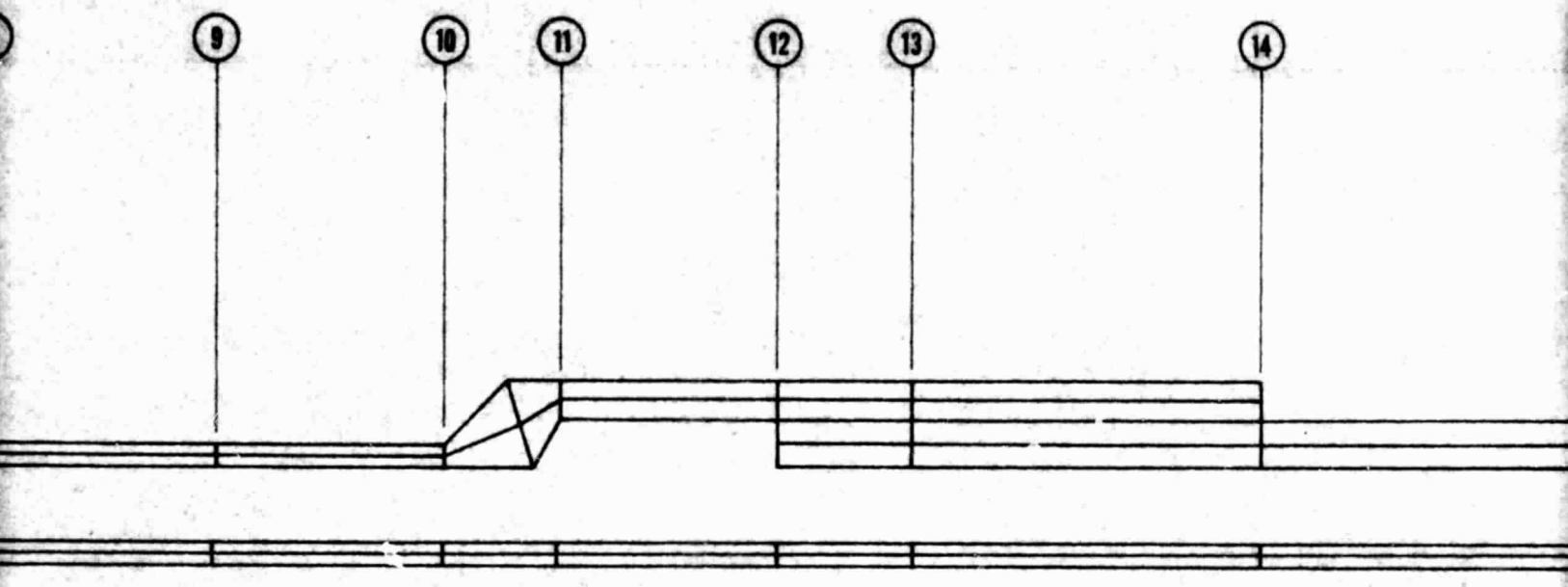

Row 13 Assembly

Row 12 Assembly

FOLDOUT FRAME 2

ORIGINAL PAGE IS
OF POOR QUALITY

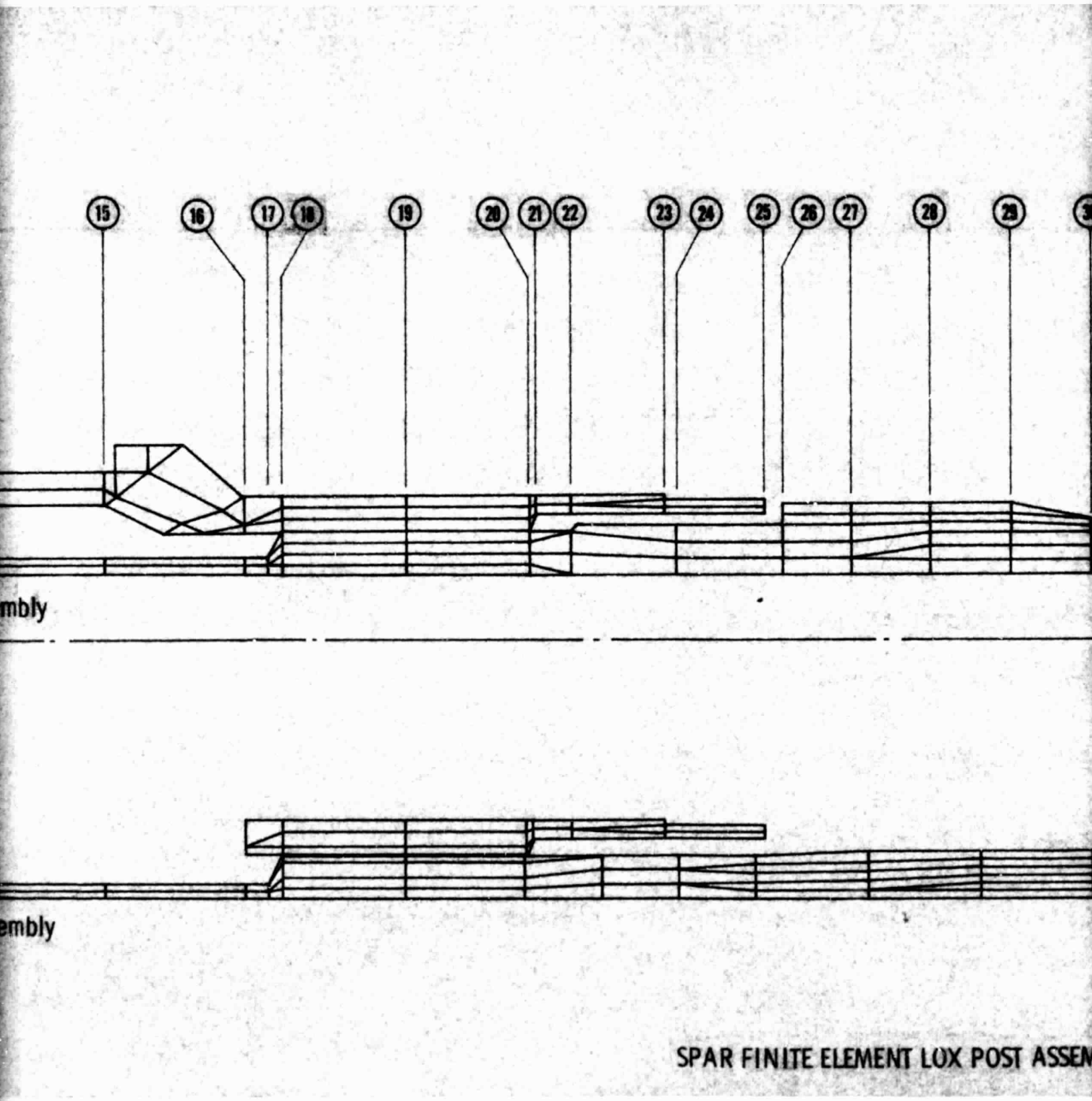

SPAR FINITE ELEMENT LOX POST ASSEM

FOLDOUT FRAME 3

ORIGINAL PAGE IS
OF POOR QUALITY

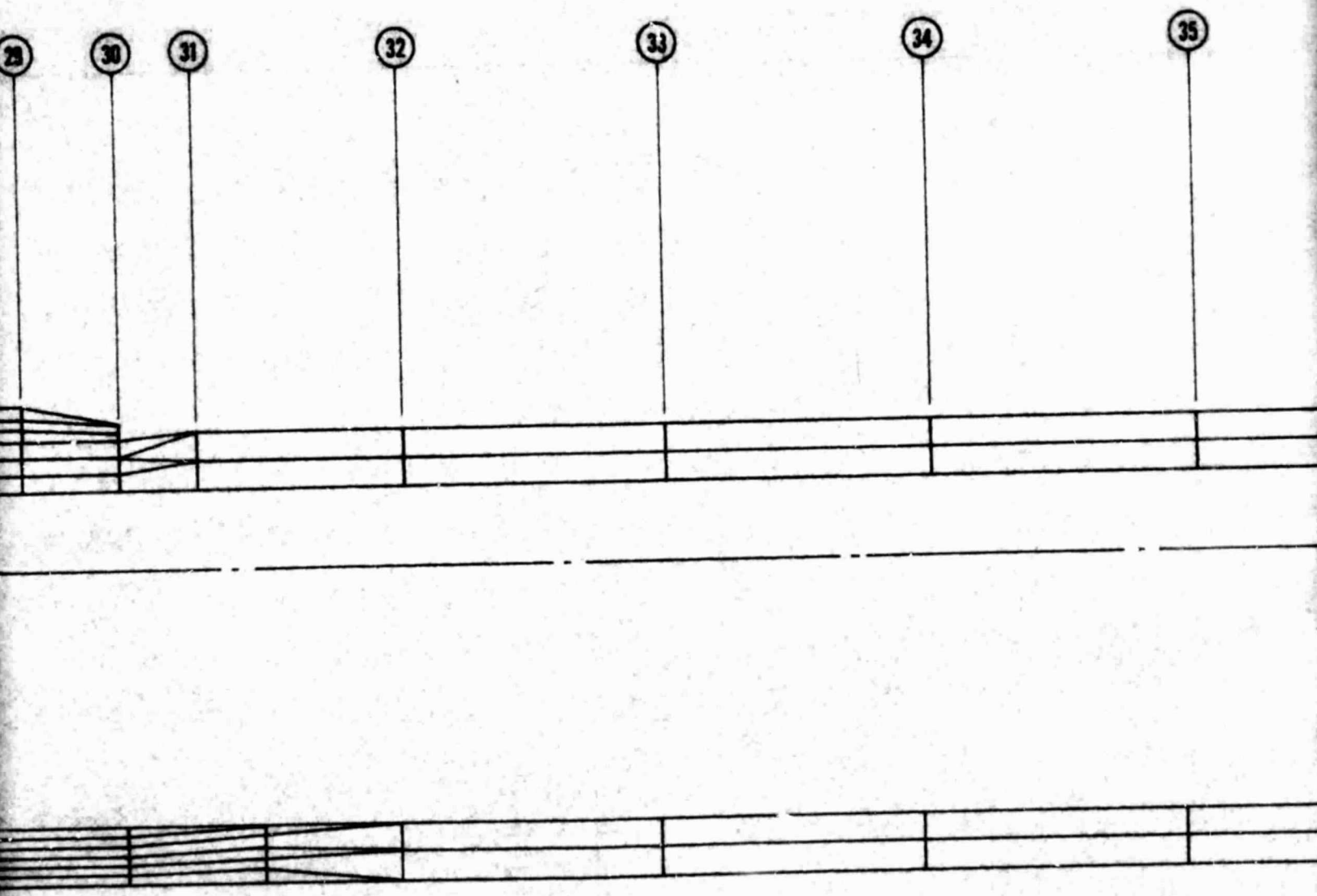

OST ASSEMBLY MODEL (Row 12 and 13)

FOLDOUT FRAME 4

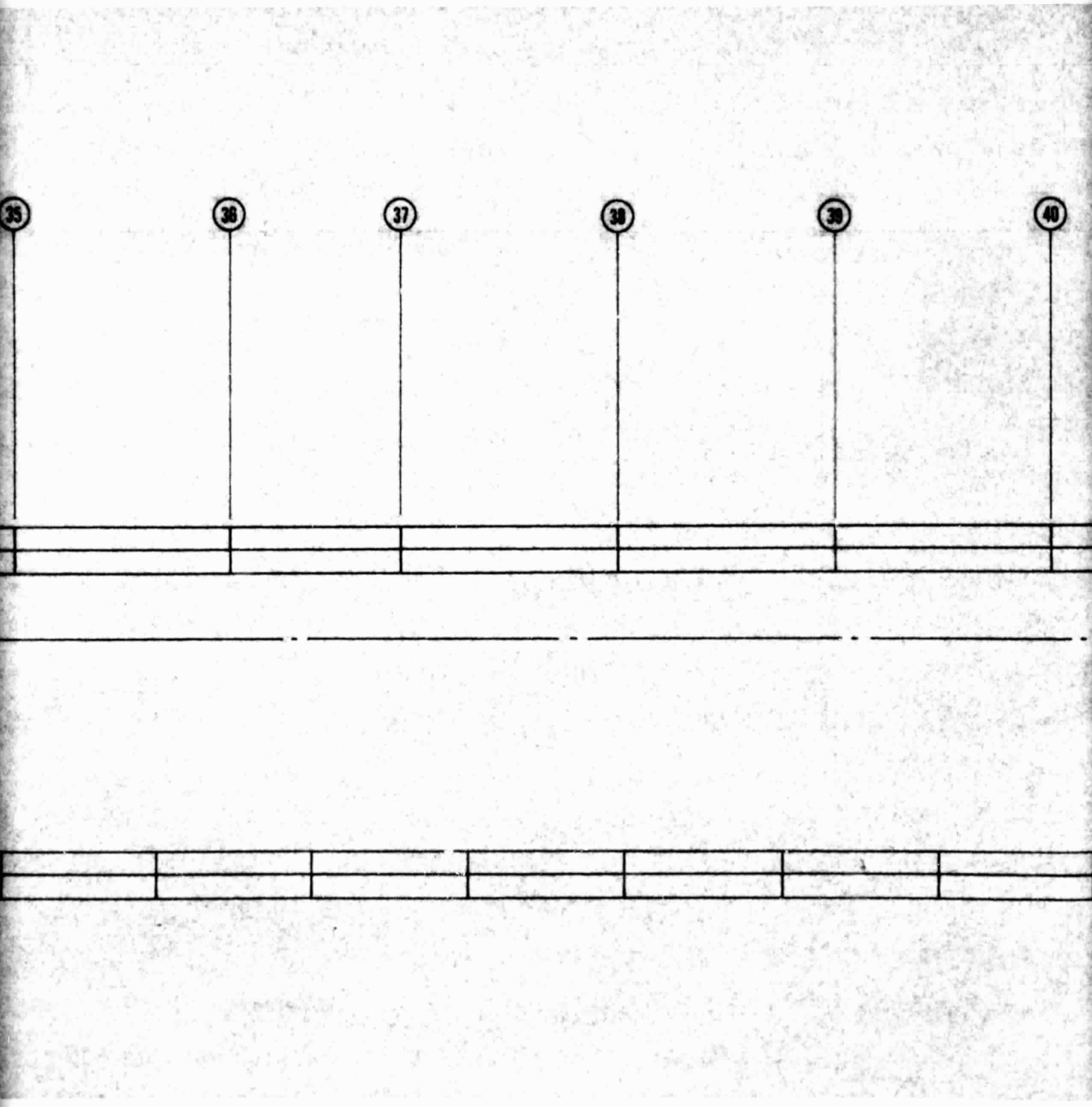

FOLDOUT FRAME 5

ORIGINAL PAGE IS
OF POOR QUALITY

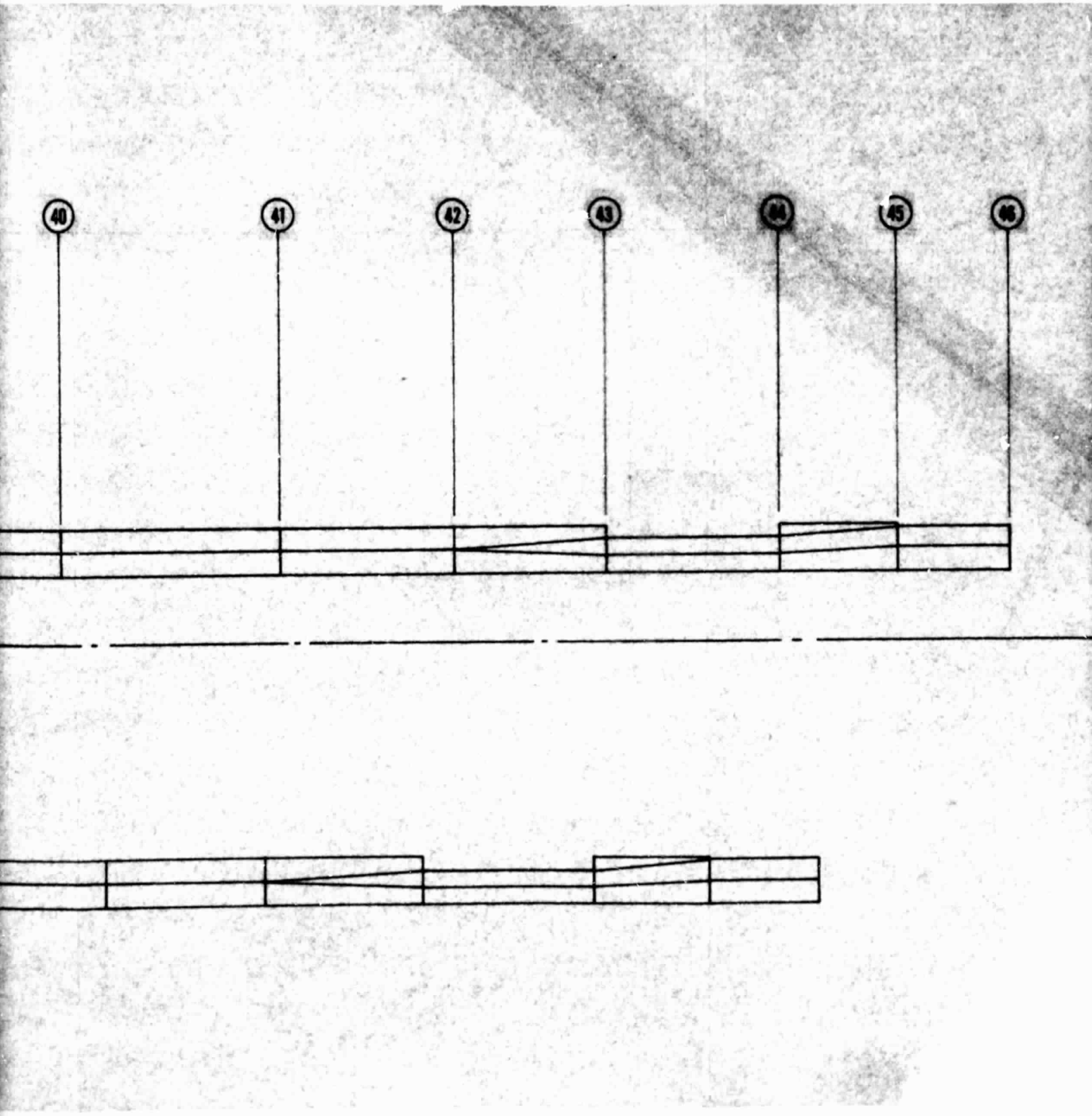

FOLDOUT FRAME 6

Not to Scale

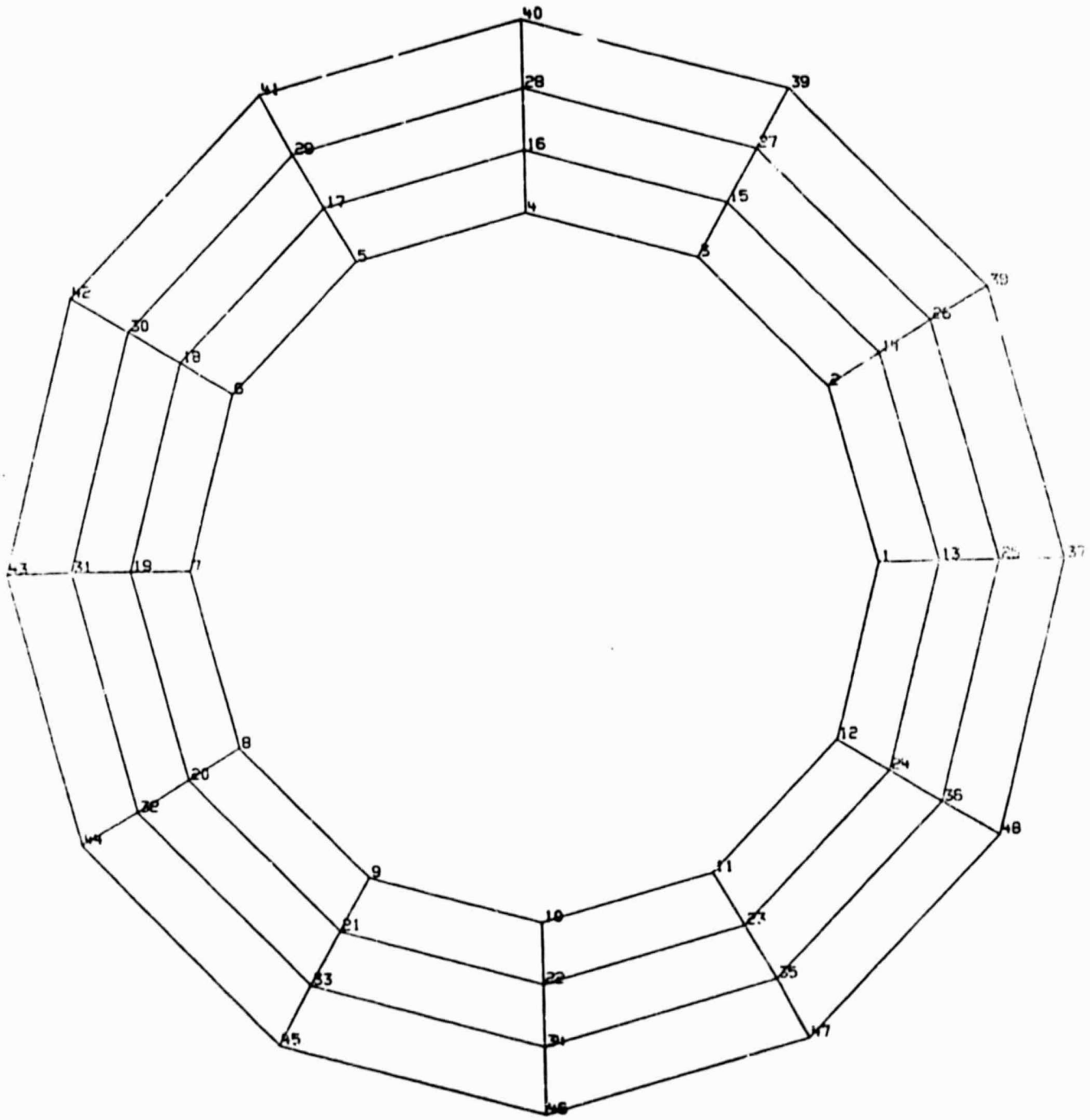

LEVEL 1

NOT TO SCALE

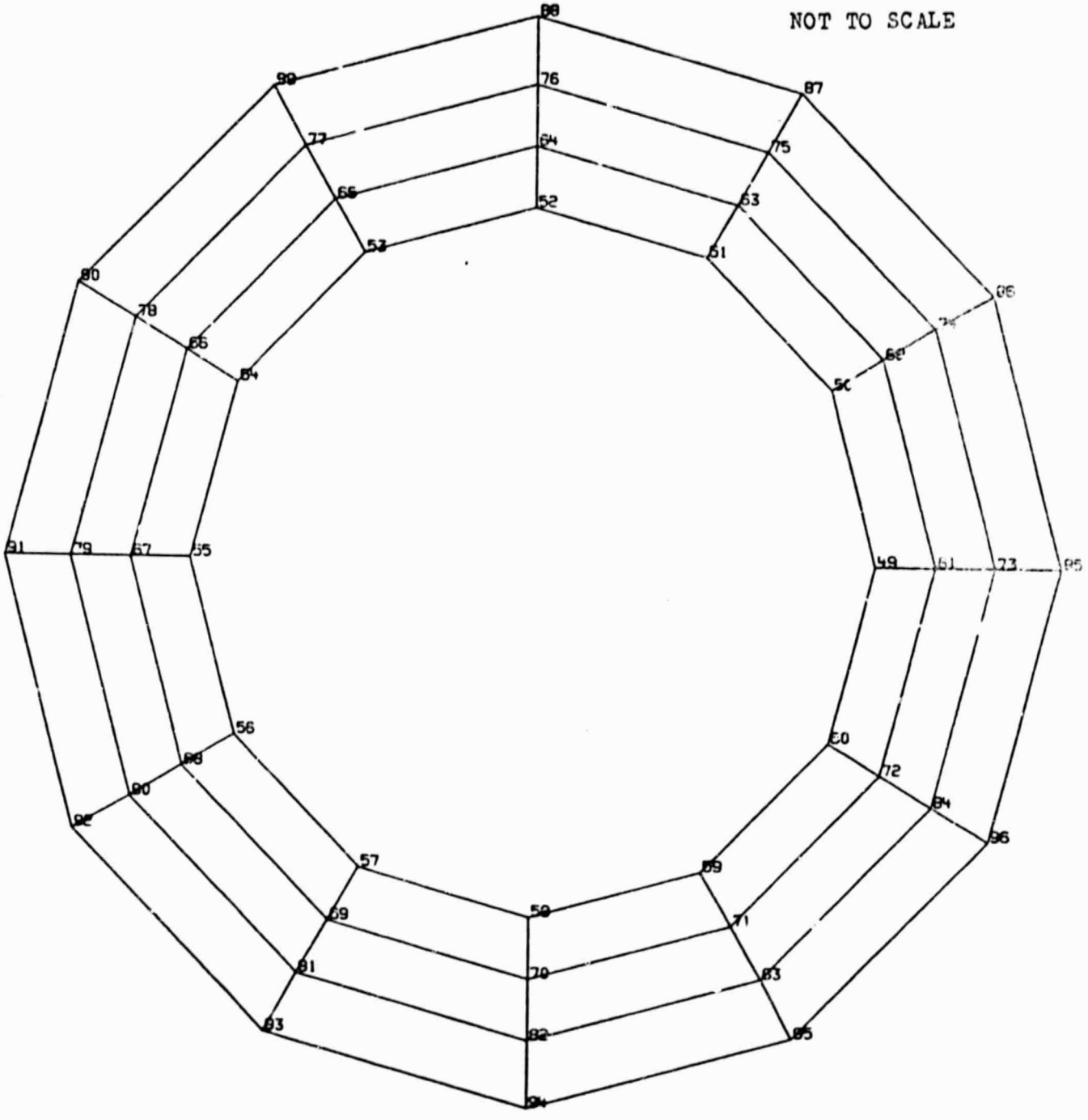

LEVEL 2

NOT TO SCALE

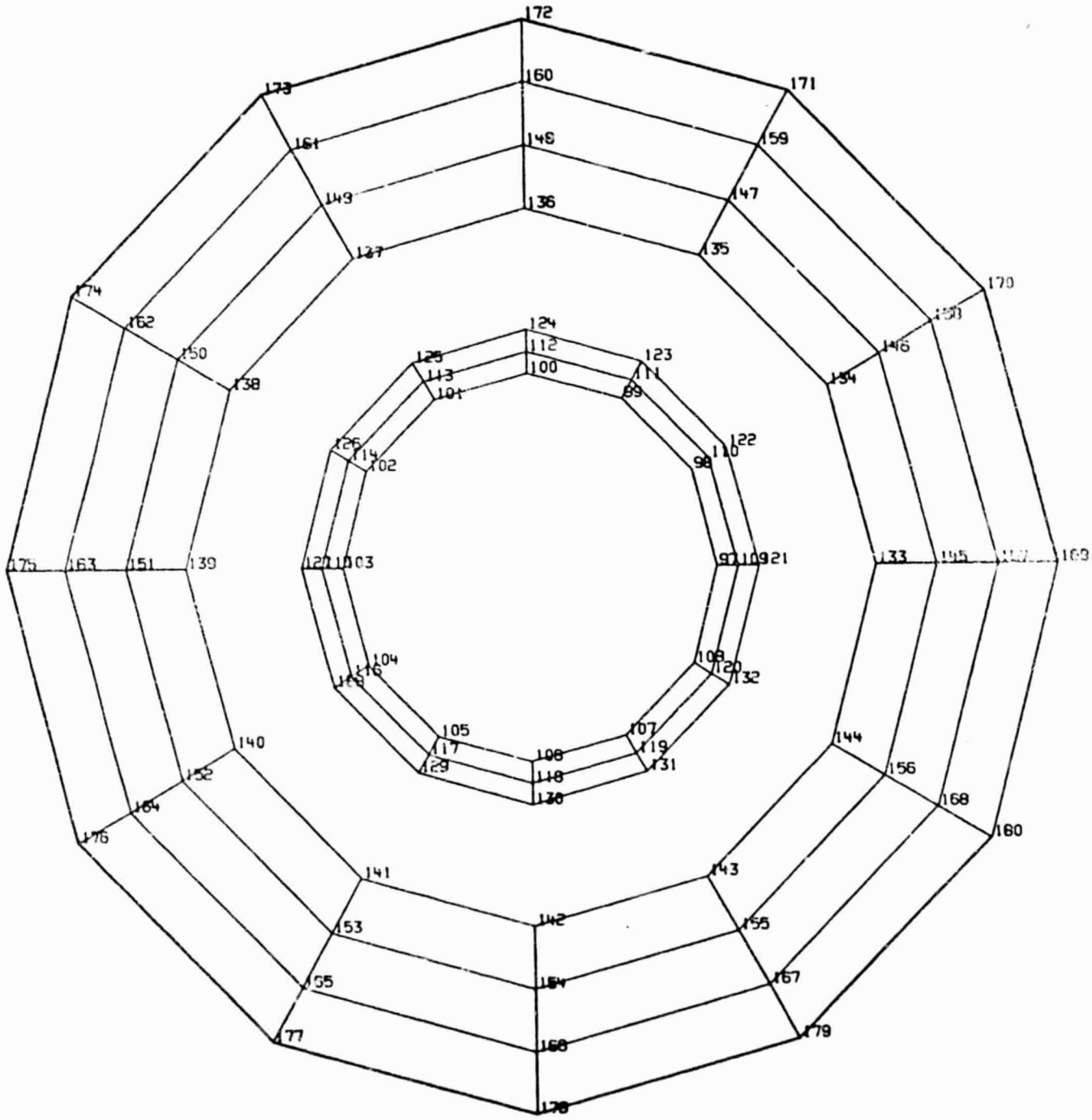

LEVEL 3

NOT TO SCALE

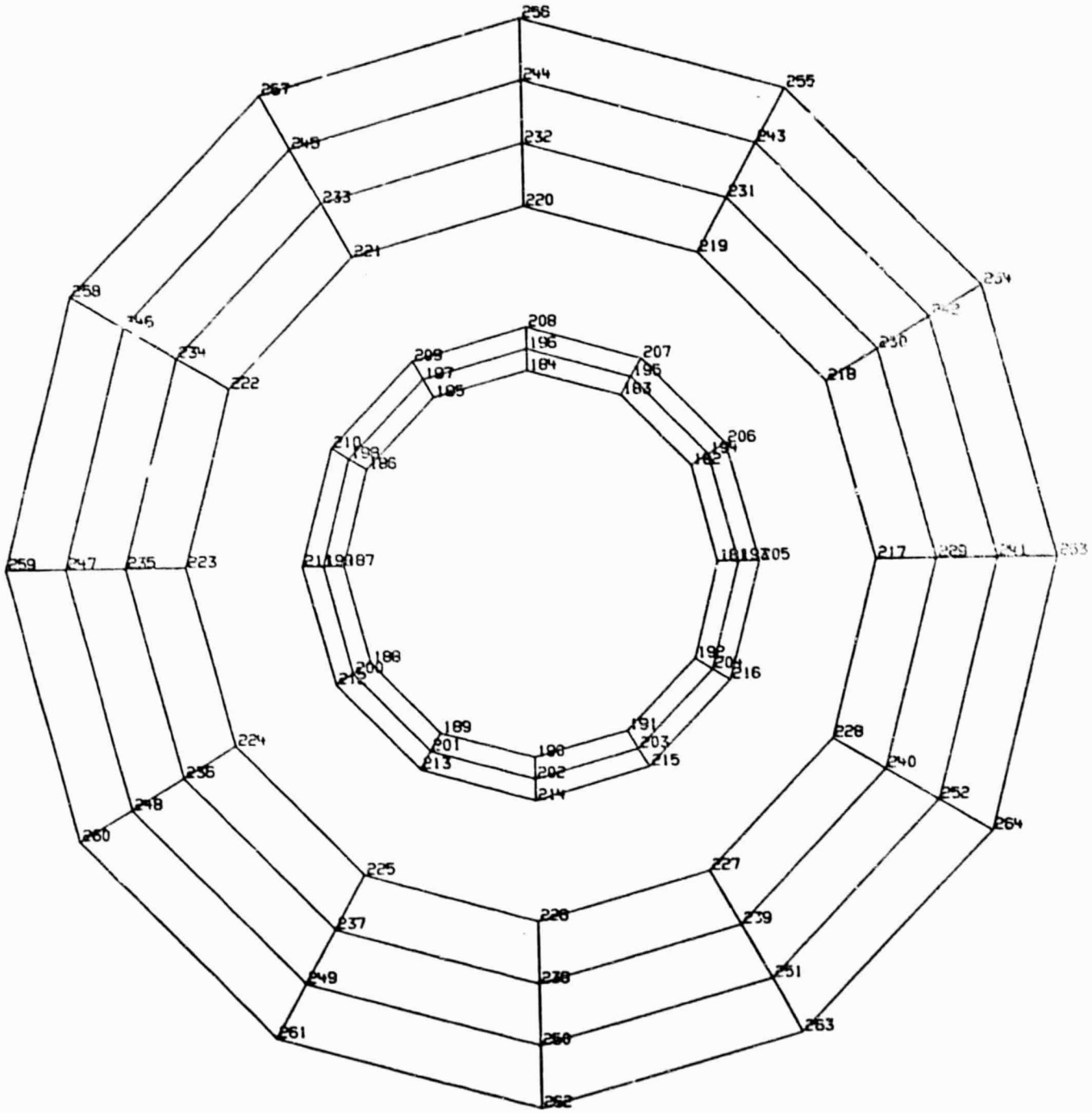

LEVEL 4

NOT TO SCALE

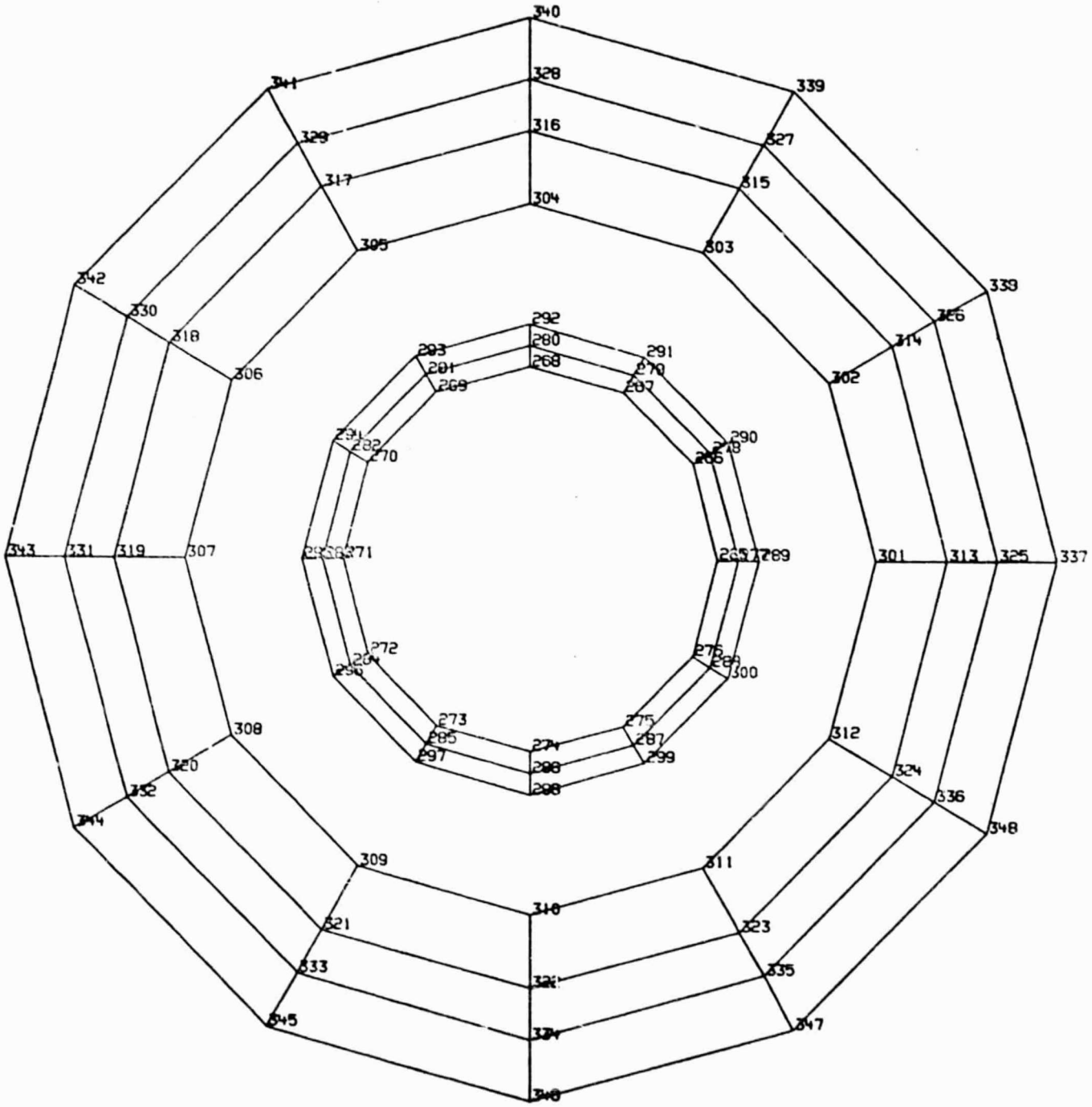

LEVEL 5

NOT TO SCALE

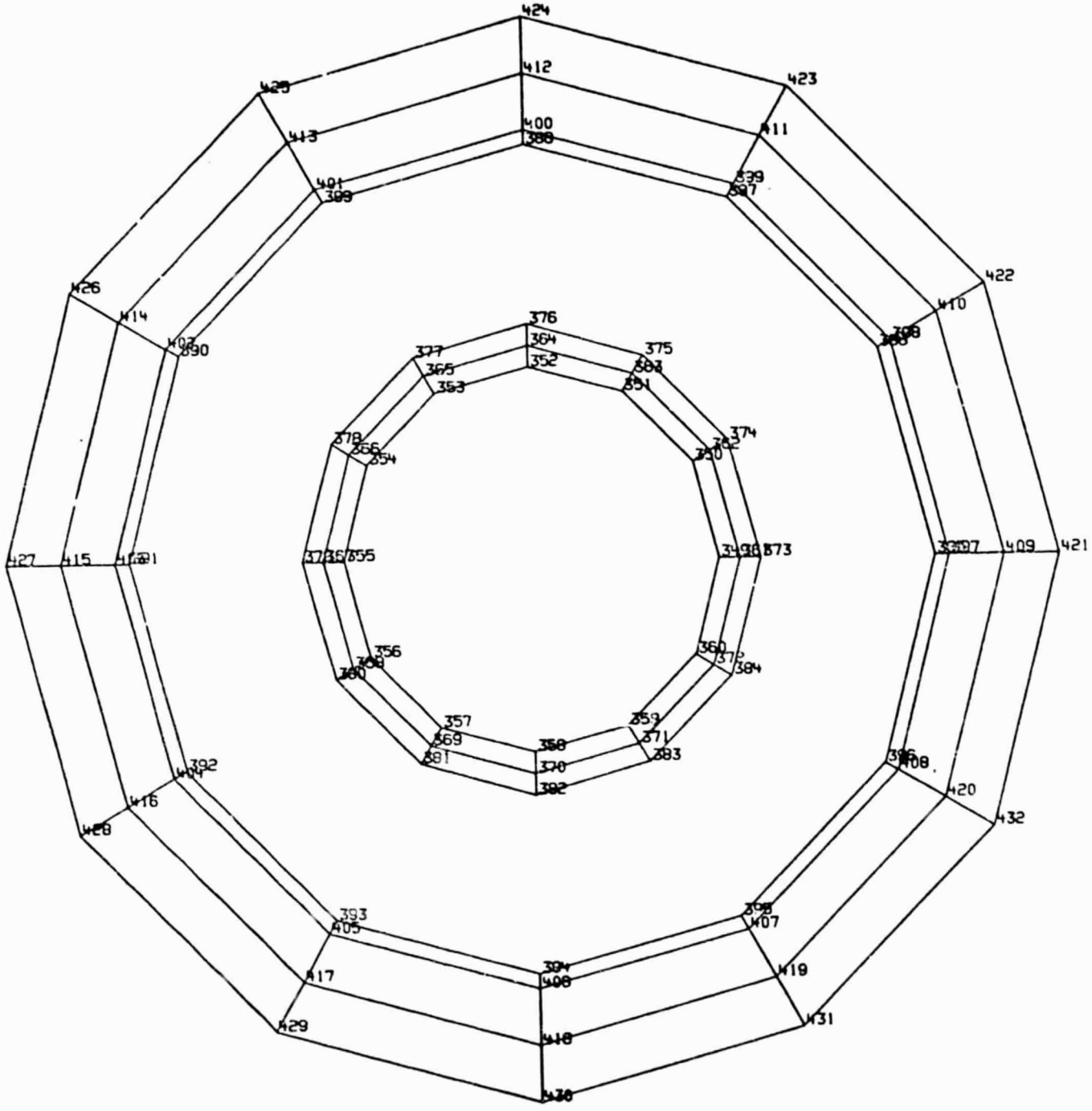

LEVEL 6

NOT TO SCALE

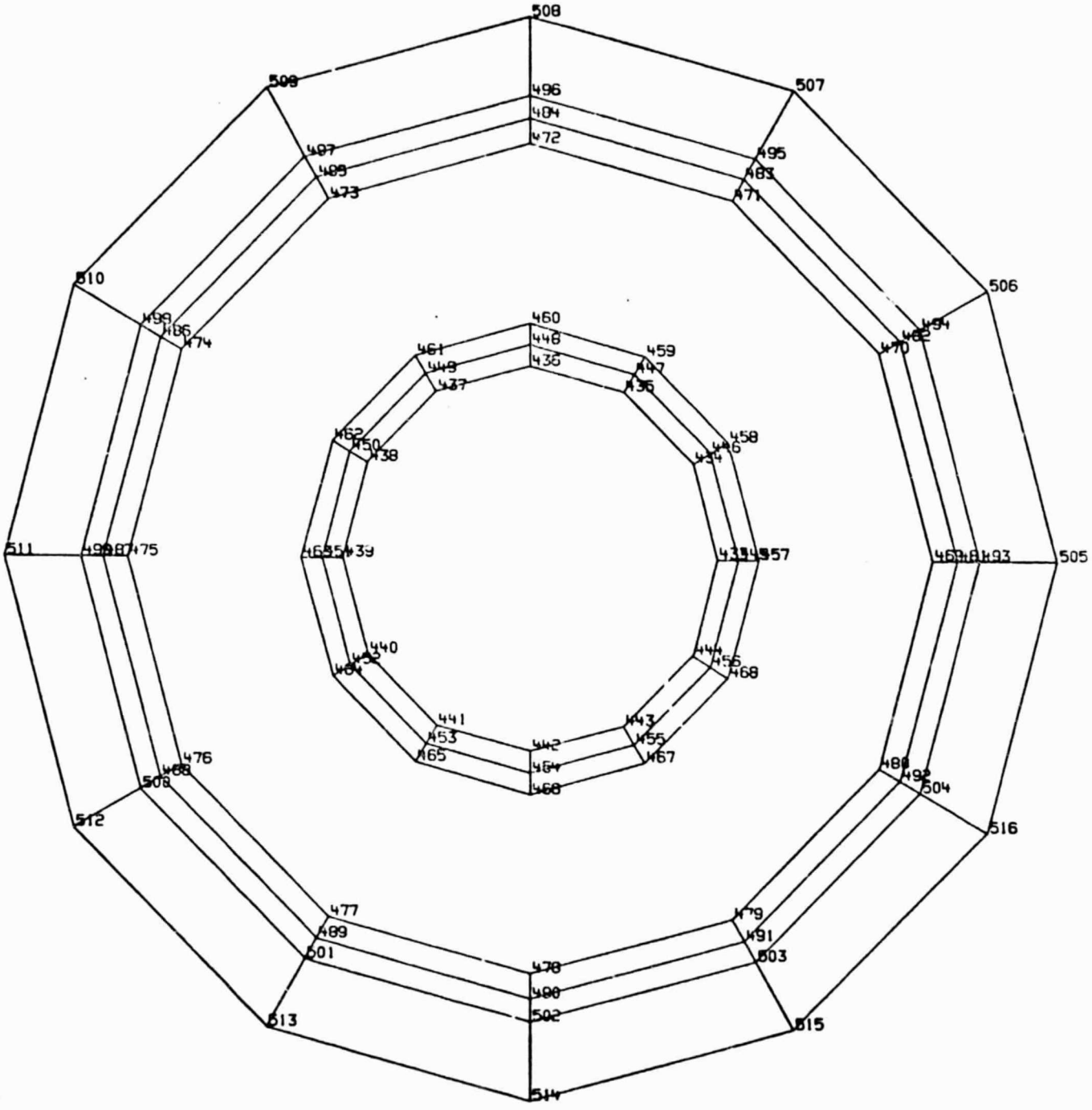

LEVEL 7

NOT TO SCALE

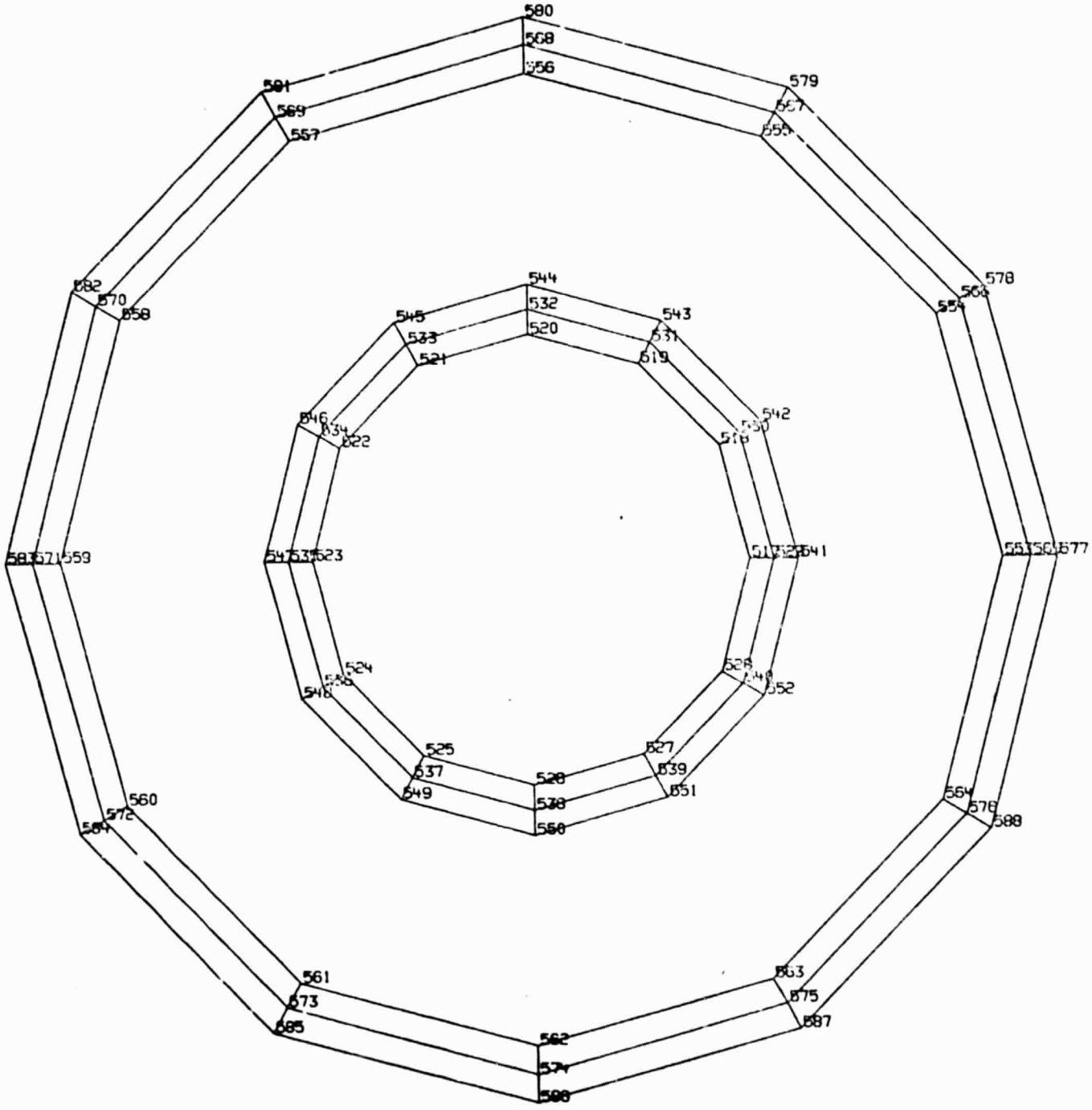

LEVEL 8

NOT TO SCALE

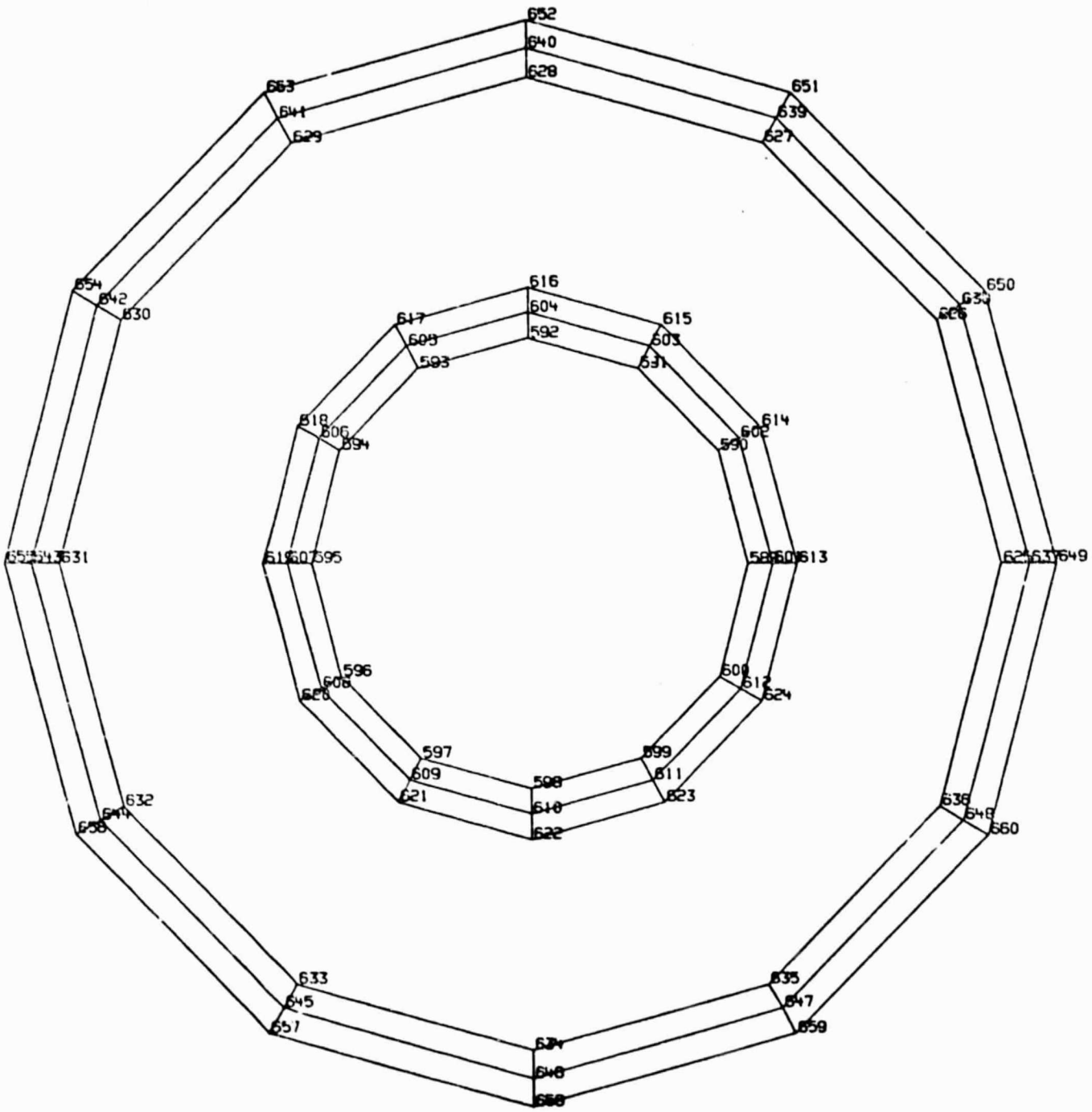

LEVEL 9

NOT TO SCALE

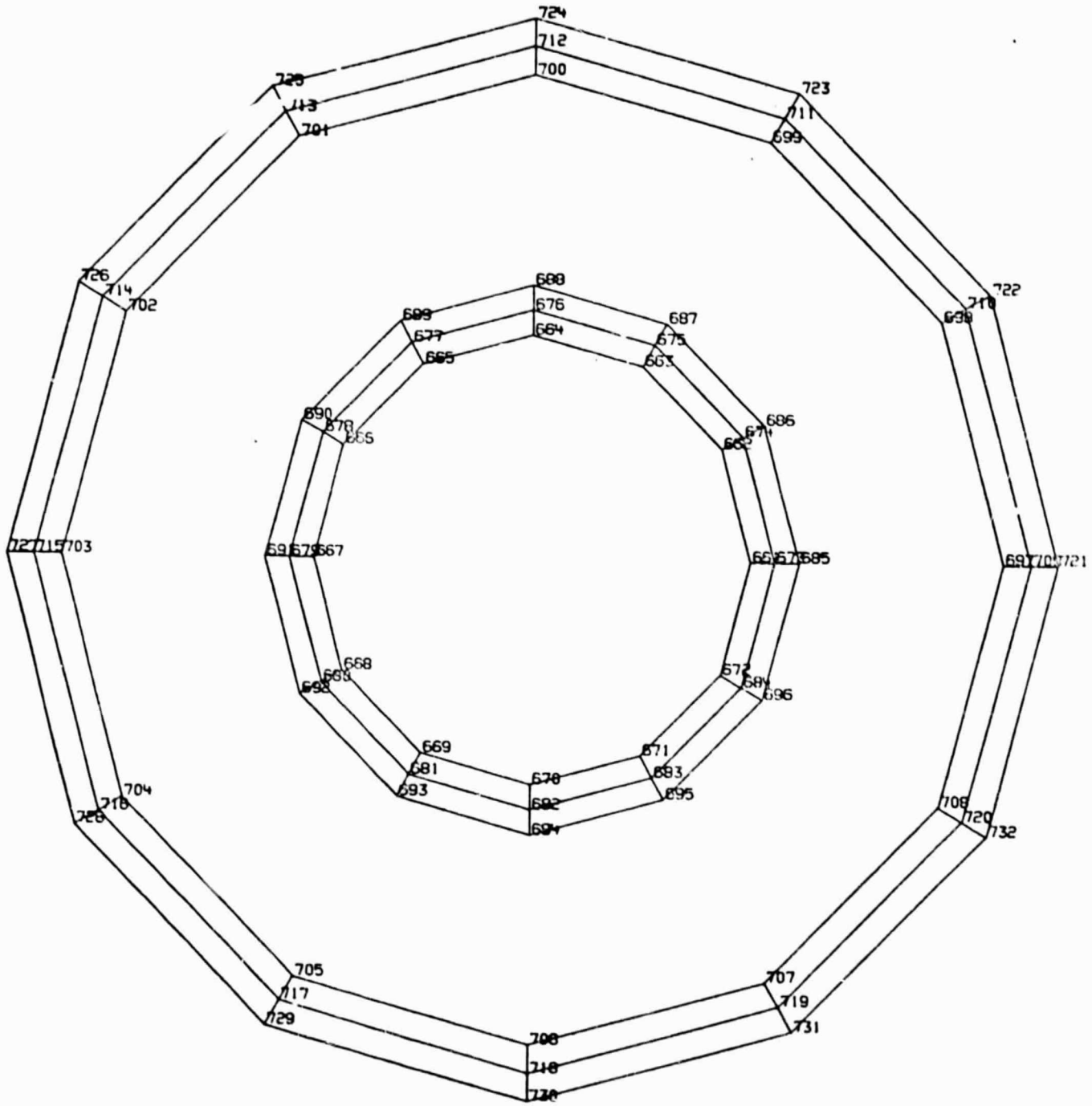

LEVEL 10

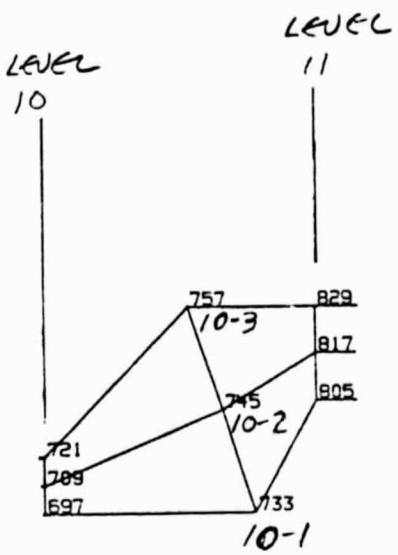

Sleeve Detail

NOT TO SCALE

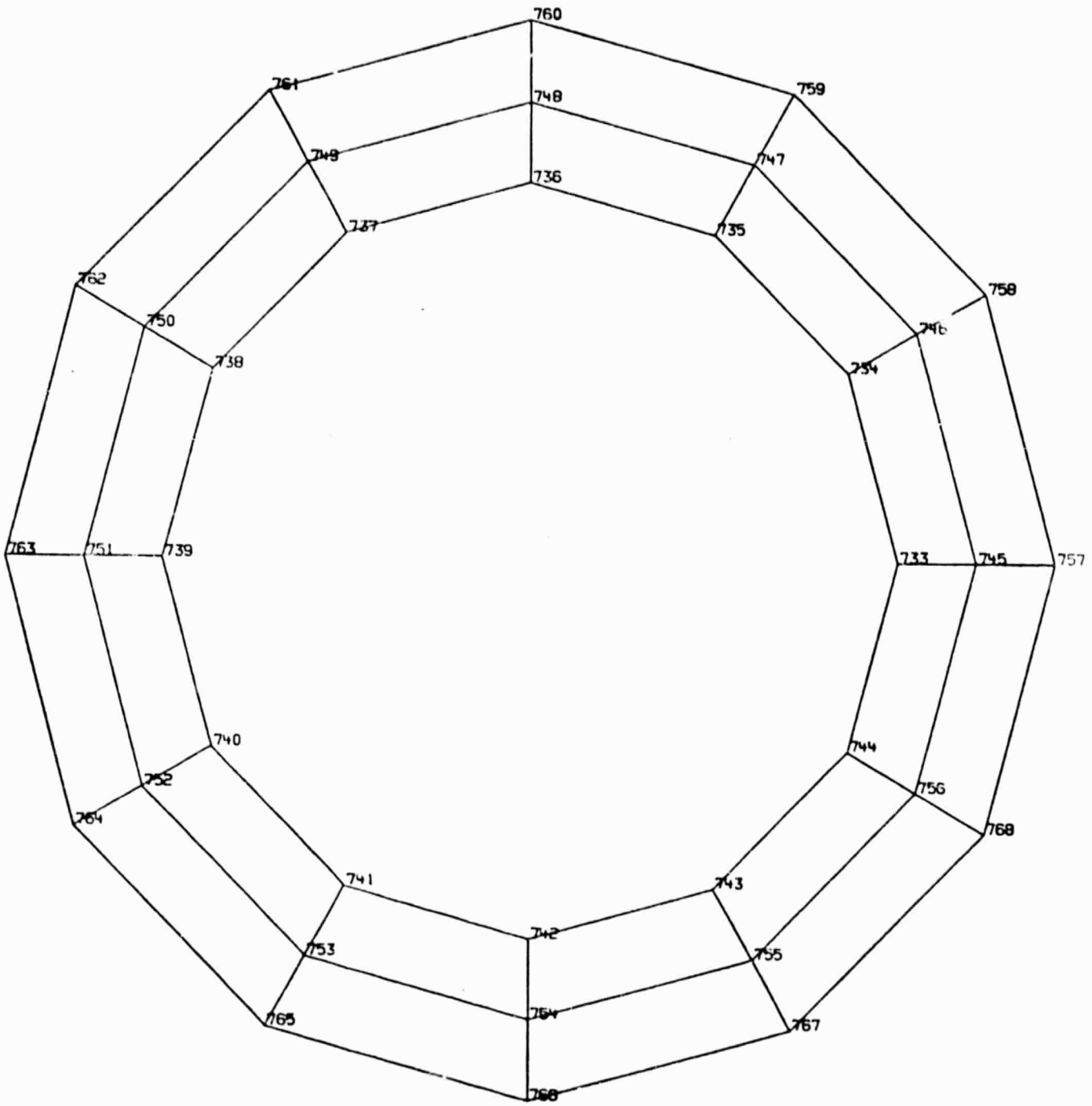

Levels 10-1, -2 and -3

NOT TO SCALE

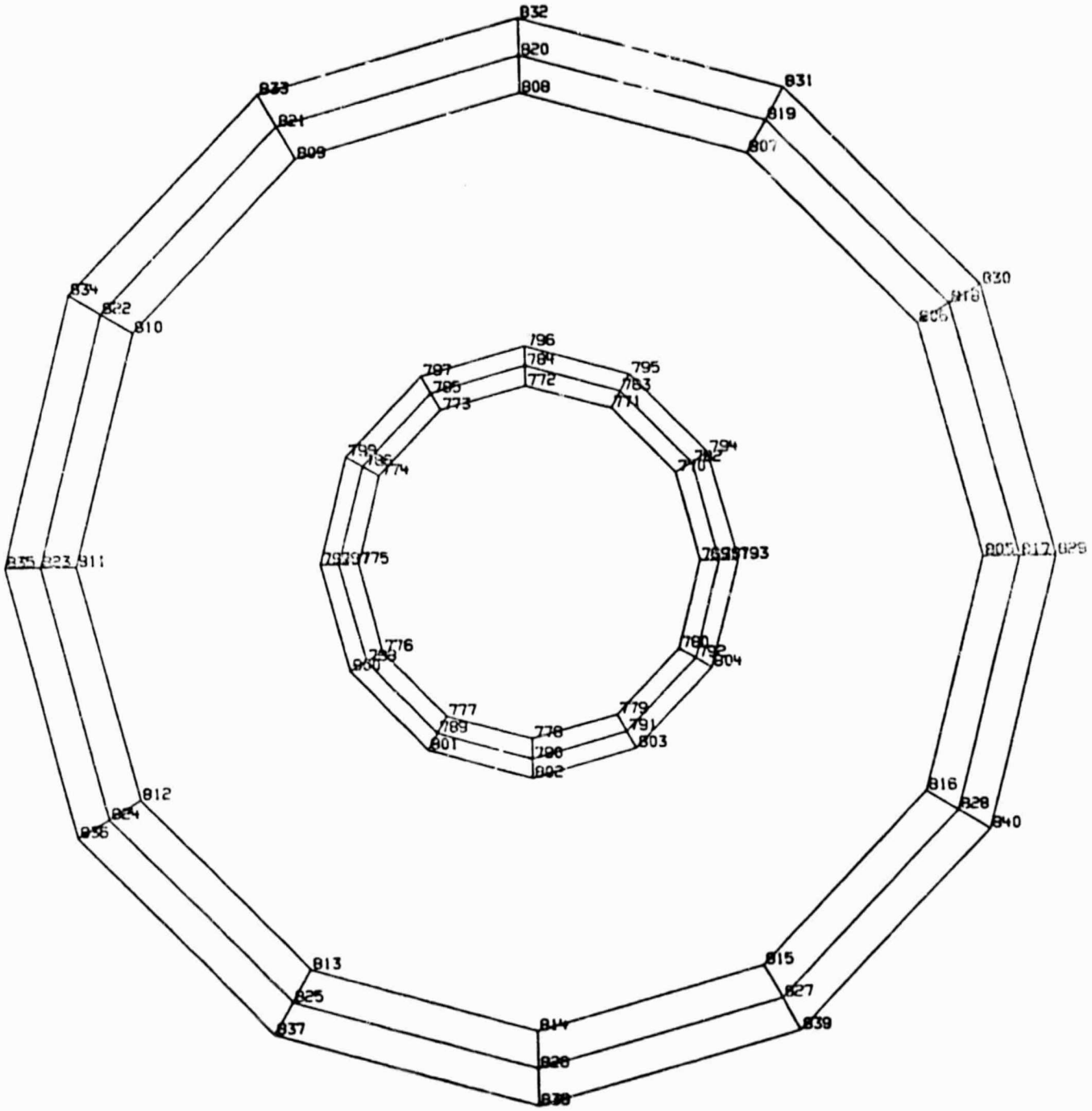

LEVEL 11

NOT TO SCALE

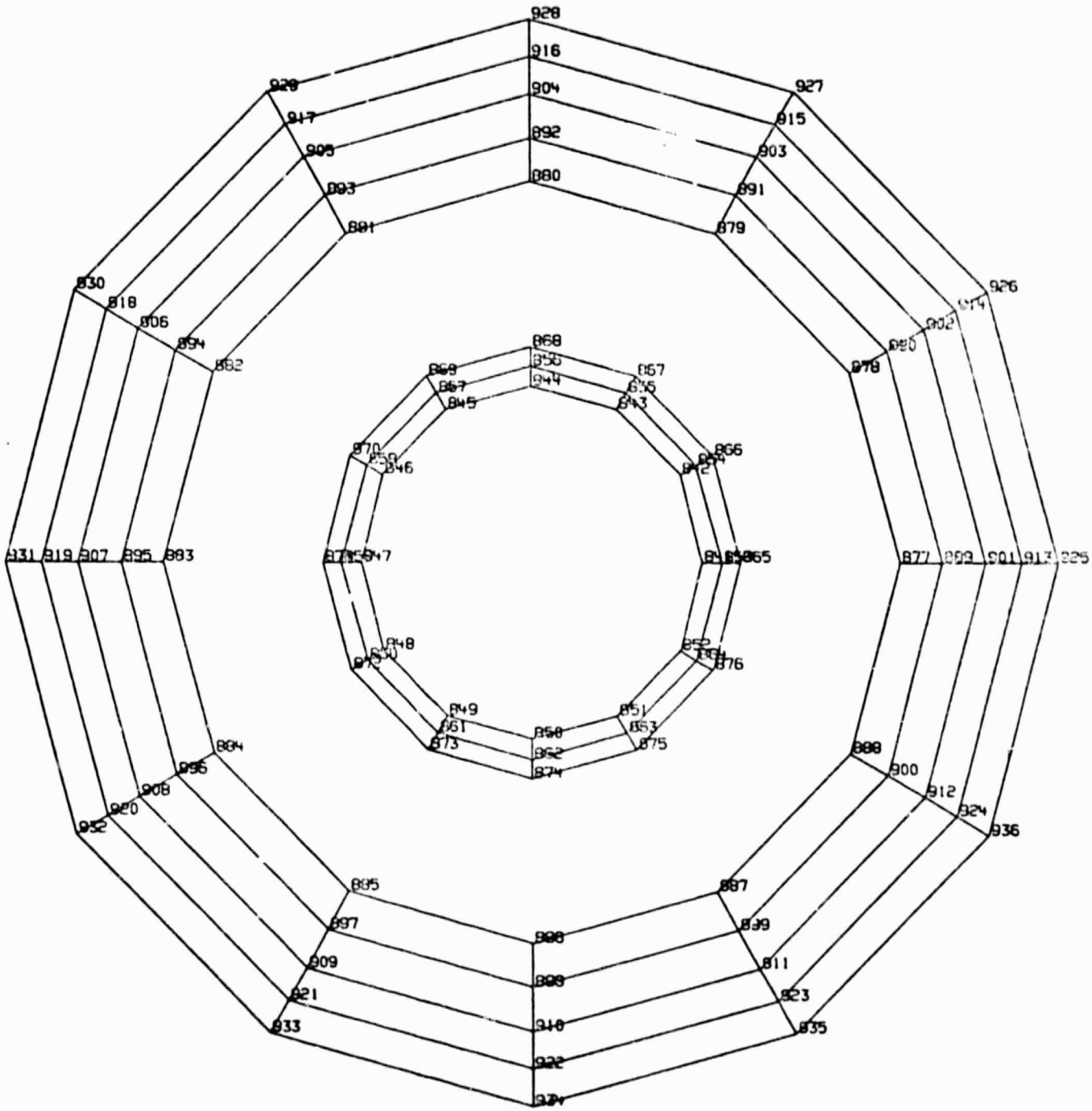

LEVEL 12

NOT TO SCALE

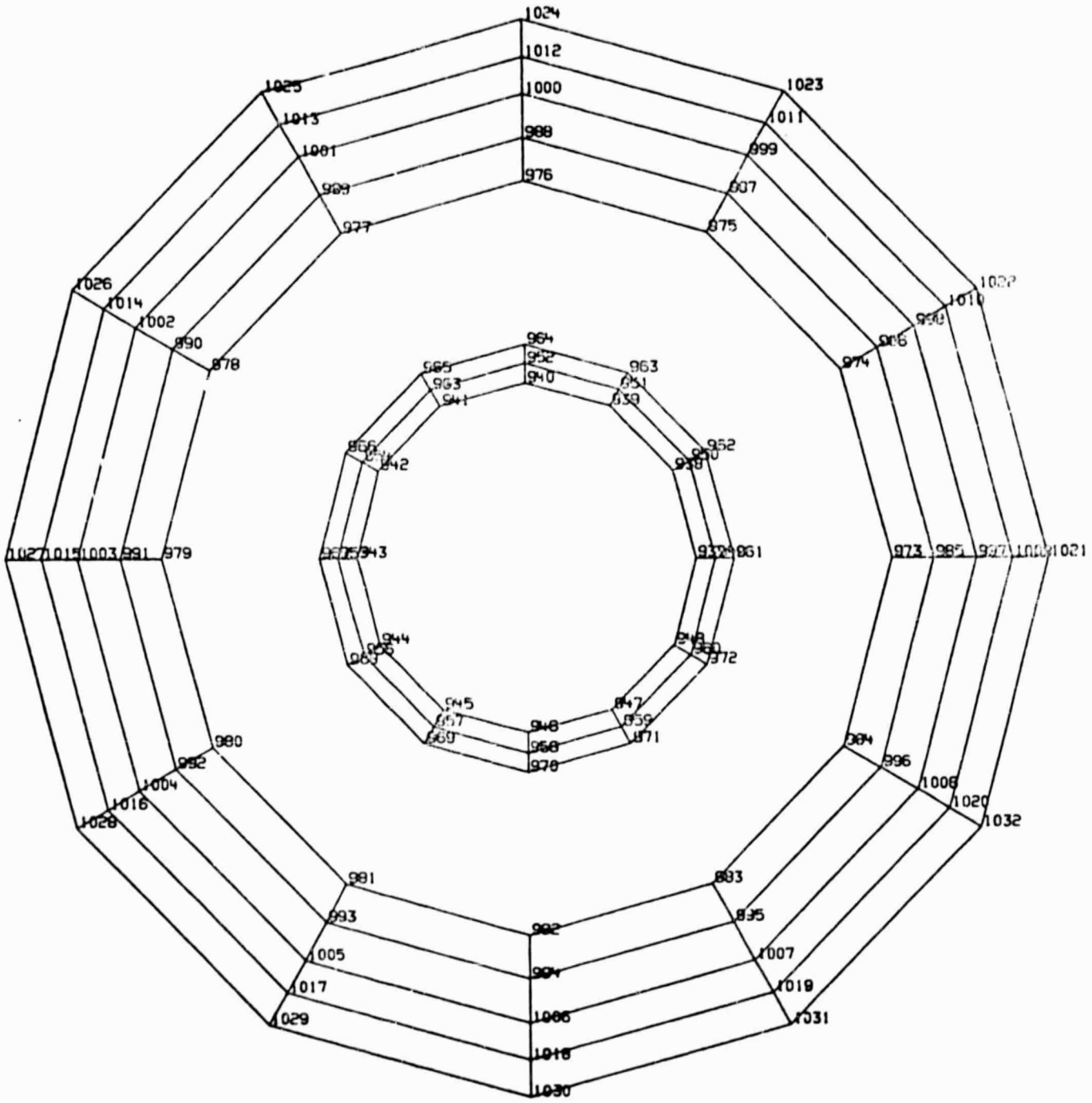

LEVEL 13

NOT TO SCALE

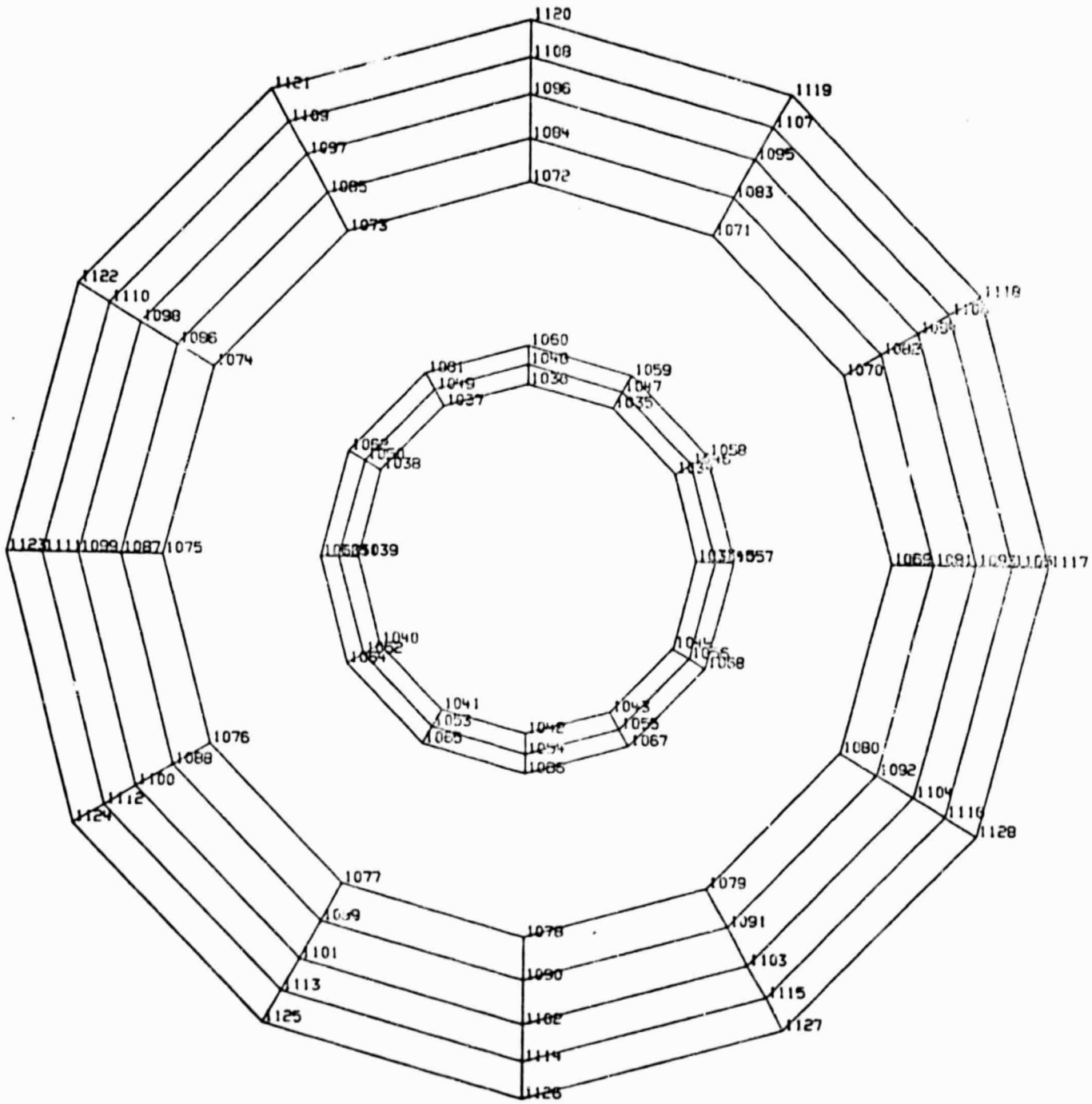

LEVEL 14

NOT TO SCALE

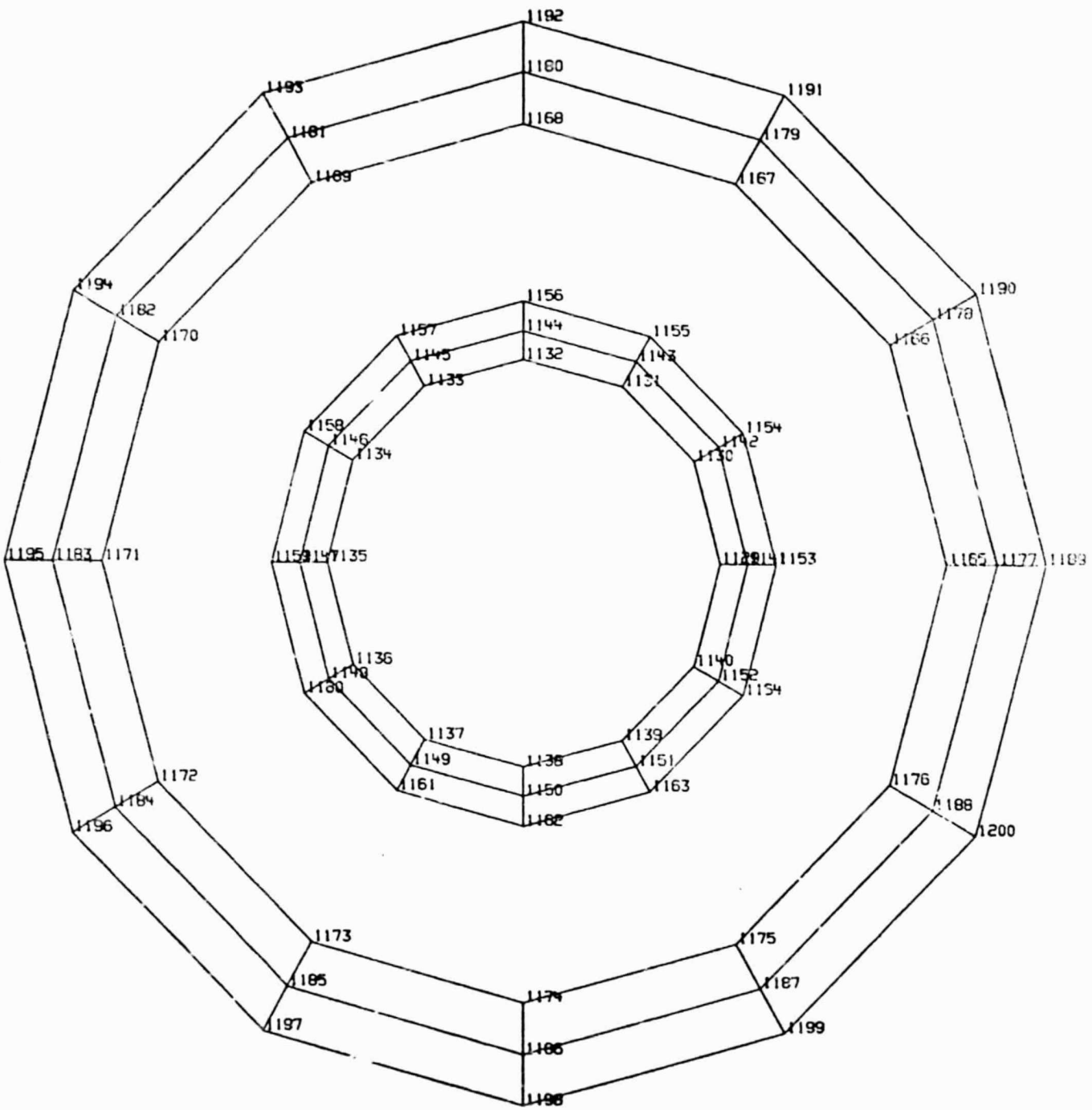

LEVEL 15

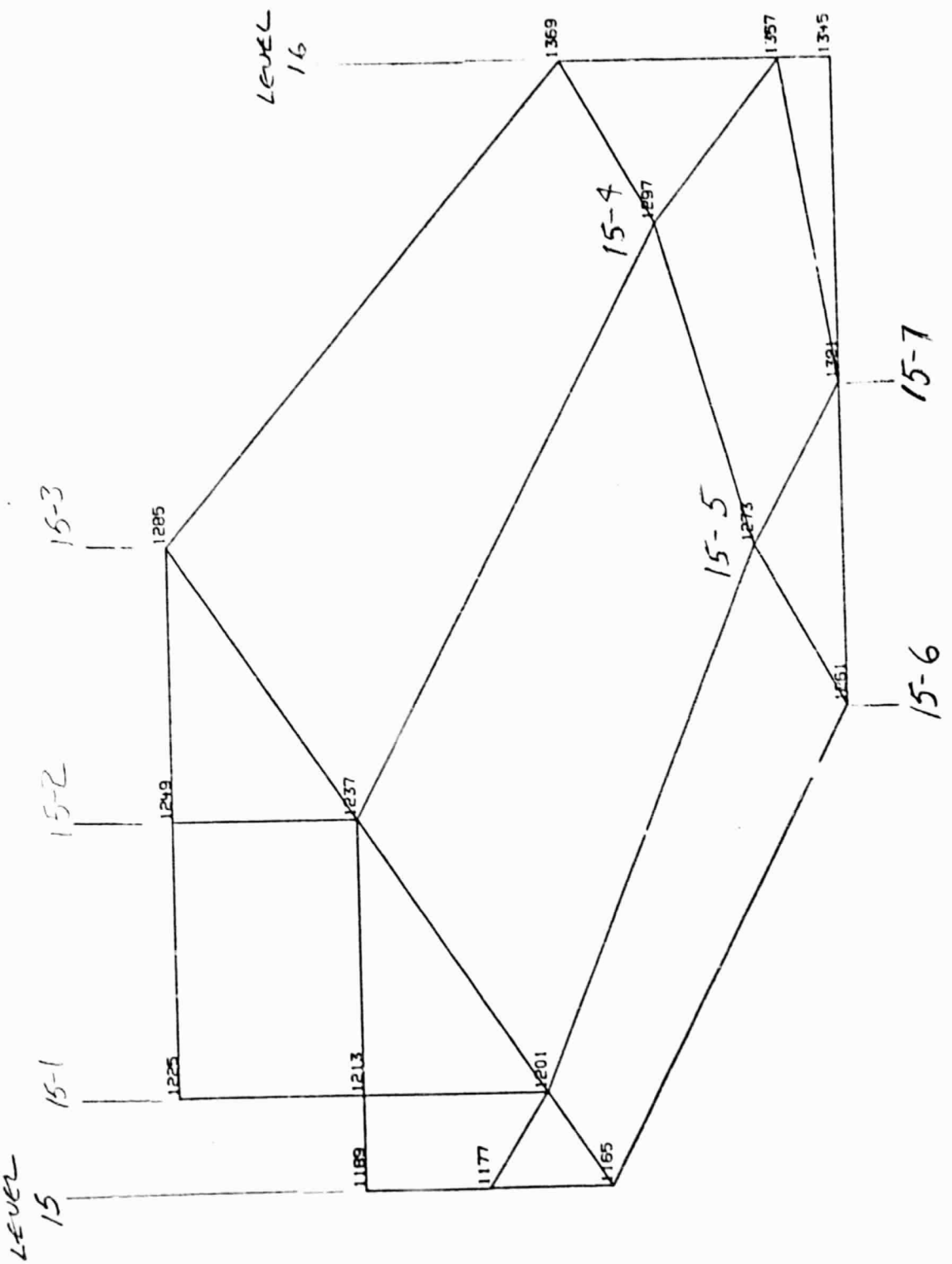

Retainer Detail

NOT TO SCALE

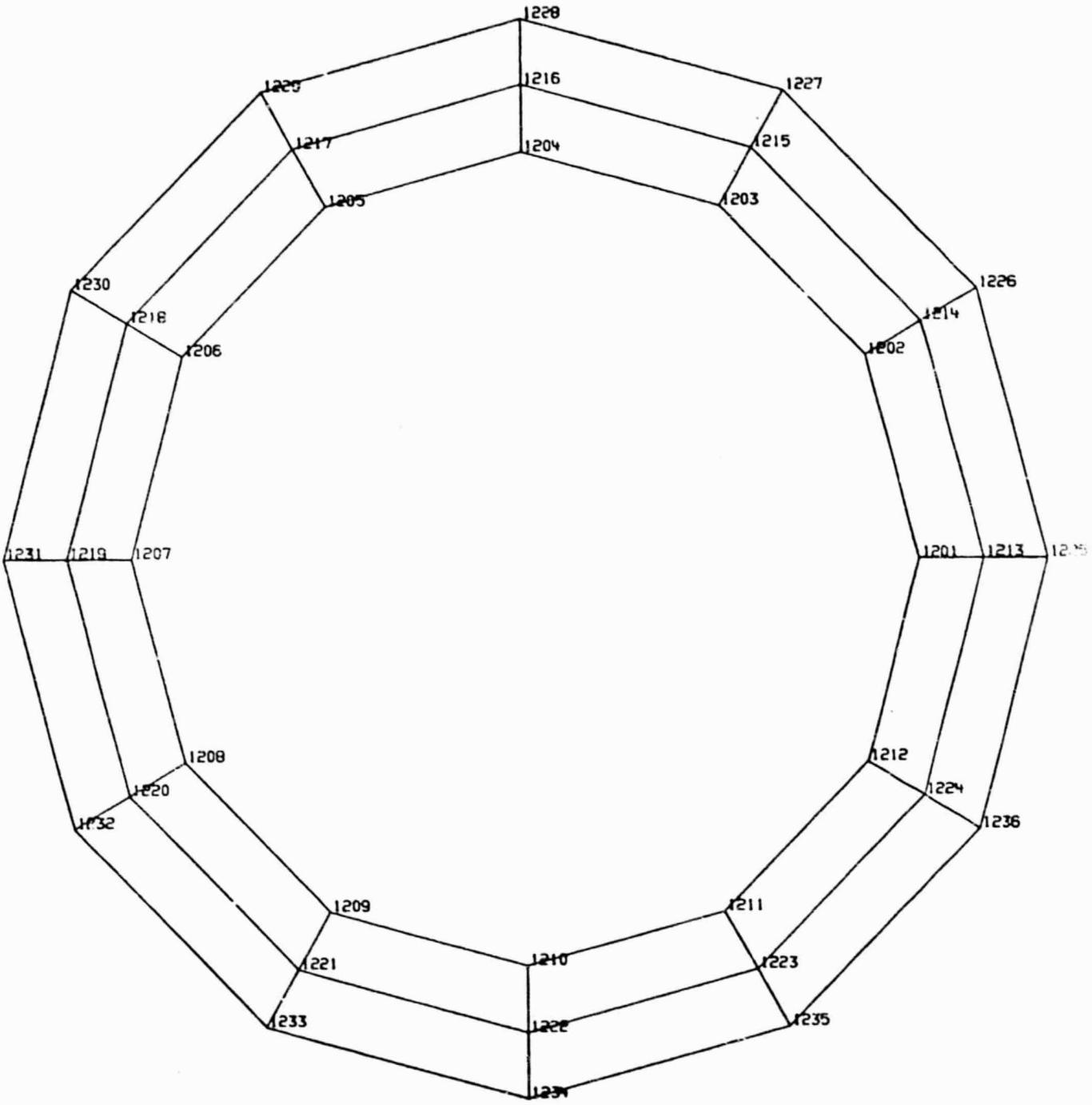

Level 15-1

NOT TO SCALE

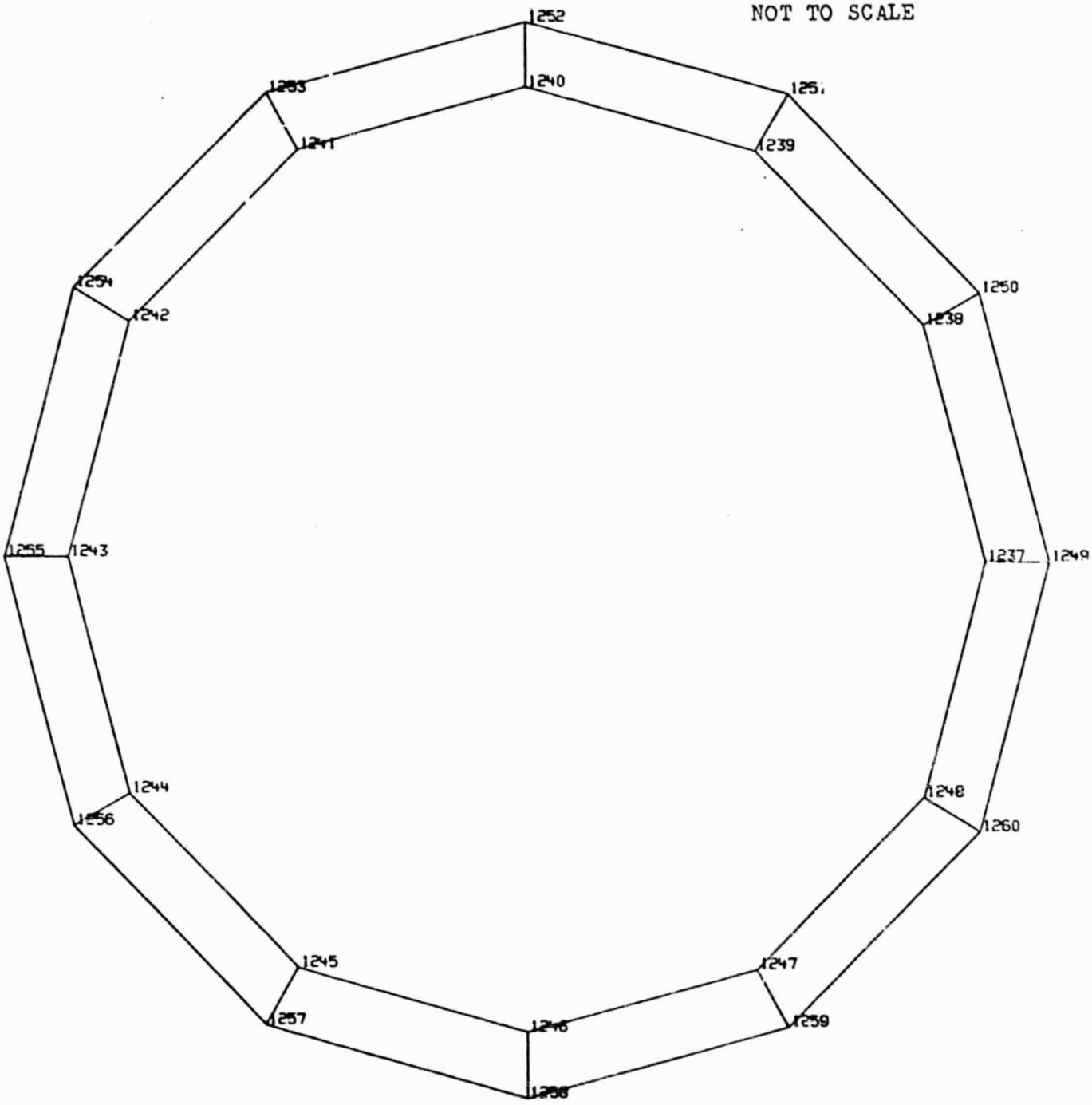

Level 15-2

NOT TO SCALE

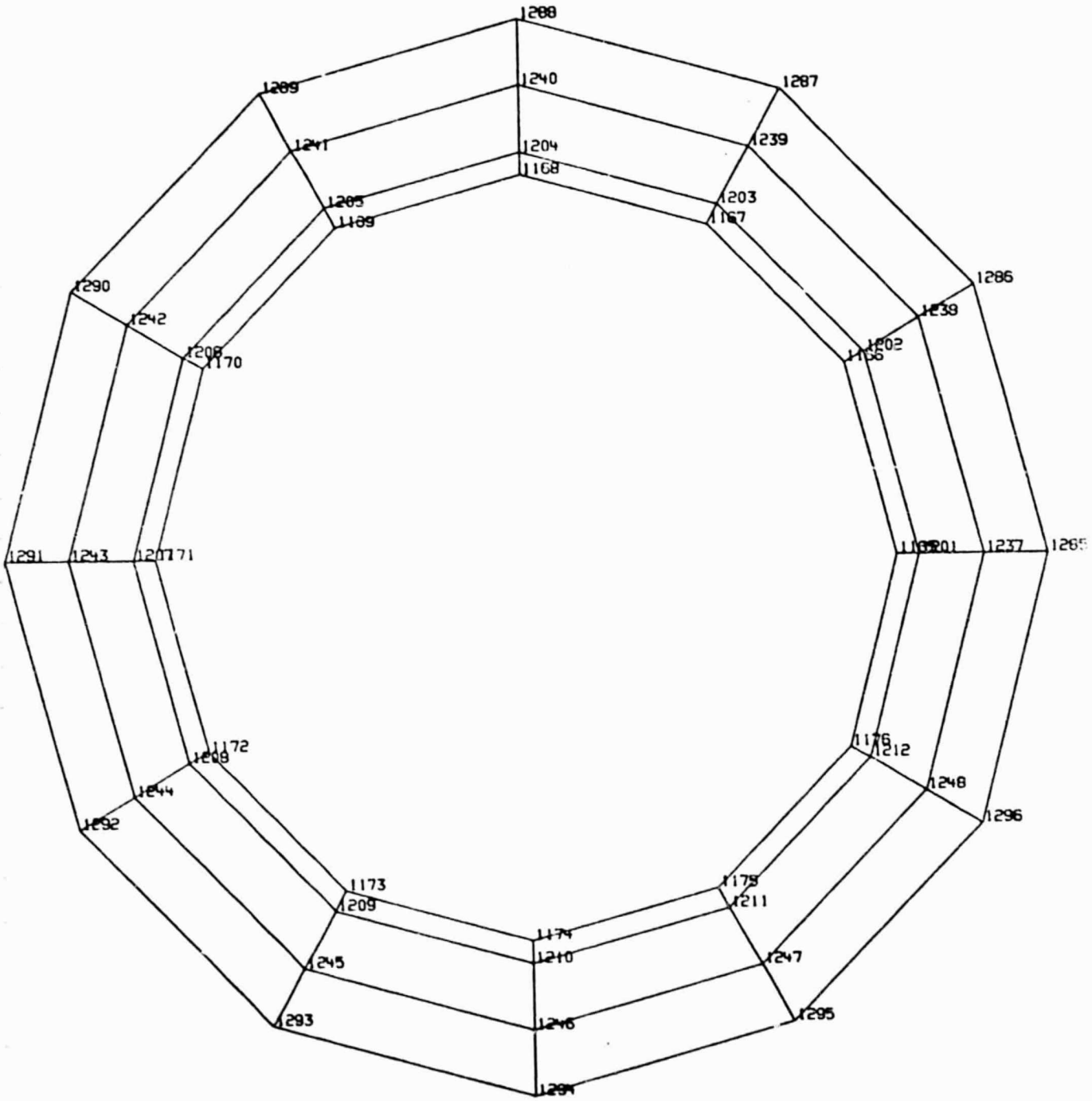

Level 15-3

NOT TO SCALE

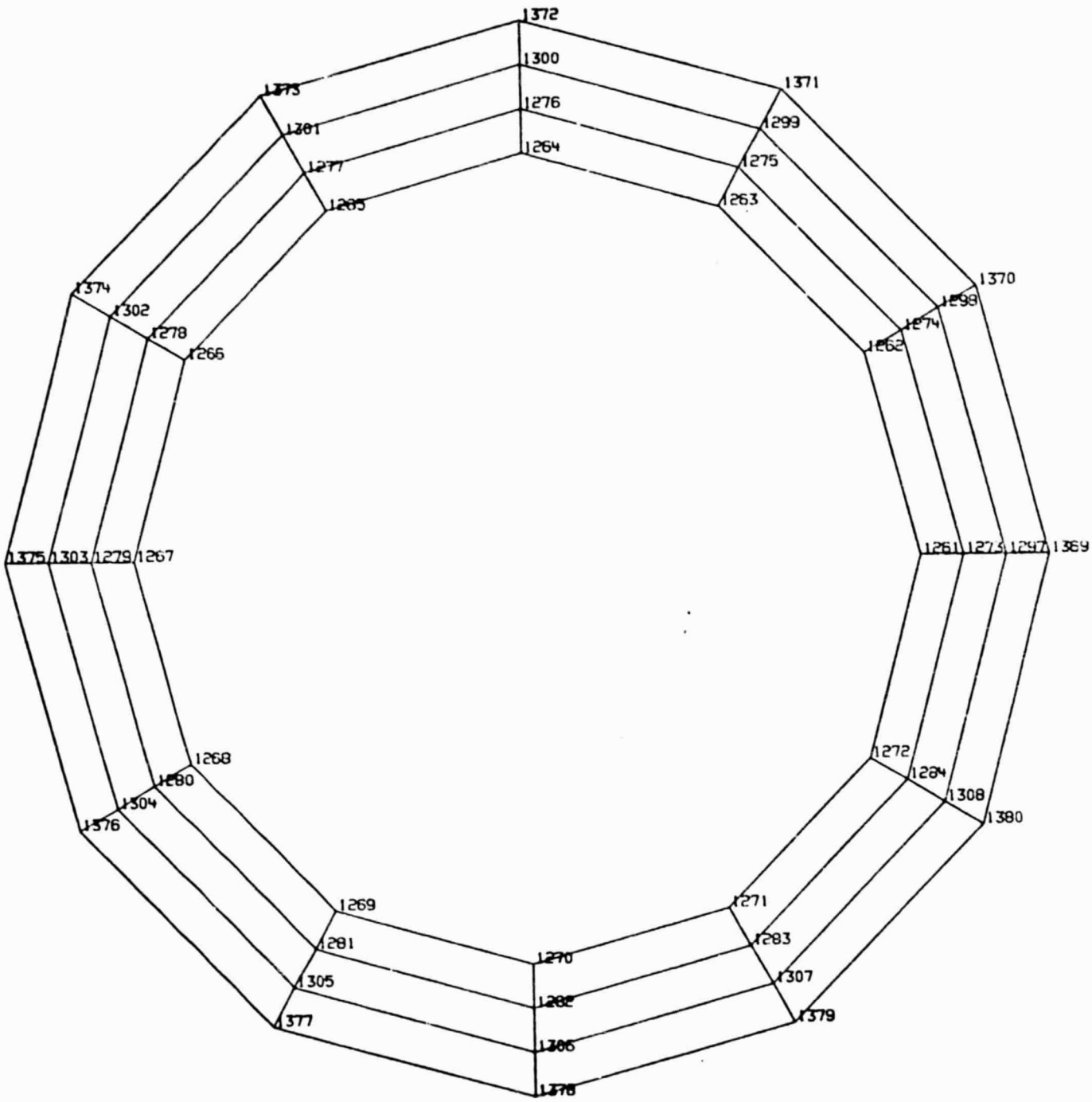

Level 16, 15-4, 5 and 6

NOT TO SCALE

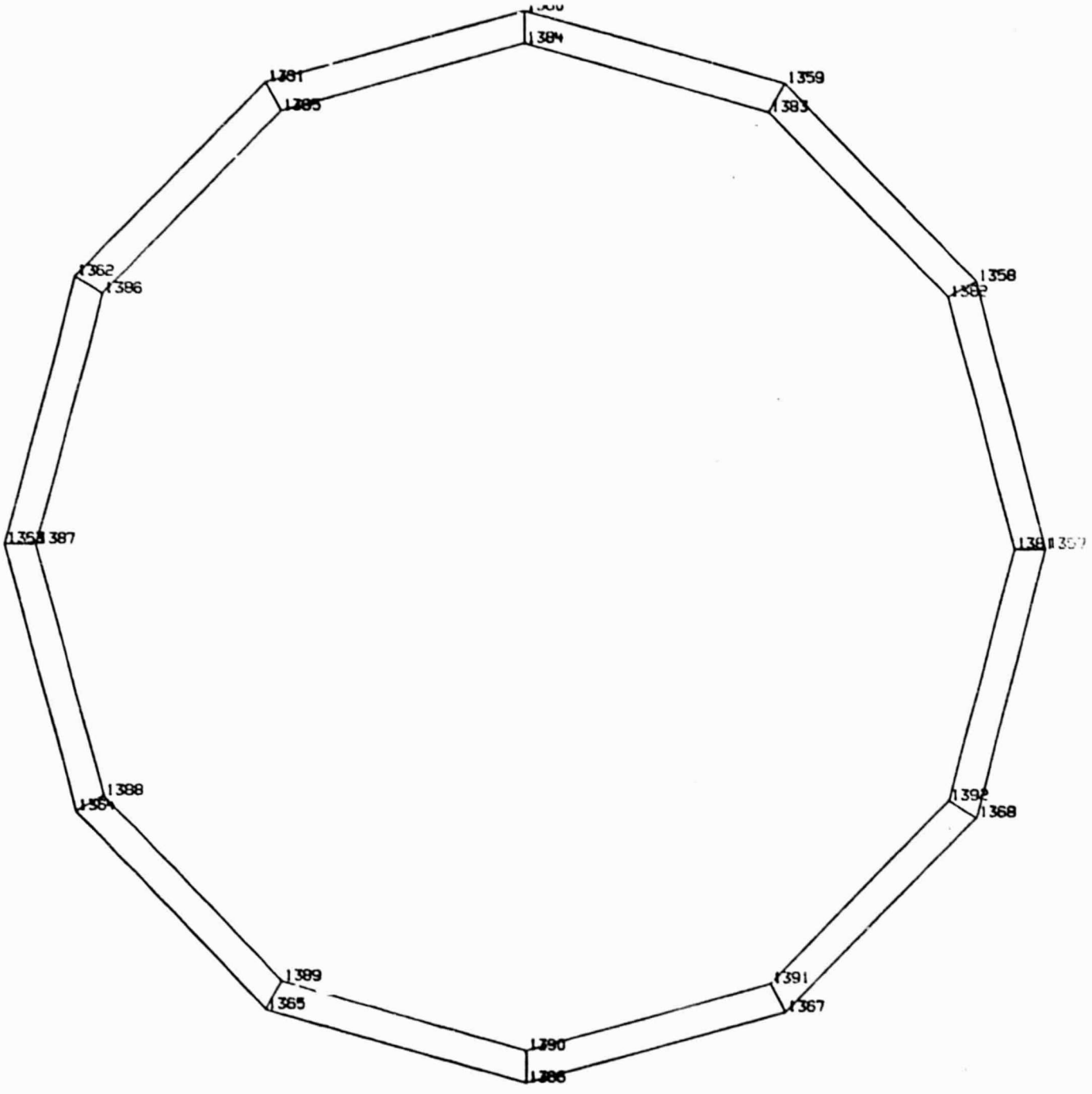

Level 16, 15-7

NOT TO SCALE

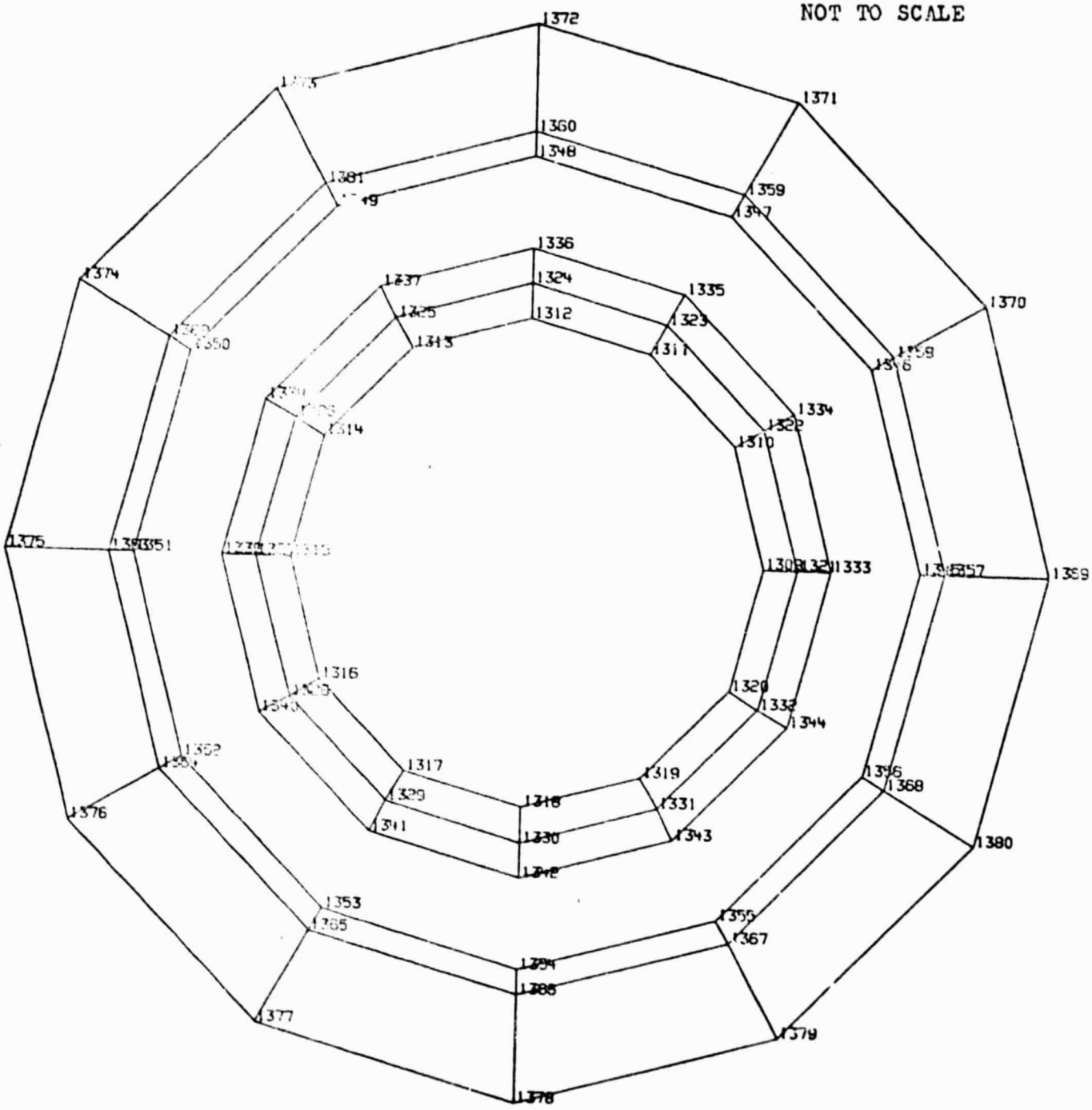

LEVEL 16

NOT TO SCALE

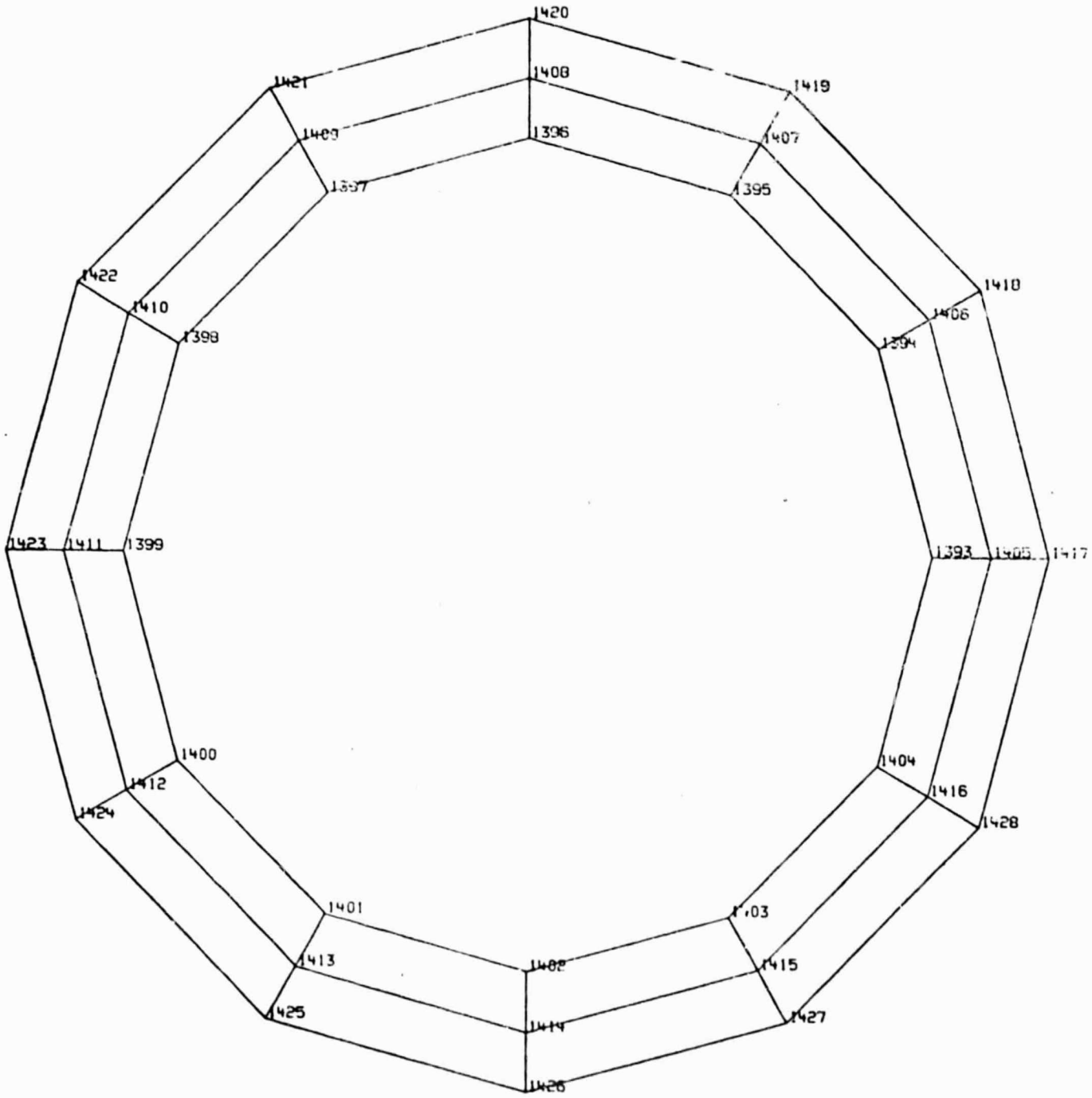

LEVEL 17

NOT TO SCALE

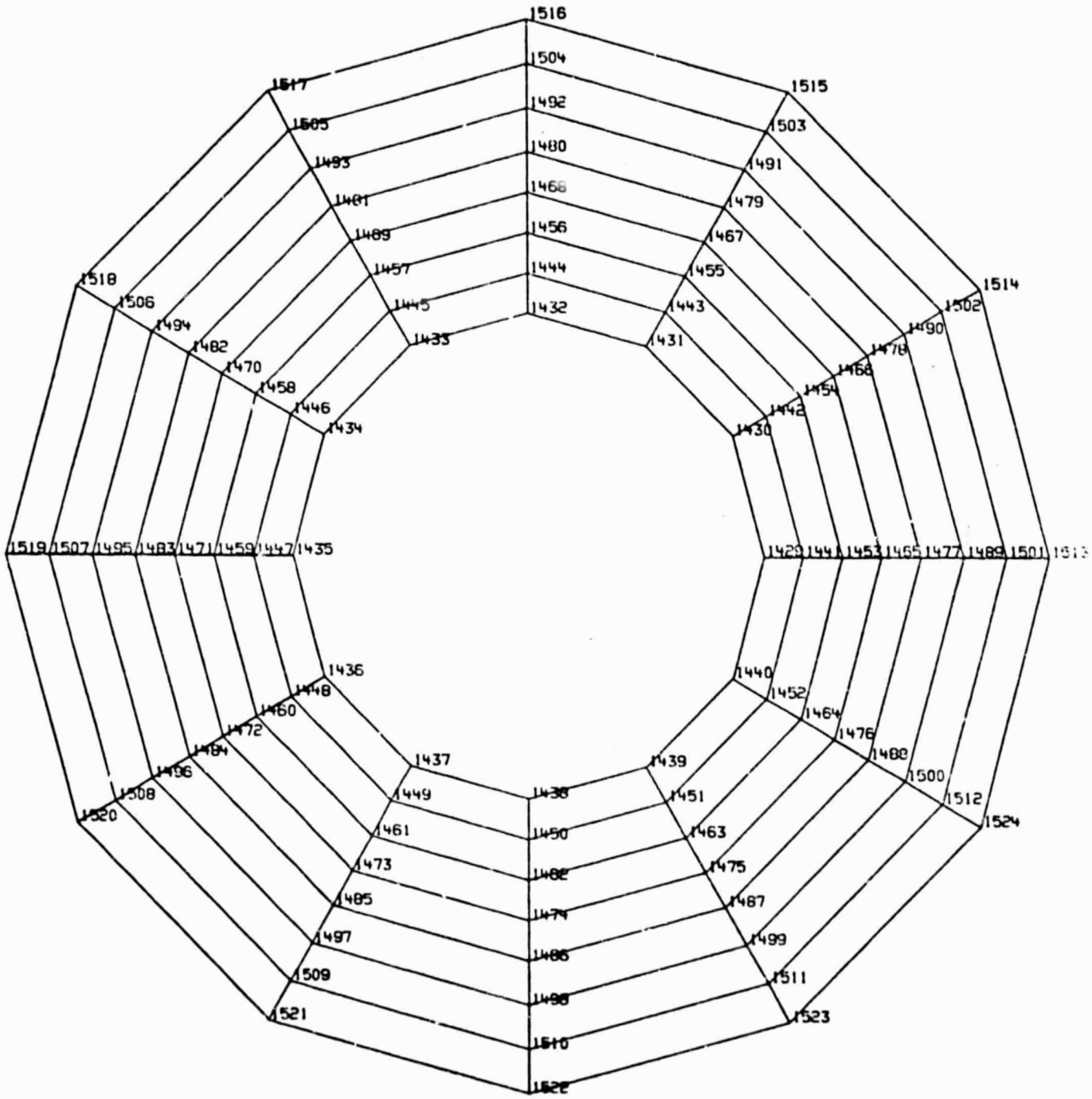

LEVEL 18

NOT TO SCALE

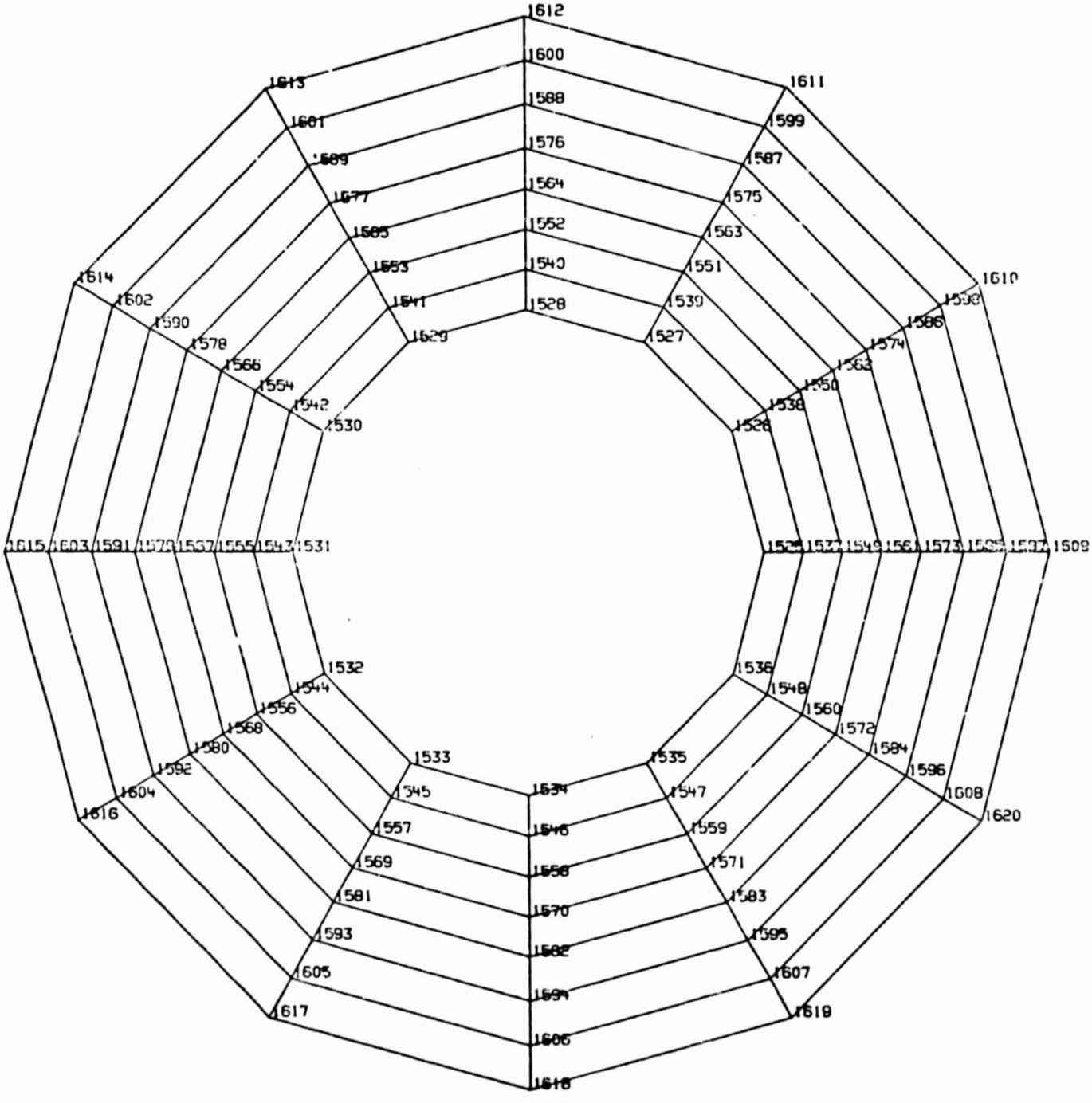

LEVEL 19

NOT TO SCALE

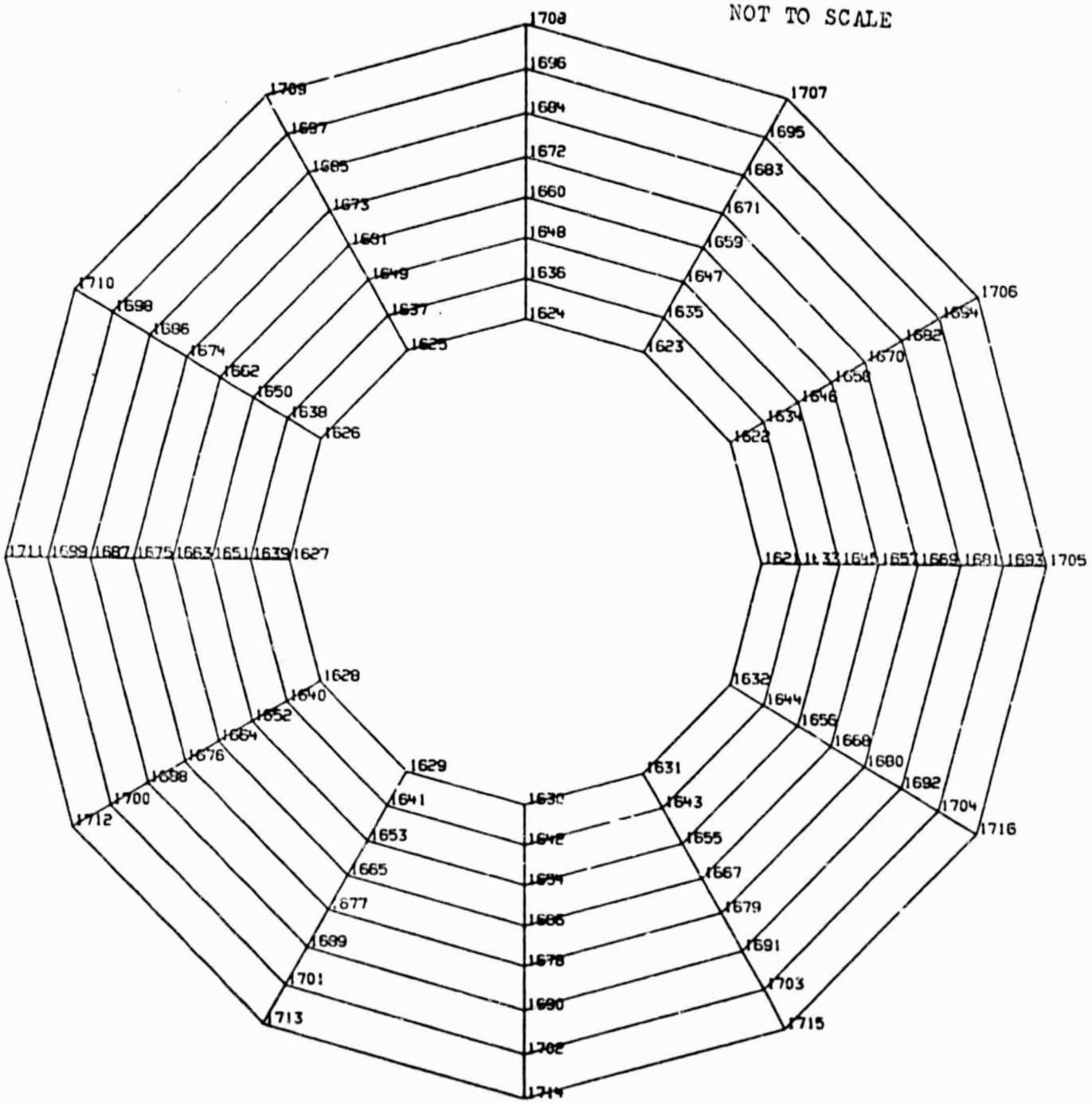

LEVEL 20

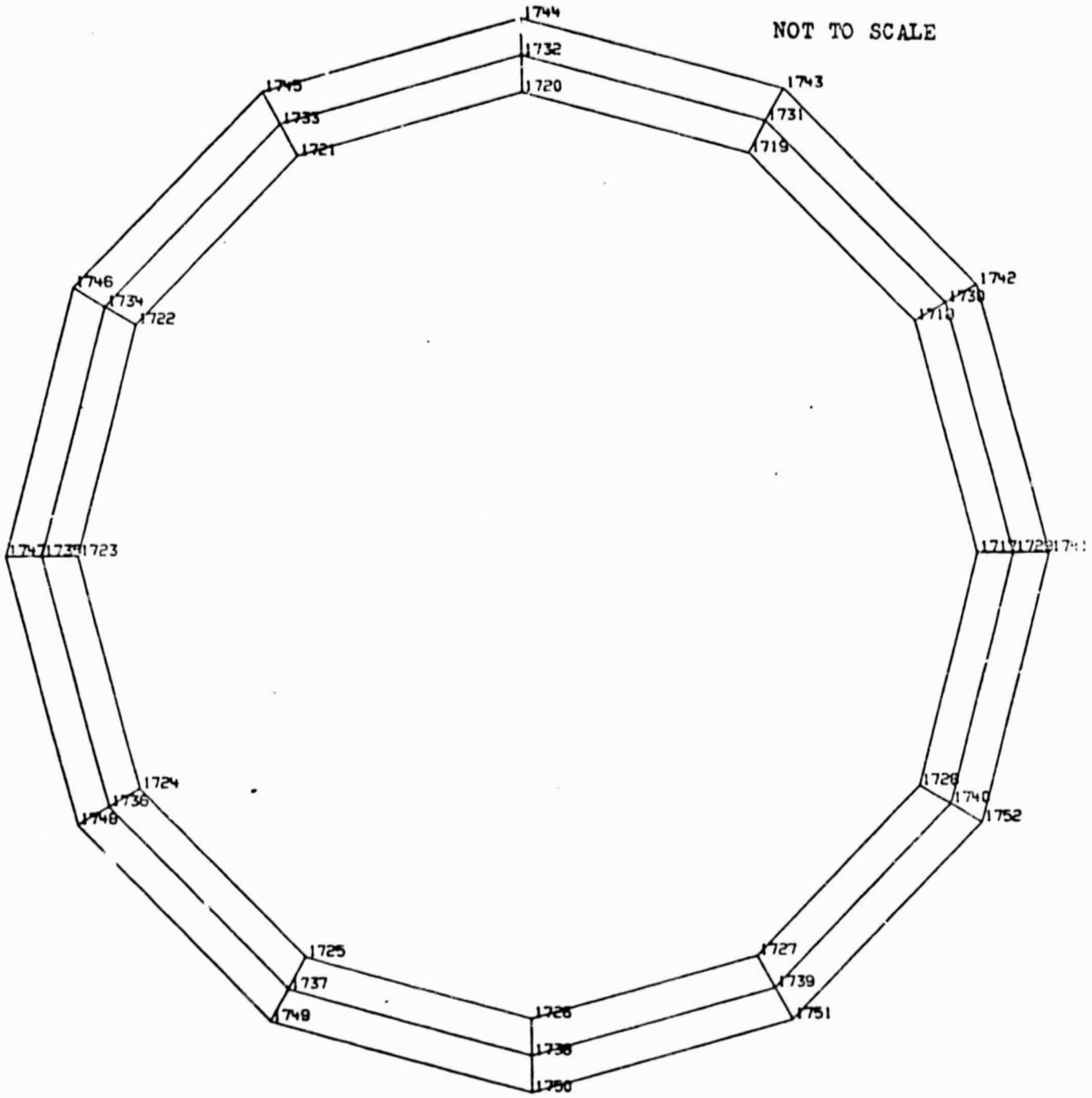
NOT TO SCALE
1744
1732
1720
1743
1731
1719
1745
1733
1721
1742
1730
1718
1746
1734
1722
1747
1735
1723
1717
1729
1741
1724
1736
1748
1728
1740
1752
1725
1737
1749
1727
1739
1751
1726
1738
1750

LEVEL 21

NOT TO SCALE

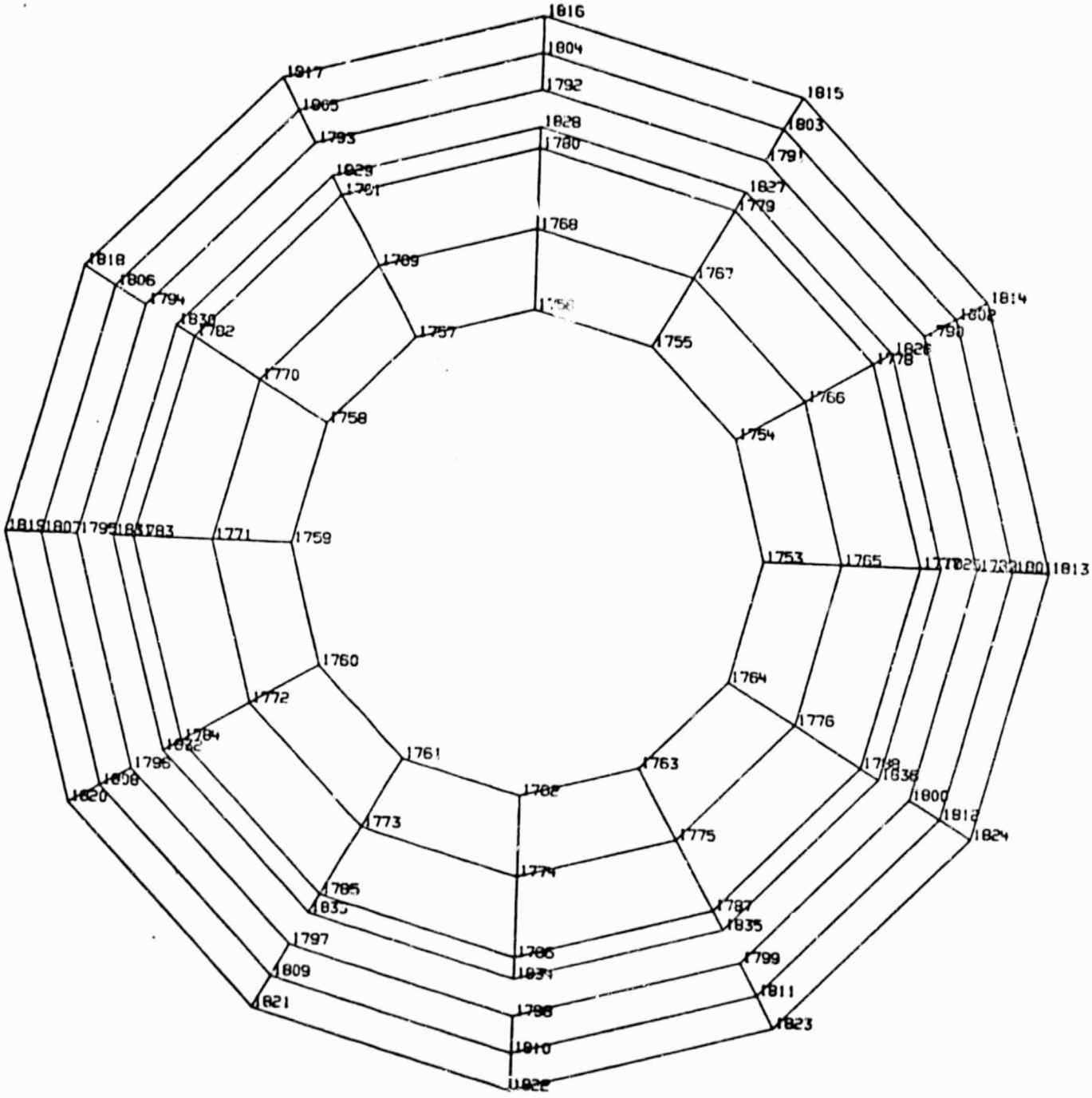

Level 22, 22-1

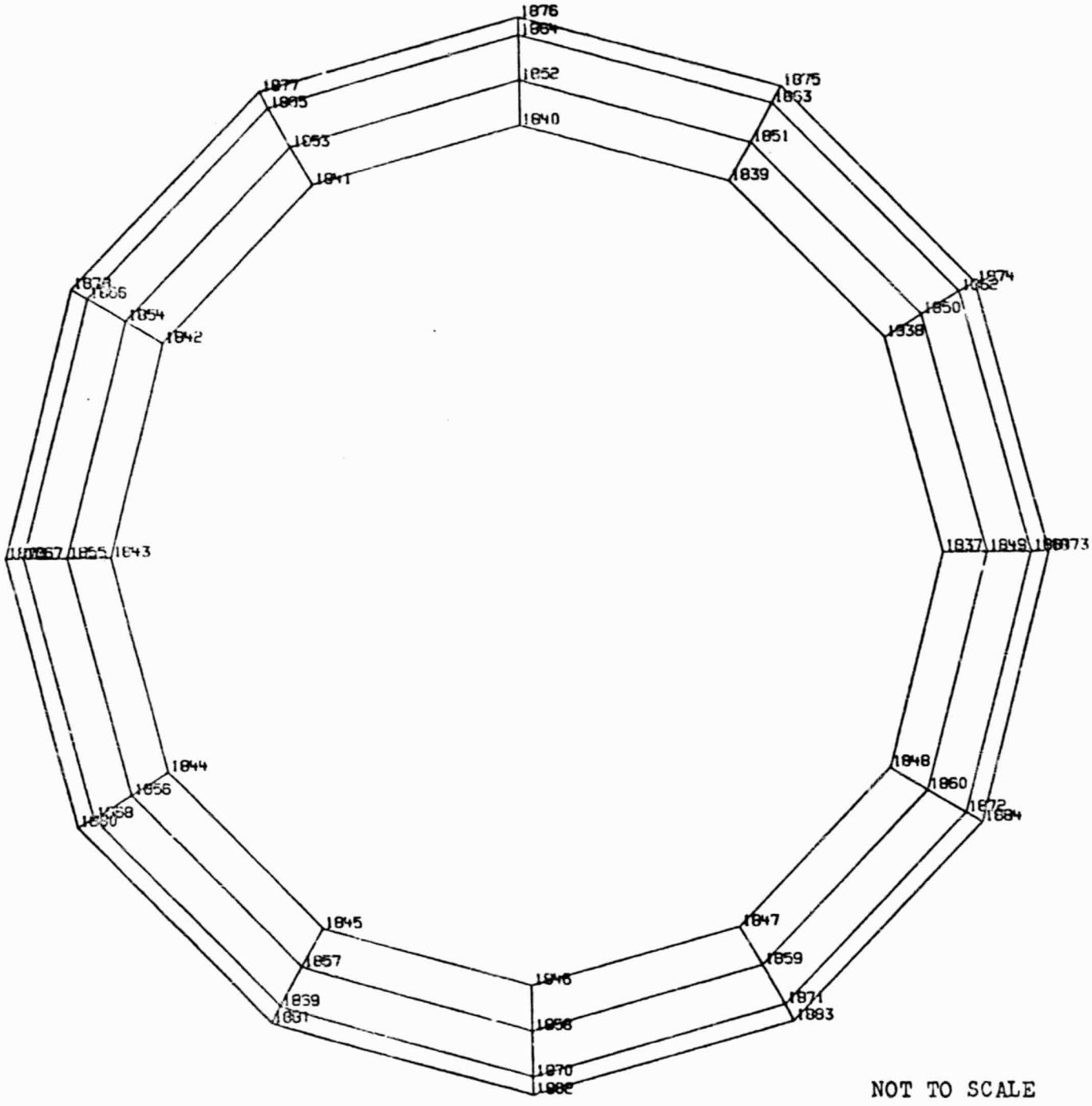

NOT TO SCALE

LEVEL 23

C-2

NOT TO SCALE

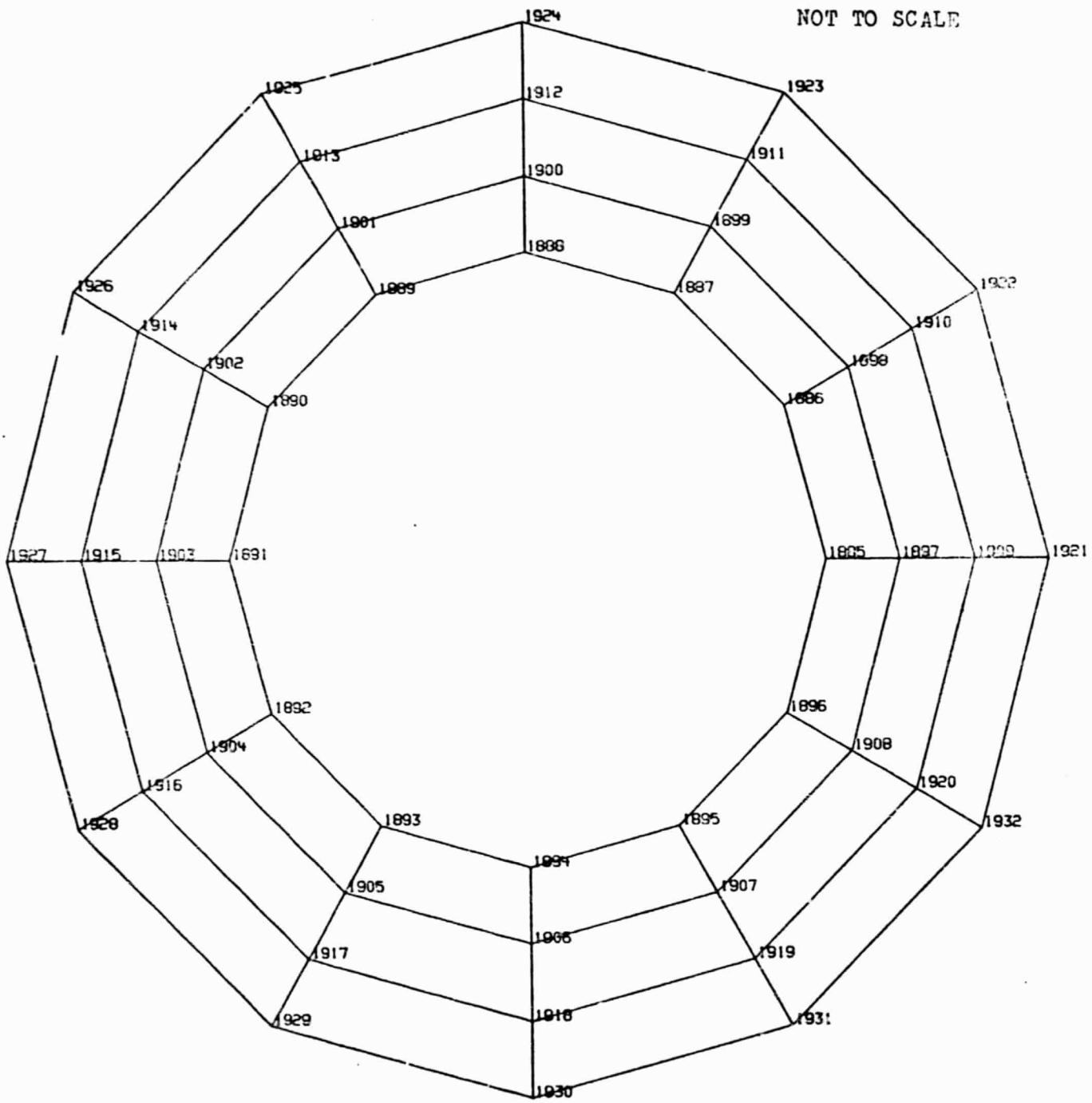

LEVEL 24

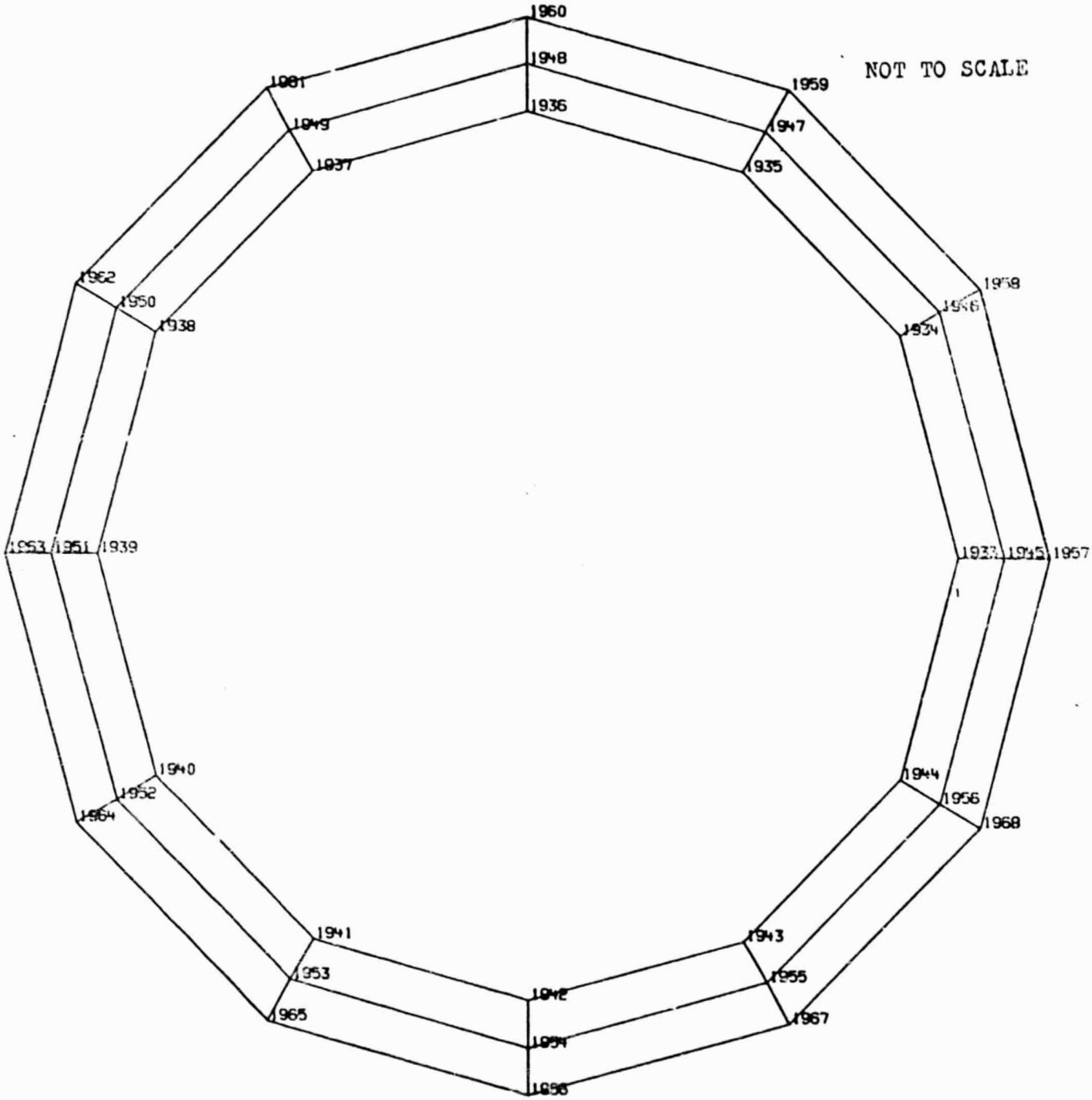
NOT TO SCALE
1960
1948
1936
1959
1947
1935
1961
1949
1937
1962
1950
1938
1958
1946
1934
1953
1951
1939
1957
1945
1933
1940
1952
1964
1944
1956
1968
1941
1953
1965
1943
1955
1967
1942
1954
1966

LEVEL 25

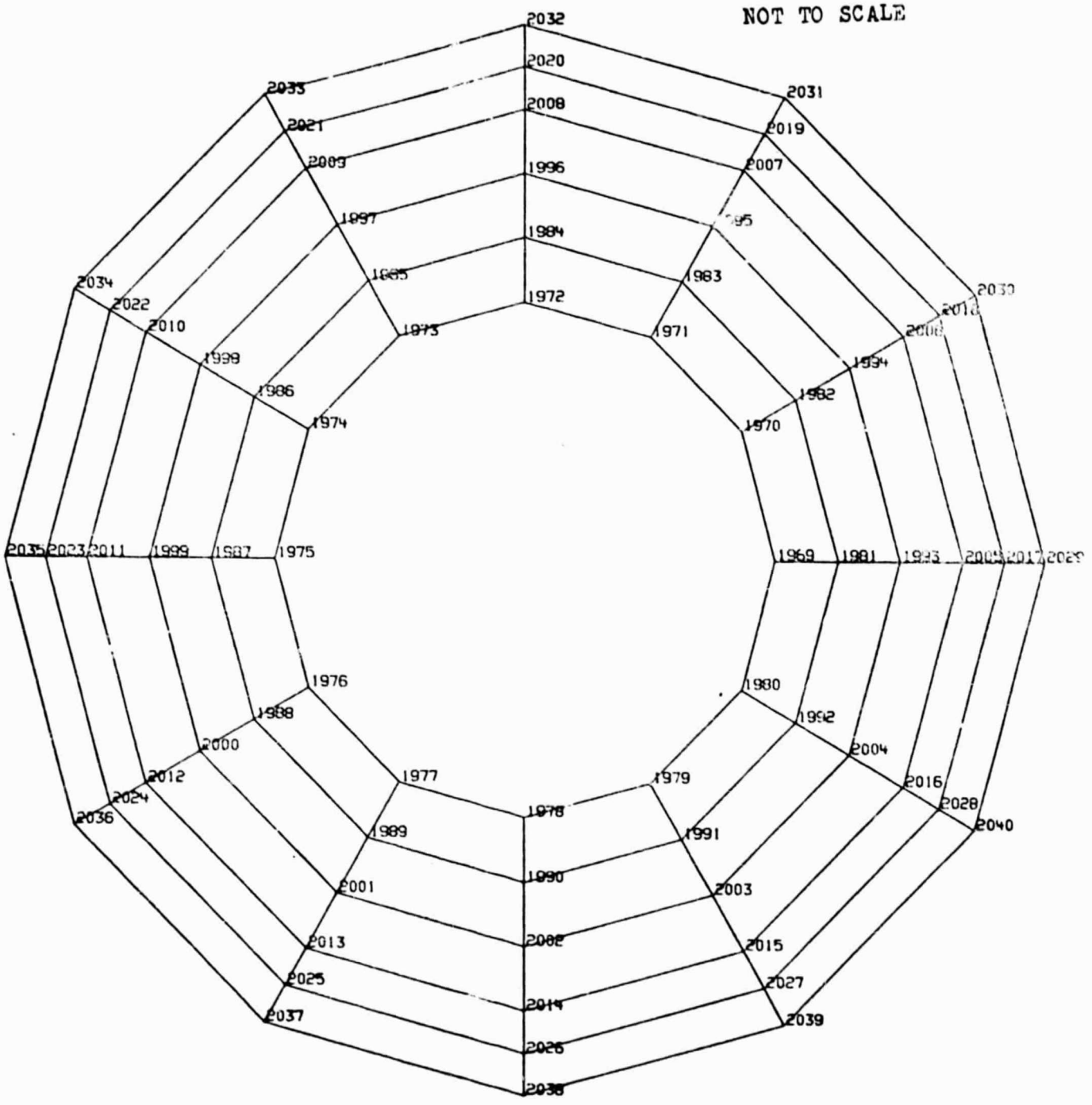
NOT TO SCALE
2032
2020
2008
1996
1984
1972
2031
2019
2007
1995
1983
1971
2030
2018
2006
1994
1982
1970
2029
2017
2005
1993
1981
1969
2028
2016
2004
1992
1980
2027
2015
2003
1991
1979
2026
2014
2002
1990
1978
2025
2013
2001
1989
1977
2024
2012
2000
1988
1976
2023
2011
1999
1987
1975
2022
2010
1998
1986
1974
2021
2009
1997
1985
1973
2040
2039
2038
2037
2036
2035
2034
2033

LEVEL 26

NOT TO SCALE

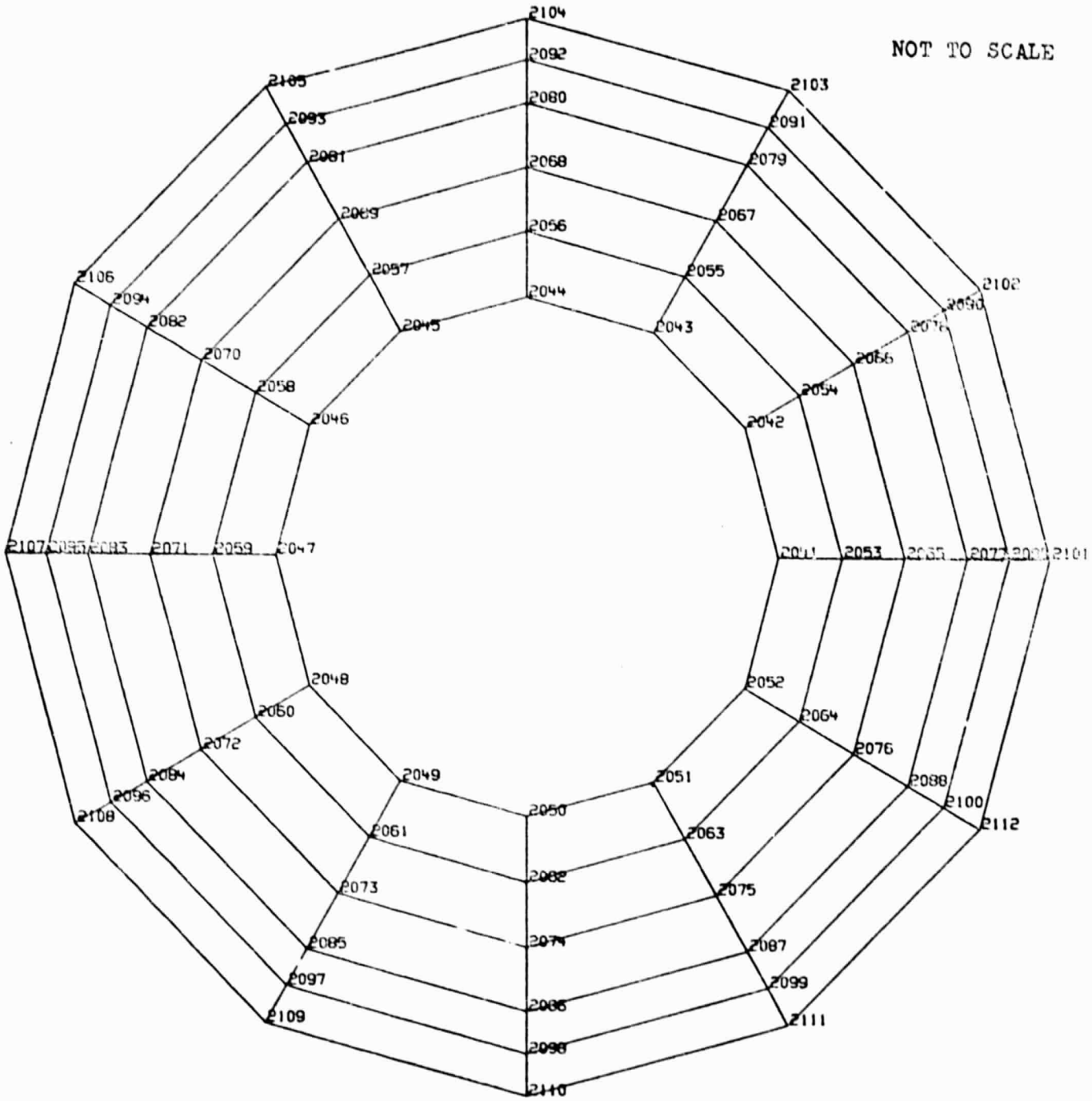

LEVEL 27

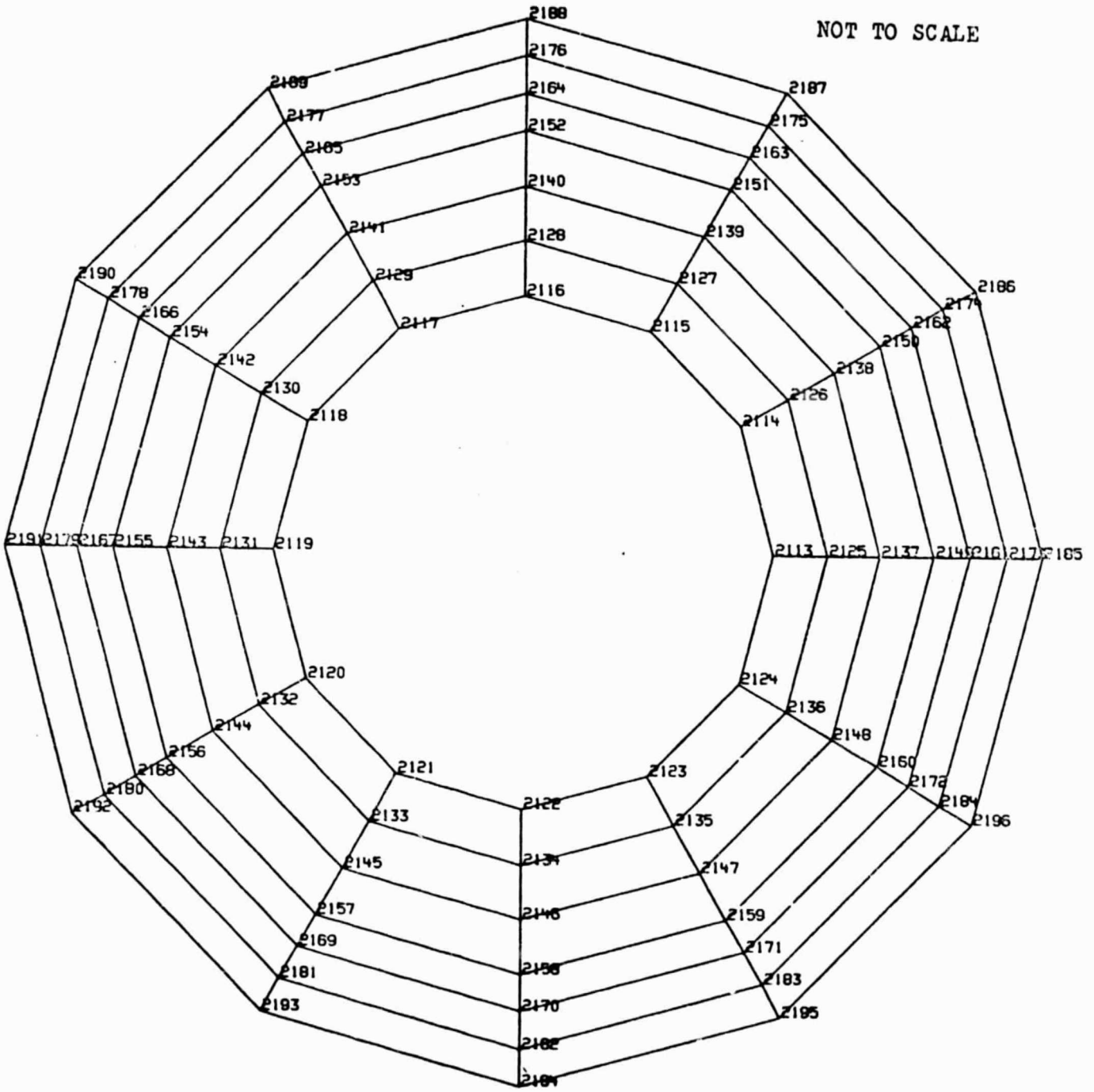
NOT TO SCALE
2188
2176
2164
2152
2140
2128
2116
2187
2175
2163
2151
2139
2127
2115
2186
2174
2162
2150
2138
2126
2114
2113
2125
2137
2149
2161
2173
2185
2196
2184
2172
2160
2148
2136
2124
2123
2135
2147
2159
2171
2183
2195
2182
2170
2158
2146
2134
2122
2121
2133
2145
2157
2169
2181
2193
2120
2132
2144
2156
2168
2180
2192
2119
2131
2143
2155
2167
2179
2191
2118
2130
2142
2154
2166
2178
2190
2117
2129
2141
2153
2165
2177
2189

LEVEL 28

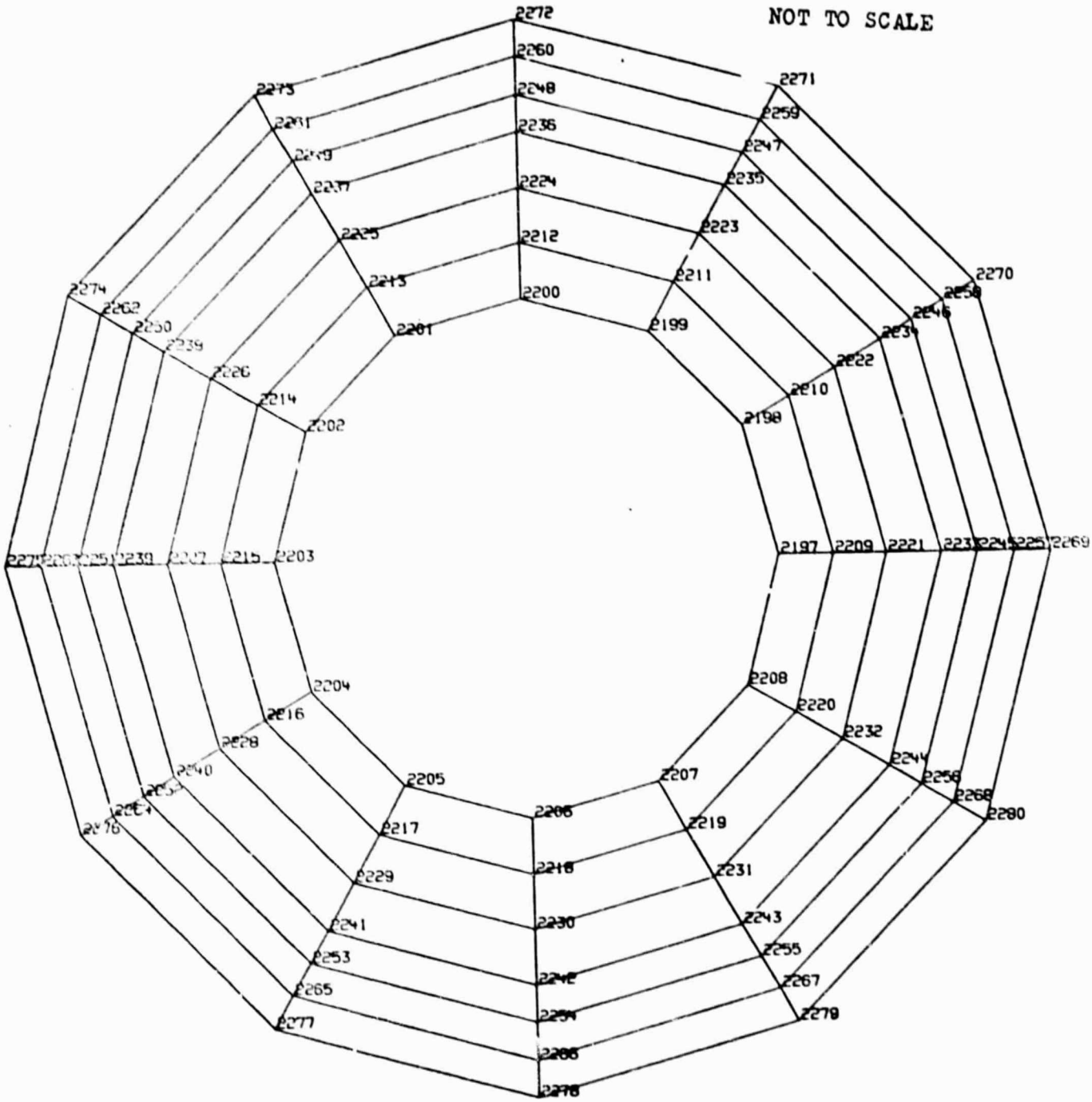
NOT TO SCALE
2272
2260
2248
2236
2224
2212
2200
2271
2259
2247
2235
2223
2211
2199
2270
2258
2246
2234
2222
2210
2198
2269
2257
2245
2233
2221
2209
2197
2268
2256
2244
2232
2220
2208
2280
2267
2255
2243
2231
2219
2207
2279
2266
2254
2242
2230
2218
2206
2278
2265
2253
2241
2229
2217
2205
2277
2264
2252
2240
2228
2216
2204
2276
2263
2251
2239
2227
2215
2203
2274
2262
2250
2238
2226
2214
2202
2273
2261
2249
2237
2225
2213
2201

LEVEL 29

NOT TO SCALE

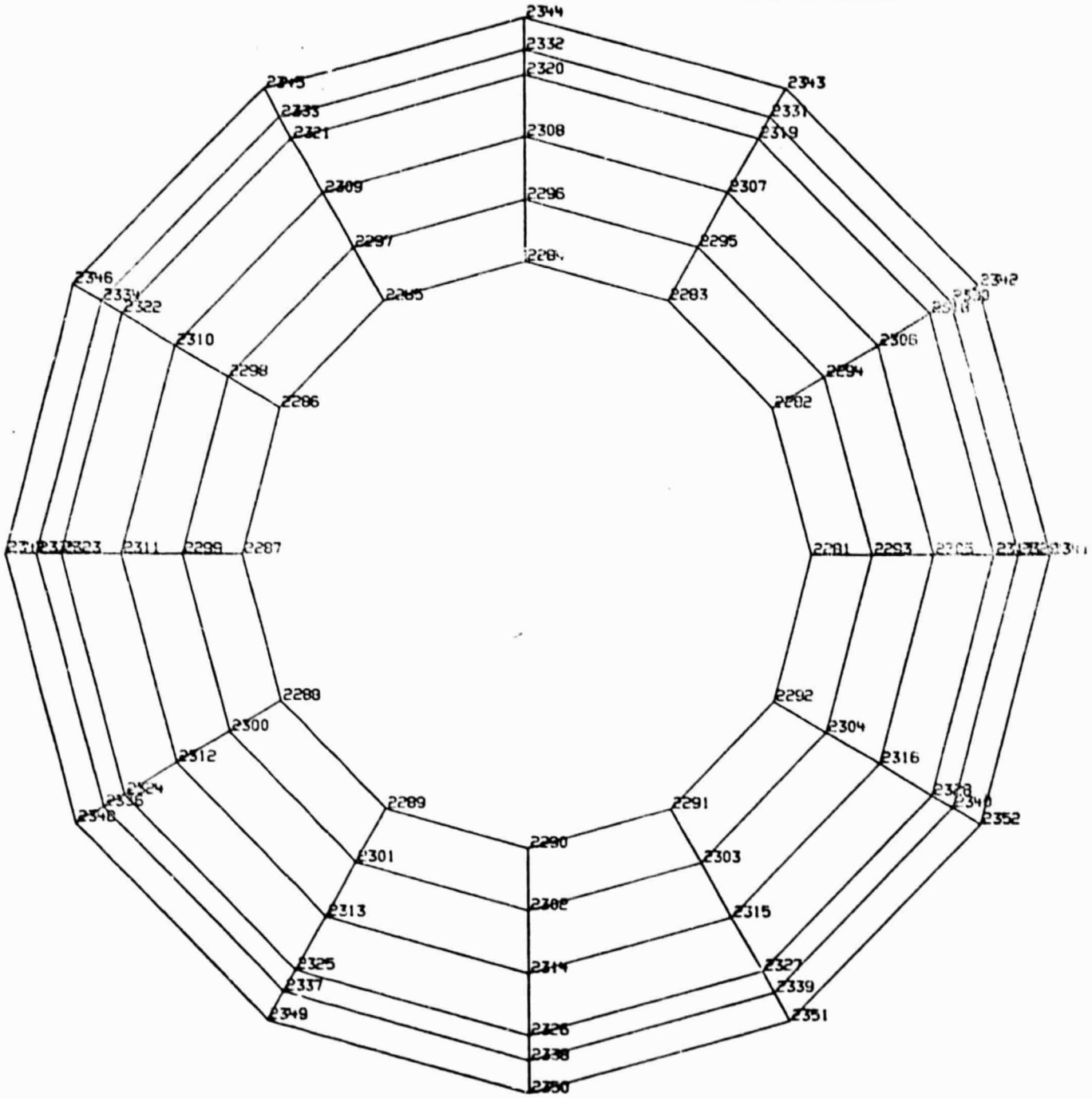

LEVEL 30

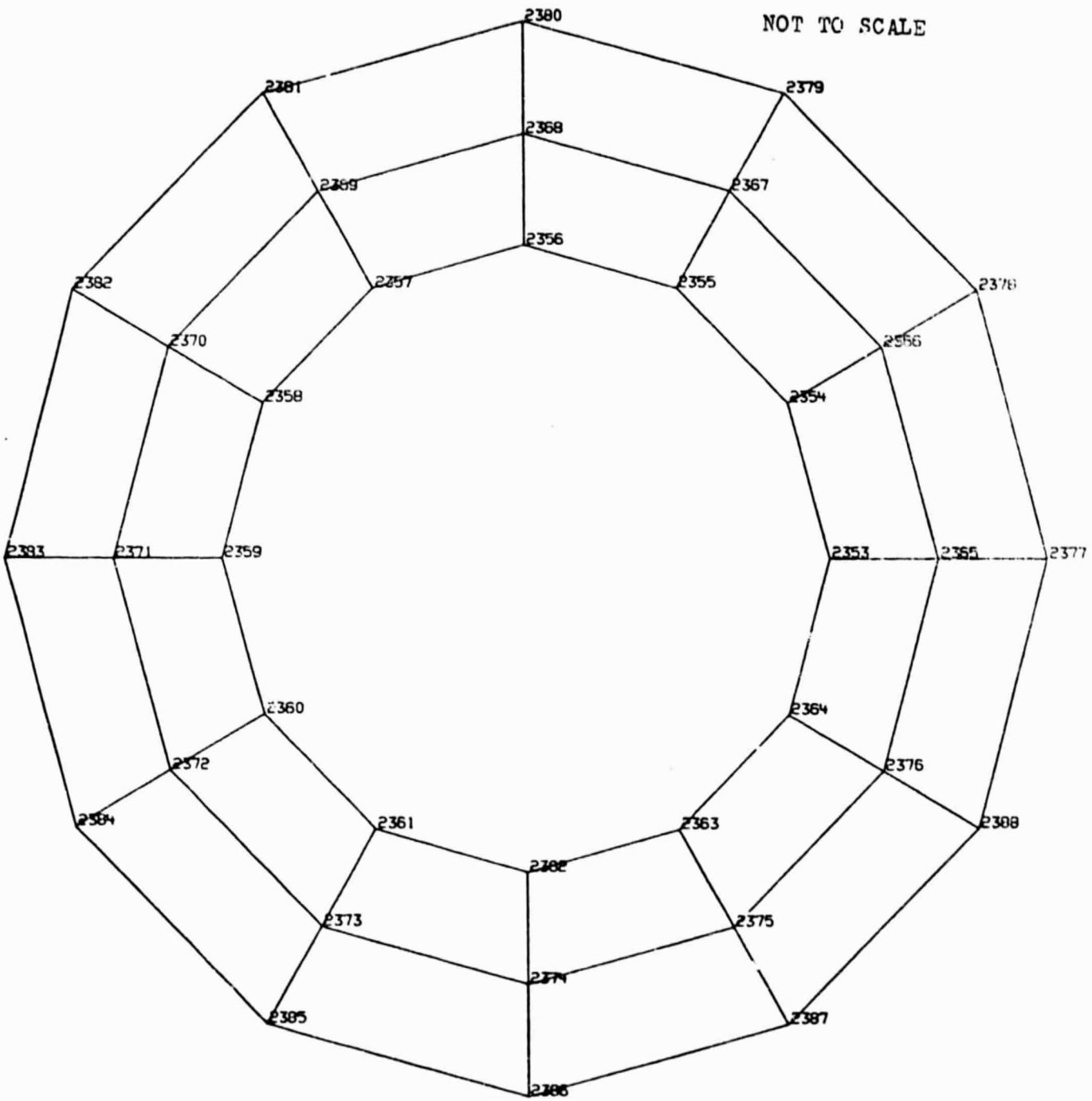
NOT TO SCALE
2380
2379
2381
2368
2367
2369
2356
2355
2357
2382
2378
2370
2366
2358
2354
2383
2371
2359
2353
2365
2377
2360
2364
2372
2376
2384
2361
2363
2308
2362
2373
2375
2374
2385
2387
2386

LEVEL 31

NOT TO SCALE

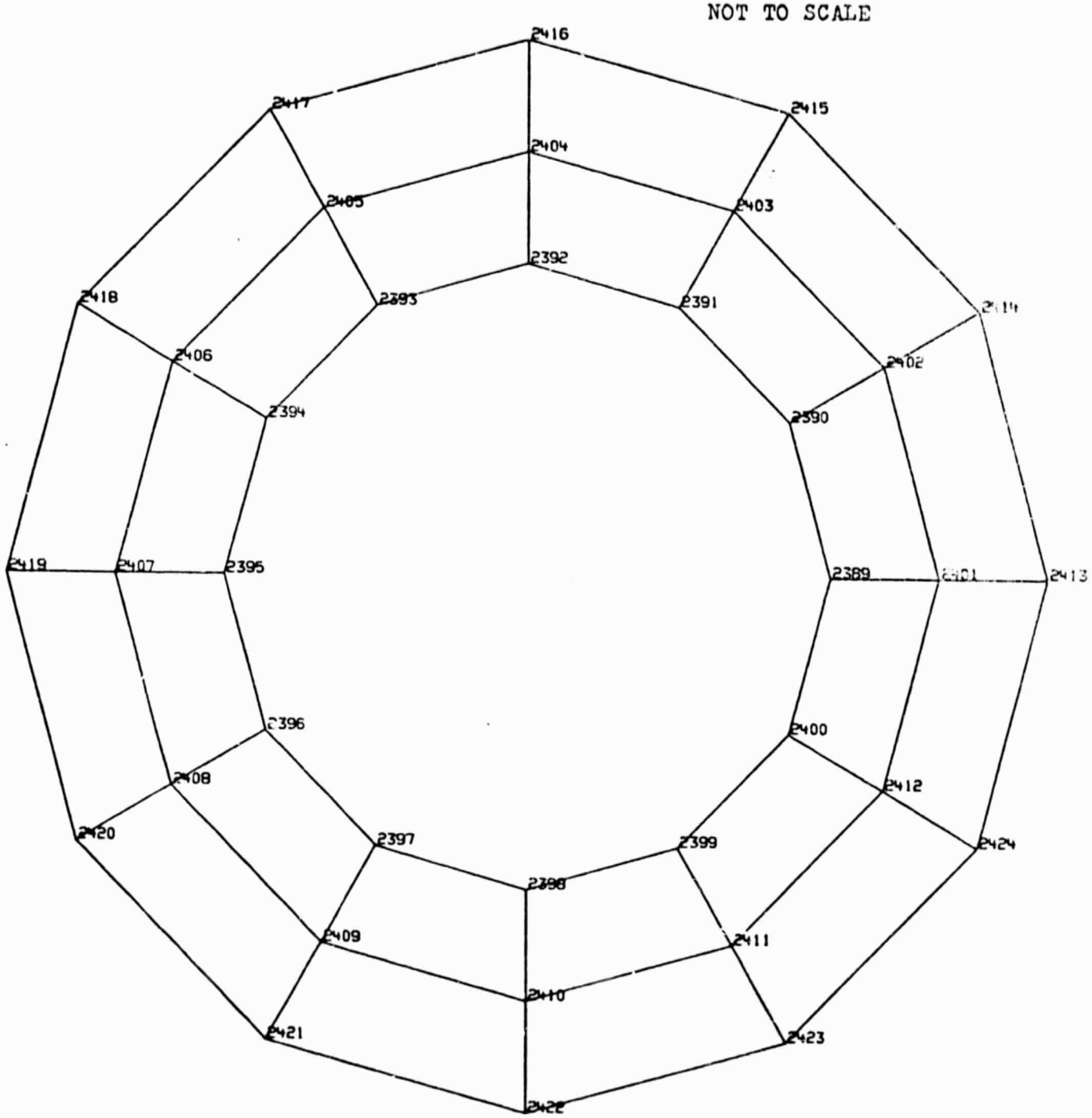

LEVEL 32

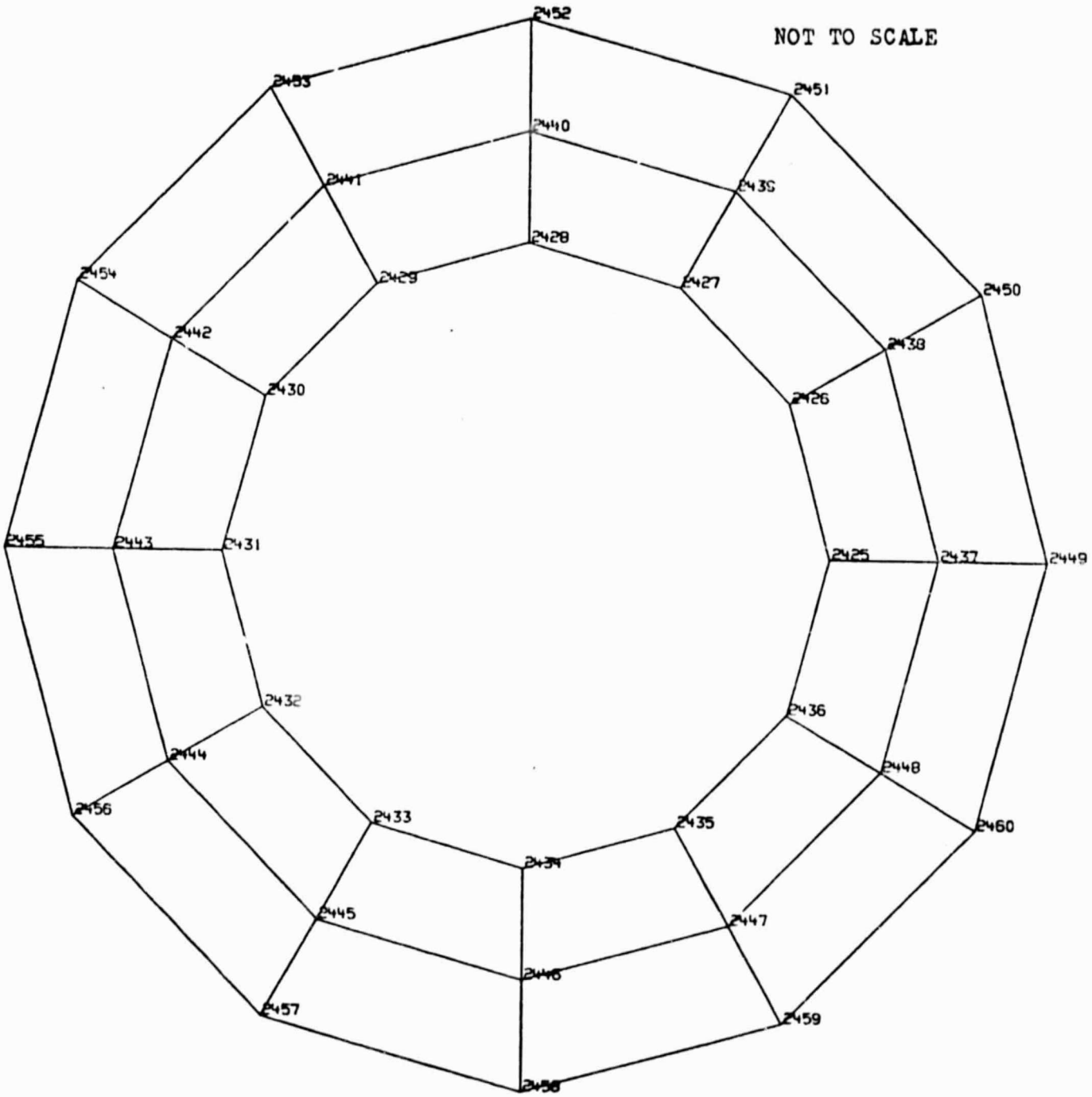
NOT TO SCALE
2452
2453
2451
2440
2441
2439
2428
2429
2427
2454
2450
2442
2438
2430
2426
2455
2443
2431
2425
2437
2449
2432
2436
2444
2448
2456
2433
2435
2460
2434
2445
2447
2446
2457
2459
2458

LEVEL 33

NOT TO SCALE

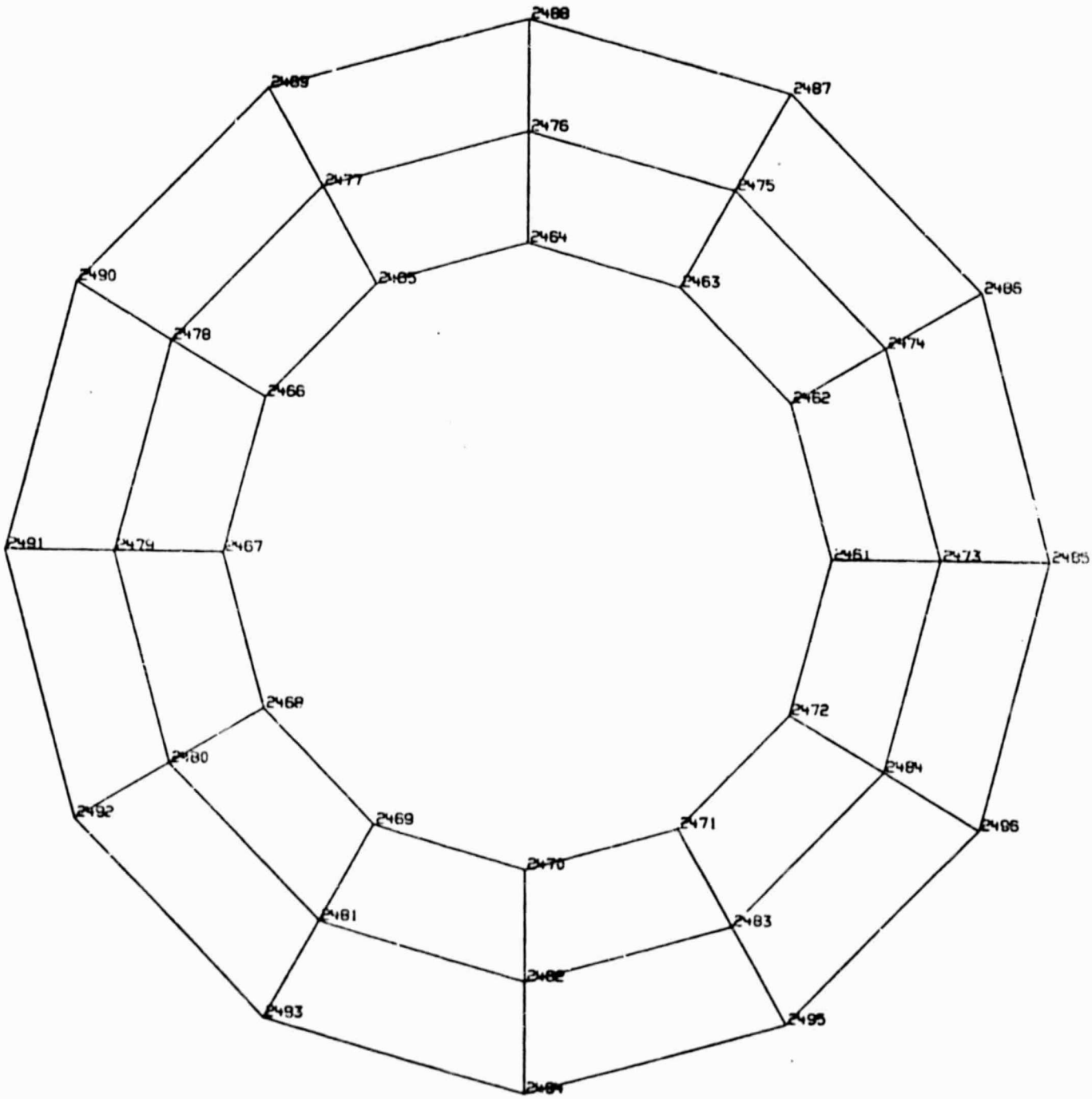

LEVEL 34

ORIGINAL PAGE IS
OF POOR QUALITY

NOT TO SCALE

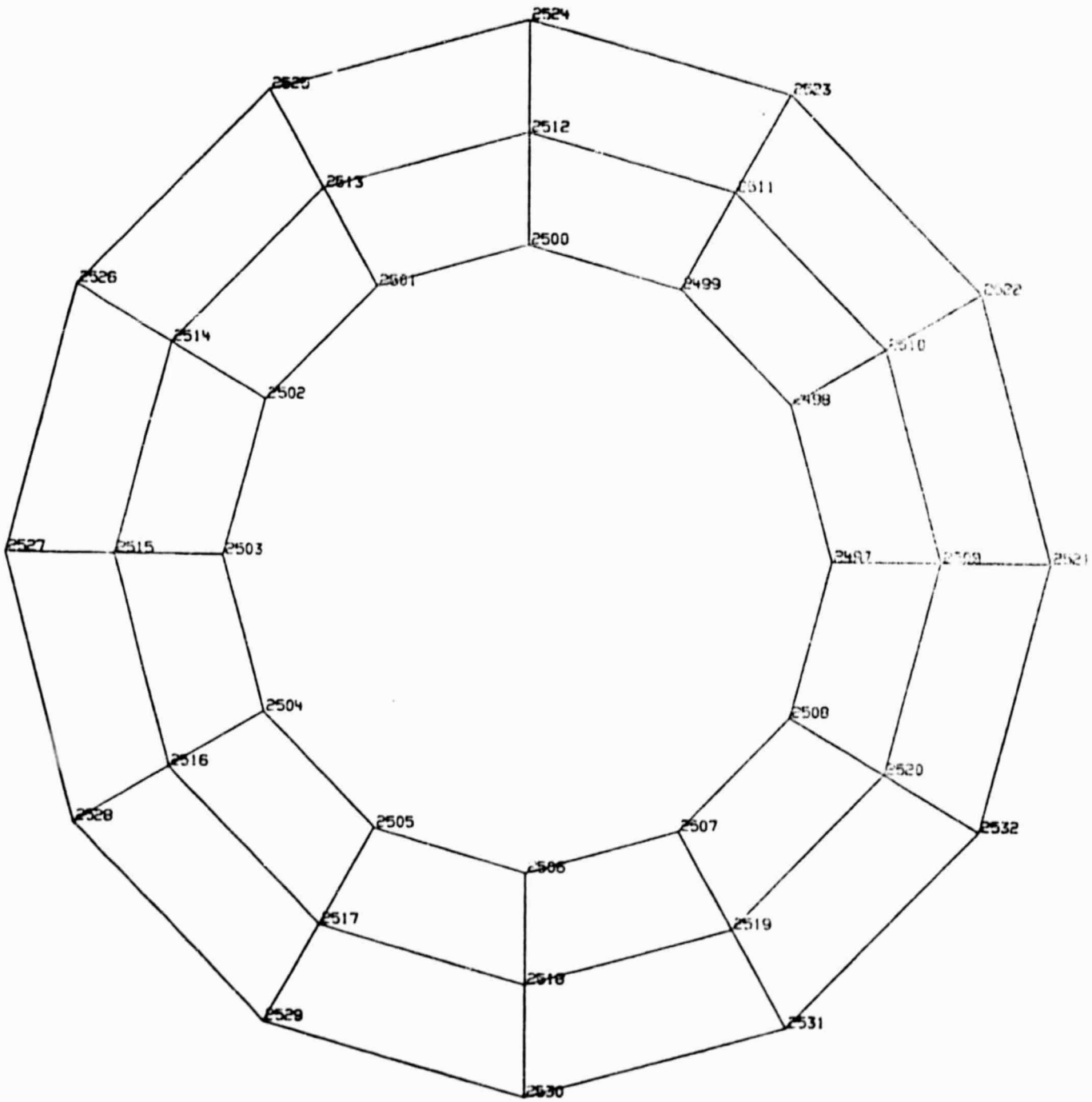

LEVEL 35

NOT TO SCALE

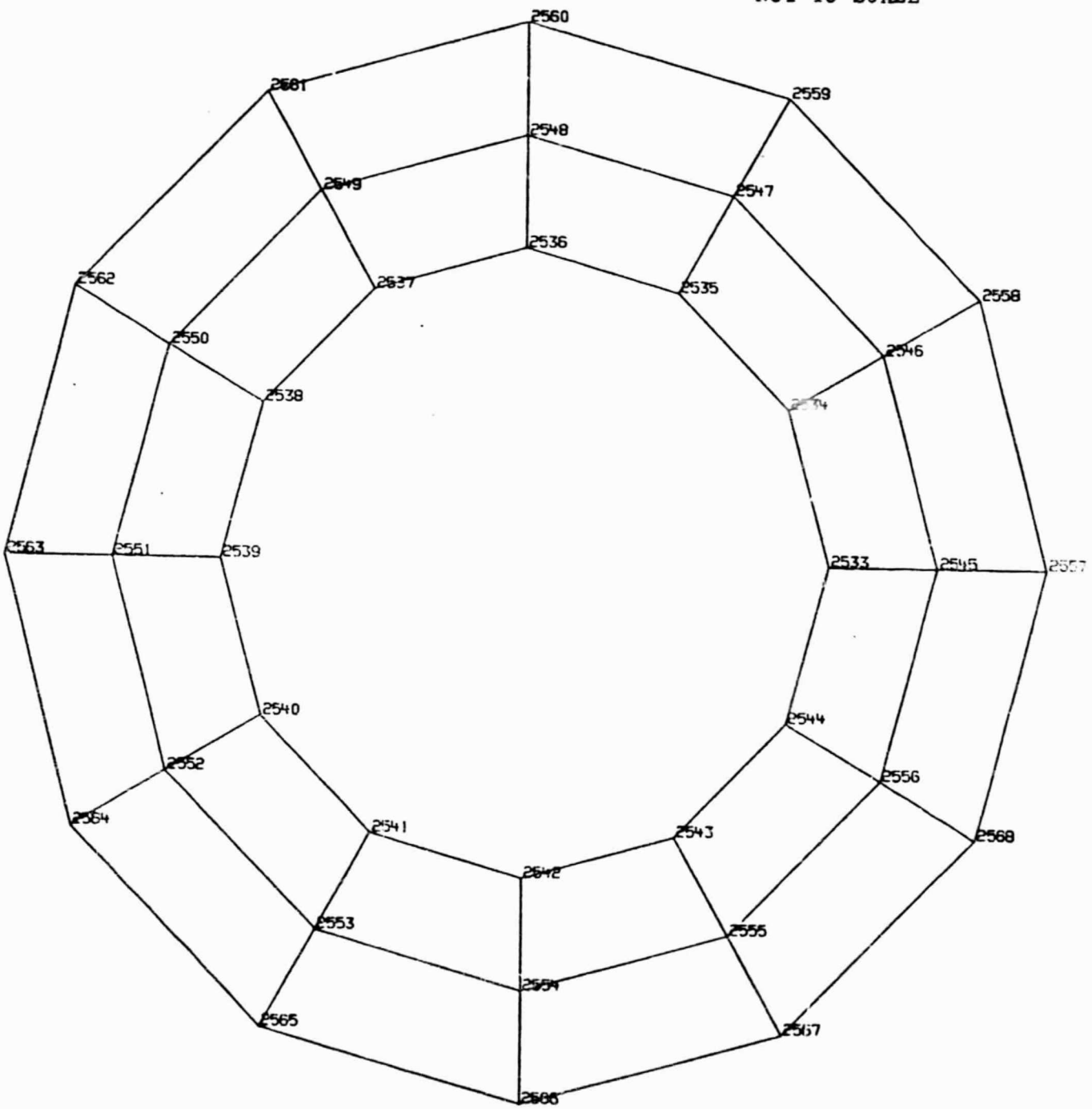

LEVEL 36

NOT TO SCALE

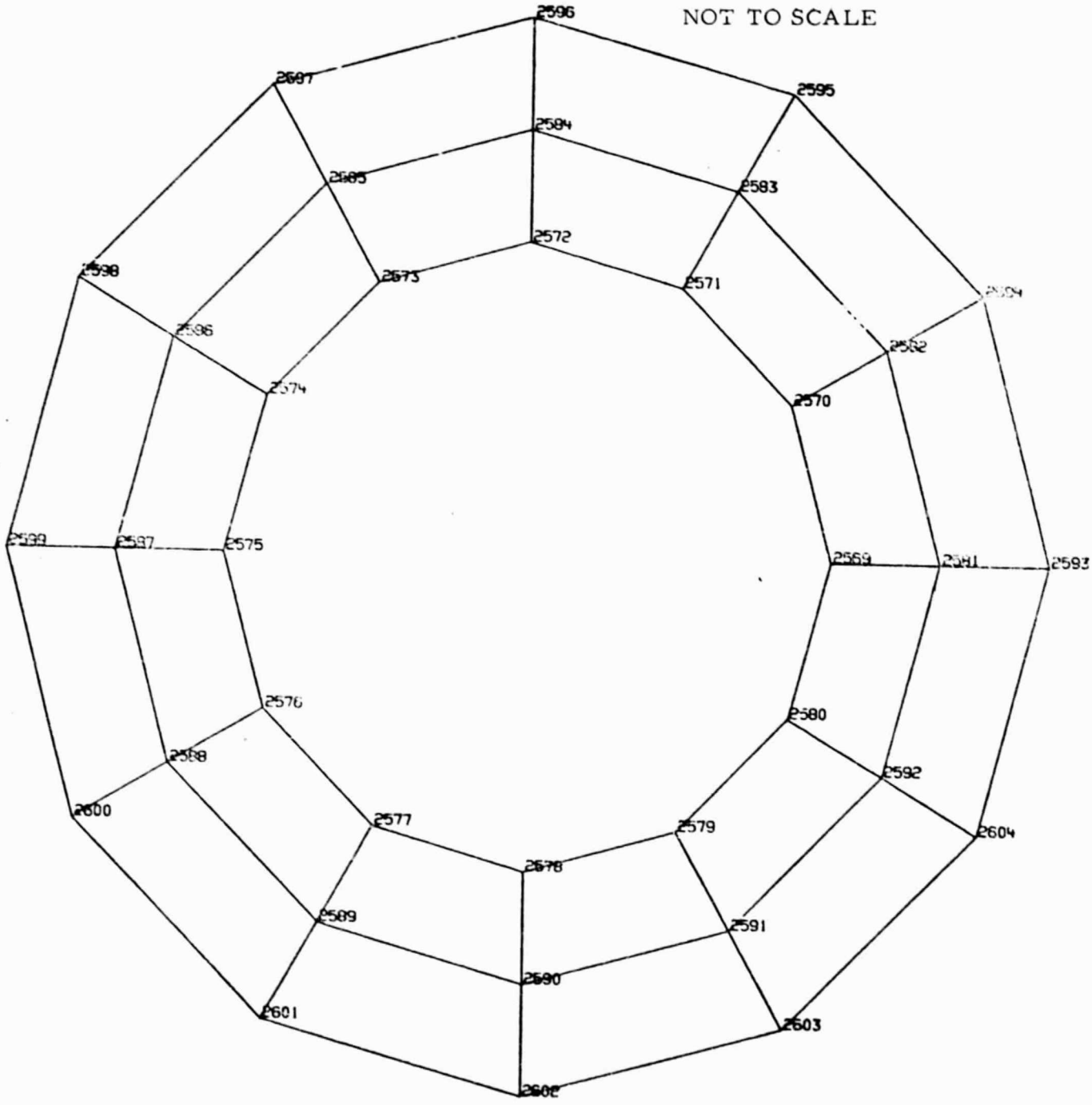

LEVEL 37

NOT TO SCALE

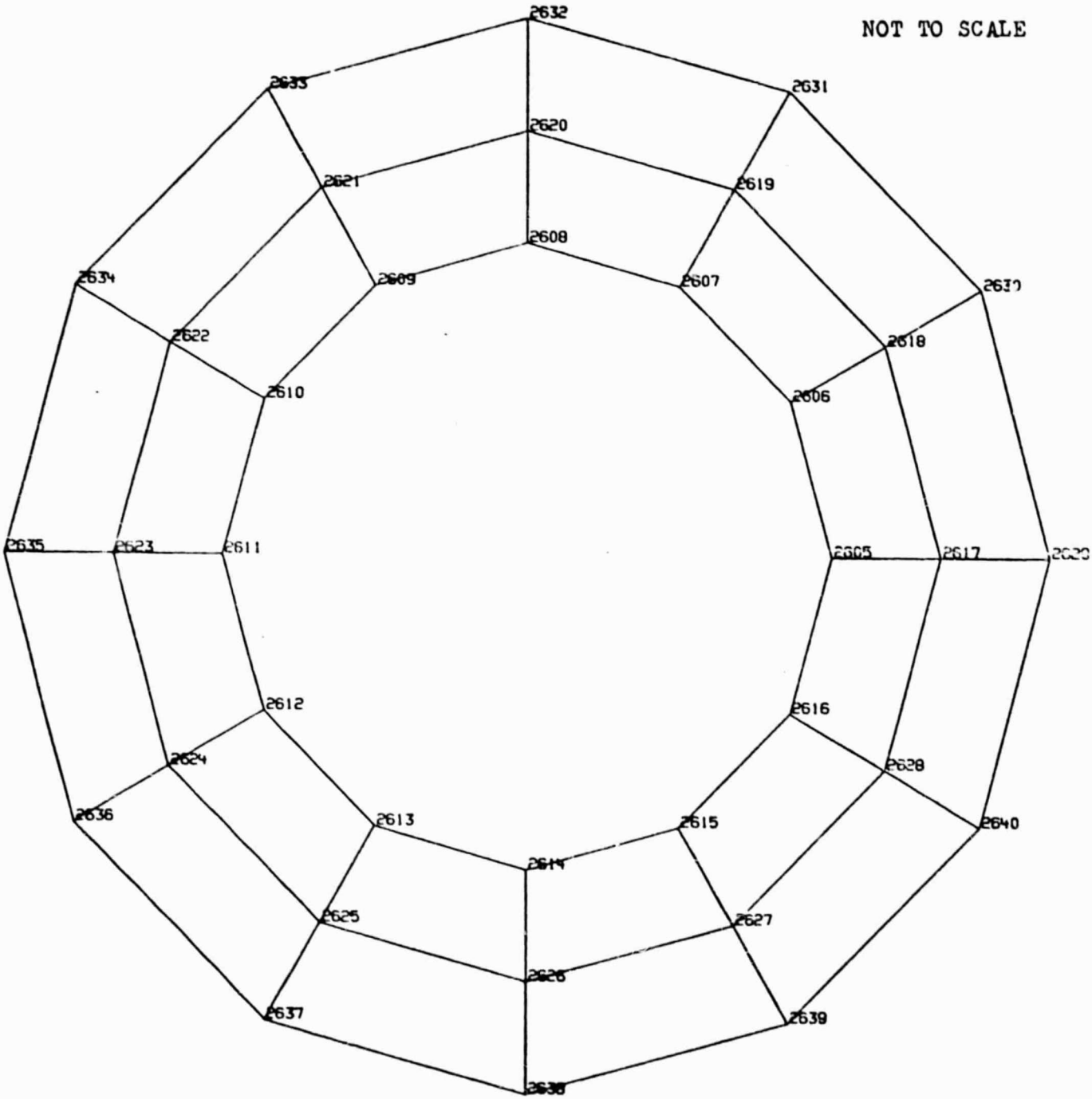

LEVEL 38

NOT TO SCALE

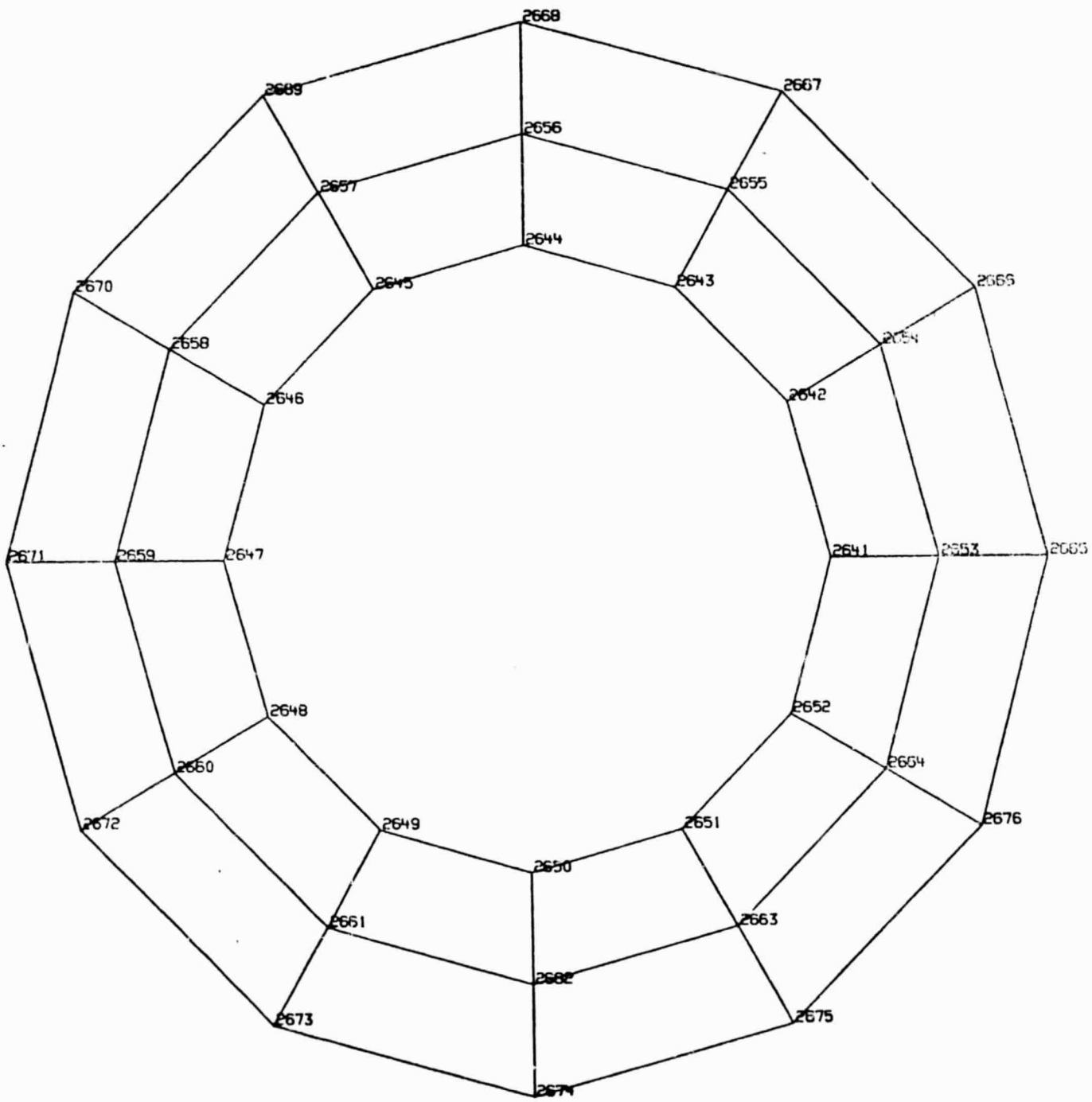

LEVEL 39

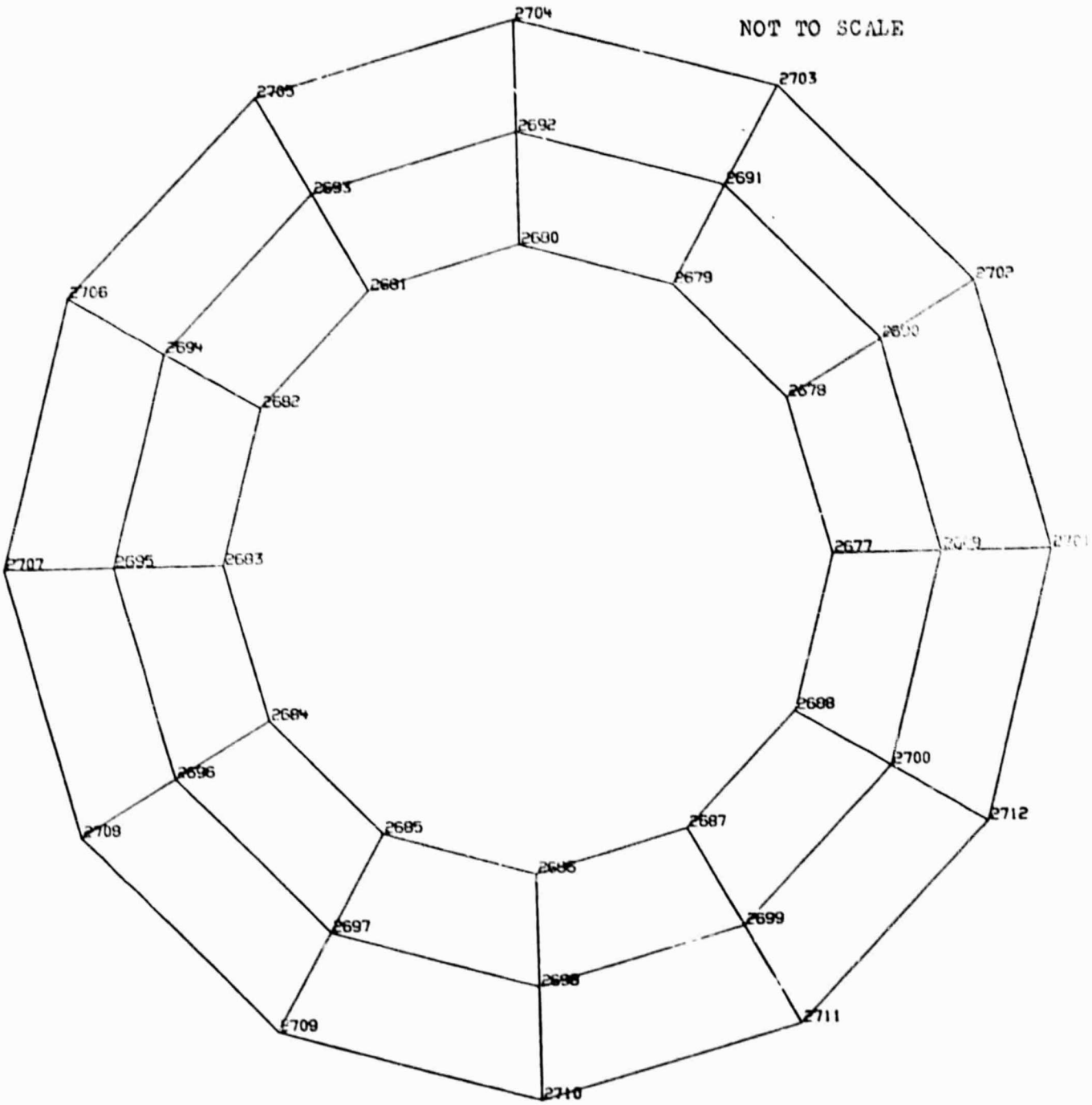
NOT TO SCALE
2704
2703
2705
2692
2691
2693
2680
2679
2681
2702
2706
2694
2678
2682
2677
2701
2707
2695
2683
2684
2708
2696
2700
2712
2709
2685
2687
2686
2699
2697
2698
2711
2709
2710

LEVEL 40

NOT TO SCALE

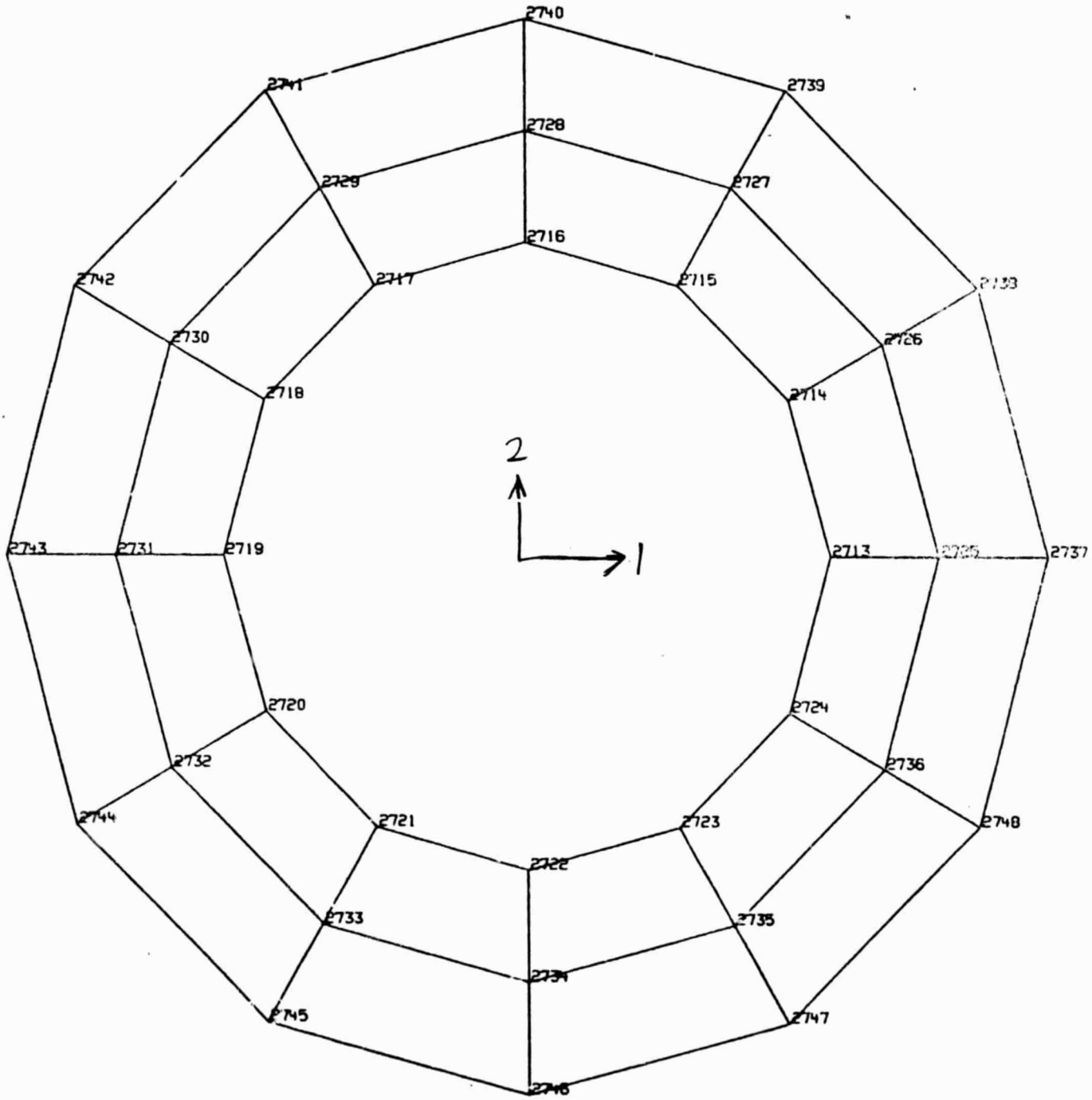

LEVEL 41

NOT TO SCALE

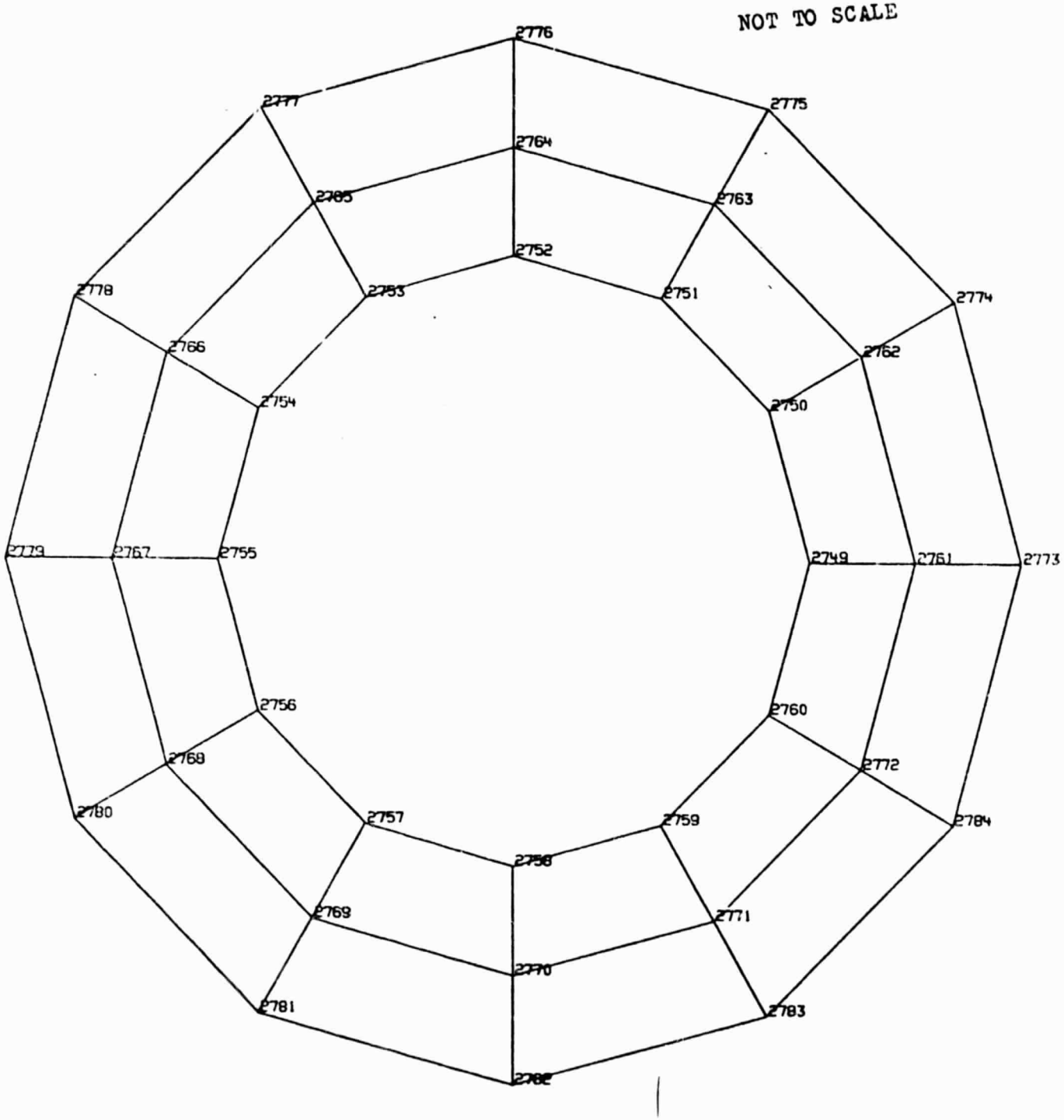

LEVEL 42

NOT TO SCALE

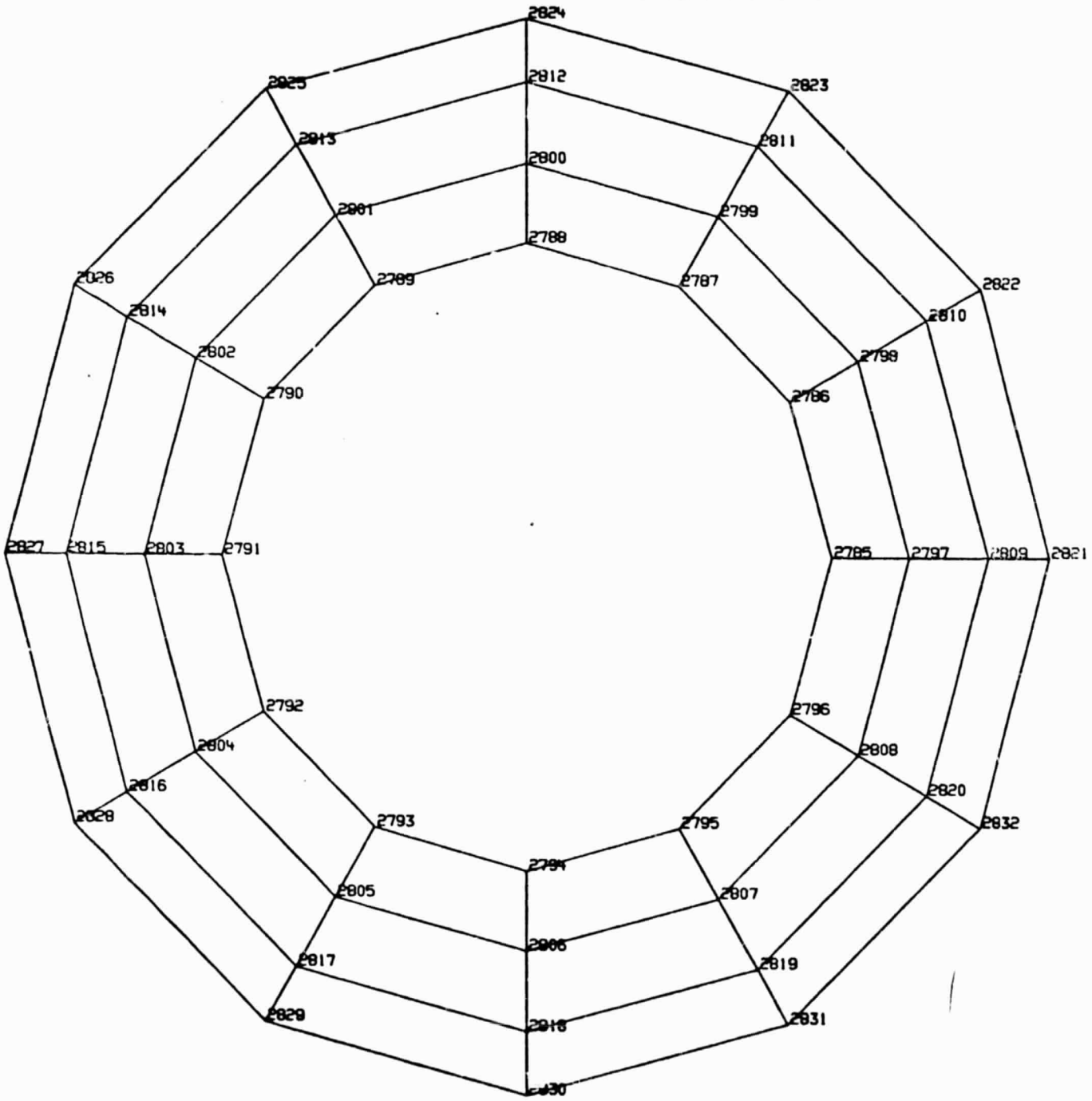

LEVEL 43

NOT TO SCALE

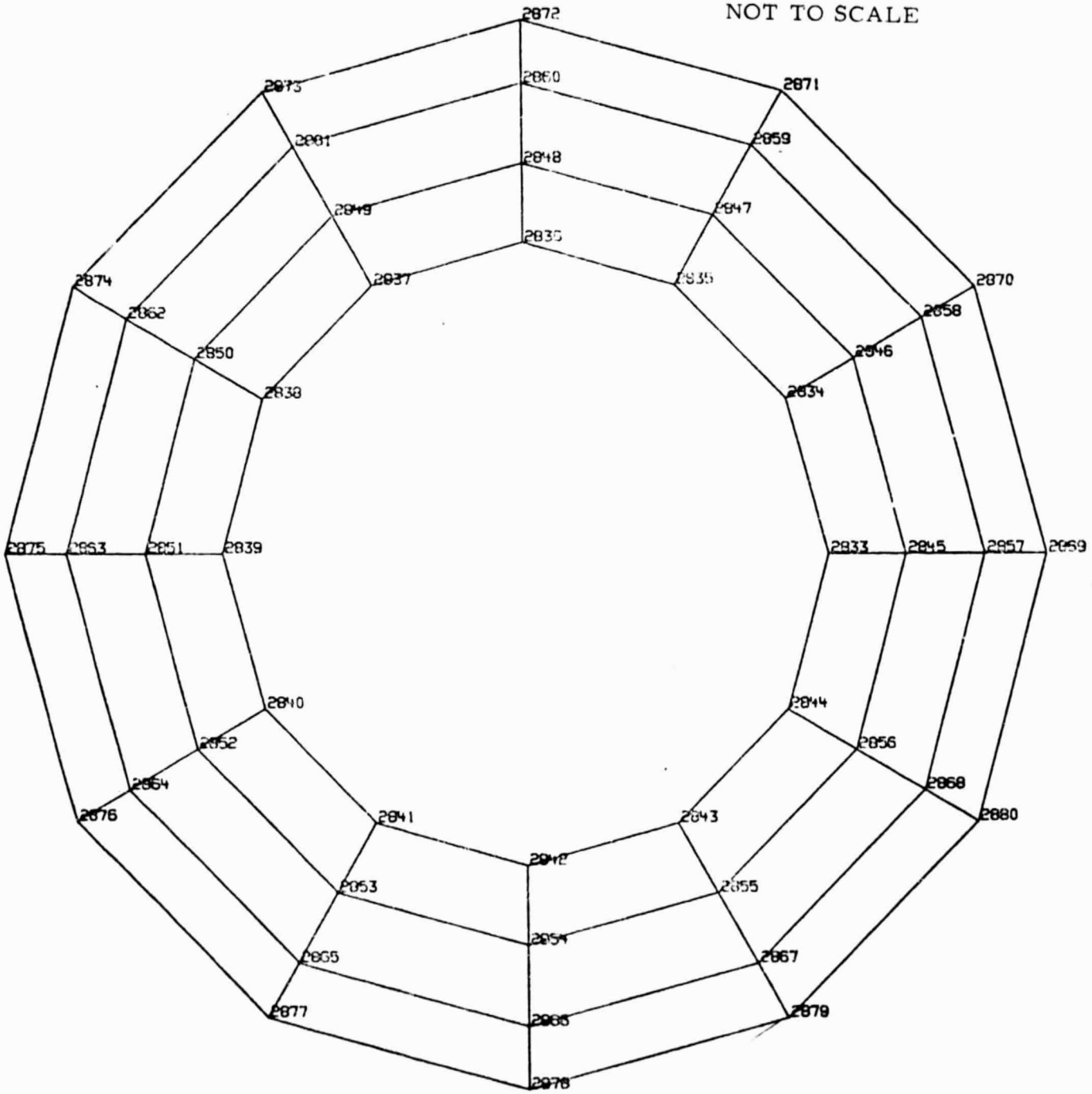

LEVEL 44

NOT TO SCALE

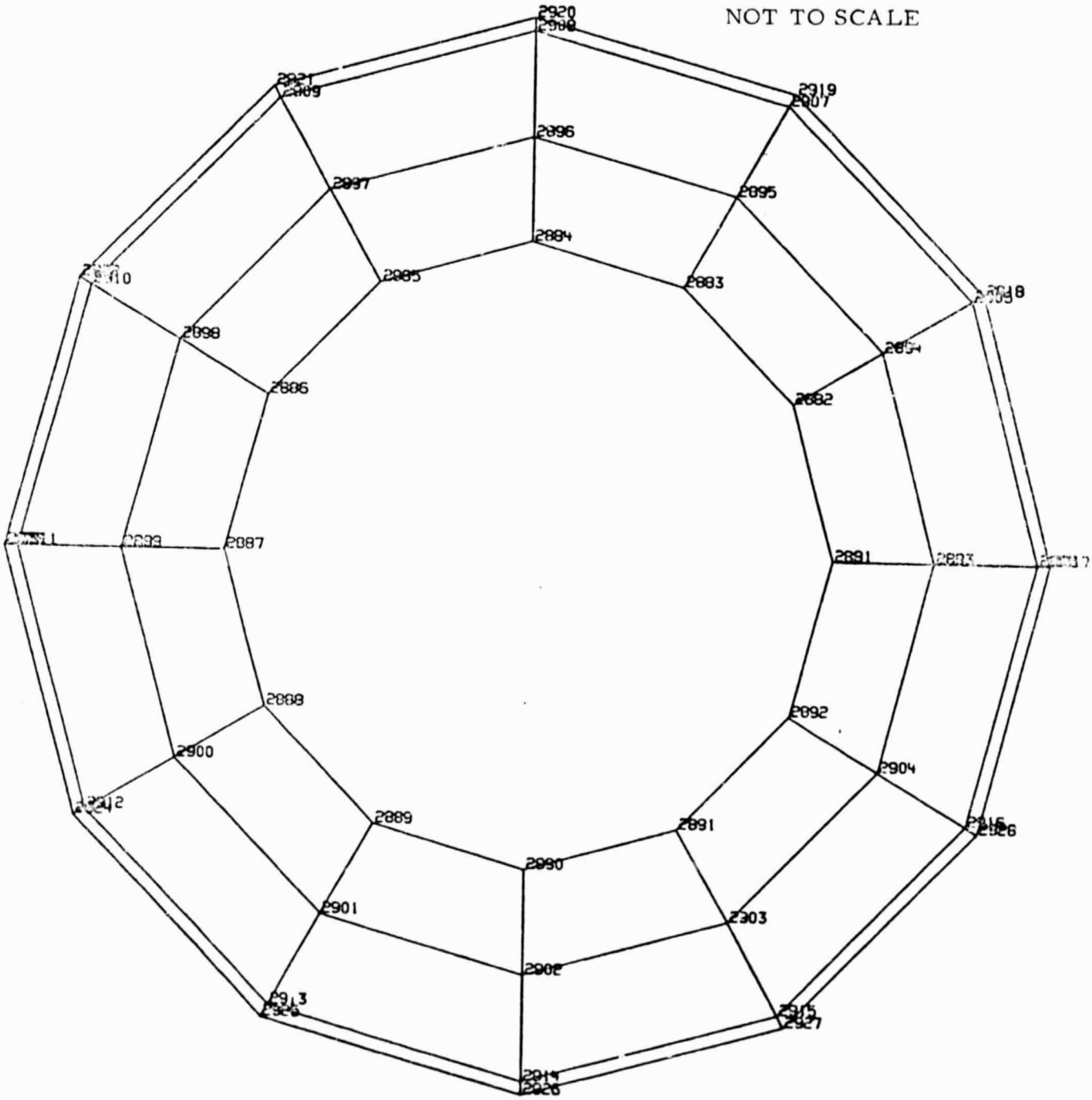

LEVEL 45

NOT TO SCALE

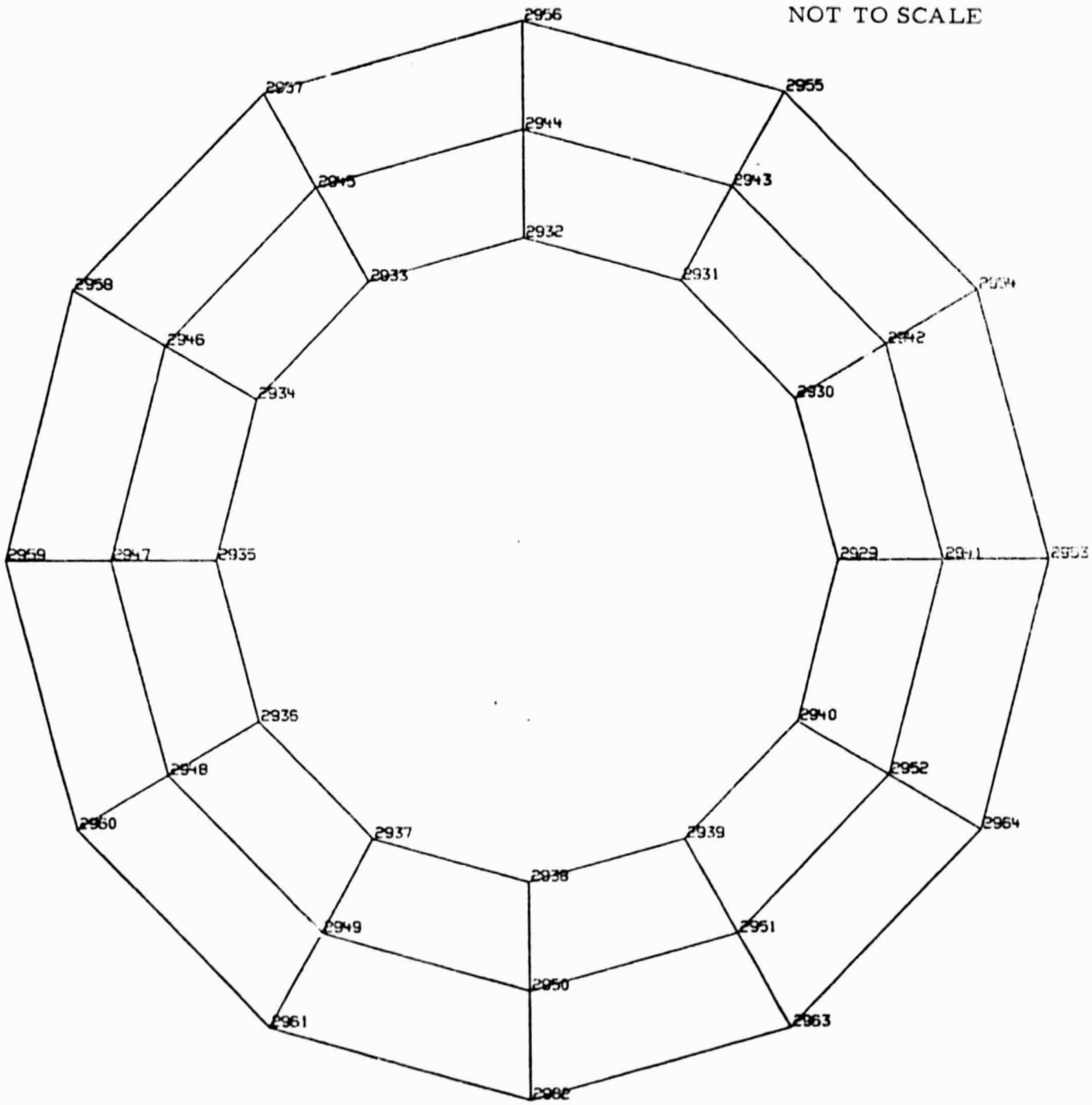

LEVEL 46

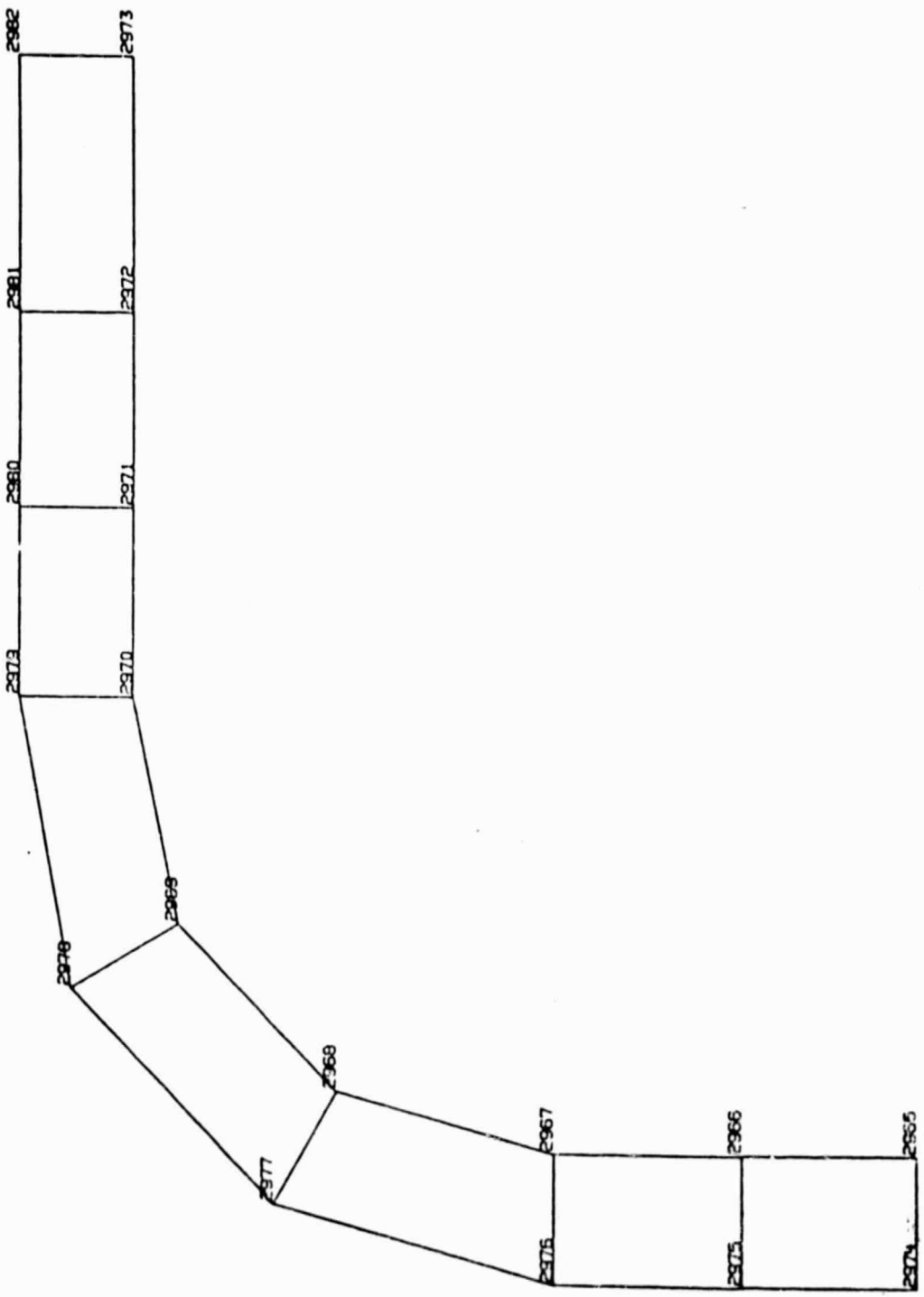

Shield Level 1

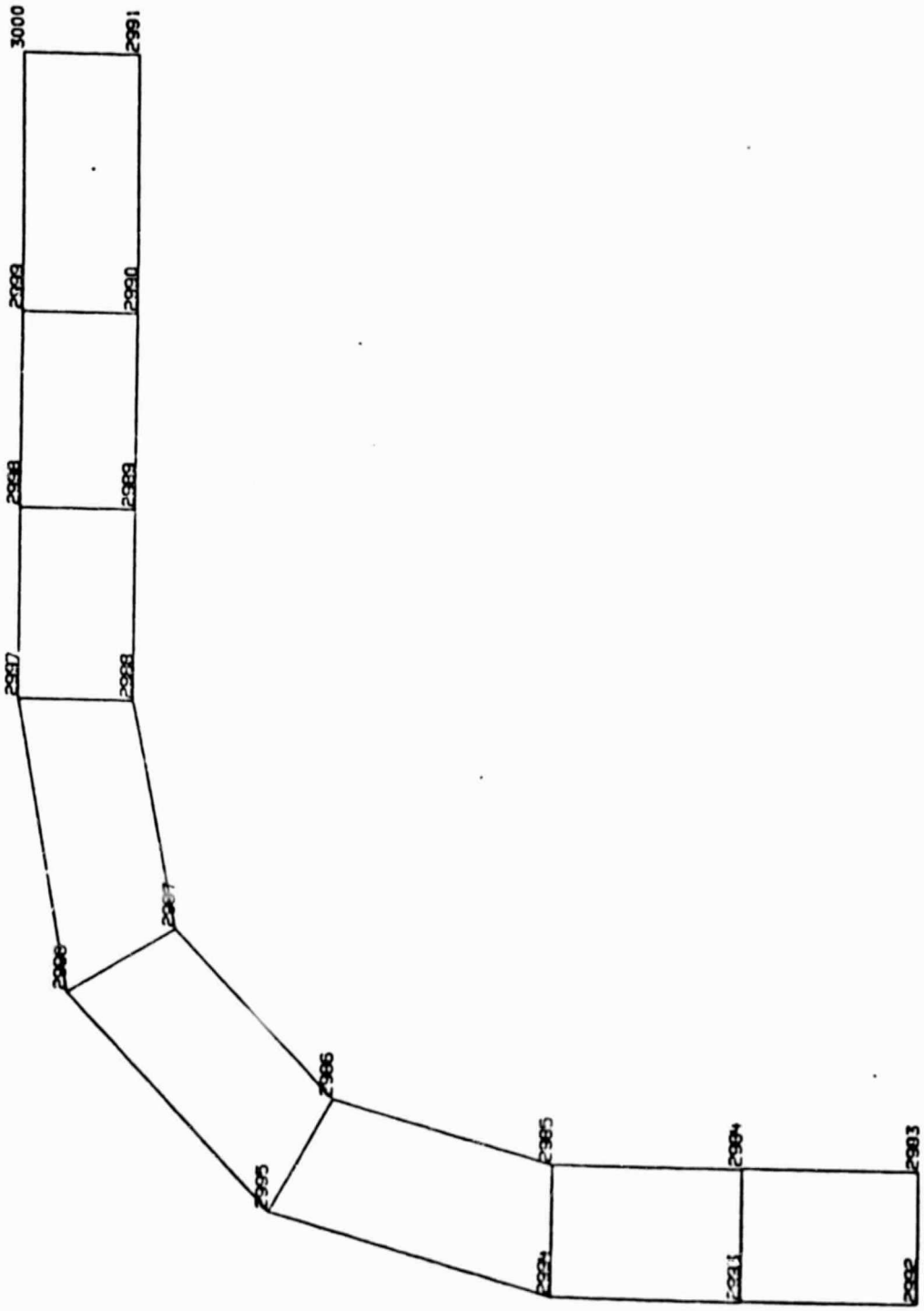

Shield Level 2

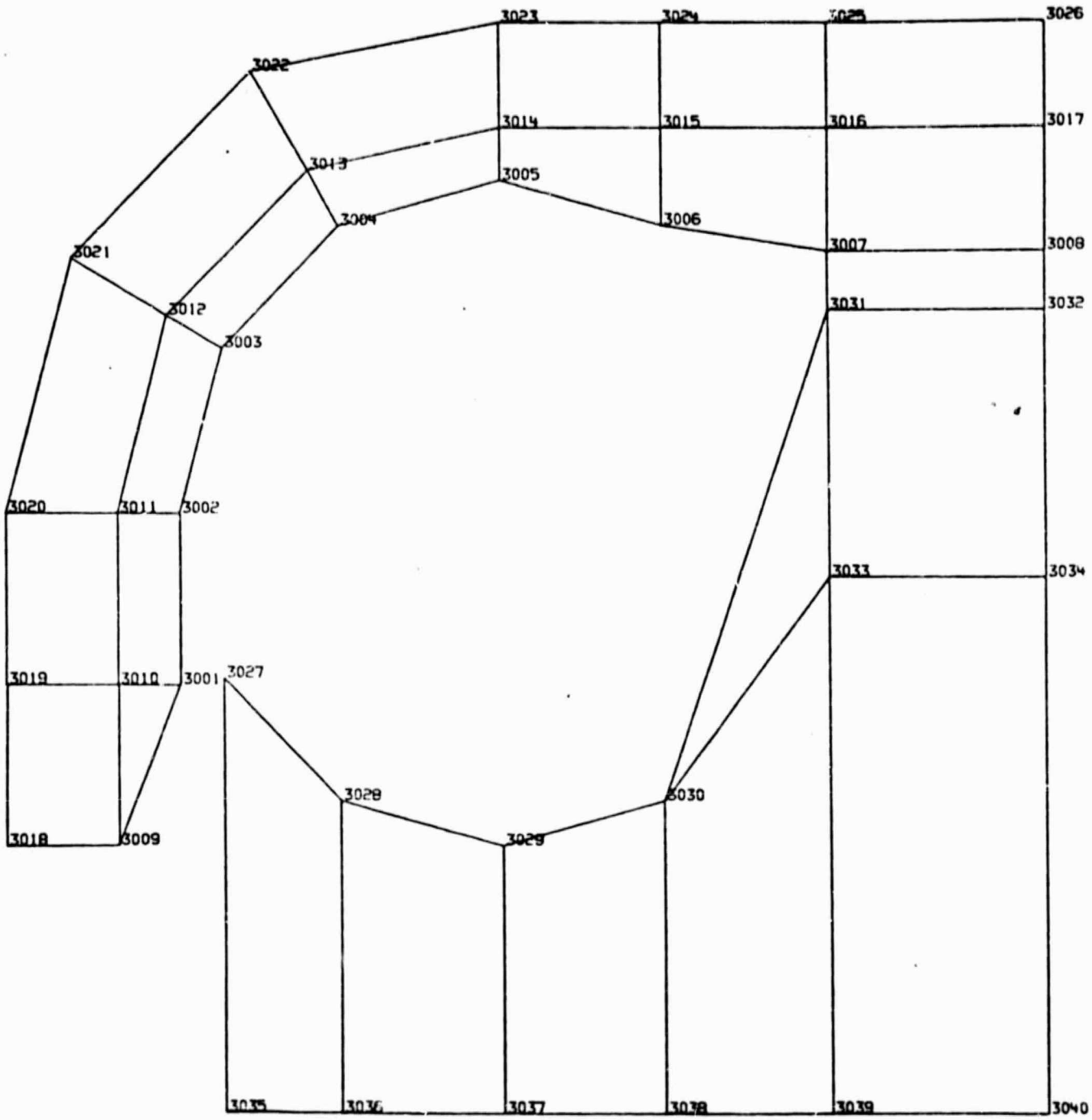

Shield Level 3

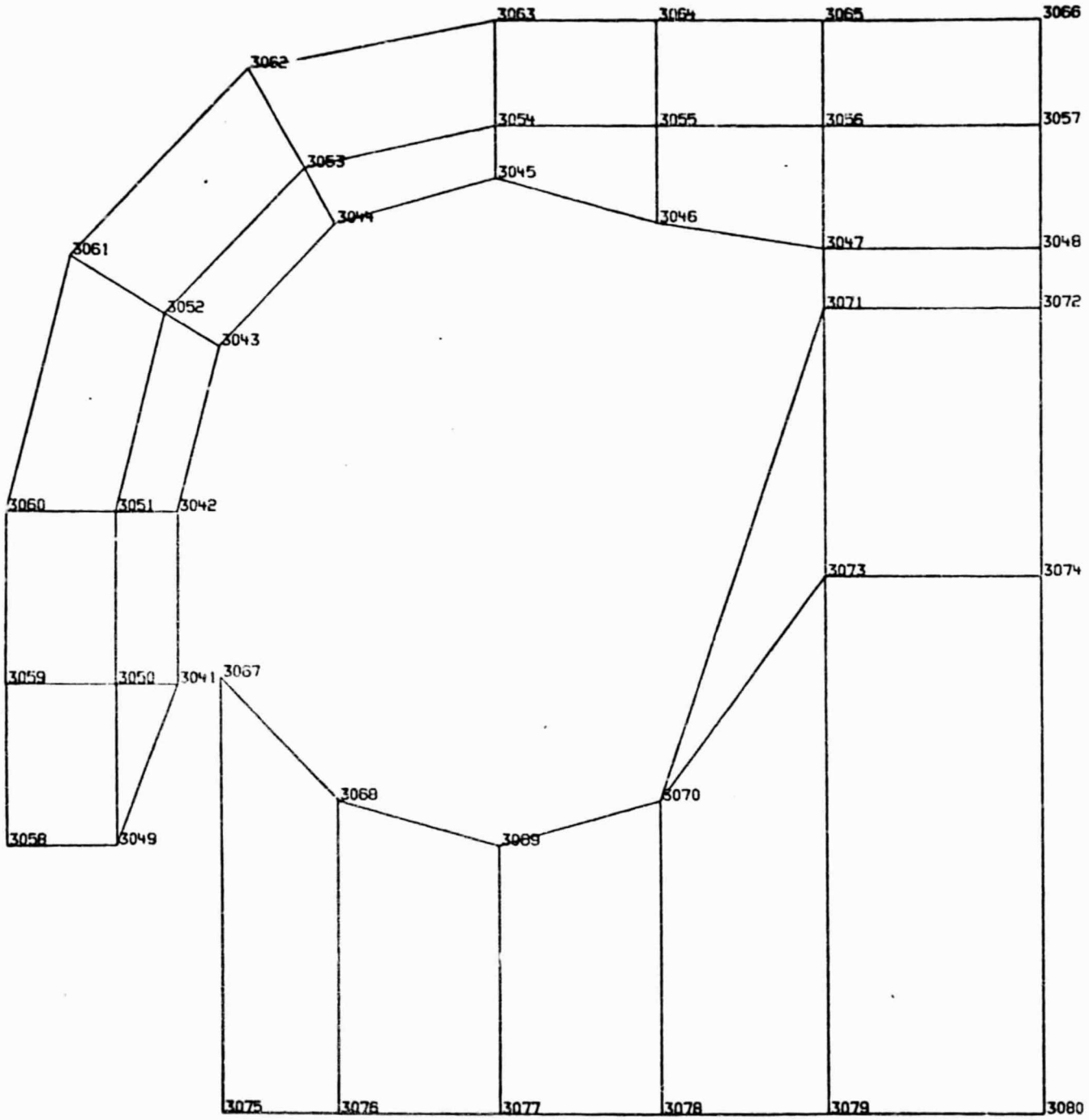

Shield Level 4

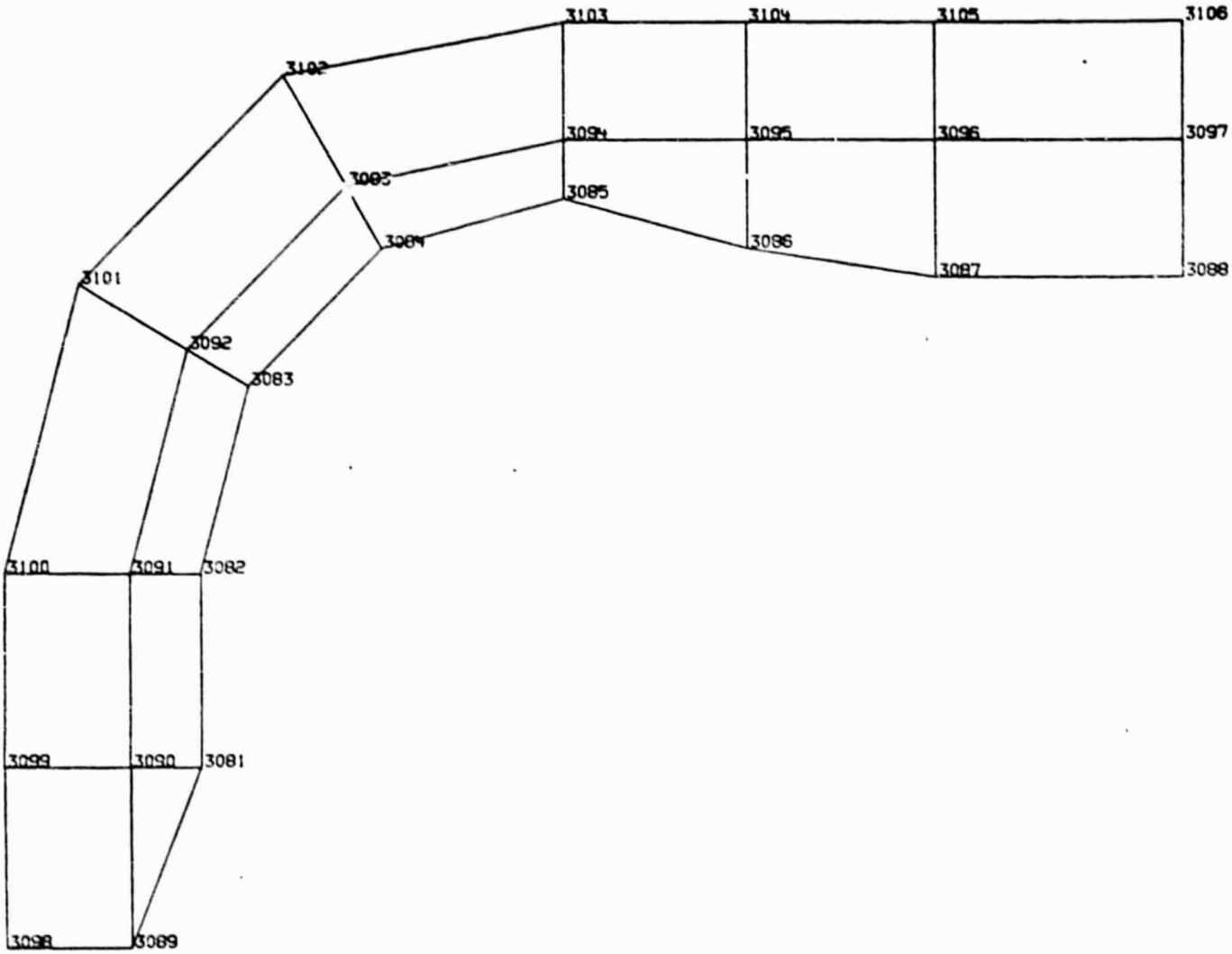

Shield Level 5

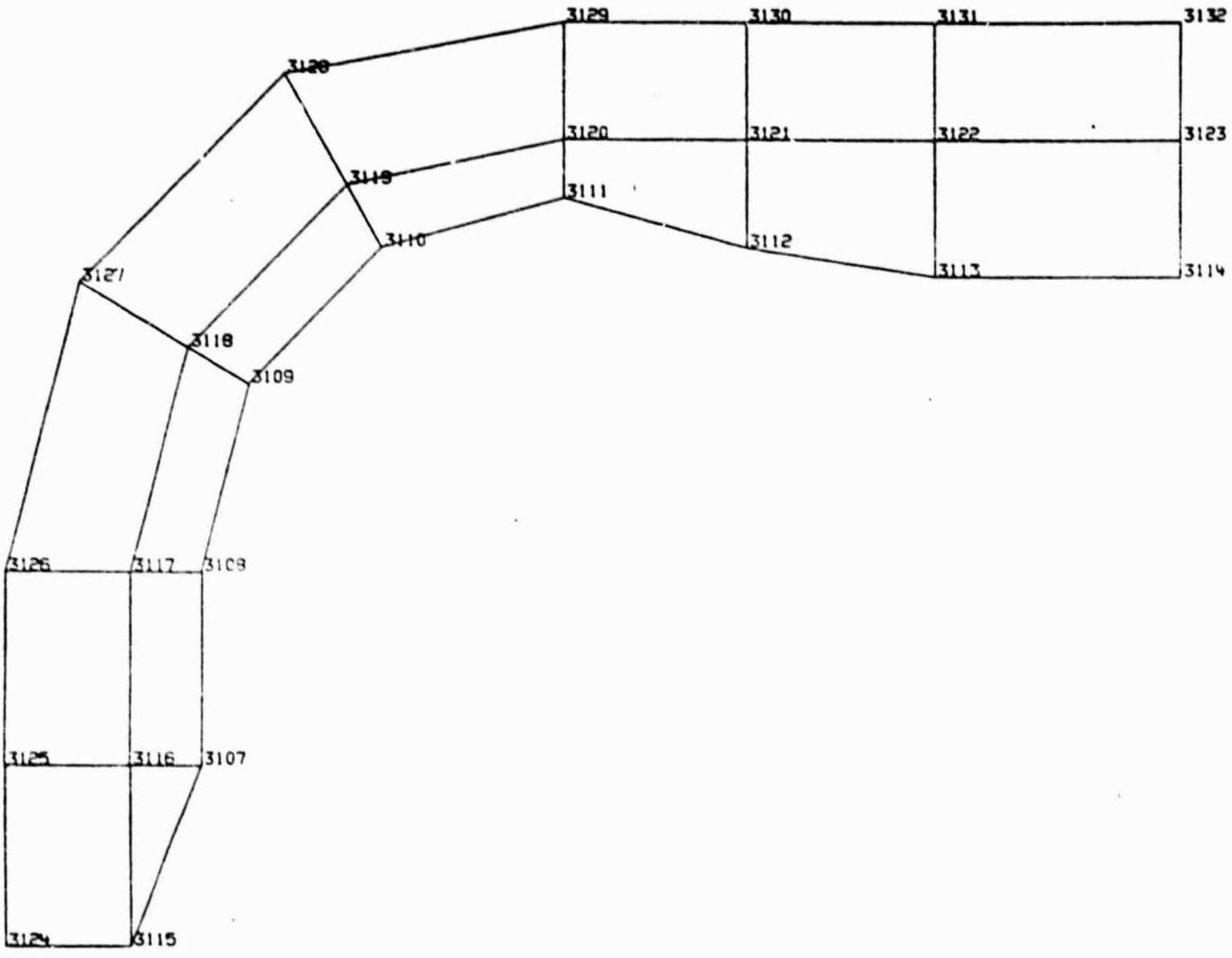

Shield Level 6

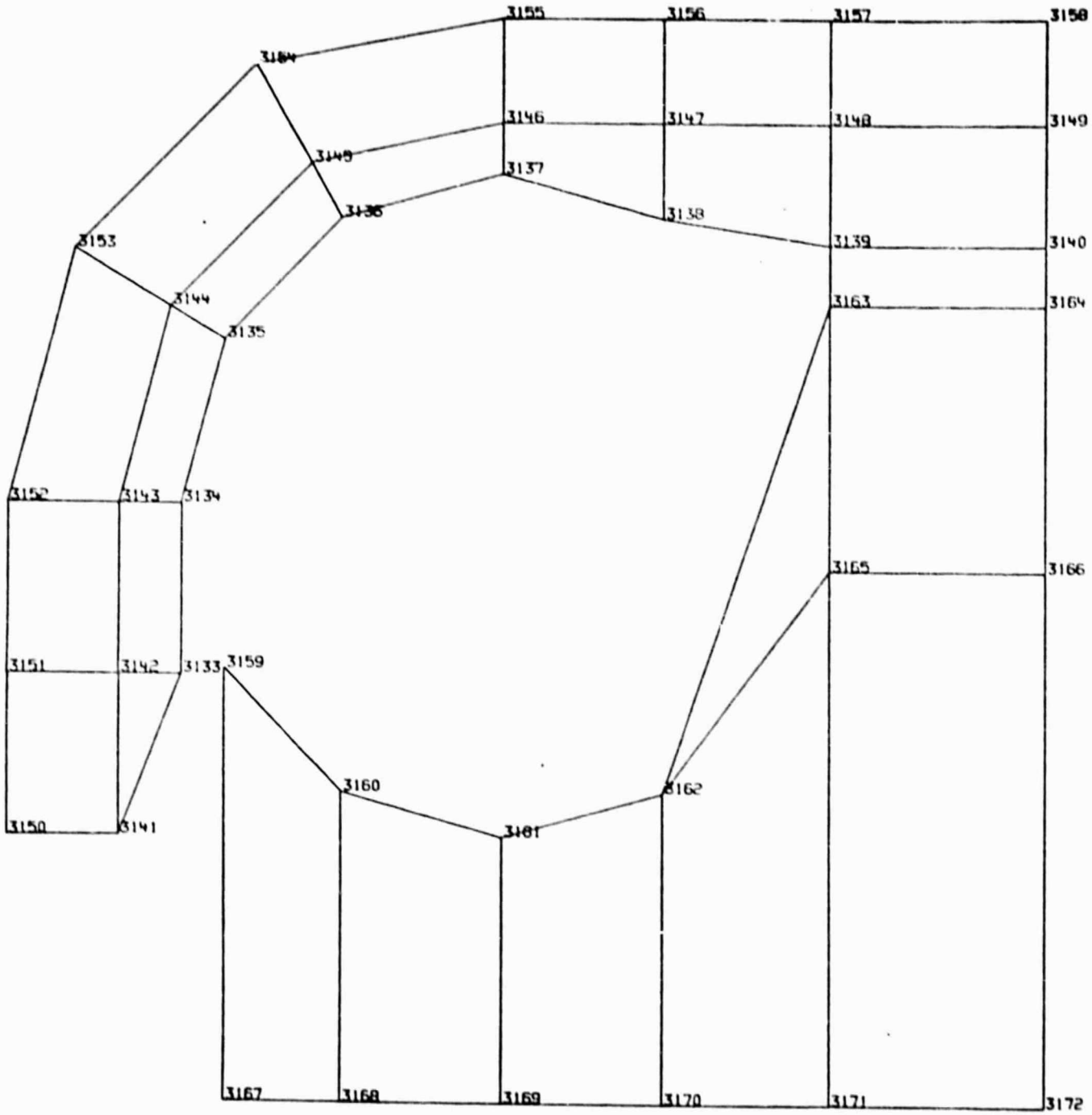

Shield Level 7

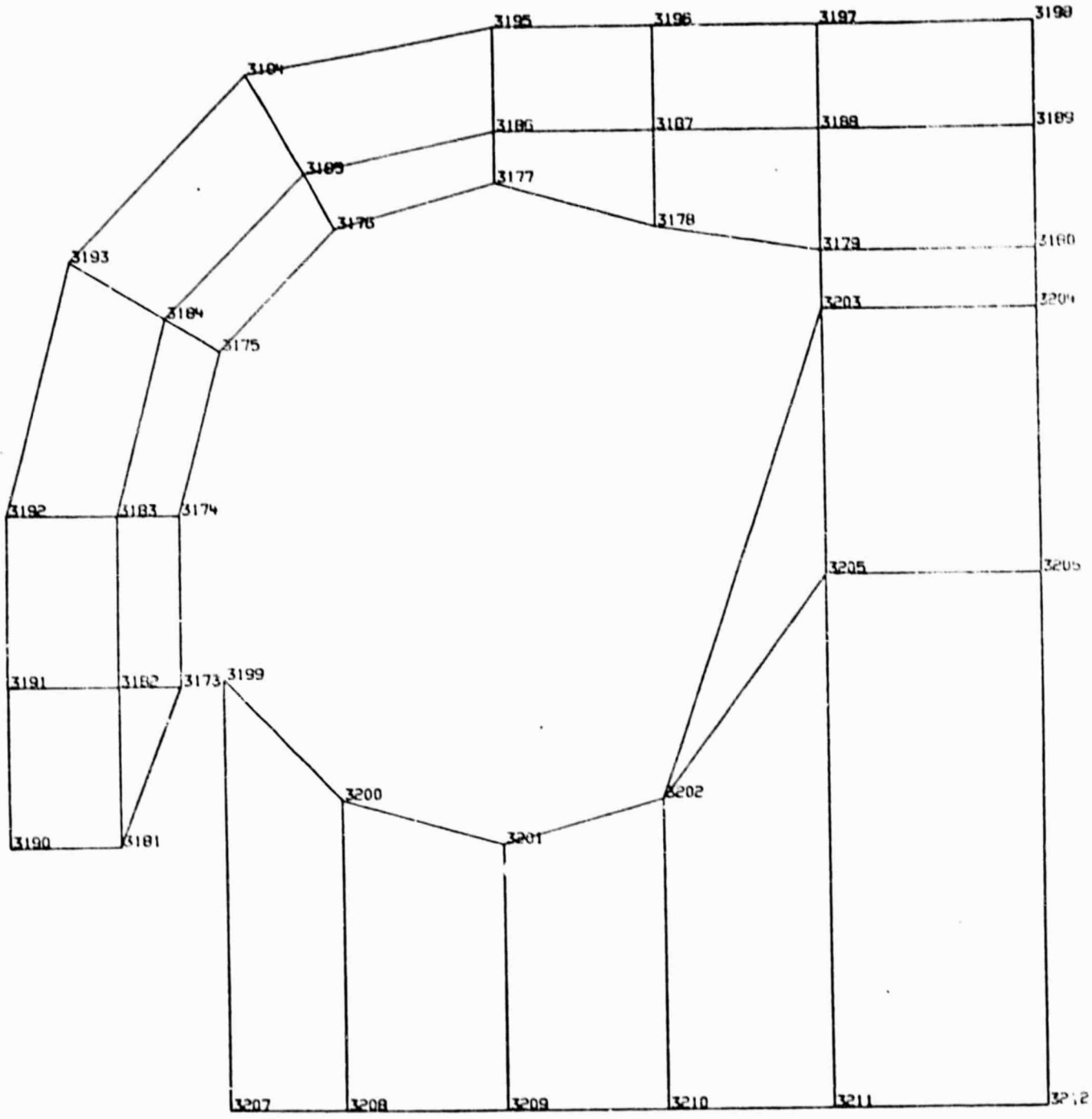

Shield Level 8

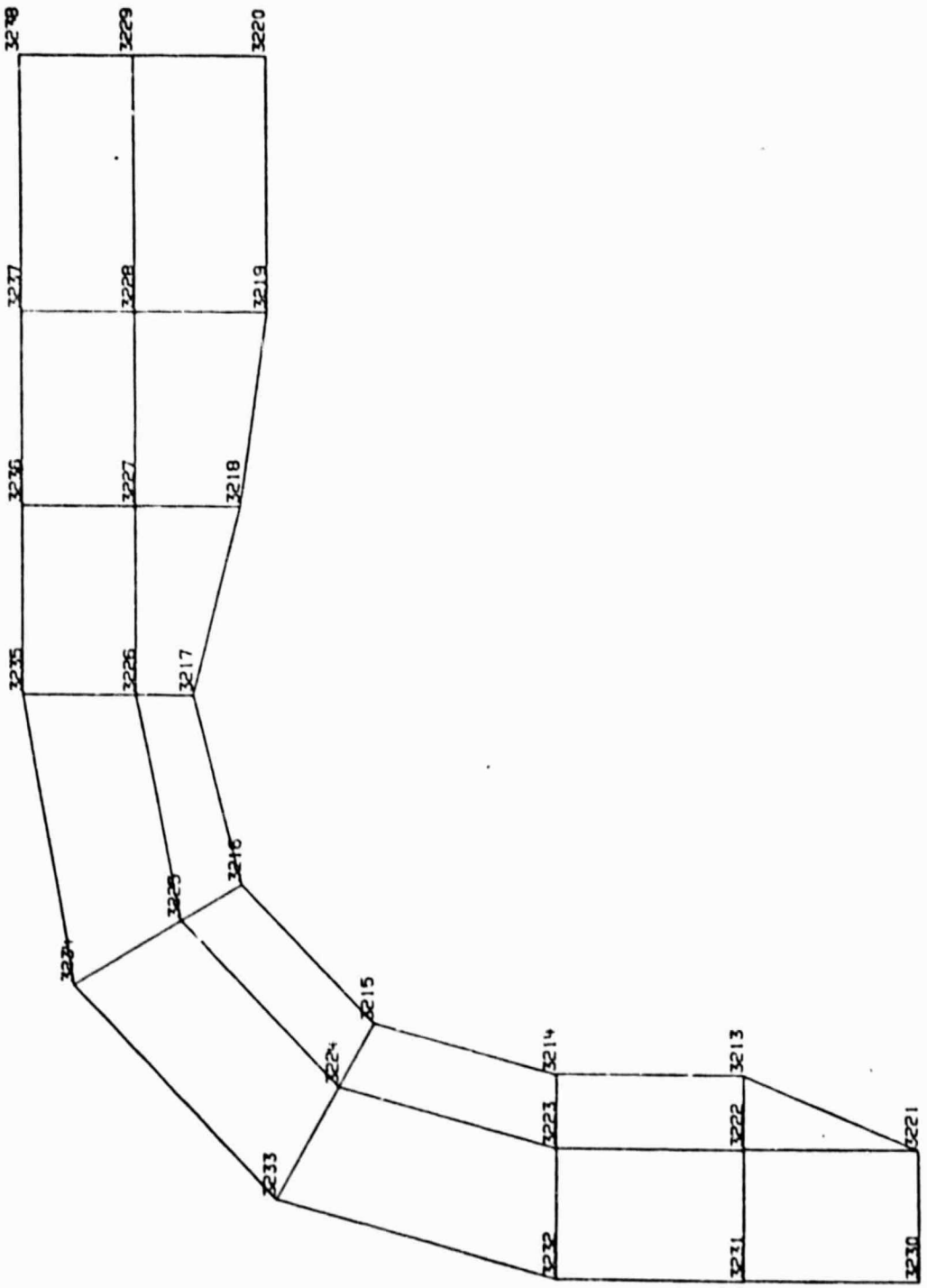

Shield Level 9

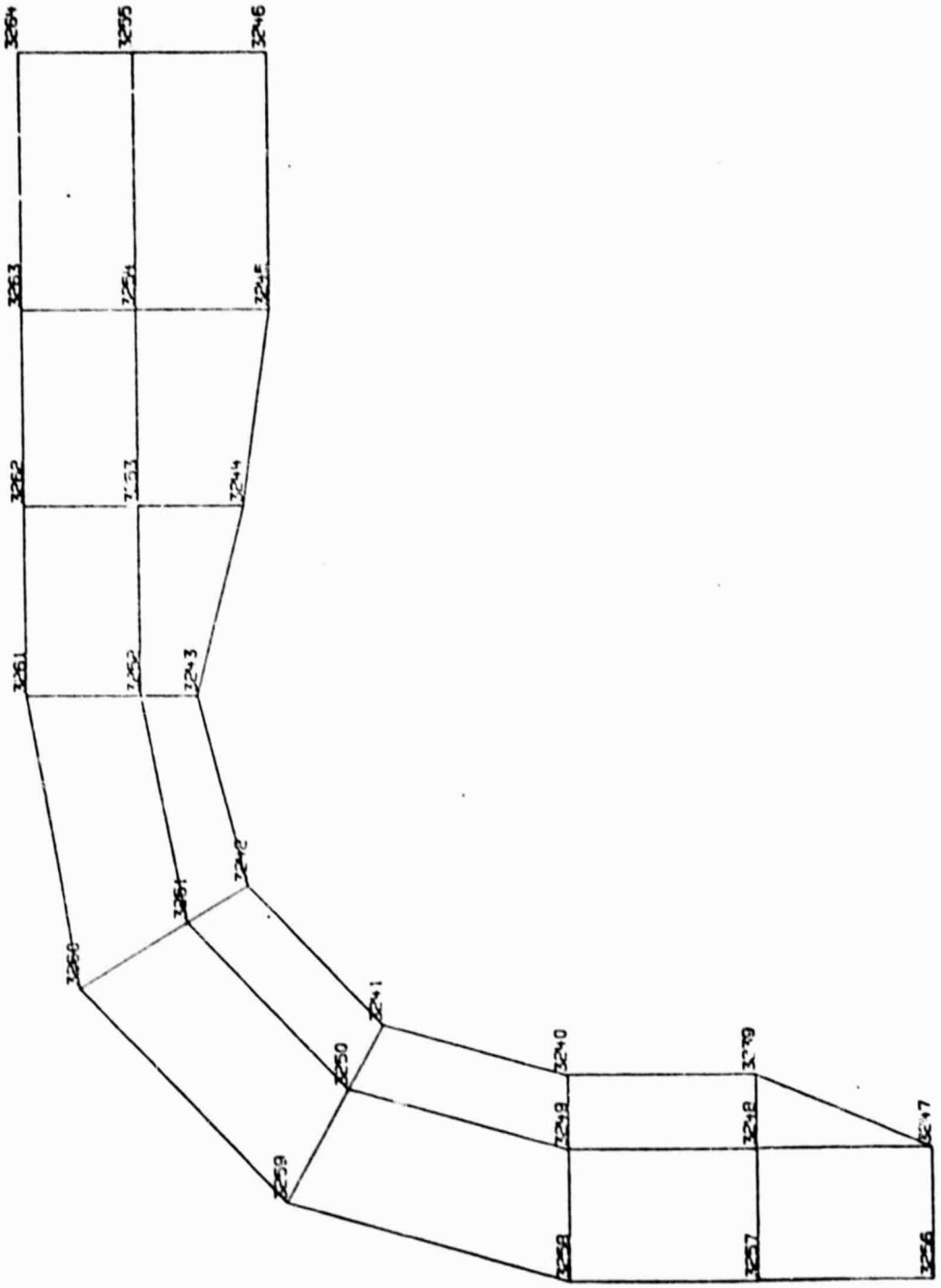

Shield Level 10

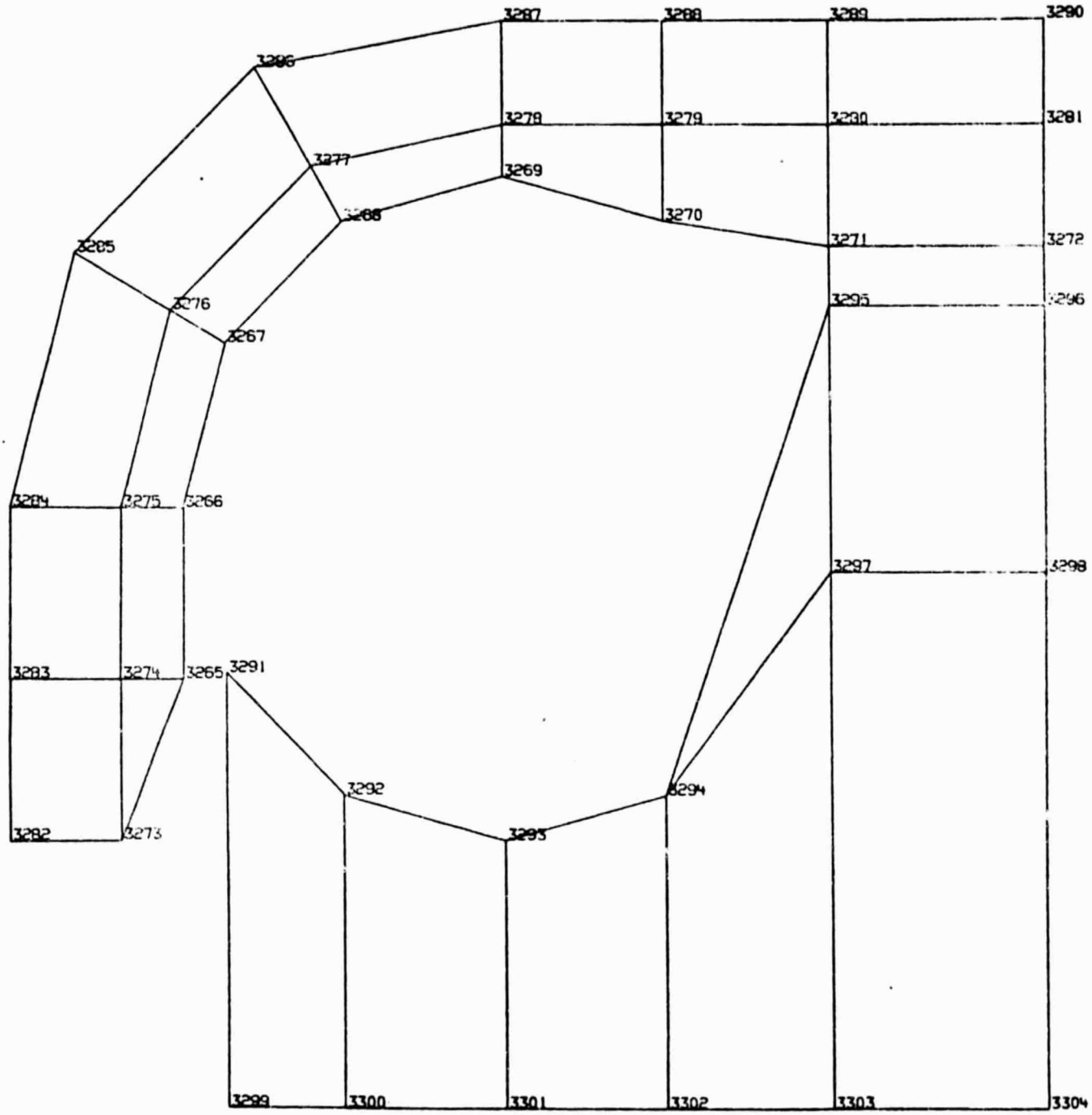

Shield Level 11

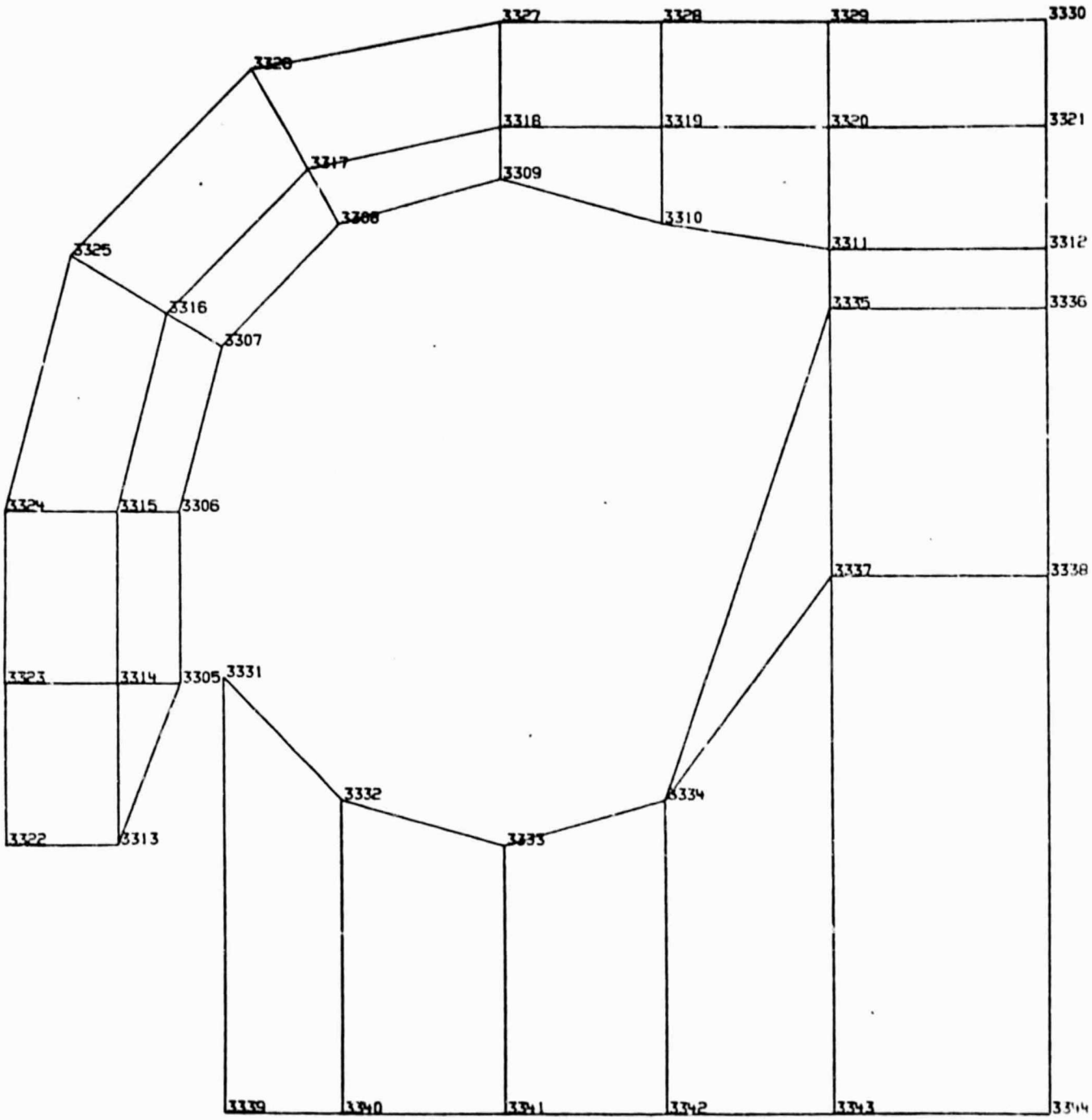

Shield Level 12

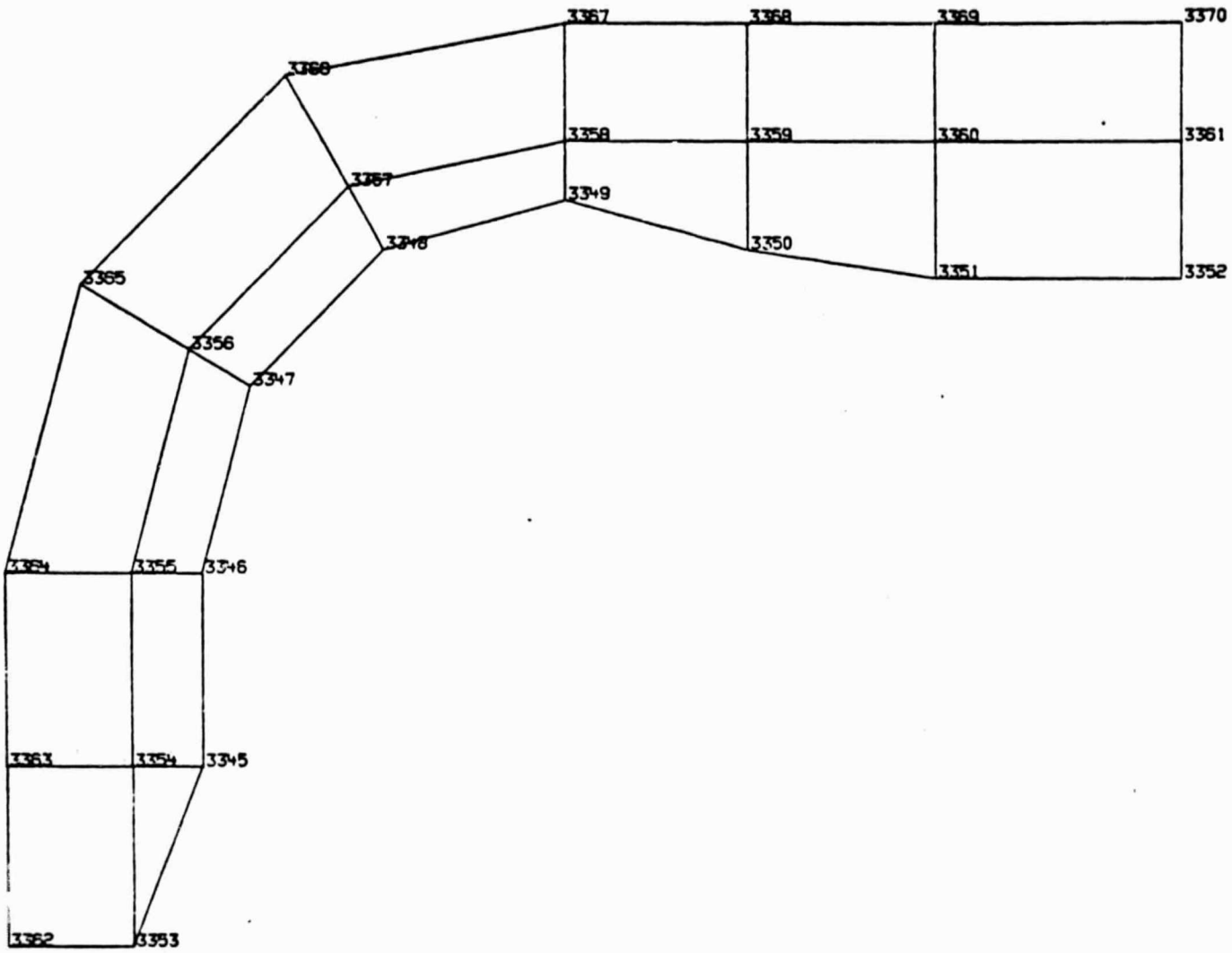

Shield Level 13

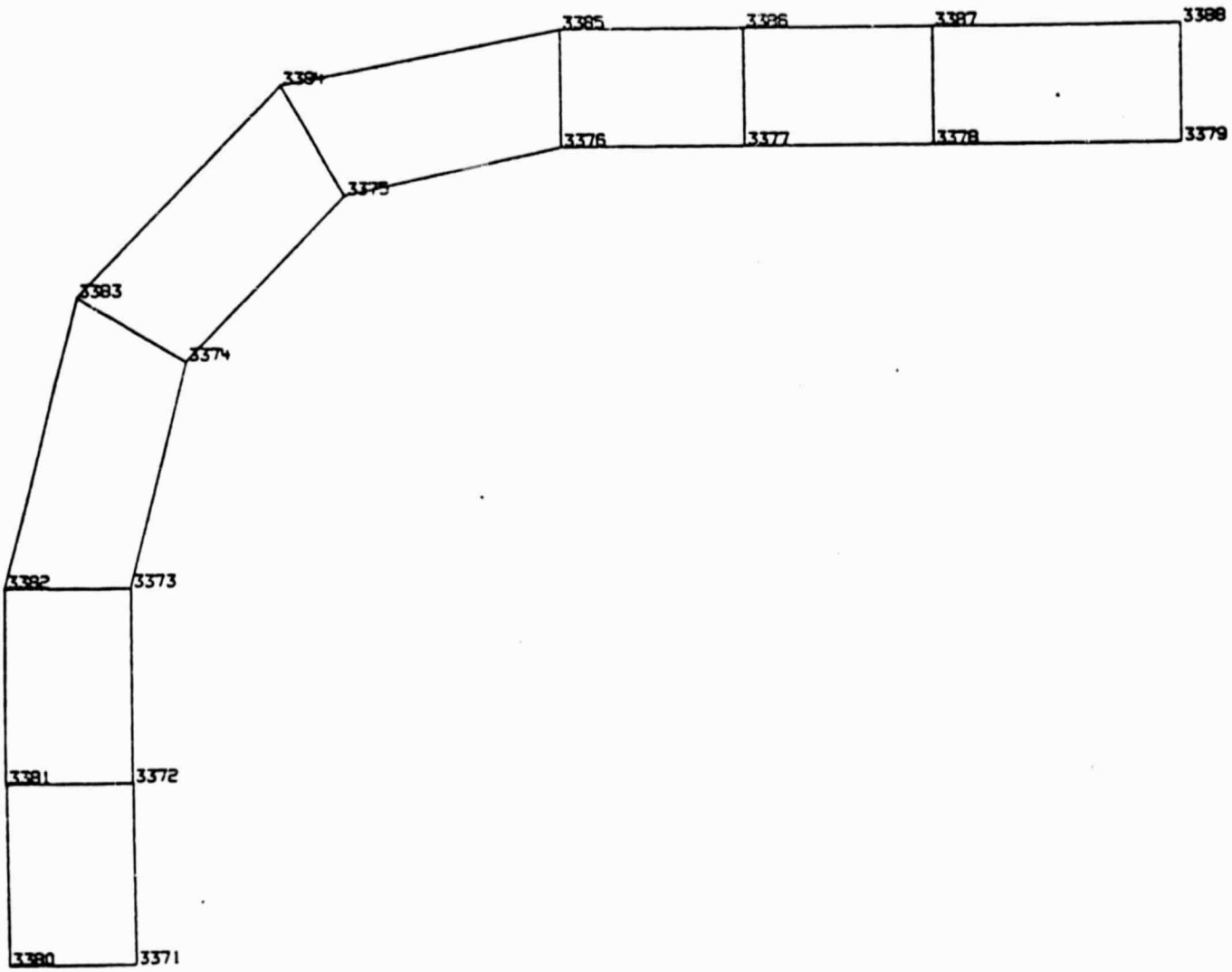

Shield Level 14

Appendix B

SPAR LOX POST ASSEMBLY MODEL COMPONENTS

ORIGINAL PAGE
BLACK AND WHITE PHOTOGRAPH

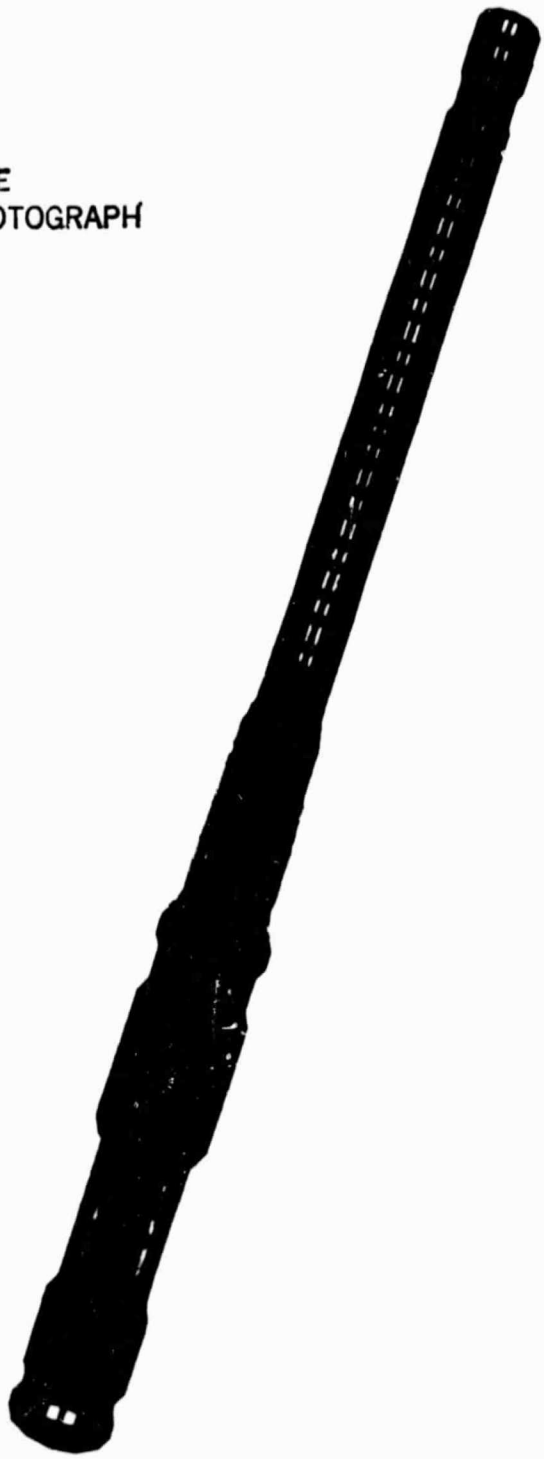

Assembled Two-Piece LOX Post

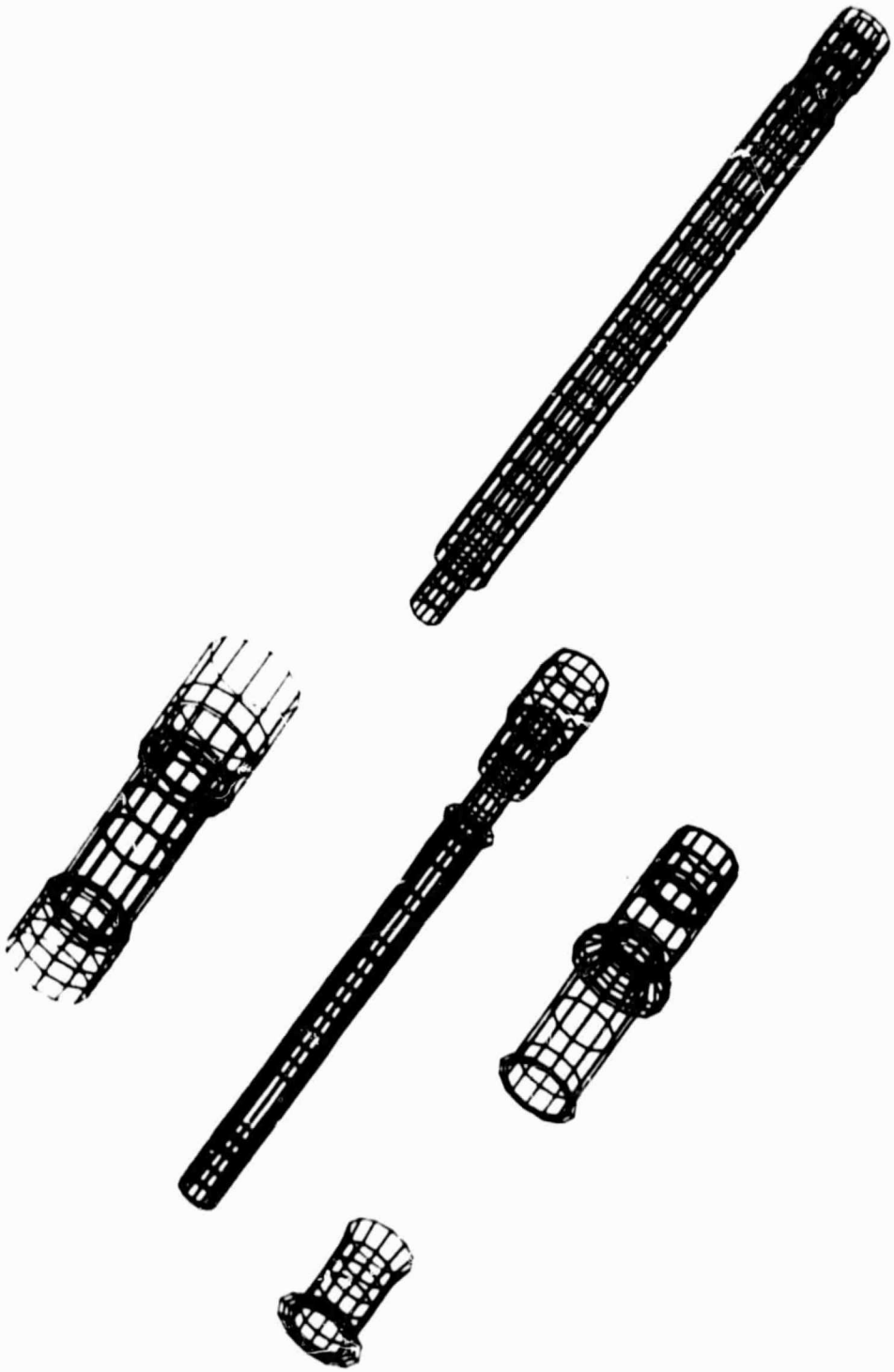

LOX Post Convective Elements to Scale

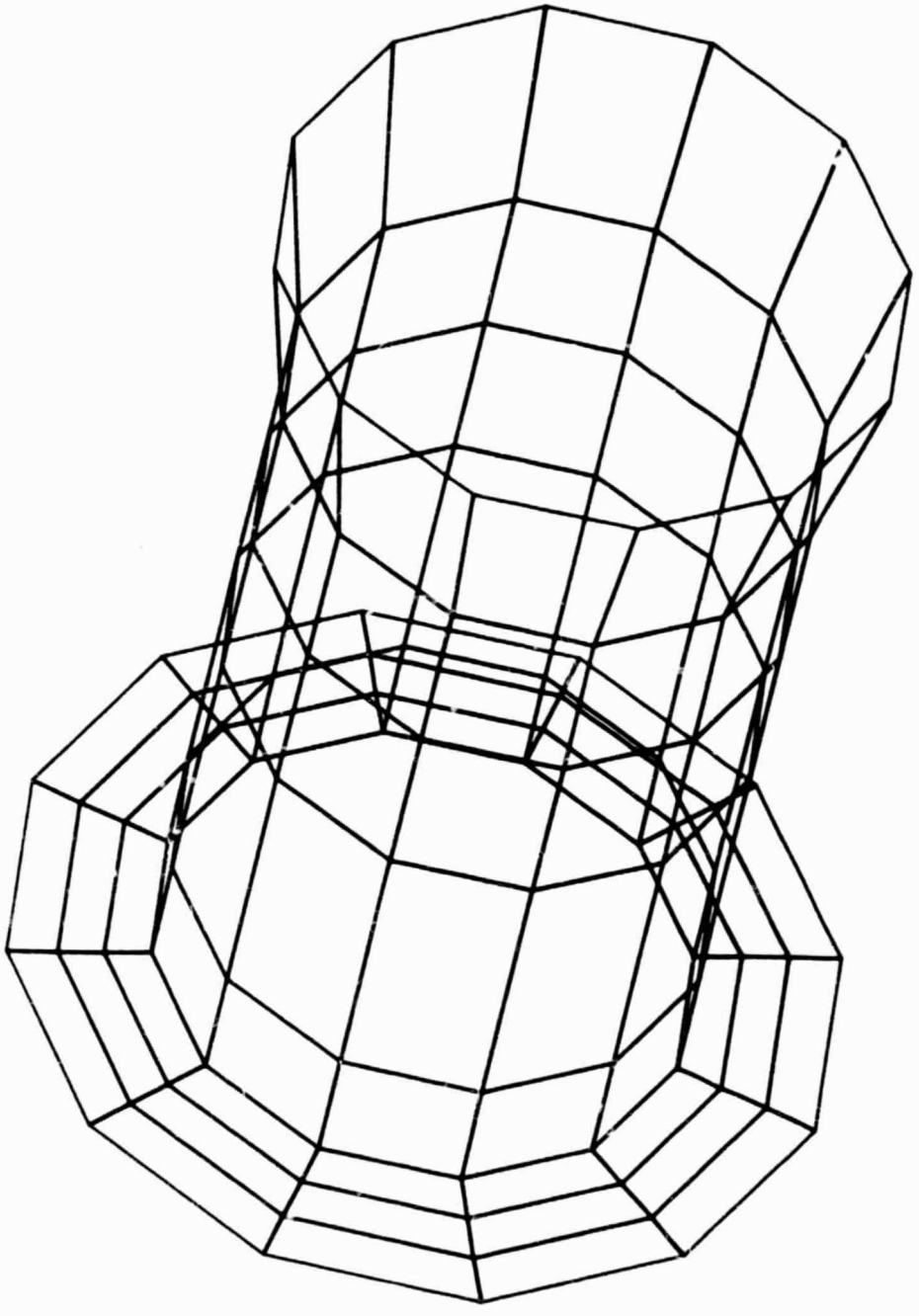

Nut Convective Elements

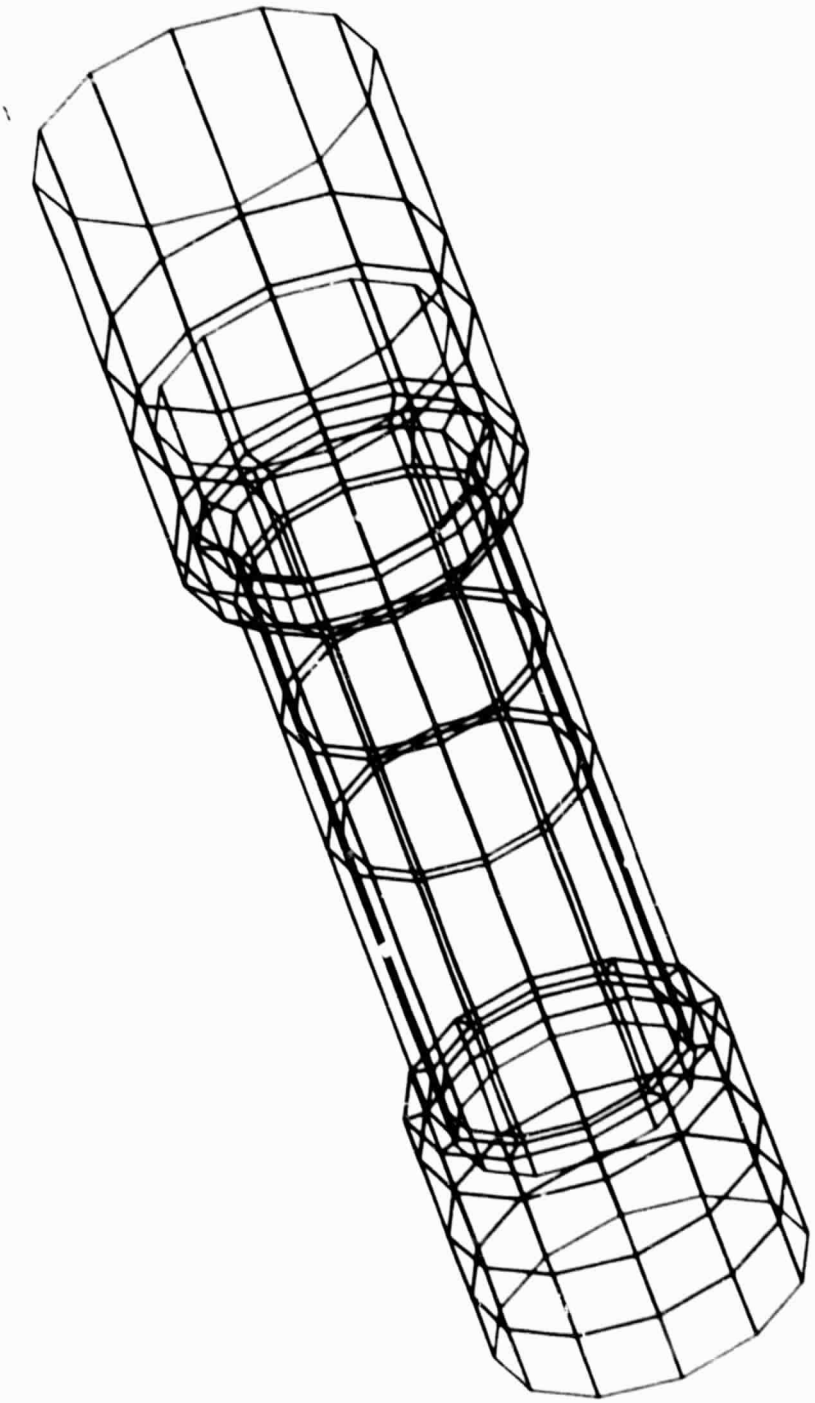

Sleeve Convective Elements

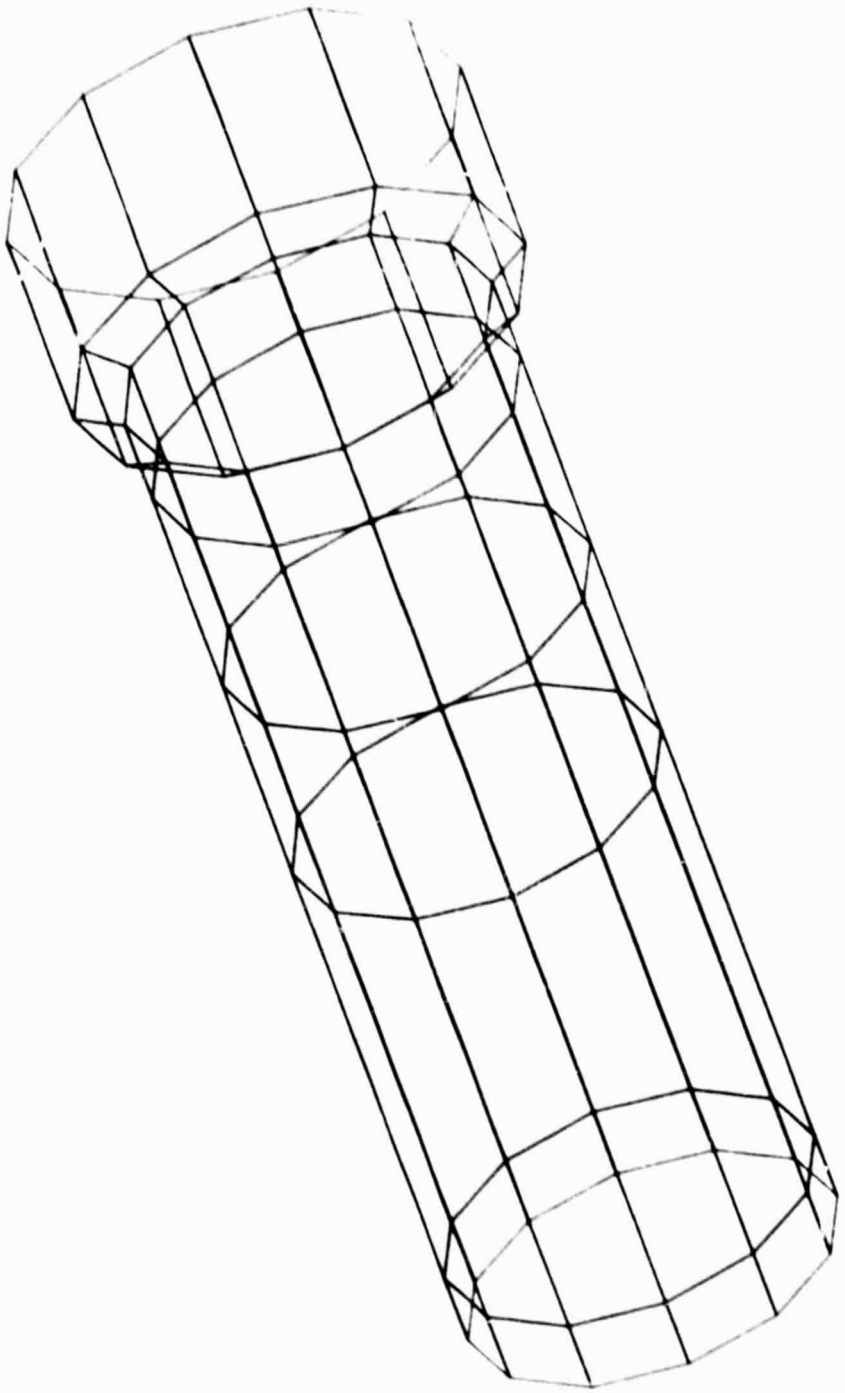

Sleeve Inner Surface Convective Elements

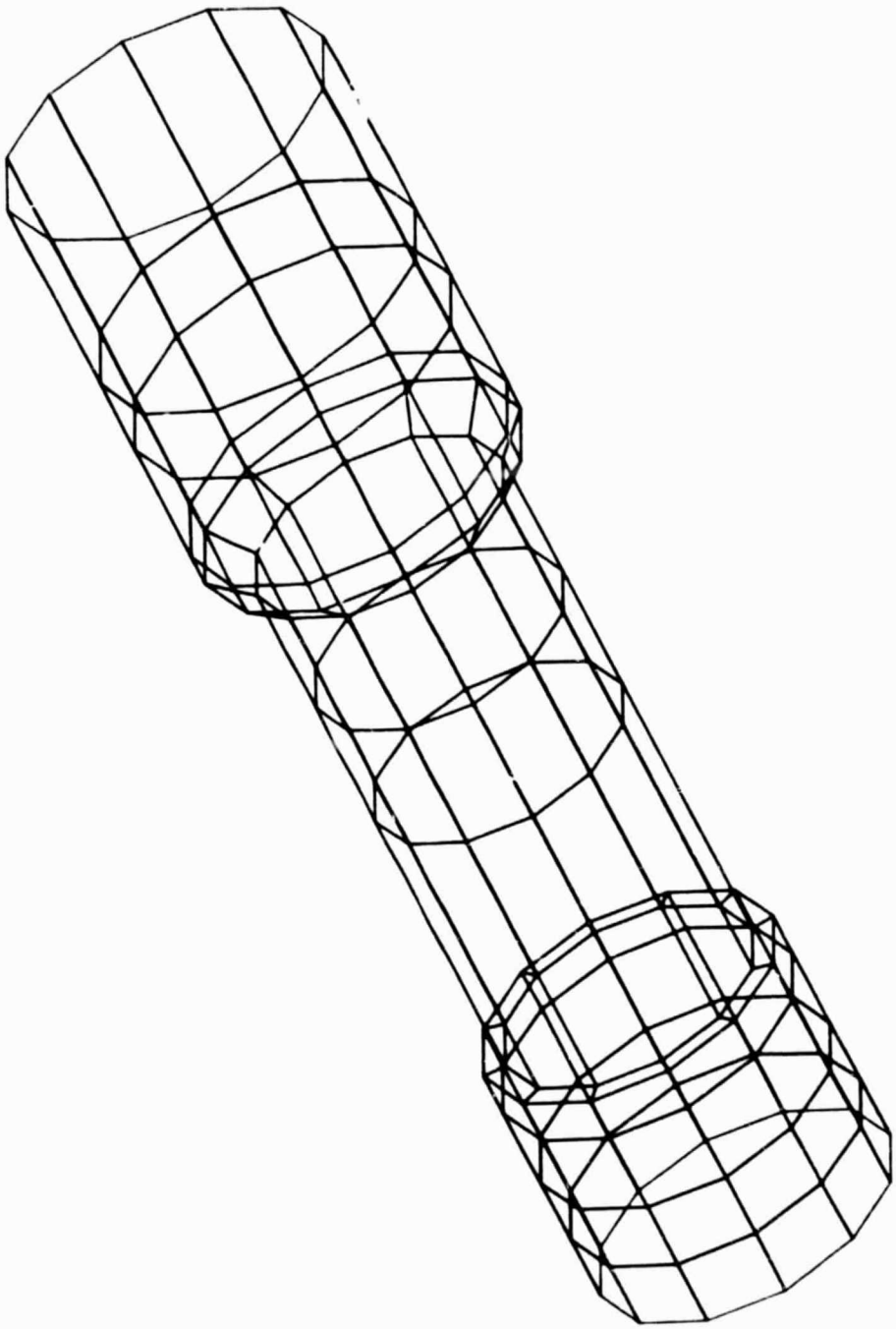

Sleeve Outer Surface Convective Elements

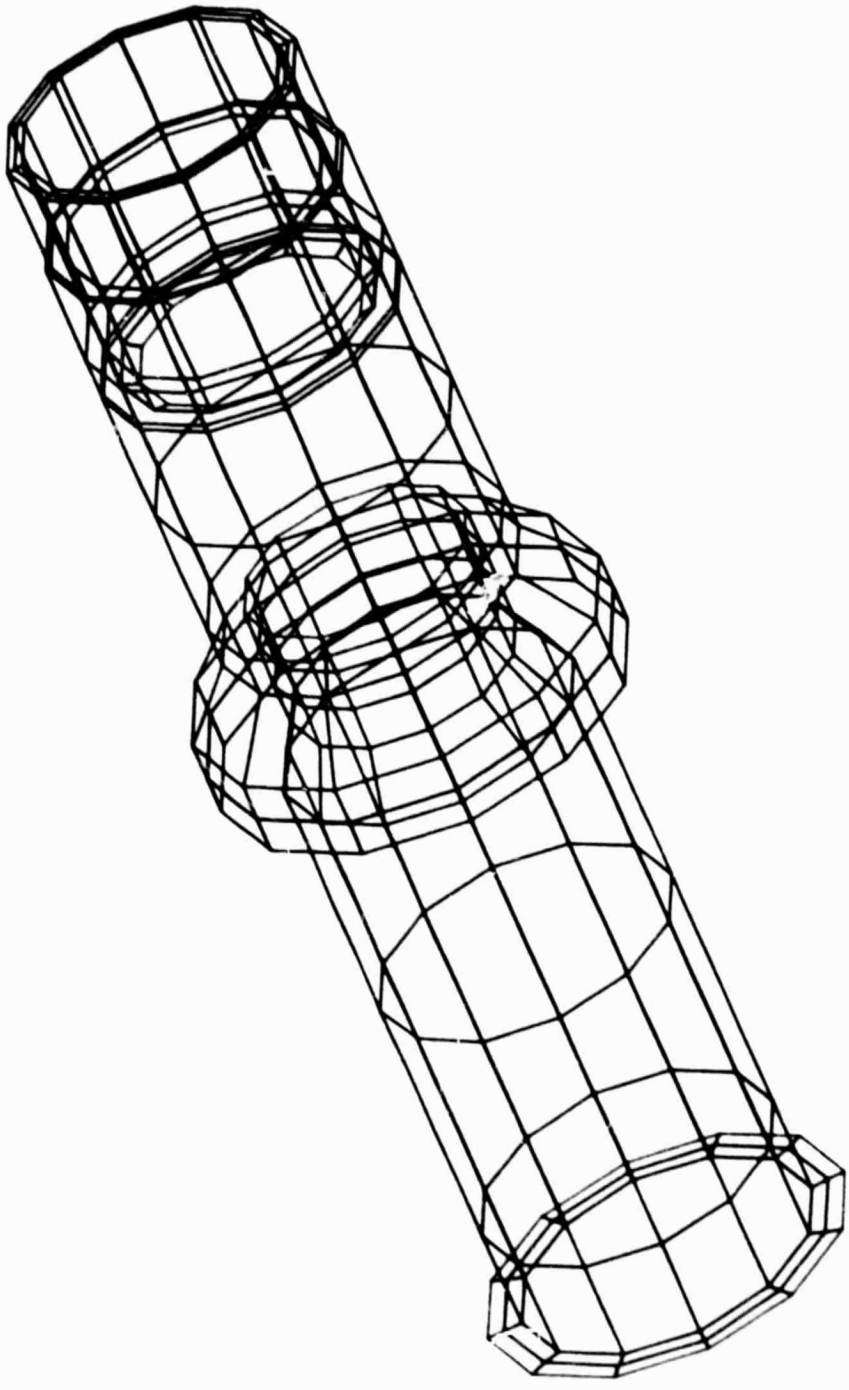

Retainer Convective Elements

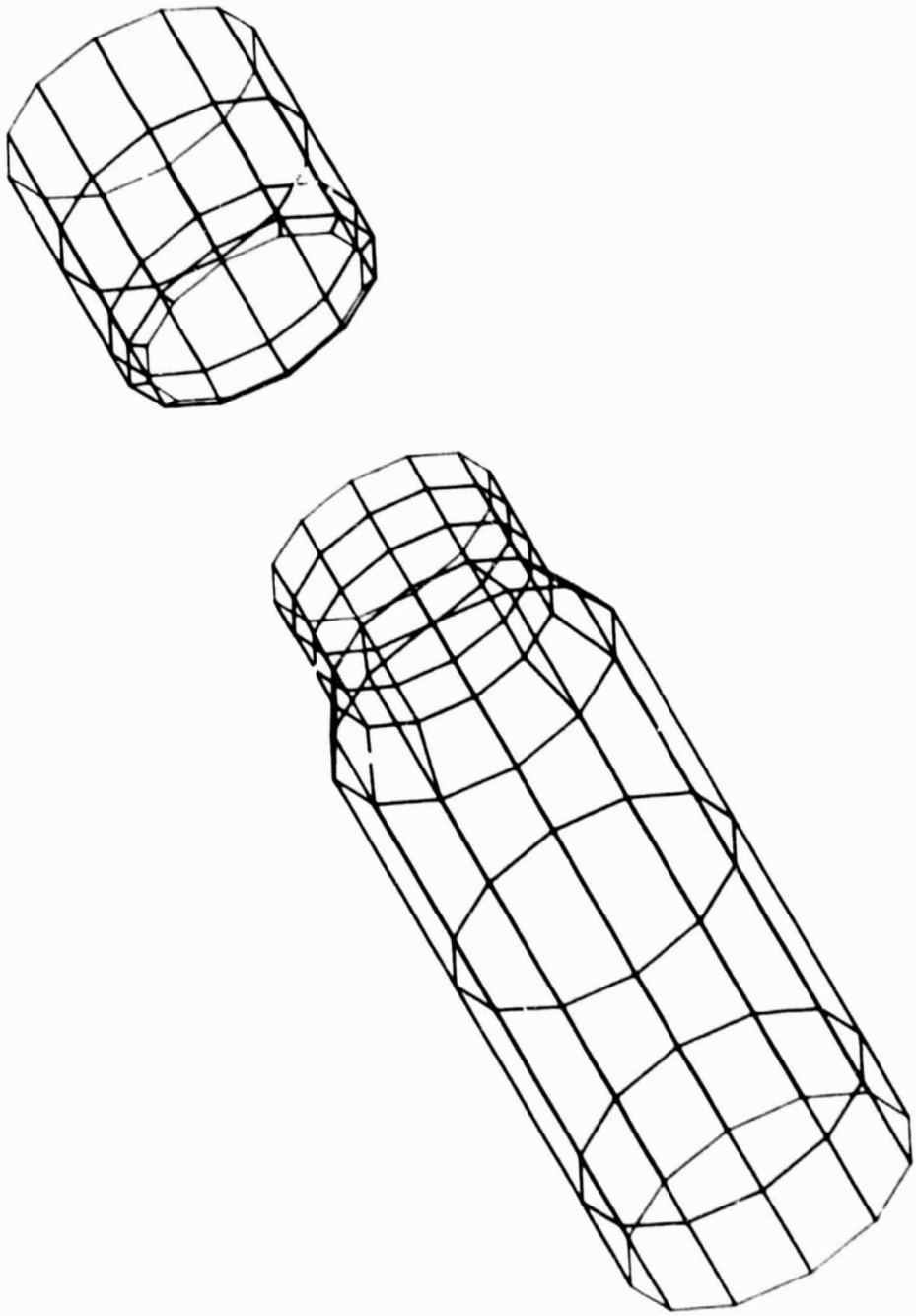

Retainer Inner Surface Convective Elements

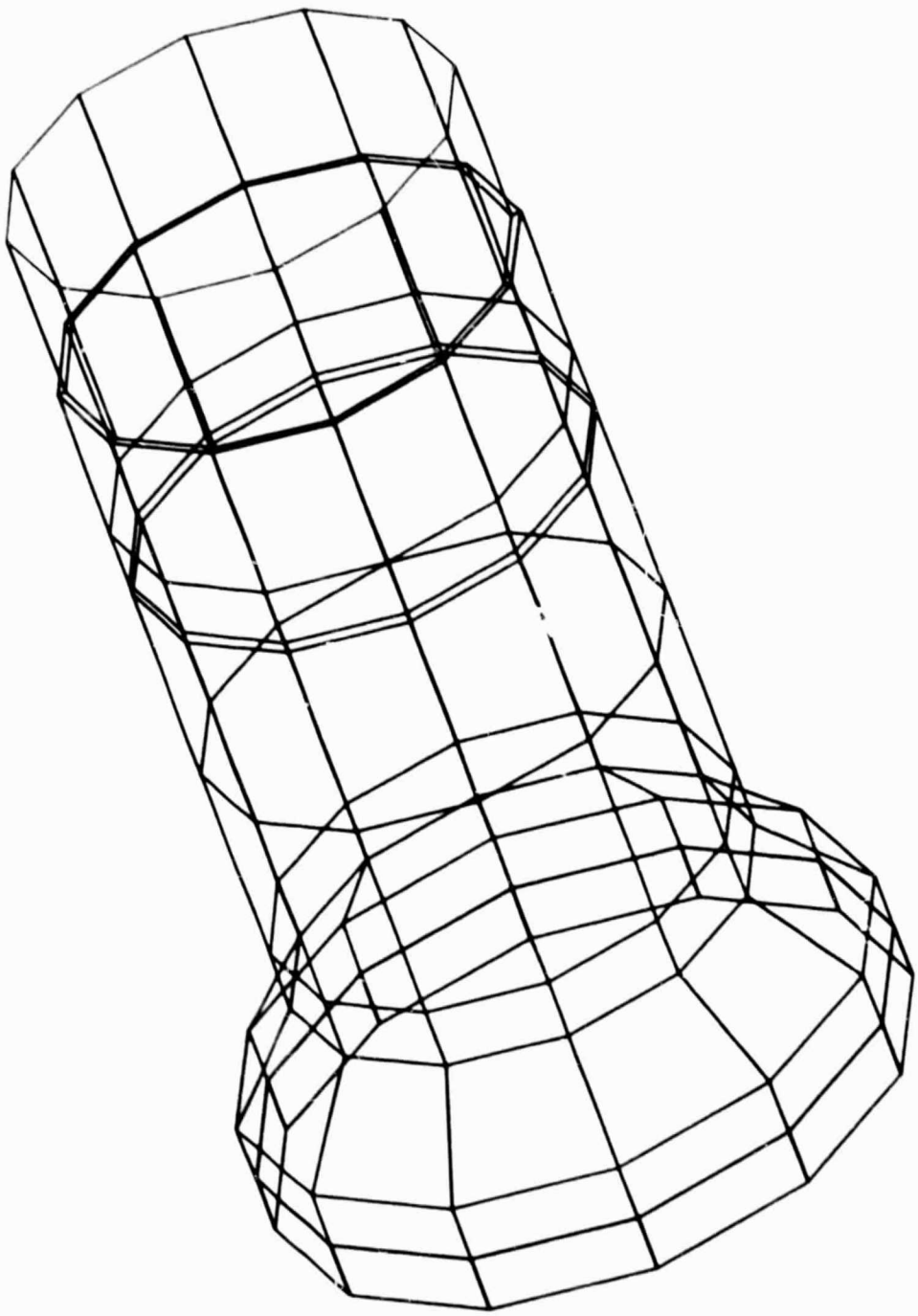

Retainer Outer Surface Convective Elements

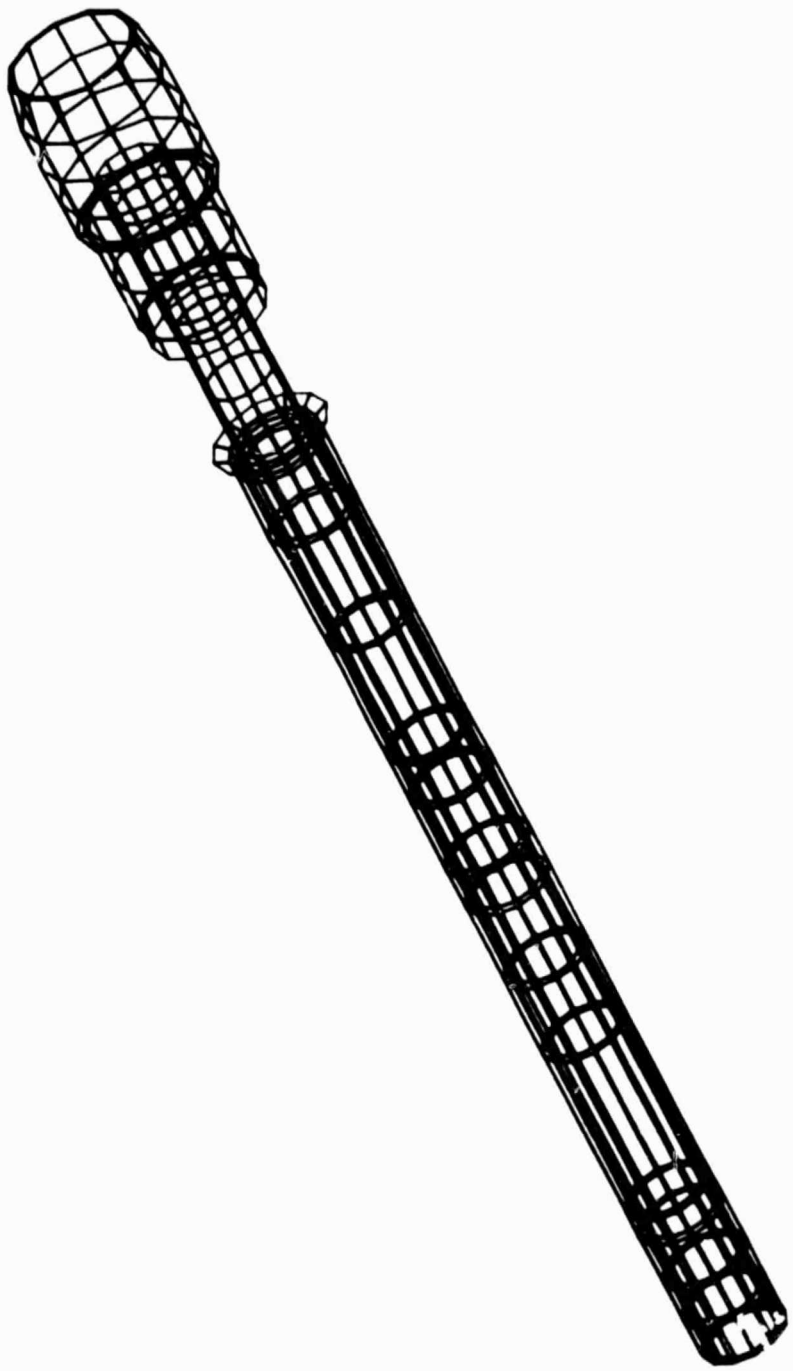

Tip Convective Elements

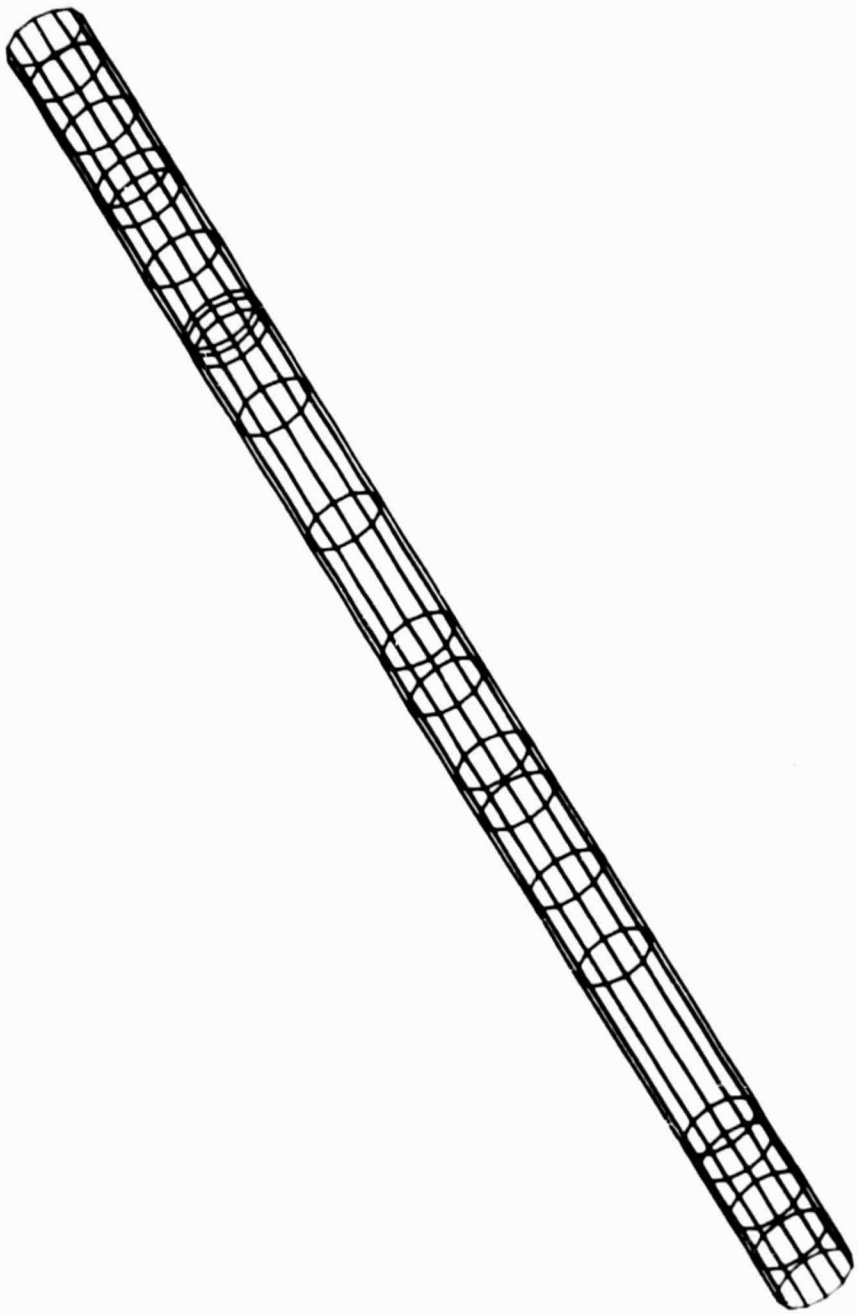

Tip Inner Surface Convective Elements

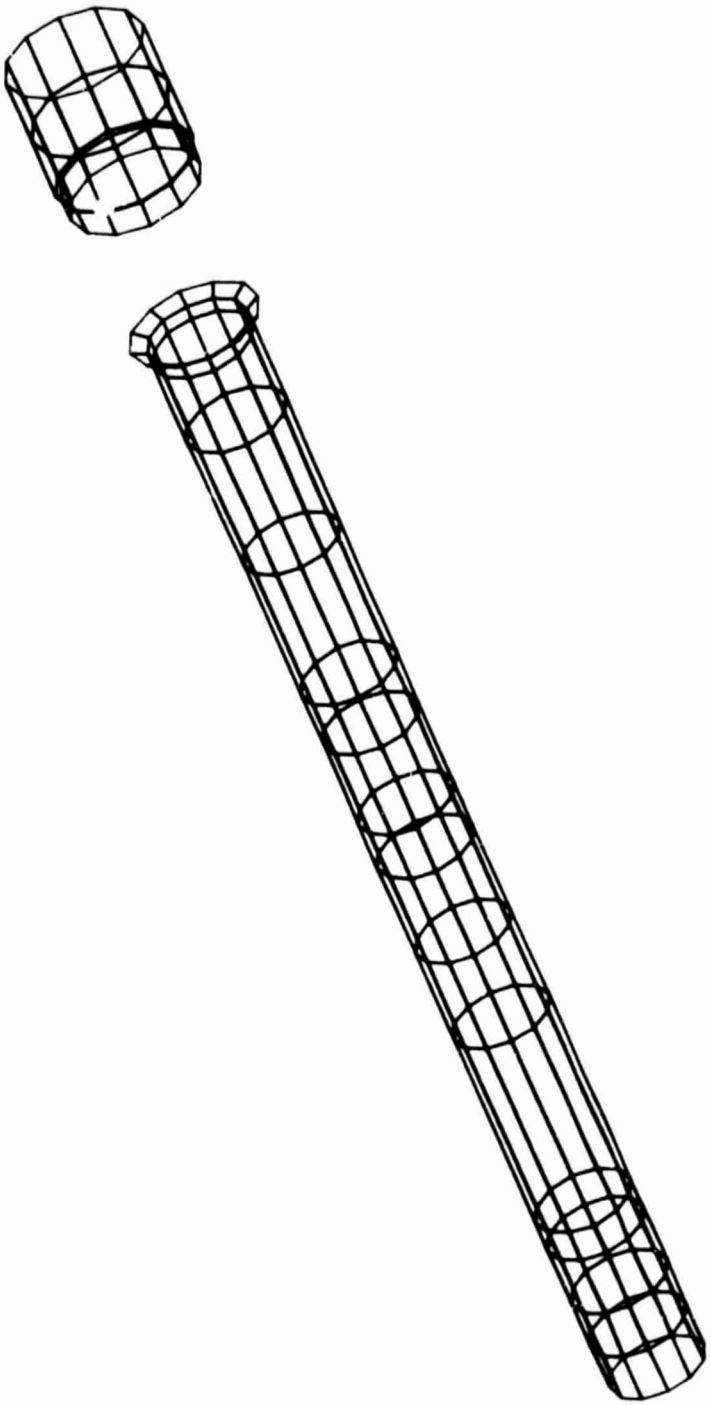

Tip Outer Surface Convective Elements

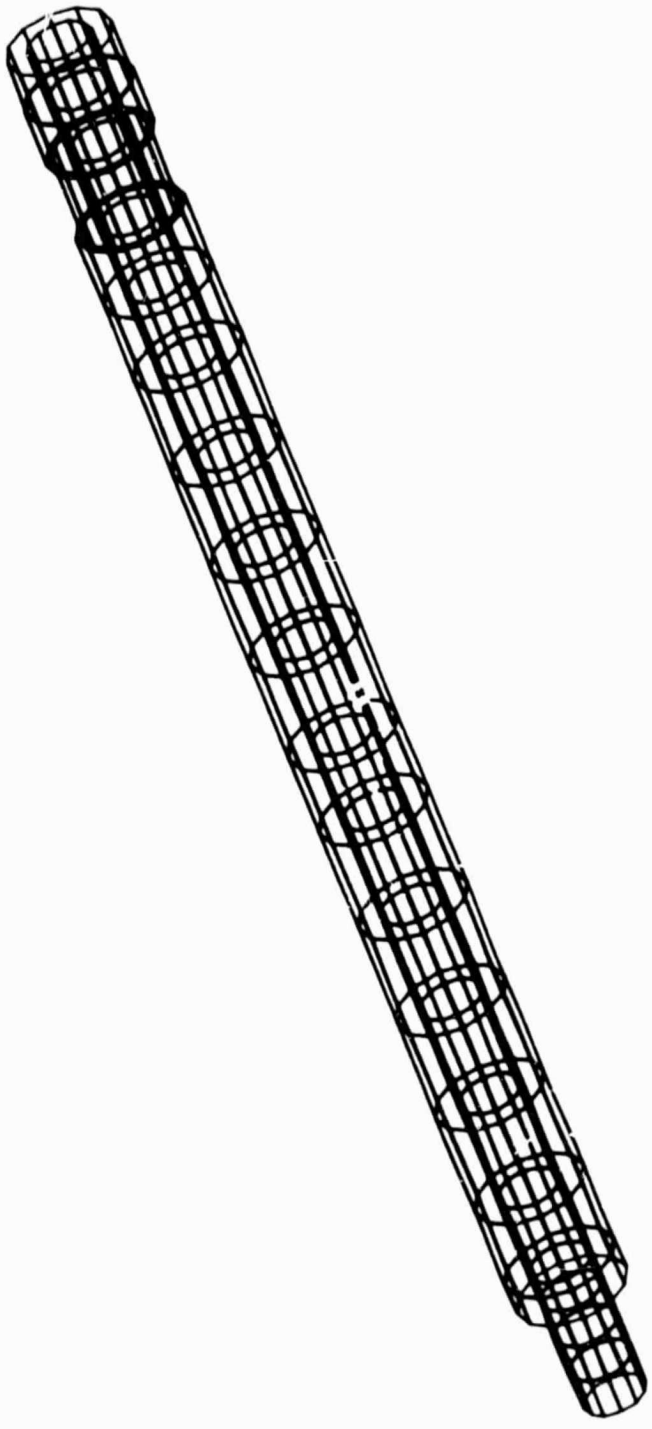

Post Convective Elements

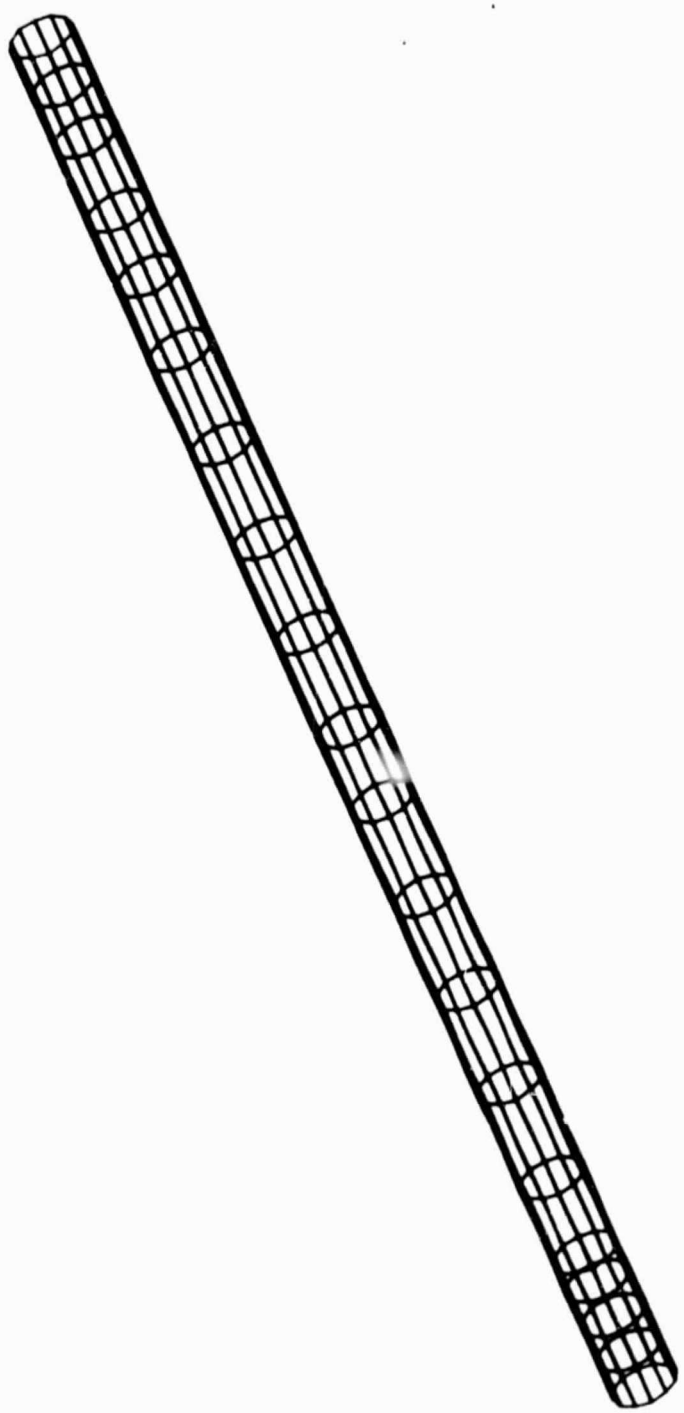

Post Inner Surface Convective Elements

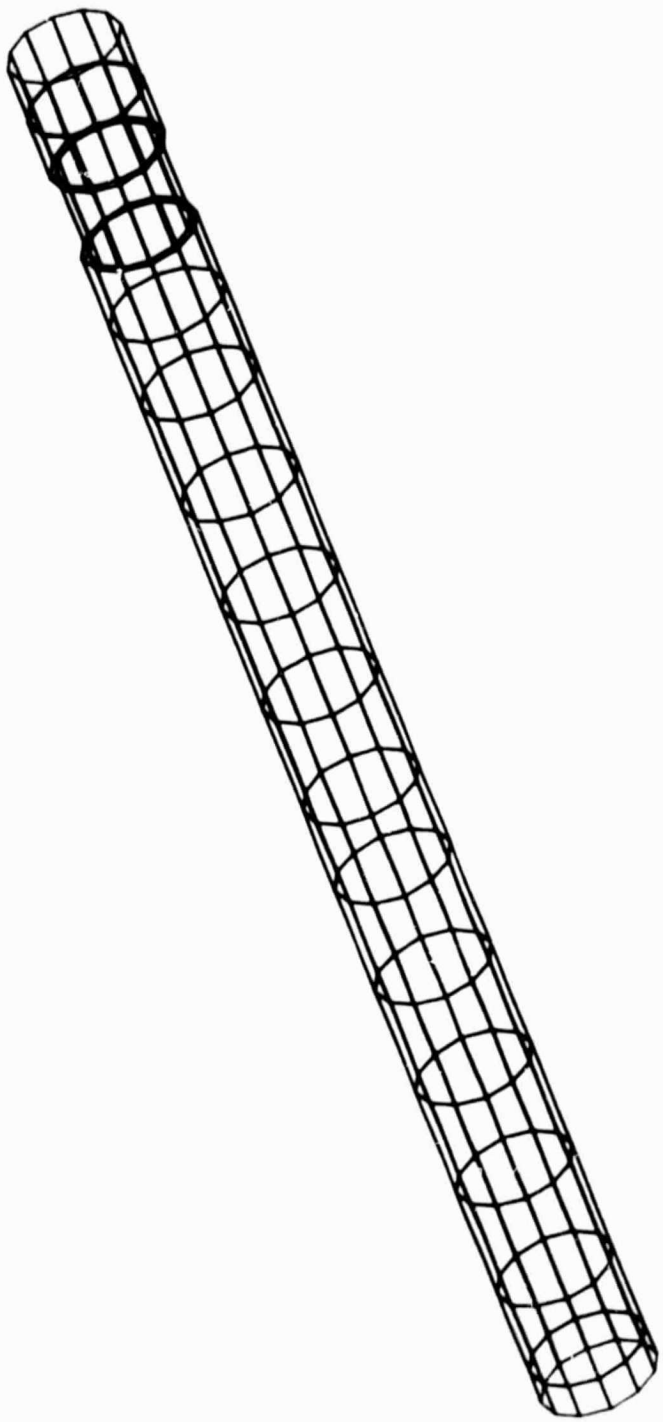

Post Outer Surface Convection Elements

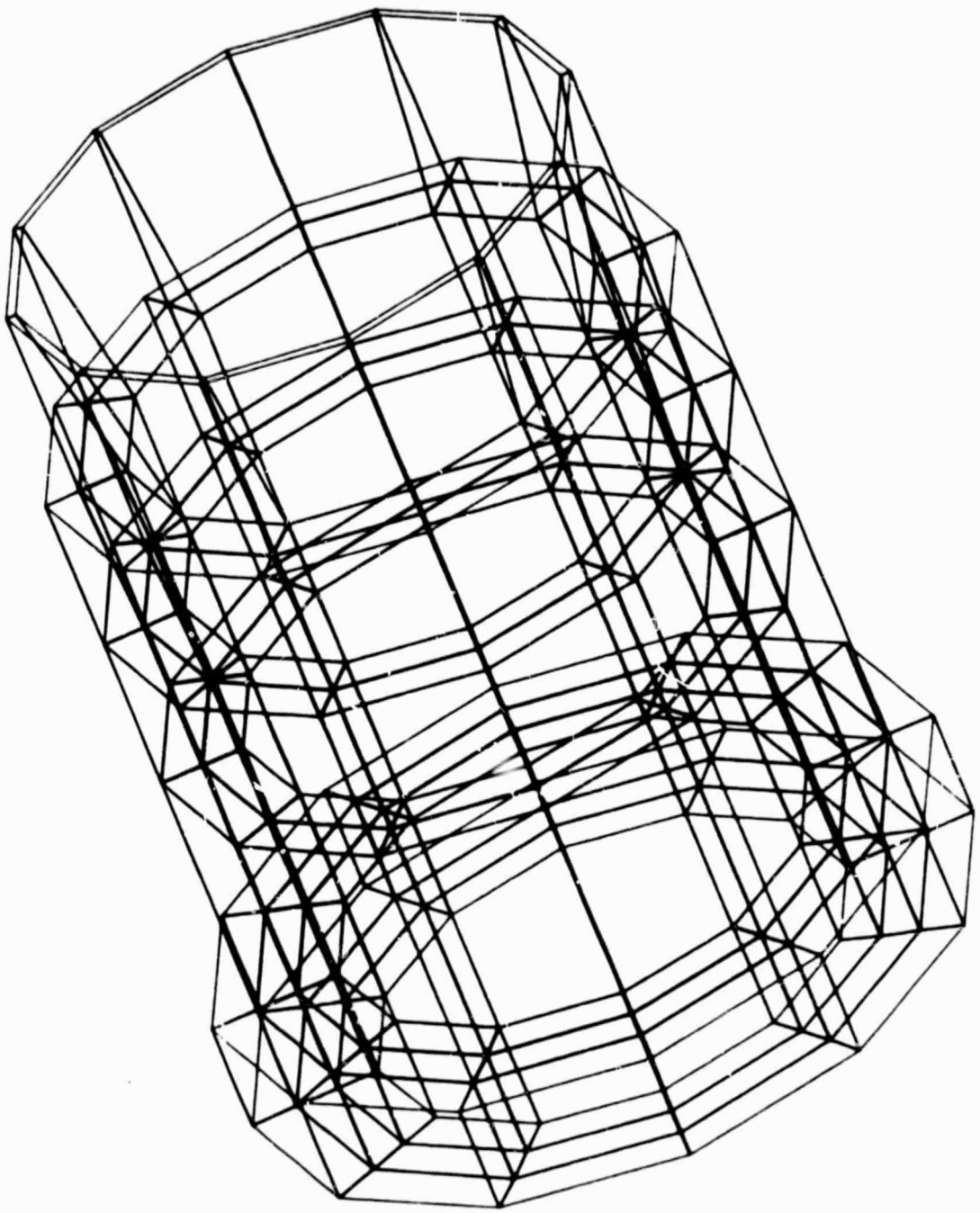

Nut Solid Elements

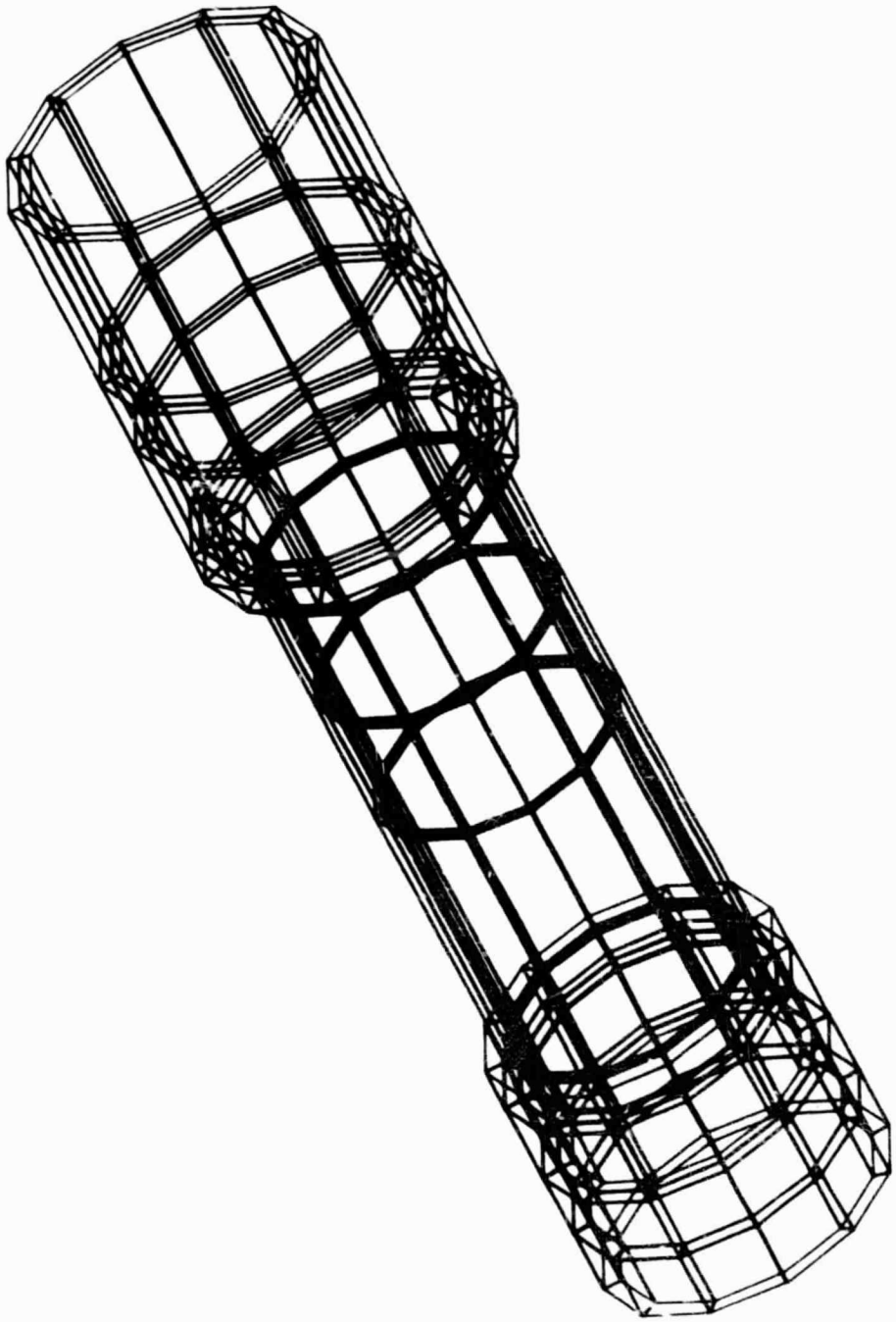

Sleeve Solid Elements

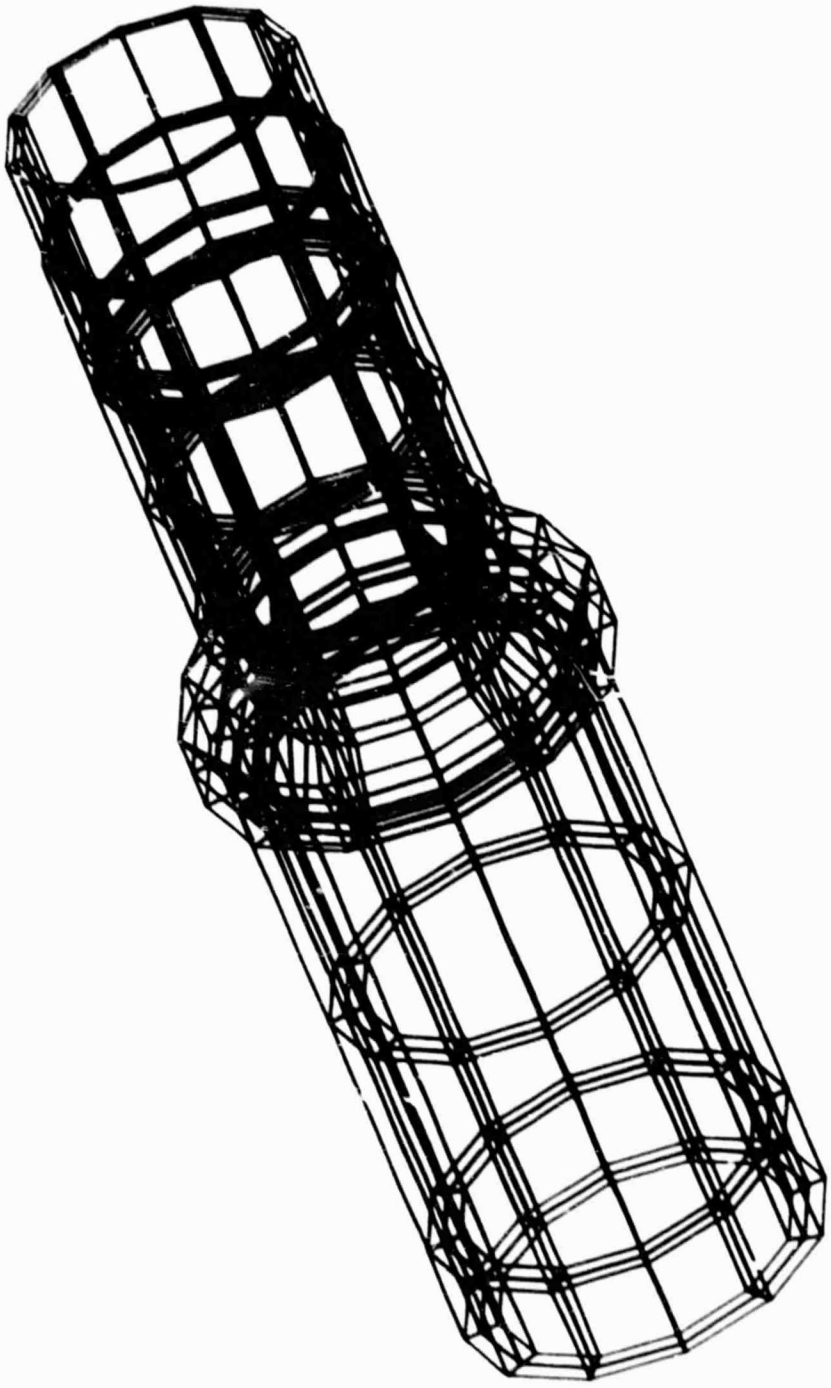

Retainer Solid Elements

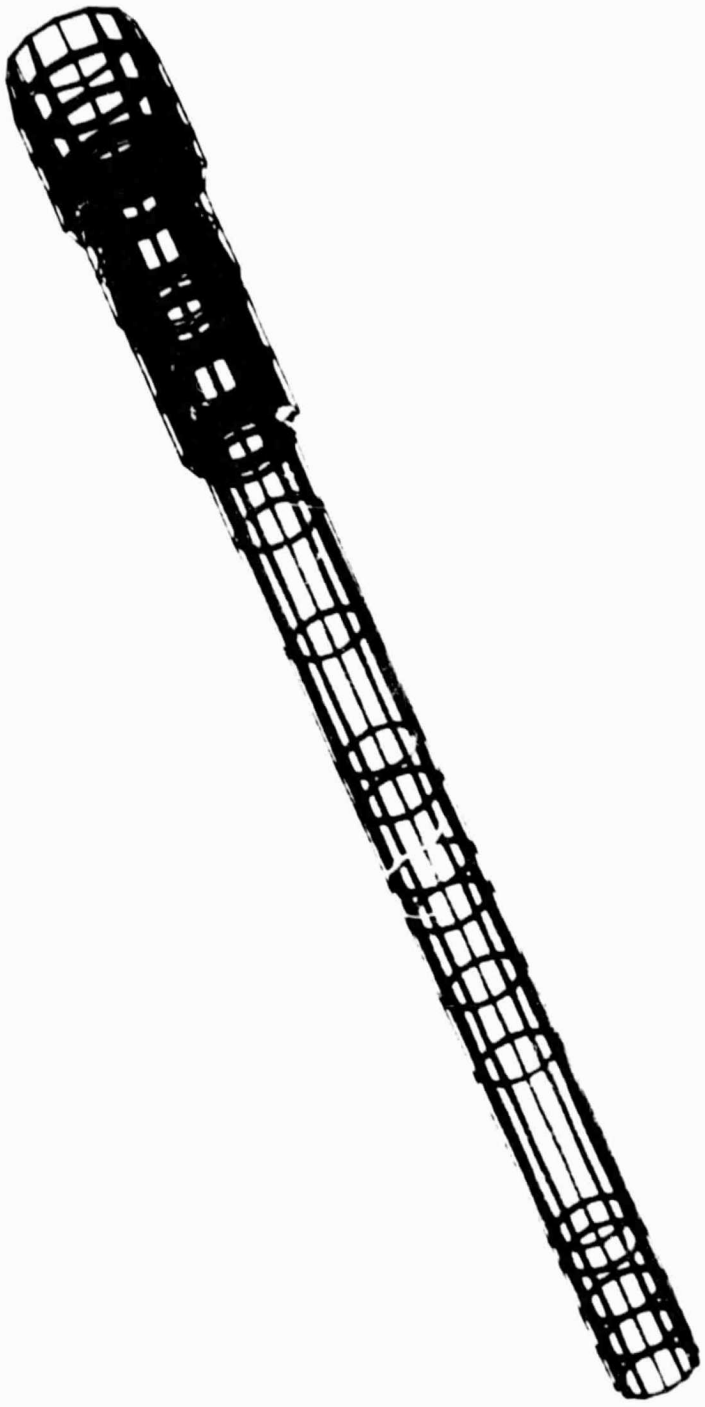

Tip Solid Elements

ORIGINAL PAGE IS
OF POOR QUALITY

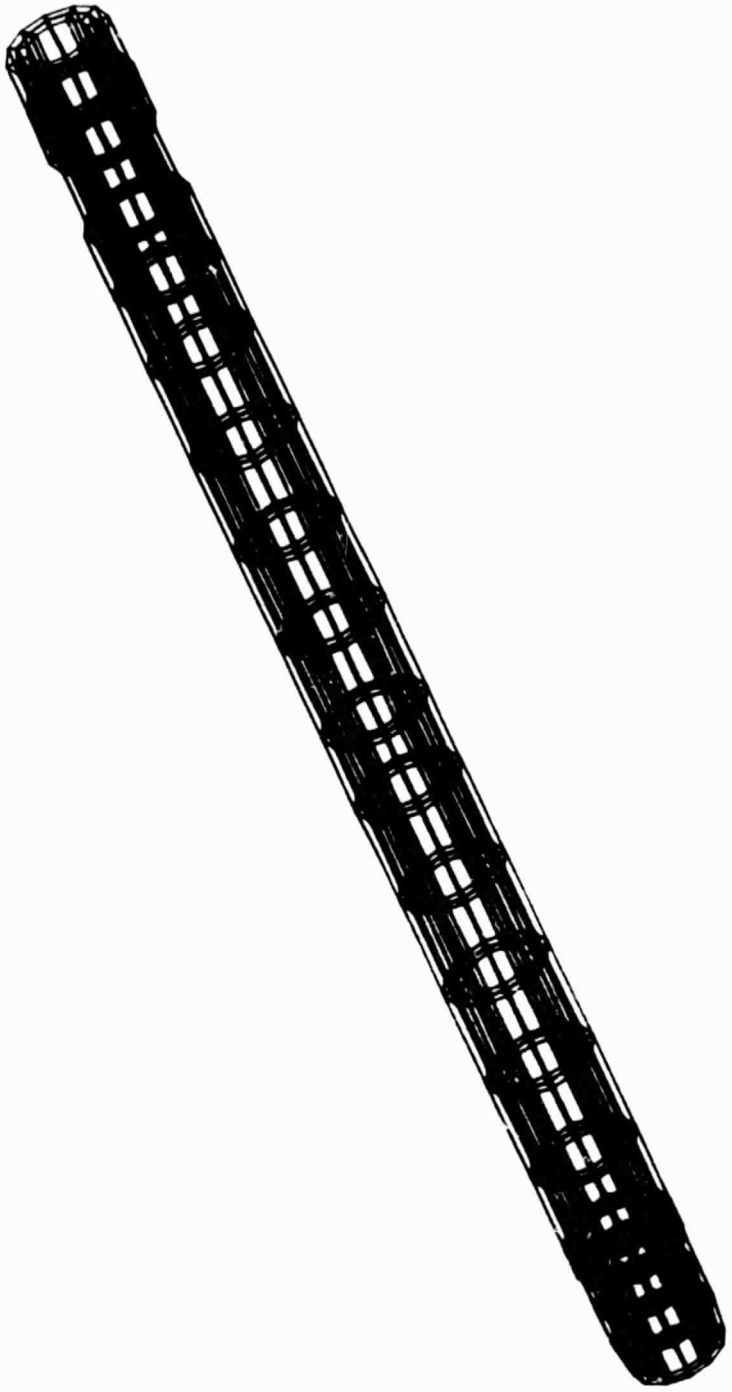

Post Solid Elements

APPENDIX C

SPAR POST/RETAINER DETAILED MODEL

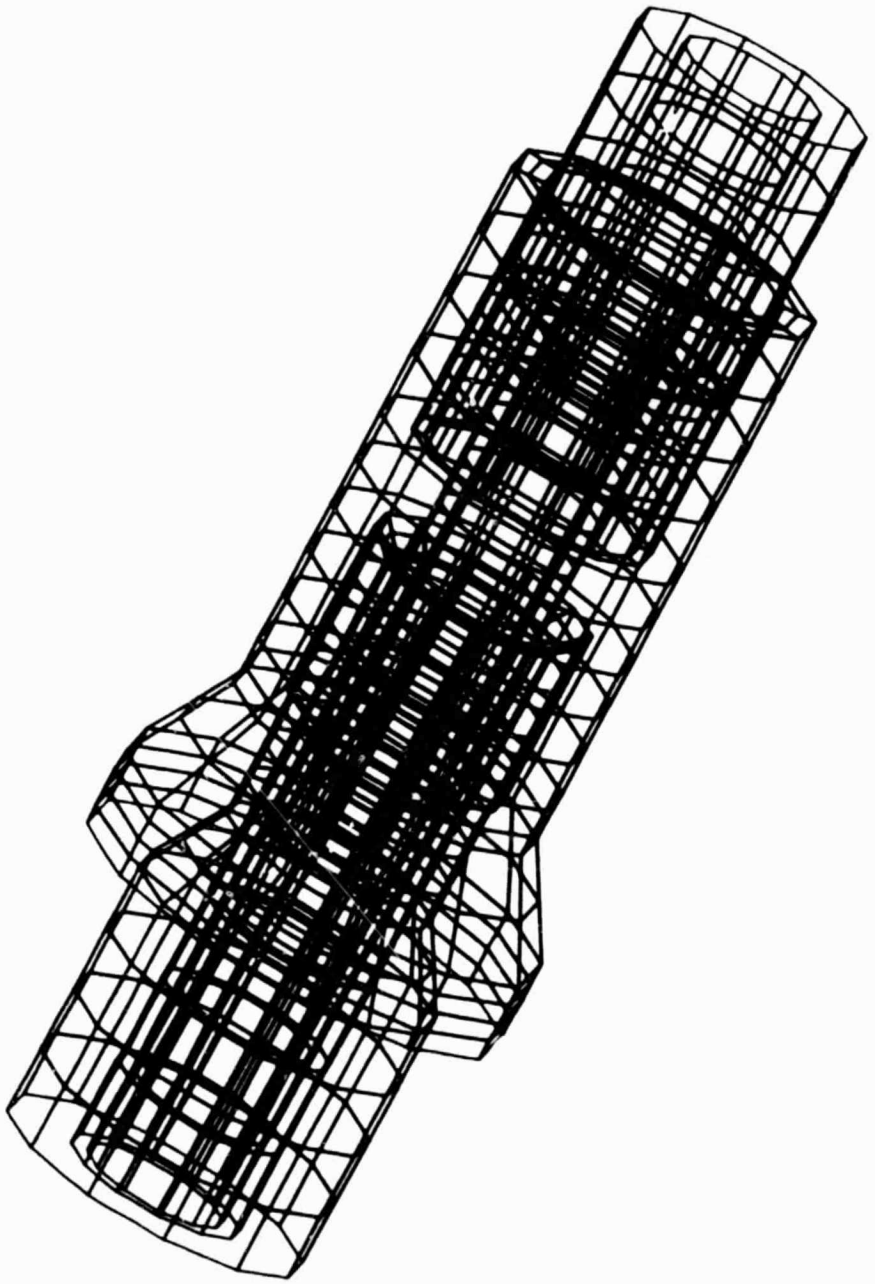

Post/Retainer Convective Elements

ORIGINAL PAGE
BLACK AND WHITE PHOTOGRAPH

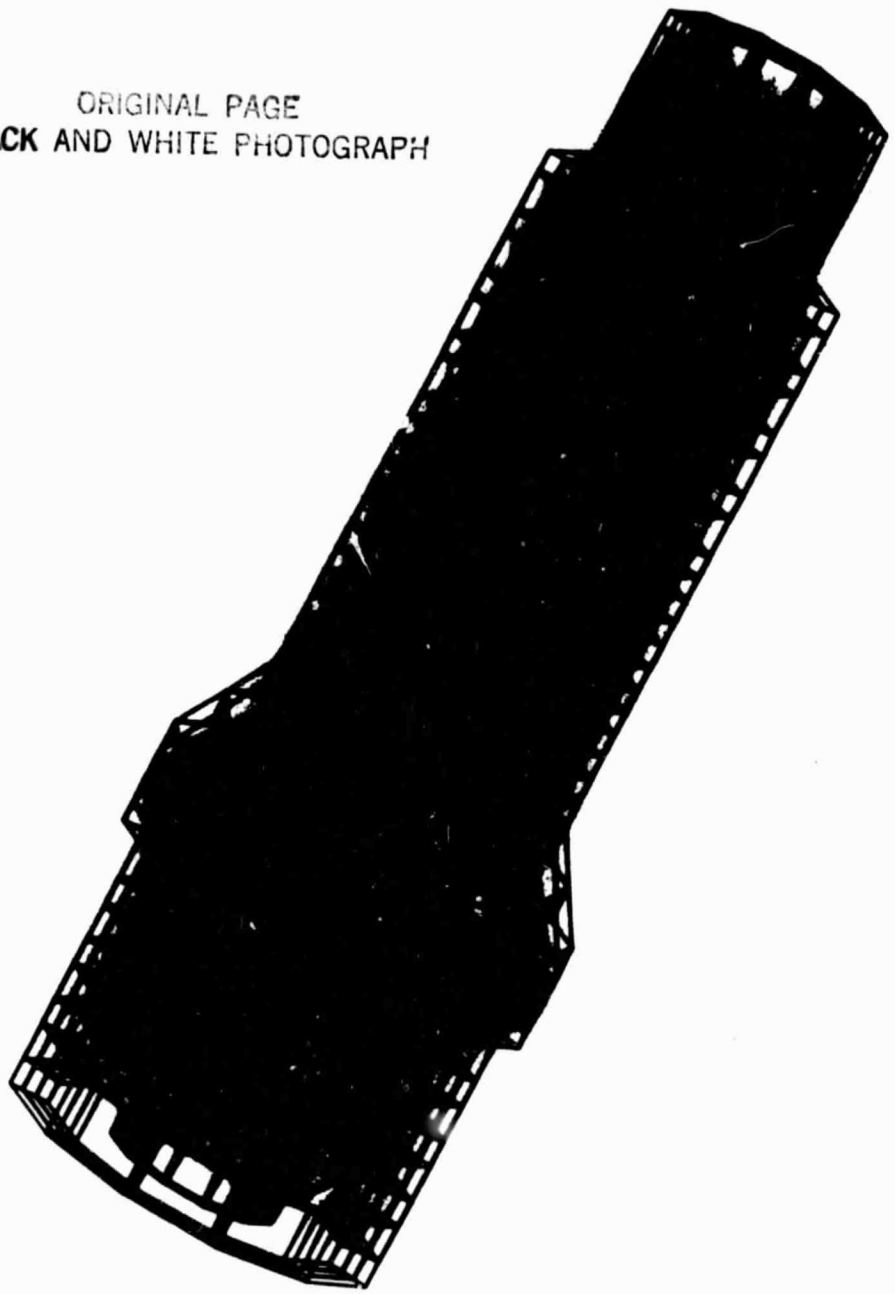

Post/Retainer Solid Elements

ORIGINAL PAGE
BLACK AND WHITE PHOTOGRAPH

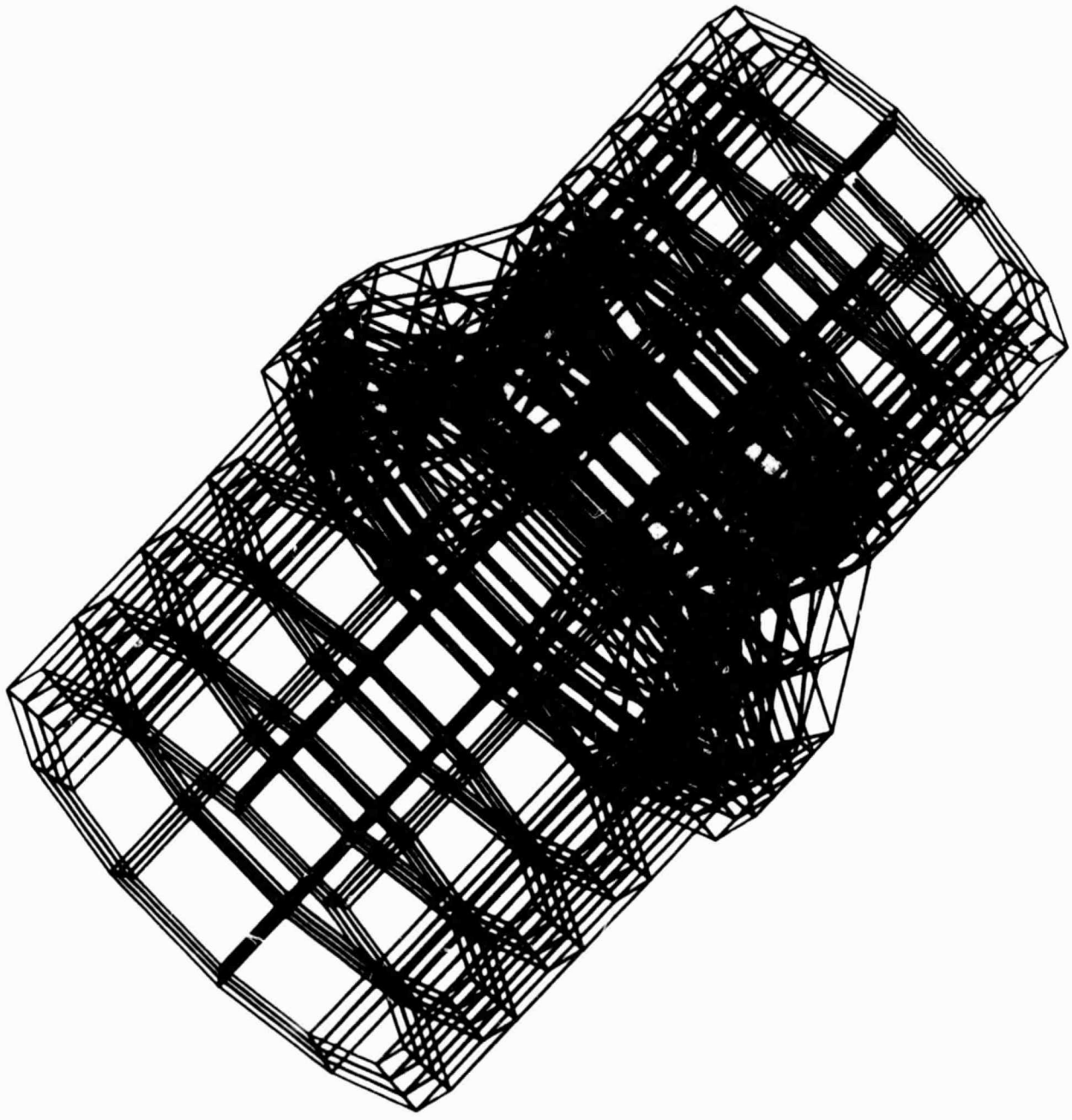

Retainer Solid Elements

ORIGINAL PAGE
BLACK AND WHITE PHOTOGRAPH

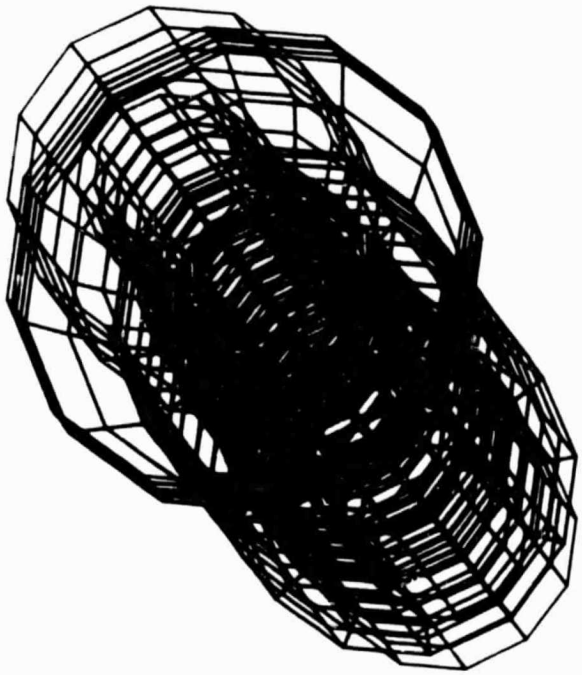

Post/Retainer Convective Elements

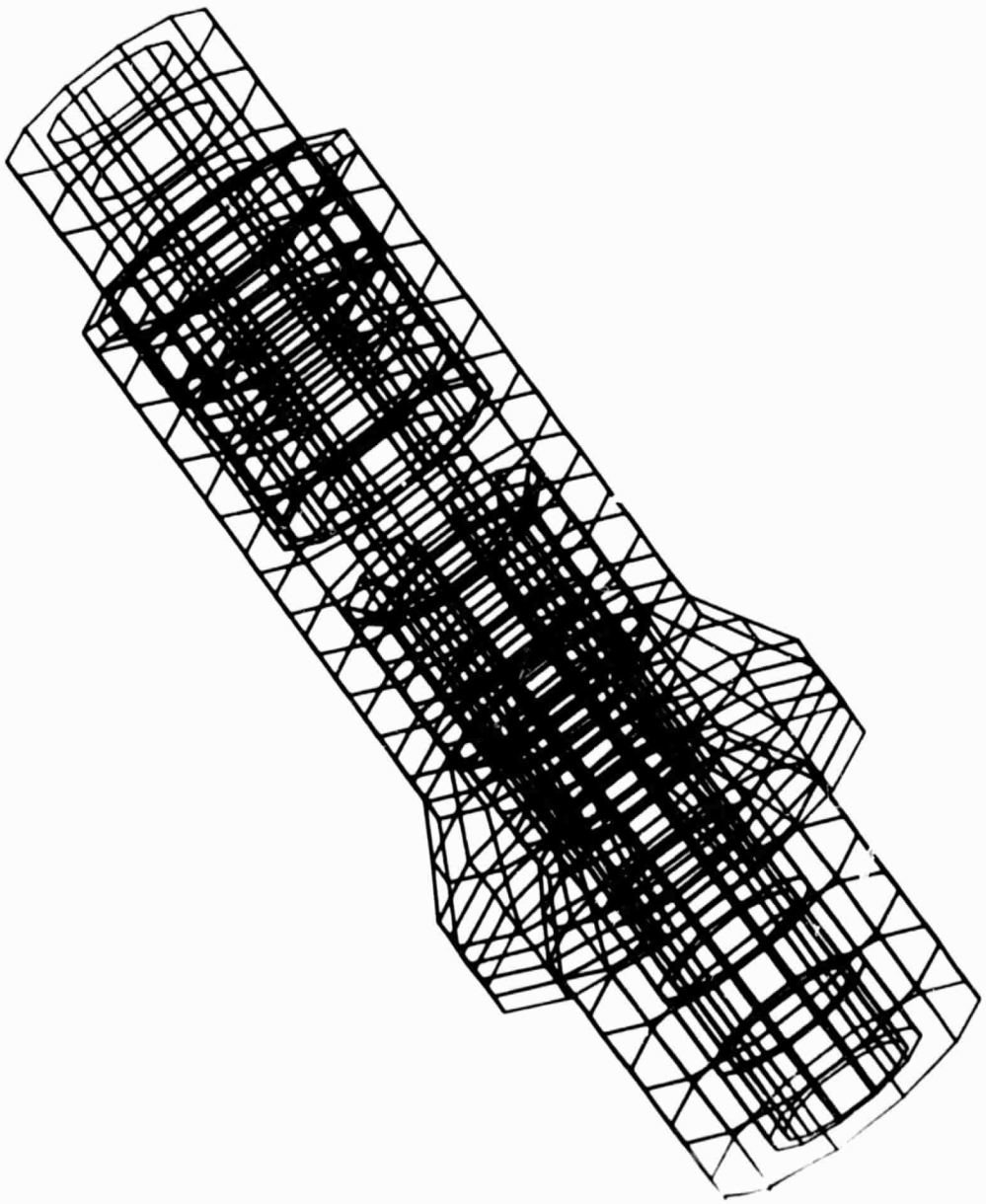

Post/Retainer Convective Elements

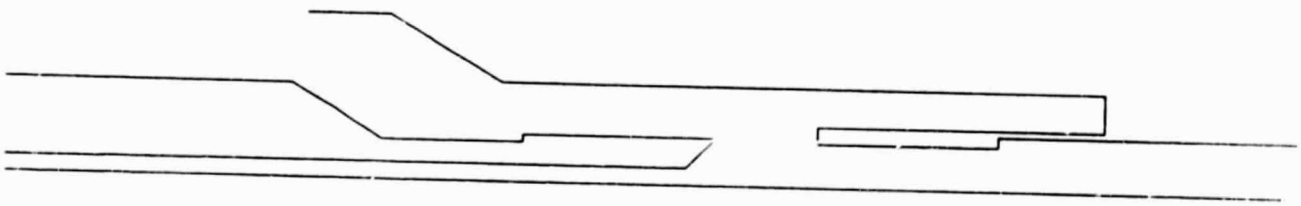

Post/Retainer 2-D Model Convective Surfaces

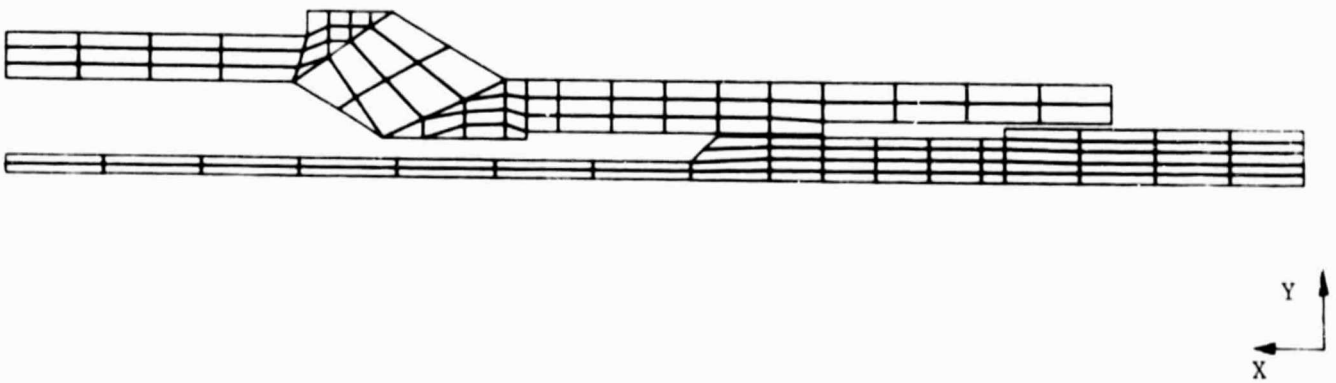

Post/Retainer 2-D Model Grid

Retainer

Post

Post/Retainer 2-D Model Numbering Scheme